Synthesis and Reactivity of Group 13 Phosphaethynolate Complexes

Daniel Wilson

Linacre College

University of Oxford

A thesis submitted for the degree of

Doctor of Philosophy

Michaelmas 2020

Abstract

Synthesis and reactivity of group 13 phosphaethynolate complexes.

Daniel W. N. Wilson Linacre College

DPhil Inorganic Chemistry Hilary 2020

This thesis describes the synthesis and reactivity of group 13 coordination complexes of the 2-phosphaethynolate anion (PCO^-). The synthesis and characterization of a stable phosphaethynolatoborane, [B]OCP ([B] = *N,N′*-bis(2,6-diisopropylphenyl)-2,3-dihydro-1H-1,3,2-diazaboryl), is described. This compound represents the first main-group, oxygen-bound isomer of the 2-phosphaethynolate anion to be structurally authenticated. The subsequent cyclisation chemistry of this compound was explored.

The reactivity of [B]OCP with a number of neutral and anionic nucleophiles was explored, the reaction outcome was found to be dependent on the properties of the nucleophile employed. Addition of catalytic amounts of ^{t}butyl-isocyanide induced isomerisation to yield the linkage isomer, [B]PCO. The mechanism of this conversion was explored experimentally and computationally.

The nucleophilicity of [B]OCP was also explored, its steric properties allow access to a series of tungsten trisphosphaalkyne carbonyl complexes. The reaction of [B]OCP with tris(pentafluorophenyl)borane demonstrated an increase in nucleophilicity with respect to the alkyl-substituted *tert*-butyl phosphaalkyne.

In an attempt to access the cyaphide anion, CP^-, the reduction chemistry of [B]OCP was explored with the aim to selectively cleave the O–C bond. The reaction outcome is dependent on the reducing agent employed, however selectivity for the desired bond was poor, giving rise to complex product mixtures. It was possible to isolate and partially characterise a magnesium cyaphide complex.

Next, a series of gallium phosphaketenes were synthesised. Both photolytic and chemical decarbonylation processes were explored, allowing access to base stabilised phosphinidenes. The ligand displacement methodology was expanded on to allow access to a compound with a gallium phosphorus double bond.

Acknowledgements

Many people have made my DPhil both possible and enjoyable. First and foremost I would like to thank my supervisor, Professor Jose Goicoechea, for giving me the opportunity to conduct this research. Without his mentorship none of this would have happened.

Thank you to all of the post-docs and D.Phil students who have I have had the pleasure of sharing this lab with over the years. Dr. Alex Hinz and Dr. David Lo, who took the time to teach me how to do synthetic chemistry when I first joined the group. Erica Faria, my long-term lab companion, for her emotional support and baked goods. Dr. Meera Mehta for reading this thesis in its entirety, in addition to her constant advice and encouragement. Dr. Sebastian Bestgen for his grumpy, but always sound, advice.

We have had a steady stream of visiting students and undergraduates come through the lab. Freddy Barnes, thank you for your contribution to this thesis, I am sorry for not giving you a working project. Though I did not supervise them, I would like to thank Cory, Harry, Gabi, Moritz, and Fabian for bringing some great attitude to the lab for the brief periods they were here.

Many people outside of the group took the time to help me with, and teach me about, various aspects of chemistry. Dr. Nick Rees, for NMR assistance and for the time spent explaining various experiments. Dr. Will Myers for the hours spent locked in a room with me aligning lasers for EPR experiments. Dr. Jamie Hicks for synthetic expertise and Dr. Petra Vasko for computational advice. Prof. John McGrady and Mauricio Franco for their work on calculations.

Thank you to my family, without whom I would not be who I am today. Particularly my Mum, who supported me going to university in the first place. Who knew I would still be here almost eight years later.

Thank you to all of my friends here in Oxford with whom I have shared innumerable lunches, coffees, and beers. Whenever life was difficult there was always someone there, without exception.

Finally, I can't imagine having done this without the care and support of Karl Dudman. I hope I can return the favour over the next few years.

List of abbreviations

12-crown-4	1,4,7,10-tetraoxacyclododecane
18-crown-6	1,4,7,10,13-pentaoxacyclopentadecane
Å	angstrom
au	atomic units
av	average
BDE	bond dissociation energy
BIAN	bisacenaphthenequinonediimine
calc	calculated
cm^{-1}	wavenumber
COD	cyclooctadiene
Cp	cyclopentadienyl
Cp*	pentamethylcyclopentadienyl
d	doublet
Da	Dalton
DFT	density functional theory
DFB	1,2-difluorobenzene
Dipp	2,6-diisopropylphenyl
EPR	electron paramagnetic resonance
ESI	electron spin resonance
G	grams
HOMO	highest occupied molecular orbital
Hz	Hertz
IMes	1,3-dimesitylimidazol-2-ylidene
^{i}Pr	*iso*-propyl
IR	infrared

J	Joules
K	kelvin
KHMDS	potassium bis(trimethylsilyl)amide
kcal	kilocalories
LUMO	lowest unoccupied molecular orbital
M	molar
m	multiplet
^{Me2}IPr	1,3-diisopropyl-4,5-dimethyl-1,3-dihydro-2λ^2-imidazole
Me	Methyl
Mes	mesityl (2,4,6-$Me_3C_6H_2$)
Mes*	mesityl terphenyl
mg	milligram
mL	millilitre
mol	mole
NHC	N-heterocyclic carbene
NICS	nucleus independent chemical shift
NMR	nuclear magnetic resonance
NRT	natural resonance theory
Ph	phenyl
ppm	parts per million
Pyr	pyridine
s	singlet
sept	septet
t	triplet
^{t}Bu	*tert*-butyl
THF	tetrahydrofuran
TMS	trimethylsilyl

tol	toluene
z	charge
γ	gyromagnetic ratio
δ	chemical shift

Contents

List of compounds

[B]	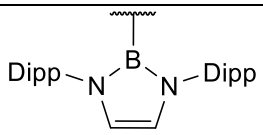
1	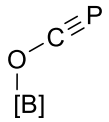
2	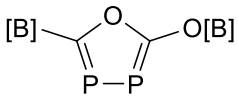
3	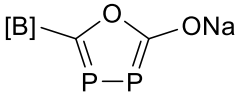
4	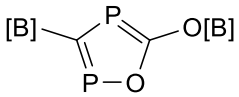
5	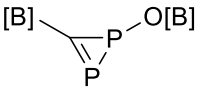
6a	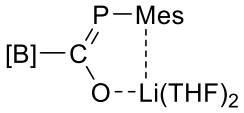
6b	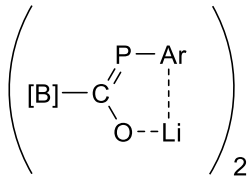
6c	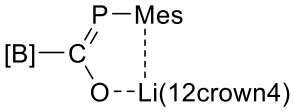
7	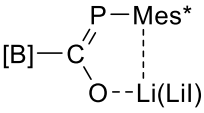
8a	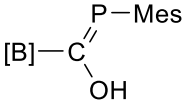
8b	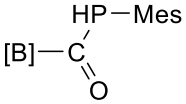
9	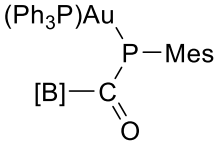
10	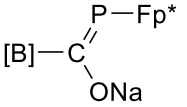

11	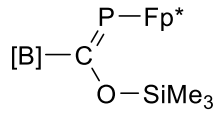
12	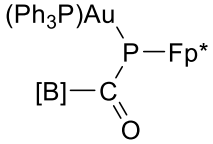
13	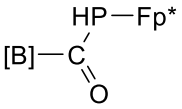
14	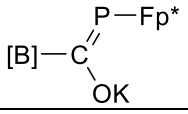
15	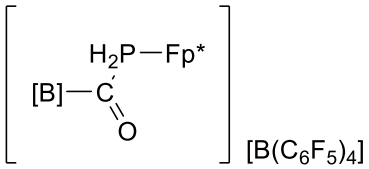
16a	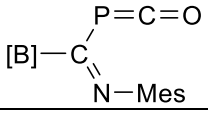
17a	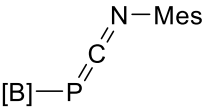
17b	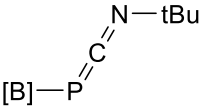
18	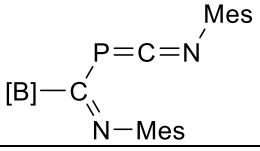
19	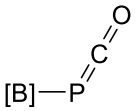
20	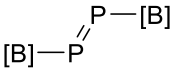
21	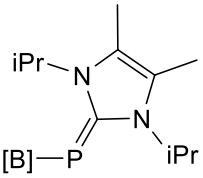
22	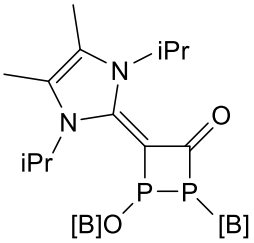

23a	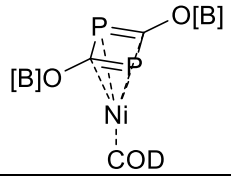
23b	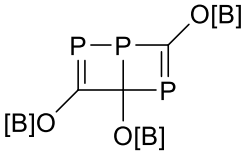
23c	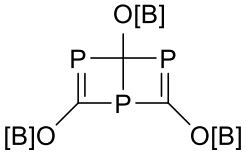
23d	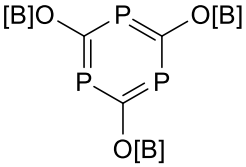
24	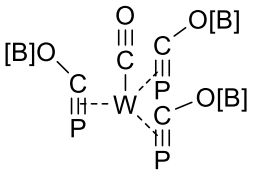
25	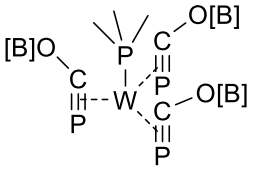
26	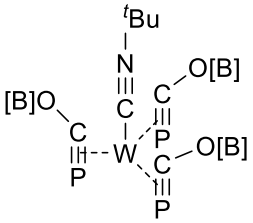
27	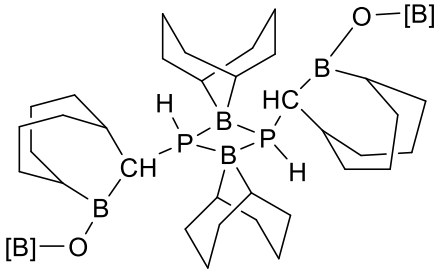
28	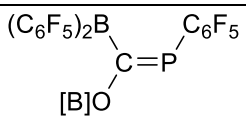
29	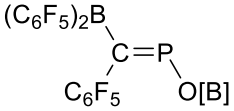

30	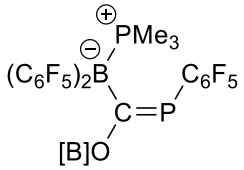
31	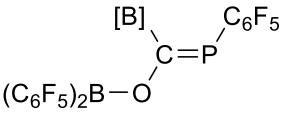
32	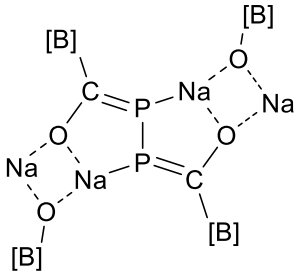
[^{Mes}Mg]	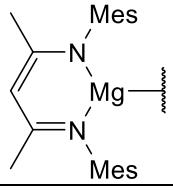
33	[B]—O—[^{Mes}Mg]
35	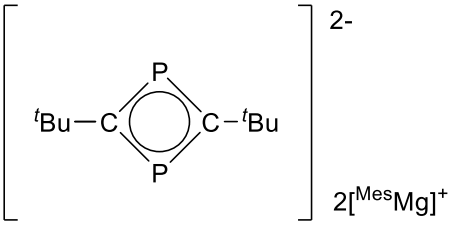
36	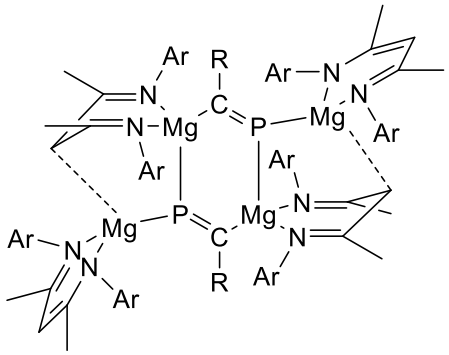
37	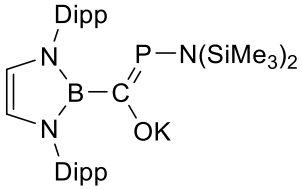
38	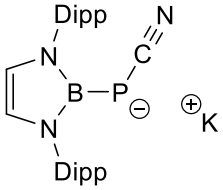

39	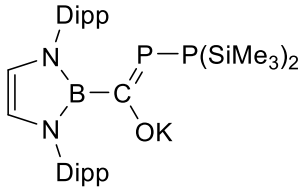
40a	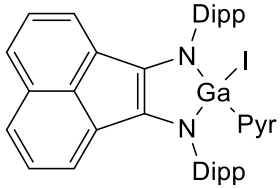
40b	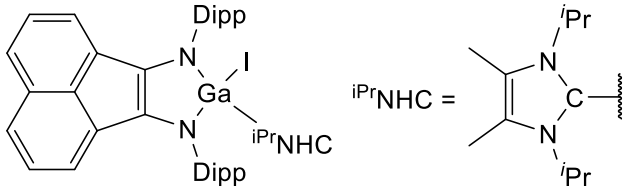
40c	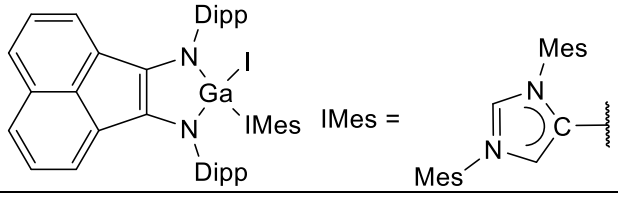
41a	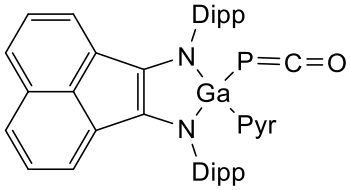
41b	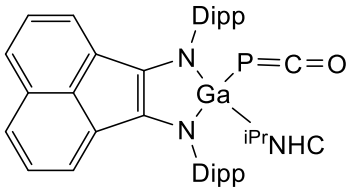
41c	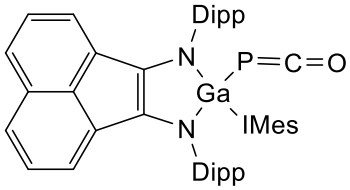
42	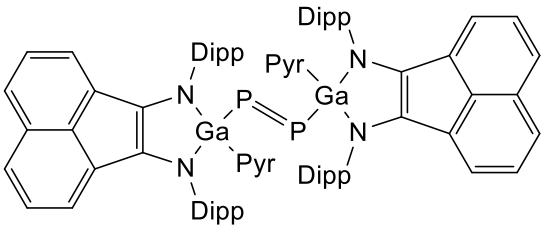
43a	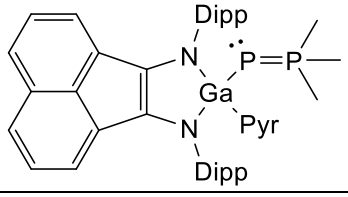

43b	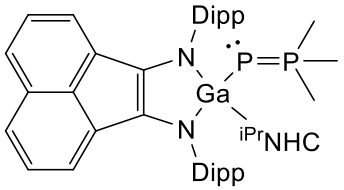 Dipp N P=P Ga N iPrNHC Dipp
44	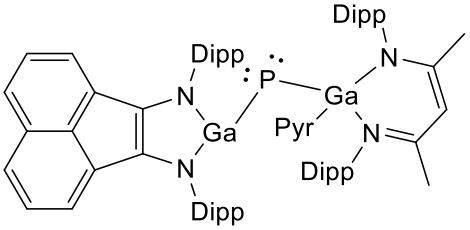 Dipp Dipp N P Ga N Pyr N N Dipp Dipp

Chapter 1
Introduction

1.1 Phosphorus in Nature

The role of phosphorus in nature is hard to overstate. Every form of cellular life relies on nicotinamide adenine dinucleotide phosphate, $NADP^+$, as a cofactor in anabolic reactions, such as those which create the nucleic acids that make up DNA.[1] Moreover, adenosine triphosphate, ATP, is the workhorse of every cellular process that requires energy. The walls of cells are built from phospholipids, and calcium phosphates deliver the rigidity for teeth and bones.[2] The chemist and writer Isaac Asimov wrote "life can multiply until all of the phosphorus has gone and then there is an inexorable halt which nothing can prevent."[3] In short, where there is life, there is phosphorus.

The first corroborated report of the discovery of elemental phosphorus took place in 1669 by the alchemist Hennig Brandt.[4] His method involved the distillation of urine, and after separation of a number of unwanted by-products, he was able to obtain a solid material that would glow in the dark, resulting in the derivation of the elements name from the Greek *phôs*, meaning light, and *phoros*, meaning bearer. The subsequent century saw alchemists from around the isolating phosphorus on mass scale. Following a stint as a cure-all medicine, with applications ranging from treating typhus to improving libido, phosphorus quickly became a staple element found in various industries.[5] The discovery that bones were high in phosphorus content allowed the large-scale manufacture of matches in the late 18th century. Technological advances, in particular the development of the Haber-Bosch process, brought on the Green Revolution of the post-World War II period. It was around the same time that it was realised that phosphorus-containing fertilizers were as important as their nitrogen-containing counterparts for improving crop yield, and in fact an excess of phosphorus was needed to reach maximum yields. It was also around this time that phosphate rock mining reached maturity, allowing for supply to meet this vast increase in demand.

Phosphate is a finite resource and, as with many mineral deposits, is not evenly distributed throughout the globe; 85% of all phosphate reserves are controlled by just five countries (Morocco, China, US, Jordan and South Africa) leading to geopolitical issues with its procurement.[6] Furthermore, little is being done to recover the phosphorus in our food 'cycle'. It is lost to waterways through both field run-off and sewage. It is our lack of phosphorus management that is the dominant contributor to a global epidemic of non-point source eutrophication; which is not only devastating for biodiversity, with the emergence of marine dead zones,[7] but also permanently removes phosphorus from the food system.[8]

1.2 Phosphorus – the Element

Elemental phosphorus can exist as several allotropes, all of which are produced from mined phosphate. Monoatomic phosphorus is known to exist but only becomes the predominant species in phosphorus vapour at temperatures around 3000 K at atmospheric pressure. Below such temperatures, 3000>2100 K, the diatomic P_2 is the dominant allotrope and further lowering the temperature results in dimerization to P_4, a tetrahedral prism consisting of exclusively sigma bonds known as white phosphorus.[9] A molecular equivalent to P_2 was reported by the Cummins group in the form of a tungsten pentacarbonyl P_2 complex generated from the $[\eta^2$-Mes*NPP)Nb(N[Np]Ar$)_3]^{1-}$ (where Mes* = 2,4,6-*tert*-butyl$_3$C$_6$H$_2$, Np = neopentyl, Ar = 3,5-$C_6H_5Me_2$) which is capable of acting as a source of P_2 upon gentle heating, which the authors subsequently trapped with cyclohexadiene.[10]

The decrease in bond order, and increase in number of σ bonds, upon cooling phosphorus gives information about the relative strength of phosphorus-phosphorus multiple bonds, particularly in comparison to its lighter congener, nitrogen. The N≡N triple bond, one of the strongest atomic bonds, is more than three times stronger than an N–N single bond (bond dissociation energy = 226 vs. 38 kcal/mol), while a P≡P triple bond is significantly

less than three times that of a P–P single bond (117 vs. 50 kcal/mol).[11] This relatively small increase in bond dissociation energy going from a P–P single bond to a P≡P triple bond is a consequence of a decreasing percentage overlap between the p-orbitals on increasing the principle quantum number from 2p to 3p. The result of this is a propensity for phosphorus to catenate upon cooling to yield a number of allotropes; assigned to three families – white, red, (and violet), and black (Figure 1.1).

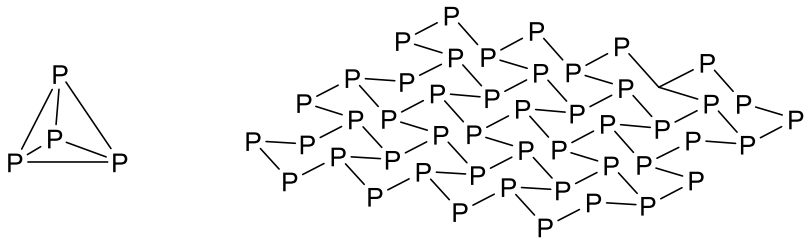

Figure 1.1. Allotropes of phosphorus: (left) white phosphorus (right) black phosphorus.

The commercial preparation of white phosphorus involves the heating of phosphate rock with sand and coke with electric furnaces which typically reach temperatures of 1400–1500 °C.[12] This process is an efficient, but energy intensive, method for the production of white phosphorus with yields of around 90% based on the phosphorus content of the phosphate mineral. The molecular structure consists of monomeric P_4 molecules arranged in a tetrahedron. P_4 is the thermodynamically least stable allotrope, with the high reactivity attributed to the strain induced by its bonding situation, represented in its high pyrophoricity. It is also highly toxic and fatal in doses of 1mg/kg of body weight.[13]

The more stable red phosphorus is created from the white allotrope on commercial scales through use of high-temperature ball mills or through exposure of white phosphorus to sunlight.[12] It is an amorphous polymeric material commonly found in household matches. The black allotrope of phosphorus is the most thermodynamically stable form and is produced by treating white phosphorus under elevated temperature and pressure.[14] The molecular structure of black phosphorus consists of a lattice of connected six-membered

rings. Treatment of black phosphorus with scotch-tape produces a two dimensional material known as phosphorene, which is realted to graphene in its structure and physical properties.[15] Aside from interest in its electronic properties, little research has been conducted into the fundamental chemistry of the black allotrope. The polymeric allotropes of phosphorus have the advantage of being non-pyrophoric and less toxic on account of the reduced solubility imparted by the polymeric structure.

The most common way of utilising red phosphorus is through reduction with alkali metals to form metal phosphides, M_3P (M = Li, Na, K). These species are highly reactive and are generally synthesized in liquid ammonia, however recent developments have found that dimethyl formate and an electron transfer reagent, such as naphthalene, are also adequate.[16] Thankfully, the reaction is for all practical purposes quantitative and allows for functionalisation of the metal phosphides *in situ* to yield mono- and di-hydrogenphosphides, M_2PH and MPH_2, which can then be easily functionalised to afford the desired organophosphorus species.[17]

Industrially, there are two main methods for accessing phosphorus. The fertiliser industry utilises phosphoric acid obtained by addition of sulphuric acid to phosphate minerals.[18] This accounts for around 90% of phosphate usage globally. The fine chemical industry favours phosphorus trichloride, PCl_3, as a general precursor to phosphorus-containing species.[19] White phosphorus can be oxidised by direct chlorination to yield PCl_3, which is then functionalised with organolithium reagents, or by reaction with halogenated organic compounds under forcing conditions. As a reagent, PCl_3 is corrosive, highly toxic and sensitive to hydrolysis. Due to these setbacks there has been recent interest in developing new phosphorus precursors for the synthesis of phosphorus containing species. Grützmacher and co-workers have been exploring the use of isolated alkali metal hydrogenphosphides as a tool for generating organophosphorus compounds, such as bis(acyl)phosphides which can

be converted to their respective bis(acyl)phosphane oxides, which find application as photoinitiators in polymer chemistry.[20,21] Cummins and co-workers are attempting to bypass the generation of white phosphorus through the reduction of trimetaphosphate, obtained from the dehydration of phosphoric acid, with trichlorosilane.[22] The product of this reaction, bis(trichlorosilyl)phosphide, has demonstrated its utility as a precursor to a range of organophosphorus species.

1.3 The double bond rule

Multiple bonds involving elements with a principal quantum number greater than two were once thought to be inaccessible due to poor (p–p)π-orbital overlap. The double bond rule only accounts for the thermodynamic factors of bond strength and does not consider the steric and electronic environment of the bond, factors which have since been exploited by chemists over the past decades to synthesize a multitude of heavy-element multiple bonds.

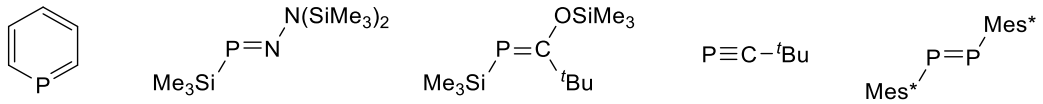

Ashe *Niecke* *Becker* *Becker* *Yoshifuji*

Figure 1.2. Early examples of phosphorus–heteroatom multiple bonds.

Early examples of stabilising explored resonance effects. For example, Ashe and co-workers demonstrated as early as 1971 that incorporating phosphorus into an aromatic ring allowed for isolation of the parent phosphorine, C_5H_5P.[23] The first example of an unsupported phosphorus-heteroelement multiple bond was reported by Niecke in 1973 in an iminophosphane derivative containing a P=N double bond stabilised by sterically demanding trimethylsilyl groups.[24] Three years later Becker reported the isolation of a compound displaying a P=C double bond, and went on to adapt his synthesis to achieve a kinetically stable compound with a P≡C triple bond, stabilised by a lone *tert*-butyl group.[25,26] The first

homoleptic multiply bound phosphorus species was published in 1981 by Yoshifuji and co-workers, in the form of a diphosphene stabilised through sterically demanding supermesitylene (Mes* = 2,4,6-$^{t}Bu_3C_6H_2$) groups.[27] While these compounds were born of academic curiosity, the understanding gained from their synthesis and isolation has led to a broad field of research, ranging from the preparation of materials with unusual electronic properties, to small molecule activation and catalysis.[28]

1.4 Phosphorus as a "carbon copy"

Phosphorus is a versatile element; comparisons to its reactivity are often made to some of its neighbouring elements. For example, there are clear comparisons in three coordinate pnictogens, which all display trigonal pyramidal geometry with a lone pair of electrons. In high valent phosphorus species comparisons in reactivity can be drawn to its period neighbour, silicon, which, for example, displays similar stereochemistry during substitution reactions.[29] The most striking resemblance, however, is to its diagonally related neighbour, carbon. This is particularly pronounced in phosphorus species with a valency of three or less and unsaturated carbon compounds, and has earned phosphorus the title of "the carbon copy", a concept that warrants further discussion.[30]

1.4.1 The isolobal analogy

The principle of isolobality was first introduced by Nobel laureate Roald Hoffmann as a rule of thumb for relating esoteric organic and inorganic molecular fragments to those of better understood compounds, with the aim of gaining insight into bonding behaviour. Hoffmann defined the fragments in question as isolobal "*...if the number, symmetry properties, approximate energy and shape of the frontier orbitals are similar – not identical, but similar.*"[31,32] This simple model was initially used for conceptualising organometallic fragments in relation to much better understood simple organic fragments. However, its

utility is broad and has been extended to the entire periodic table. The simplicity of this model makes no attempt to account for kinetic or thermodynamic stability of a molecule derived from a stable isolobal analogue.

The most relevant analogy for this work is the relationship between a phosphorus atom and a methine fragment, C–H (Figure 1.3). The similarity in the partially occupied sp^3 orbitals of these species indicate the potential to replace methine with phosphorus in an organic molecule.

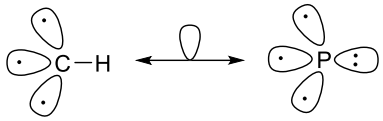

Figure 1.3. The isolobal relationship between a methine fragment a phosphorus atom.

In addition to isolobality, the diagonal relationship between phosphorus and carbon further enhances their similar reactivity. The diagonal relationship is a result of competing, and often inverse, factors of moving across the period and down a group. This results in pairs of elements from the second and third periods exhibiting similar properties.[33] Carbon and phosphorus form one of these pairs, and display some similarity in their electronic and chemical properties. The σ electronegativity of phosphorus is lower than that of carbon (χ_P = 2.19, χ_C = 2.55), however it is a much closer than to its group-neighbour, nitrogen (χ_N = 3.04), while the π electronegativity is approximately the same.[34] The resulting similarity in reactivity has resulted in the birth of phospha-organic chemistry, with some prominent examples discussed in greater detail.

1.4.2 Phosphaalkenes

Some of the earliest and most prevalent examples of unsaturated phospha-organic compounds are phosphaalkenes. The synthesis and reactivity of these compounds have been reviewed numerous times.[30,35] Over the years many synthetic routes have been identified to

form these species, however only the two most general routes will be discussed in this thesis (Scheme 1.1). The first example of a general route to phosphaalkenes was reported by Becker.[25] Becker's synthesis involved the addition of bis(trimethylsilyl)phosphine to an acyl chloride, the resulting acyl phosphine undergoes a 1,3-silyl migration from a phosphine to a proximal oxygen, driven by the oxaphilicity of silicon. This now eponymous migration was adapted to create a series of phosphaalkenes from the reaction of bis(trimethylsilyl)phosphine with CO_2,[36] CS_2,[37] and carbodiimides,[38] all driven by the preference of silicon to form bonds with oxygen, sulphur, or nitrogen, respectively, over phosphorus. The second general route was first reported in 1984 by Bickelhaupt, involving a base-promoted 1,2-elimination of HCl, allowing access to a range of aryl-substituted phosphaalkenes.[39]

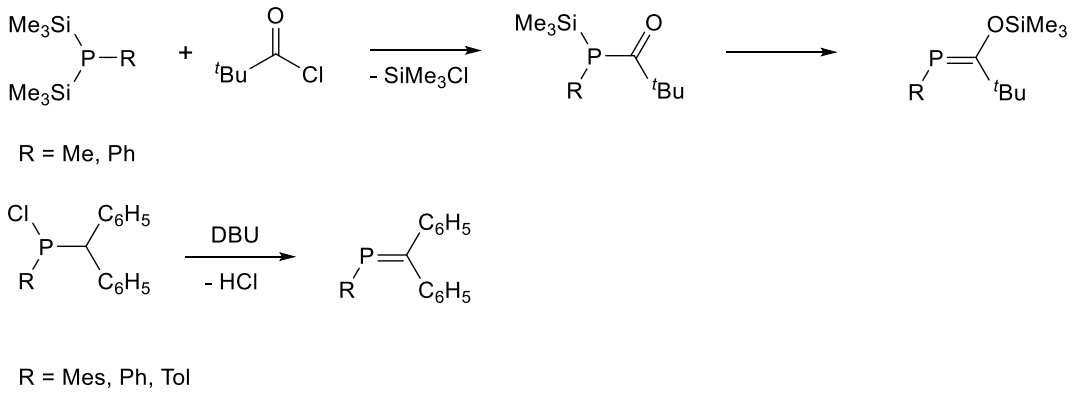

Scheme 1.1. Two general synthetic routes to phosphaalkenes. Top: 1,3-silyl migration pathway. Bottom: Base promoted 1,2-elimination pathway (DBU = 1,8-diazabicyclo[5.4.0]undec-7-ene).

In line with the electronegativity values for the respective elements, the P=C bond is polarised towards the carbon centre. UV photoelectron spectroscopy on the parent compound, $HP=CH_2$, reveals that the HOMO lies predominantly on the π-bond, with the lone pair at phosphorus being slightly lower in energy.[40] The similarity in energy between the HOMO and HOMO–1 can result in ambiguity between the two sites during reactions.[41] However, reactions typically occur at the double bond with the expected regiochemical outcome. For the reasons stated in the double-bond rule, the C=P bond is significantly

weaker than the corresponding C=C bond (bond dissociation energy of 43 kcal/mol *vs.* 65 kcal/mol),[11] resulting in this class of compounds being significantly more reactive than their carbon analogues. Therefore, these species require stabilisation to prevent oligomerisation, either in the form of sterically protecting ligands, electronic stabilisation through resonance, or through coordination to a Lewis-acid centre. There has also been interest in controlling the oligermerisation of phosphaalkenes by choice of appropriate steric groups with the aim to form polymeric materials in reactions analogous to olefin polymerisation.[42]

1.4.3 Phosphaalkynes

The parent phosphaalkyne, HC≡P, was first detected in 1961 by Gier, in quite an unusual synthesis, PH_3 was decomposed inside an electric arc between graphene electrodes and HC≡P was detected using IR spectrsocopy and mass spectrometry.[43] The synthesis was improved 15 years later by Nixon and Kroto, who expanded the number of detectable phosphaalkynes to include FC≡P and MeC≡P *via* a double dehydrohalogenation of RCH_2PCl_2, however both of these species were unstable at ambient temperature.[44] It was another five years before a kinetically stable phosphaalkyne was isolated in the form of Becker's *tert*-butyl phosphaalkyne, ^{t}BuC≡P.[26] Becker's synthesis expanded on the 1,3-silyl migration utilised for the synthesis of phosphaalkenes, however by using a base (such as potassium *tert*-butoxide) as a promoter a second 1,3-silyl migration occurred resulting in complete deoxygenation to yield the first isolable compound containing C≡P triple bond (Scheme 1.2).

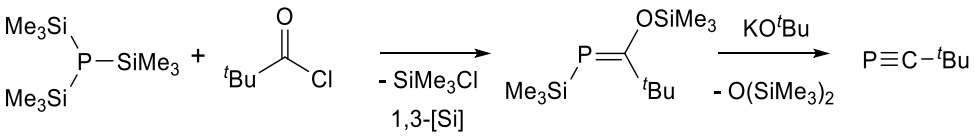

Scheme 1.2. Becker's synthesis of *tert*-butyl phosphaalkyne.

UV photoelectron spectroscopy studies into ^{t}BuC≡P revealed a HOMO residing on the degenerate π-bonds, while the lone pair at the phosphorus centre is significantly lower in energy.[45] This correctly predicts that the chemistry of phosphaalkynes is likely to be dominated by the nucleophilicity of the π-manifold.[46,47] Later work by Becker, Nixon and Regitz expanded the range of substituents capable of stabilising phosphaalkynes, in addition to exploring their utility for the synthesis of phosphorus-containing molecules.[46–48] It was found that phosphaalkynes display a rich [2+3] cycloaddition chemistry towards reagents with a 1,3-dipole such as azides or nitrile oxides.[49]

1.4.4 Phosphaketenes

The final class of organophosphorus compounds that will be discussed in this section are phosphaketenes, the heavier phosphorus analogues of isocyanates. Prior to the discovery of stable salts of the 2-phosphaethynolate anion, which will be discussed in section 1.5, the chemistry of phosphaketenes had been less developed than the previously mentioned phosphaalkenes and phosphaalkynes. A literature search for such compounds synthesised prior to 2012 unearths two hydrocarbon substituted examples. The first of these to be characterised was the *tert*-butyl phosphaketene, ^{t}BuP=C=O, which is stable below –60 ˚C but rapidly dimerises upon warming to give a 1,3-diphosphetane-2,4-dione.[50] Increasing the steric bulk of the phosphaketene substituent, from *tert*-butyl to supermesityl, increased the stability substantially, allowing the monomer to be isolated at room temperature.[51] The synthesis of both phosphaketenes involved the addition of bis(trimethylsilyl)phosphine with phosgene, resulting in loss of two equivalents of trimethylsilyl chloride to give the phosphaketenyl species.

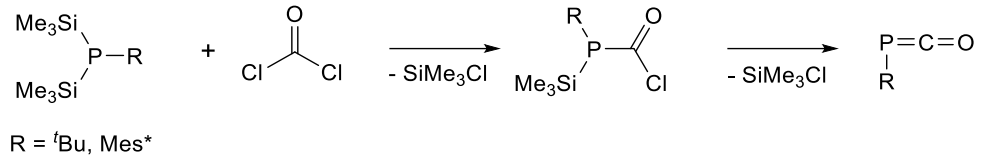

Scheme 1.3. Synthesis of alkylphosphaketenes.

The further reactivity of phosphaketenes has historically been limited to the thermally stable supermesityl derivative. UV photolysis induces decarbonylation to yield a transient triplet phosphinidene, the phosphorus analogue of a triplet carbene, which reacts with a nearby methyl group on the supermesityl to yield a phosphaindane. Decarbonylation can also be induced catalytically using palladium(0) to yield the diphosphene.[52]

1.5 The 2-phosphaethynolate ion

The first rational synthesis of the 2-phosphaethynolate anion was reported in 1992 in the form of its lithium salt, $Li(DME)_2(PCO)$ (DME = 1,2-dimethoxyethane), obtained through reaction of lithium bis(trimethylsilyl)phosphide and dimethyl carbonate (Scheme 1.4).[53] Though the authors managed to characterise the anion, issues associated with scaling up the synthesis and the poor stability of the lithium salt resulted in limited investigations into species over the following two decades.

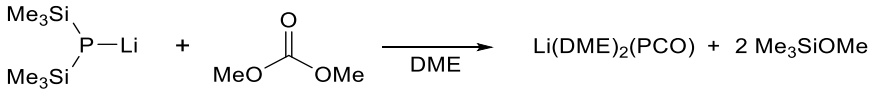

Scheme 1.4. The original synthesis of PCO^-.

One attempt to advance the field was made by Westerhausen, who modified Becker's original synthesis to obtain alkaline earth metal phosphaethynolate salts, however these salts were similarly unstable.[54] In 2011 two independent reports from the groups of Grützmacher and Cummins reported the synthesis of the sodium salt and noted a much improved stability, with the authors of the former study noting the sodium phosphaethynolate salt *"...is*

remarkably stable and can be handled in air without decomposition".[55,56] Though these original syntheses of the sodium salts were quite impractical, the Grützmacher group published a simple, scalable synthesis starting from inexpensive materials in 2014.[57] This synthesis involves the *in situ* generation of sodium phosphide, from red phosphorus, sodium metal, and *tert*-butanol, which is then reacted with ethylenecarbonate carbonate in DME to liberate alcohol and the desired sodium salt.

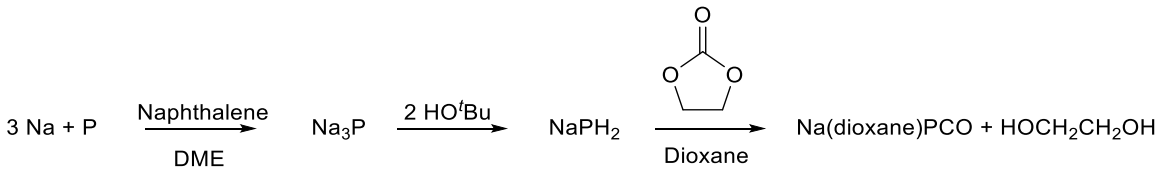

Scheme 1.5. Scalable synthesis of the more stable sodium salt of PCO^-.

The Goicoechea group entered the field in 2013 with the synthesis of K(18-crown-6)(PCO) by direct carbonylation of DMF (DMF = *N*,*N*-dimethylformamide) solutions of K_3P_7.[58] This is quite an unusual reaction, as the P_7^{3-} ion can be thought of as three monoanionic phosphides inserted into three faces of a P_4, this synthesis represents abstraction of those P^- fragments by gaseous CO. This potassium salt displays comparable stability to the sodium salts.

Following the discovery of these stable salts, the 2-phosphaethynolate anion is fast becoming a diverse reagent for the delivery of low valent phosphorus to metals, main group species and for the preparation of phosphorus containing heterocycles. While we will explore some of the more pertinent chemistry of the compound here, a more comprehensive review of the properties and reactivity of the 2-phosphaethynolate anion can be found in recent reviews.[59–61]

1.5.1 Electronic and structural properties

The stability of the 2-phosphaethynolate ion, which lacks the steric protection of previously reported isolable phosphaalkynes and phosphaalkenes, is due to resonance stabilisation and Coulombic repulsion. There are two principal tautomeric forms for the ion (Figure 1.4.), the largest contributor being the phosphaethynolato form, with a formal triple bond between the carbon and phosphorus centre, a single bond between the oxygen and carbon and the negative charge residing on the oxygen. The second most significant resonance structure is the phosphaketenyl form, with double bonds between the phosphorus and carbon, and carbon and oxygen and the negative charge localised at the phosphorus centre. There is also a small contribution from a third resonance form, which is in essence Lewis adduct between carbon monoxide and monoanionic phosphide. Though a small contributor to the hybrid resonance structure, this last form is important in rationalising the relative weakness of the P–CO bond which is a notable trait of this anion.

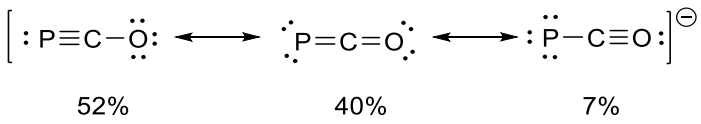

Figure 1.4. The resonance forms of the 2-phosphaethynolate ion and their percentage contributions, from NRT analysis.

The known ionic salts of the 2-phosphaethynolate ion display similar structural features. The P-C-O bond angles are all approximately linear, ranging between 178.3(3)° and 179.9(2)°. The C–P bond length varies, however fall within the range of a double (1.69 Å) and triple (1.54 Å) bond, with values ranging between 1.555(3) and 1.634(3) Å.[62] The C–O bond is less varied, falling between 1.198(4) and 1.213(1) Å, around the range of a double bond (1.24 Å).

1.5.2 Coordination chemistry

These resonance structures, in combination with the Lewis basicity bestowed by the negative charge, impart ambiphilicity to the 2-phosphaethynolate anion; which is able to coordinate as either a phosphaethynolate or a phosphaketenyl (Figure 1.5). In general terms, soft, polarisable elements coordinate to the phosphorus centre, while hard, electron dense elements favour the oxygen coordination mode. The first example of a phosphaketenyl bound PCO^- was the rhenium complex [Re(triphos)$(CO)_2$(PCO)], reported in 2013.[63] The bonding mode of the PCO^- is approximately 90°, a result of increased π-orbital contribution to the bond. This bond angle is apparent in all examples of structurally authenticated phosphaketenes reported to date. The authors also note that PCO^- is a reducing agent, a limiting factor when selecting suitable metal complex candidates.

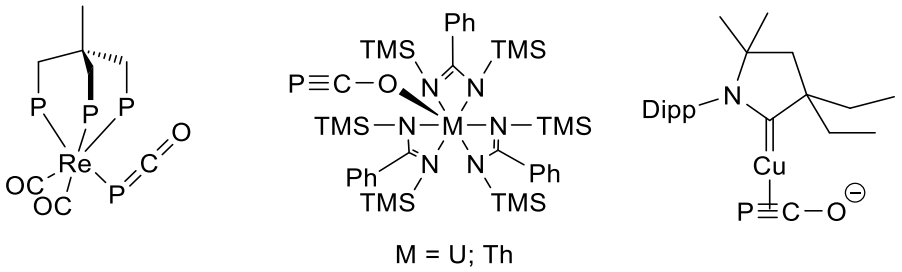

Figure 1.5. The first examples of phosphaketenyl and phosphaethynolato coordination complexes, and the first example of an η^2 PCO^- complex.

The first reported example of an oxygen bound phosphaethynolate came shortly later, in 2015, in the form of $(amid)_3M(OCP)$ (M = U, Th; L = *N*,*N*'-bis-(trimethylsilyl)benzamidinate), confirming the need for a hard Lewis acidic metal centre to achieve this bonding mode.[64] Interestingly, later reports of early d-block complexes of vanadium and titanium, which are also considered 'hard' electrophiles, also display the phosphaketenyl bonding mode.[65,66] This surprising observation is likely due to the thermodynamic advantage of forming a very strong C–O π–bond at the expense of a significantly weaker C–P π-bond. This results in the majority of structurally authenticated

examples of coordination complexes of PCO^- displaying the phosphaketenyl bonding mode, with the phosphaethynolato mode typically reserved for complexes of the s-, and f-block elements, in addition to one example of a scandium(III) phosphaethynolato species.[67]

The ion is also able to coordinate through the π-manifold in a manner that is more common of phosphaalkynes, the first reported example of such being in the cyclic alkyl amino carbene stabilised copper complex in which the PCO^- is bound in an η^2–coordination mode (Figure 1.5).[68]

1.5.3 Cycloaddition chemistry

As with phosphaalkynes, the 2-phosphaethynolate anion has developed a rich cyclisation chemistry; allowing access to three-, four-, five- and six-membered heterocycles. Becker proposed a transient four-membered heterocycle as an intermediate in the conversion of PCO^- to its heavier analogue, PCS^-. In this reaction, the lithium salt of PCO^- was reacted with carbon disulphide (Scheme 1.6).[69] The P≡C and C=S π-bonds cyclise to form the heterocycle, then undergo a cycloreversion to yield PCS^- and SCO.

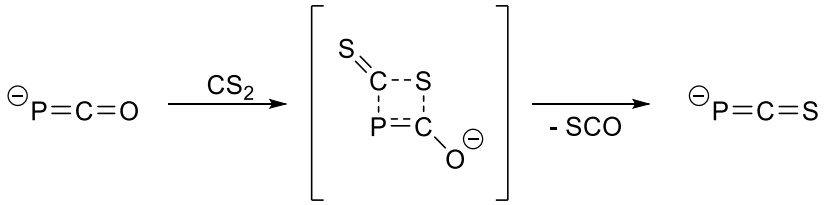

Scheme 1.6. Conversion of PCO^- to PCS^- *via* a transient heterocycle.

Similar reactivity allows for isolation of stable 4-membered heterocycles by variation of the heteroallene selected, for example CO_2 reacts with two equivalents of PCO^- to yield a dianionic 4-membered heterocycle with a carboxylate group attached to one of the phosphorus centres.[57] This species displays broad resonances in the ^{31}P NMR spectrum, indicating fluctional behaviour between the heterocycle and CO_2.

1.5.4 Brønsted-Lowry Acid Base chemistry

Unlike other phosphaallenes, theoretical calculations predicted protonation of the PCO^- anion to occur exclusively at the phosphorus centre, yielding HPCO, the analogue of isocyanic acid, HNCO.[70] HPCO was recently spectroscopically characterised by heating Na(dioxane)[PCO] with solid stearic acid under vacuum, and condensing the volatiles into an NMR tube containing deuterated solvent allowing for solution-phase characterisation of the acid in addition to a number of its oligermerisation products.[71] This species is a postulated intermediate in a number of transformations involving the ion. The most notable of which being the addition of PCO^- to ammonium salts, which results in phosphinecarboxamide, a product of an initial deprotonation of ammonium, followed by a cyclisation to yield the phosphinecarboxamide (Scheme 1.7).[72–74] This is a rare example of PCO^- displaying similar reactivity to its lighter congener, NCO^-. In Wöhler's landmark synthesis of urea, he reported the decomposition of ammonium cyanate to ammonia and cyanic acid, which in turn react to form urea.[75]

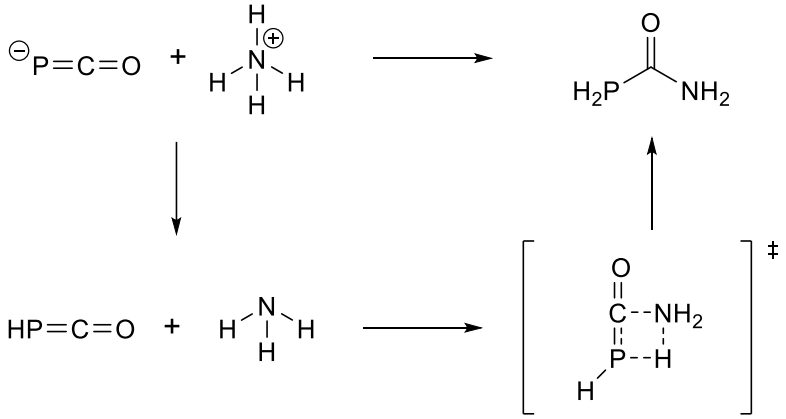

Scheme 1.7. Formation of phosphinecarboxamide *via* a Wöhler-type synthesis.

Wöhler went on study the thermal decomposition of urea, which upon heating releases ammonia and forms isocyanic acid, HNCO.[76] The tautomer of isocyanic acid, cyanic acid (HOCN), is highly unstable and rapidly decomposes. However, solutions of isocyanic contain around 3% of this tautomer, which cyclotrimerises to yield cyanuric acid $(OCPH)_3$.

The phosphorus analogue of this species was spectroscopically characterised from a cyclotrimerisation reaction of NaPCO with (–)-B-chlorodiisopinocampheylborane ($(ipc)_2BCl$), followed by addition of *tert*-butanol to yield the desired product.[77]

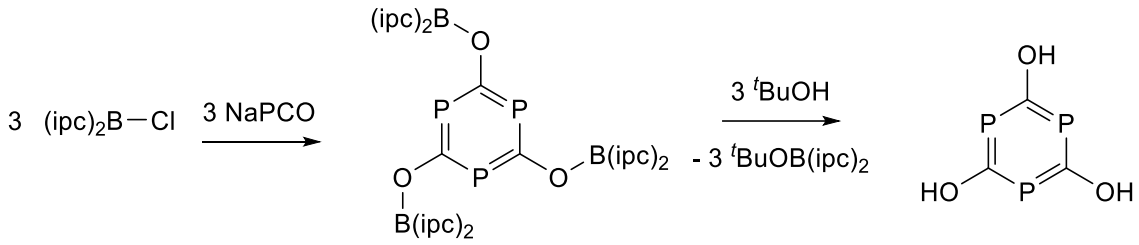

Scheme 1.8. Synthesis of the phosphorus analogue of cyanuric acid.

1.5.5 Monoanionic phosphide (P^-) donor

Another defining reactivity mode of 2-phosphaethynolate is its utility as a source of monoanionic phosphide, P^-, through decarbonylation reactions. This reactivity can be rationalised through the smallest contributing resonance form of PCO^-, which is essentially a carbon monoxide adduct of P^-. In the same way that the isoelectonic azide ion, N_3^-, can be utilised as a source of N^-, PCO^- can be utilised as a source of P^-. This reactivity mode was first reported upon reaction of PCO^- with imidazolium salts, which results in the carbene adducts of the parent phosphandiyl, PH (Scheme 1.9). This reaction is proposed to proceed *via* an initial deprotonation of the imidazolium to give the transient HPCO, which is decarbonylated by the generated carbene.[78]

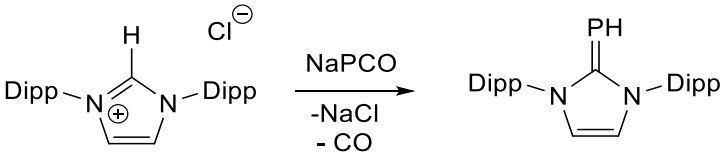

Scheme 1.9. Synthesis of a carbene stabilised phosphandiyl.

The groups of Bertrand and Grützmacher independently synthesized a series of phosphanyl phosphaketenes, with unsaturated and saturated imine backbones, respectively.[79,80] It was found those with saturated backbones decarbonylated upon

irradiation with a medium pressure mercury lamp. When the ligand substituents were relatively small, for example diisopropylphenyl groups, the sole product of the reaction was the diphosphene, suggesting a decarbonylation reaction followed by dimerization. The authors hypothesized that the intermediate in this reaction was a transient phosphinidene, which they were able to spectroscopically characterise by dramatically increasing the steric bulk on the ligand backbone to 2,6-bis[(4-*tert*-butylphenyl)methyl]-4-methylphenyl) groups (Scheme 1.10).

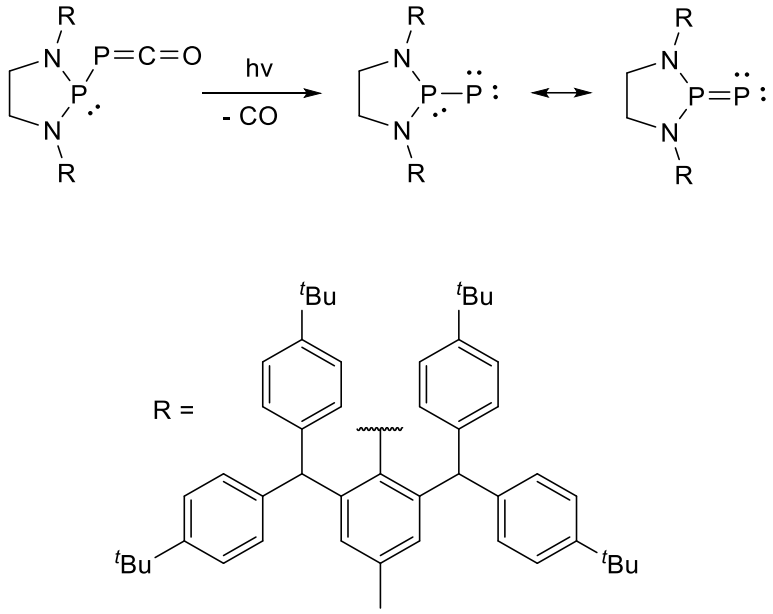

Scheme 1.10. Synthesis of a singlet phosphinidene.

In addition to light-driven decarbonylation reactions, addition of Lewis bases, such as phosphines or isocyanides, to phosphanyl phosphaketenes results in a ligand displacement reaction at the phosphinidene centre and release of carbon monoxide to generate a new class of compounds known as base-stabilised phosphinidenes.[81,82] The authors noted that it was possible to add a series of bases, in order of increasing donor strength (CO < PR_3 < CNR < NHC < CAAC), to perform sequential ligand displacement reactions. The bonding in the base-stabilised phosphinidenes can be rationalised in a similar fashion to phosphaketenes, with two major resonance forms; either as a Lewis adduct or as bonds made of shared

electrons, formally resulting in a double bond between the base and phosphinidene (Figure 1.6). In the case of the trimethylphosphine stabilised phosphinidene the authors report a RP–PMe_3 bond length of 2.197(1) with a ^{31}P NMR $^{1}J_{P-P}$ coupling of 496 Hz, indicating a strong interaction between the two atoms.

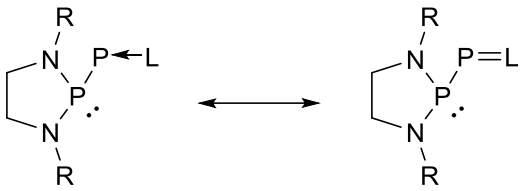

Figure 1.6. Resonance forms of base stabilised phosphinidenes. L = Lewis base.

1.5.6 Isomerisation chemistry

Owing to its ambiphilic nature PCO^- is theoretically cable of forming linkage isomers; coordination compounds in which the overall molecular formula is the same, differing only in the connectivity of the ligand to the metal. The first example of linkage isomers was reported in 1856, in the form of the xantho and isoxantho complexes of colbalt(III).[83] However, the phenomena itself was not defined until 1907 when Nobel Laureate Alfred Werner included 'salt isomerism' in his seven-fold complex classification system.[84] The first rational synthesis of linkage isomers was reported by Basolo and co-workers in the 1960s who prepared a series of $[M(NH_3)_5(NO_2\text{-}\kappa\text{-}O)]^{n+}$ (M = Co(III), Cr(III), Rh(III), Ir(III), and Pt(IV)) complexes which, with the exception of the chromium complex, isomerise in solution and in the solid state to yield the NO_2-κ-N isomers (Scheme 1.11).[85,86]

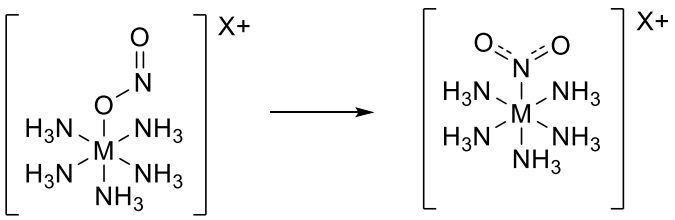

Scheme 1.11. Linkage isomerism in a transition metal complex (M = Rh(III), Ir(III), and Pt(IV)).

The difficulty of rationally preparing these systems has resulted in little further development in this field. Reports on the number of linkage isomers range between 10 and 29 pairs (in rather old reviews), depending on structural authentication or simply spectroscopically detection.[87,88] There are three requirements to the observation of linkage isomers: the first being the requirement that the ligand be capable of multiple coordination modes, of which there are numerous candidates (NO_2^-, SCN^-, CN^-, NCO^-, among others); there must also be a small energy difference between the two isomers; and finally an isomerisation barrier high enough to prevent rapid conversion to the thermodynamically more stable product.

The first spectroscopic evidence of linkage isomerism of PCO^- was the detection of both the phosphaketenyl and phosphaethynolato species upon addition of PCO^- to a solution containing triphenylsilyl triflate at low temperatures (Scheme 1.12).[89] The authors observe ^{31}P NMR signals consistent with the existence of both isomers, however upon warming the solution rapid, uncontrolled oligermerisation occurs preventing isolation of either species. This report will be discussed in detail in Chapter 2.

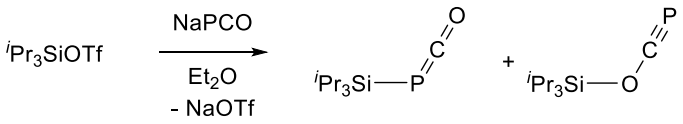

Scheme 1.12. The first spectroscopically detected linkage isomers of PCO^-.

Constitutional isomerism, in which the molecules or ions have the same molecular formula but differ in terms of connectivity or branching, has a profound effect on the reactivity of molecules. For example, while the cyanate ion, NCO^- is a stable species, a simple reorganisation of the bonding situation to the constitutionally identical fulminate ion, CNO^-, produces drastically different reactivity. Salts of the fulminate ion are highly explosive, friction sensitive materials. Nitrile oxides, RC≡N–O, upon heating rearrange to their constitutionally isomeric isocyanides, RN=C=O, a rearrangement first reported by

Heinrich Wieland.[90] Investigation into the mechanism of this rearrangement by Taylor concluded that it proceeds *via* formation of polymeric nitrile oxide with an initial nucleophilic attack between the oxygen and carbon centre of a second molecule (Scheme 1.13).[91] This facilitates transfer of the alkyl group to the nitrogen, with concerted cleavage of the N–O bond to yield the isocyanide.

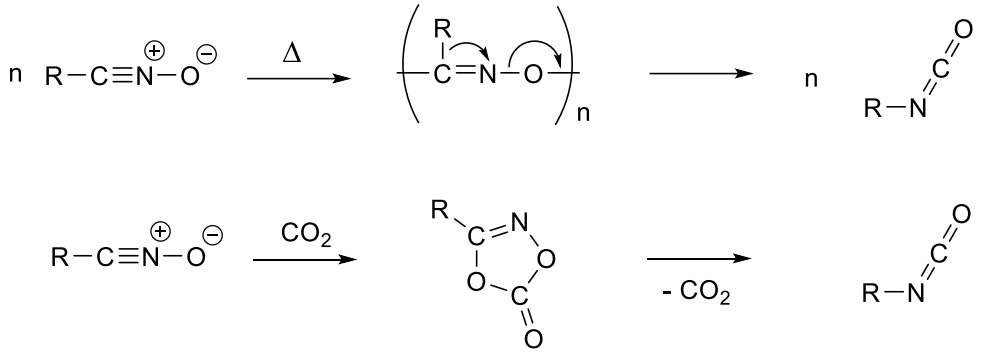

Scheme 1.13. Thermal and catalytic isomerisation of nitrile oxides to isocyanides.

In a separate study by Trickes and Meier, the same rearrangement could be catalysed by the addition of sulphur dioxide.[92] The role of the catalyst is to act as a dipolarophile, forming a 5-membered heterocycle with the nitrile oxide which then releases the isocyanide *via* an R-group migration/decyclization. The analogous reactivity is not known for the heavier congeners, CPO^- and PCO^-, as no report of RCPO type species exist. However, a report from the group of Grützmacher group found that addition of N-heterocyclic carbenes to phosphanyl phosphaketenes results in the opposite rearrangement, where the PCO core of the phosphaketene rearranges to its constitutional isomer, OPC (Scheme 1.14).[93] It should be noted that this reactivity is sensitive to the electronic configuration of the diimine backbone of the phosphanyl, with saturated backbones instead resulting in oxygen transfer from the core chain to the phosphanyl phosphorus.

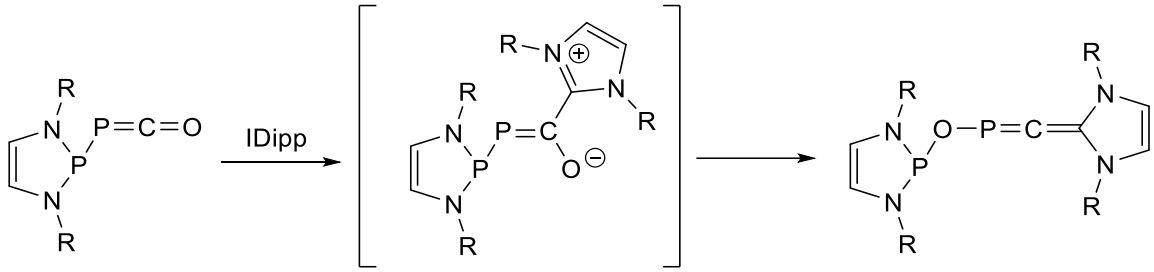

Scheme 1.14. An example of carbene-induced isomerisation of a phosphaketene. R = Dipp.

Further expansion on the deoxygenation chemistry of phosphanyl phosphaketenes allowed for isolation of phosphanyl cyanophosphide salts. In a synthesis reminiscent of earlier organometallic work which explored the conversion of metal carbonyls to metal isocyanides ([LM(CO)] to [LM(CN)$^{-}$]),[94] the authors exploited the oxaphilicity of trimethylsilane in order to selectively replace the oxide, O^{2-}, with the isoelectronic nitride, N^{3-}, through addition of alkali metal bis(trimethylsilyl)amide salts to give the phosphanyl cyanophosphide salt and liberate siloxane (Scheme 1.15).[95]

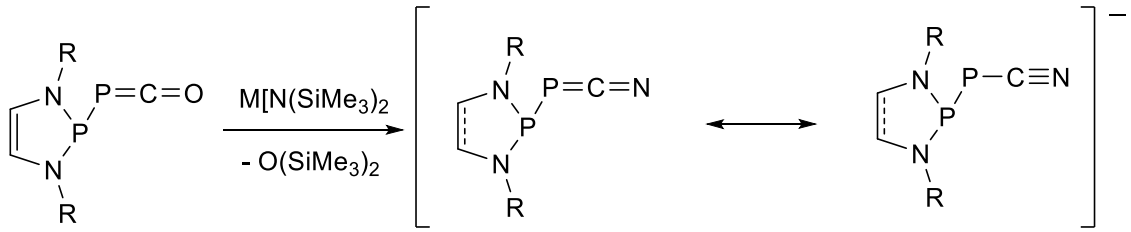

Scheme 1.15. Synthesis of phosphanyl cyanophosphide salts from phosphaketenes. M = Na, K, R = Dipp, Mes.

1.6 Project aims

At the time of starting this project, the understanding of the reactivity of the 2-phosphaethynolate anion was still in its infancy. In terms of coordination chemistry, there were select cases of group 14 and 15, as well as transition metal and actinide, complexes of the salt reported in the literature. We aimed to explore the coordination chemistry of the 2-phosphaethynolate anion towards group 13 halides, utilising salt metathesis strategies to

obtain coordination complexes of PCO^-. We hypothesized that by employing the hard Lewis acidic boron it may be possible to obtain a covalently bound phosphaethynolate species. The synthesis of the phosphaethynolatoborane ([B]OCP), which can also be described as a boryloxyphosphaalkyne, is outlined in Chapter 2, in addition to a computational analysis of its electronic properties. The following chapters are dedicated to exploring the reactivity of this unusual molecule; Chapter 3 explores the role of the phosphaethynolatoborane as an electrophile and the varying reactivity induced by different nucleophiles. Chapter 4 assesses the nucleophilicity of [B]OCP, in a role typical of phosphaalkynes.

We propose that by targeting a phosphaethynolate with a very strong oxygen Lewis acid bond we would be able to reductively cleave the O–C bond to yield the cyaphide anion, $C{\equiv}P^-$, the smallest possible organophosphorus building block. Our attempts towards this molecule are outlined in Chapter 5. The final chapter will explore gallium complexes of PCO^-, which form the phosphaketenyl isomer. The reactivity of these compounds was somewhat more limited, however ligand substitution reactions could be observed at the phosphinidene site upon addition of Lewis bases and the chemistry achieved from such reactions will be discussed.

1.7 References

[1] M. Karki, C. Gibard, S. Bhowmik, R. Krishnamurthy, *Life.* **2017**, *7*, 1–28.

[2] G. M. Filippelli, *Elements* **2008**, *4*, 89–95.

[3] I. Asimov, *Asimov on Chemistry.*, Anchor Books, **1974**.

[4] R. J. Huxtable, *Nature.* **2000**, *405*, 15–16.

[5] K. Ashley, D. Cordell, D. Mavinic, *Chemosphere* **2011**, *84*, 737–746.

[6] M. Heckenmüller, D. Narita, G. Klepper, *Kiel Work. Pap.* **2014**, 26.

[7] M. Selman, S. Greenhalgh, *Renew. Resour. J.* **2010**, *26*, 19–26.

[8] J. R. Vallentyne:, *Int. Rev. der gesamten Hydrobiol. und Hydrogr.* **1977**, *62*, 181–181.

[9] H. Bock, H. Muller, *Inorg. Chem.* **1984**, *23*, 4365–4368.

[10] N. A. Piro, J. S. Figueroa, J. T. McKellar, C. C. Cummins, *Science.* **2006**, *313*, 1276–1279.

[11] R. A. Howald, *Chemical Bonds and Bond Energy*, Academic Press, **1971**.

[12] G. Villalba, Y. Liu, H. Schroder, R. U. Ayres, *J. Ind. Ecol.* **2008**, *12*, 557–569.

[13] *Toxicity of Military Smokes and Obscurants*, National Academies Press, Washington, D.C., **1999**.

[14] P. W. Bridgman, *J. Am. Chem. Soc.* **1914**, *36*, 1344–1363.

[15] L. Li, Y. Yu, G. J. Ye, Q. Ge, X. Ou, H. Wu, D. Feng, X. H. Chen, Y. Zhang, *Nat. Nanotechnol.* **2014**, *9*, 372–377.

[16] D. J. Peterson, S. Township, *Preparation of Alkali Metal Phosphides*, **1968**.

[17] K. D. Troev, *Reactivity of P-H Group of Phosphorus Based Compounds*, Elsevier, **2018**.

[18] N. N. Greenwood, A. Earnshaw, *Chemistry of the Elements*, **1998**.

[19] R. Engel, J. I. Cohen, *Synthesis of Carbon-Phosphorus Bonds*, CRS Press, **2004**.

[20] A. Huber, A. Kuschel, T. Ott, G. Santiso-Quinones, D. Stein, J. Bräuer, R. Kissner, F. Krumeich, H. Schönberg, J. Levalois-Grützmacher, et al., *Angew. Chem. Int. Ed.* **2012**, *51*, 4648–4652.

[21] J. Wang, G. Siqueira, G. Müller, D. Rentsch, A. Huch, P. Tingaut, J. Levalois-Grützmacher, H. Grützmacher, *Chem. Commun.* **2016**, *52*, 2823–2826.

[22] M. B. Geeson, C. C. Cummins, *Science.* **2018**, *359*, 1383–1385.

[23] A. J. Ashe, *J. Am. Chem. Soc.* **1971**, *93*, 3293–3295.

[24] E. Niecke, W. Flick, *Angew. Chem. Int. Ed.* **1973**, *12*, 585–586.

[25] G. Recker, *ZAAC - J. Inorg. Gen. Chem.* **1976**, *423*, 242–254.

[26] G. Becker, G. Gresser, W. Uhl, *Zeitschrift fur Naturforsch. - Sect. B J. Chem. Sci.* **1981**, *36*, 16–19.

[27] M. Yoshifuji, I. Shima, N. Inamoto, K. Hirotsu, T. Higuchi, *J. Am. Chem. Soc.* **1981**, *103*, 4587–4589.

[28] P. P. Power, *Nature.* **2010**, *463*, 171–177.

[29] R. R. Holmes, *Chem. Rev.* **1996**, *96*, 927–950.

[30] M. Regitz, *Book Review, Phosphorus: The Carbon Copy, from Organophosphorus to Phosphaorganic Chemistry*, Wiley, **1999**.

[31] R. Hoffmann, *Angew. Chem. Int. Ed.* **1982**, *21*, 711–724.

[32] M. Elian, M. M. L. Chen, D. Michael, P. Mingos, R. Hoffmann, *Inorg. Chem.* **1976**, *15*, 1148–1155.

[33] D. A. Phillips, *Essential Trends in Inorganic Chemistry (Mingos, D. M. P.)*, Oxford

University Press, **2000**.

[34] *Quantities, Units and Symbols in Physical Chemistry*, Royal Society Of Chemistry, **2007**.

[35] A. C. Gaumont, J. M. Denis, *Chem. Rev.* **1994**, *94*, 1413–1439.

[36] R. Appel, B. Laubach, M. Siray, *Tetrahedron Lett.* **1984**, *25*, 4447–4448.

[37] R. Appel, P. Fölling, L. Krieger, M. Siray, F. Knoch, *Angew. Chem. Int. Ed.* **1984**, *23*, 970–971.

[38] K. Issleib, H. schmidt, H. Meyer, *J. Organomet. Chem.* **1980**, *192*, 33–39.

[39] T. C. Klebach, R. Lourens, F. Bickelhaupt, *J. Am. Chem. Soc.* **1978**, *100*, 4886–4888.

[40] S. Lacombe, D. Gonbeau, J. L. Cabioch, B. Pellerin, J. M. Denis, G. Pfister-Guillouzo, *J. Am. Chem. Soc.* **1988**, *110*, 6964–6967.

[41] T. A. van der Knaap, T. C. Klebach, R. Lourens, M. Vos, F. Bickelhaupt, *J. Am. Chem. Soc.* **1983**, *105*, 4026–4032.

[42] T. Baumgartner, R. Réau, *Chem. Rev.* **2006**, *106*, 4681–4727.

[43] T. E. Gier, *J. Am. Chem. Soc.* **1961**, *83*, 1769–1770.

[44] H. W. Kroto, J. F. Nixon, N. P. C. Simmons, *J. Mol. Spectrosc.* **1980**, *82*, 185–192.

[45] J. C. T. R. James, M. A. King, H. W. Kroto, J. F. Nixon, R. J. Suffolk, *J. Chem. Soc. Dalt. Trans.* **1983**, 755–759.

[46] M. Regitz, *Chem. Rev.* **1990**, *90*, 191–213.

[47] J. F. Nixon, *Endeavour* **1991**, *15*, 49–57.

[48] W. Rösch, U. Hees, M. Regitz, *Chem. Ber.* **1987**, *120*, 1645–1652.

[49] W. Rösch, M. Regitz, *Angew. Chem. Int. Ed.* **1984**, *23*, 900–901.

[50] R. Appel, W. Paulen, *Tetrahedron Lett.* **1983**, *24*, 2639–2642.

[51] R. Appel, W. Paulen, *Angew. Chem. Int. Ed.* **1983**, *22*, 785–786.

[52] M. A. David, D. K. Wicht, D. S. Glueck, G. P. A. Yap, L. M. Liable-Sands, A. L. Rheingold, *Organometallics* **1997**, *16*, 4768–4770.

[53] G. Becker, M. Schmidt, W. Schwarz, M. Westerhausen, *ZAAC - J. Inorg. Gen. Chem.* **1992**, *608*, 33–42.

[54] M. Westerhausen, S. Schneiderbauer, H. Piotrowski, M. Suter, H. Nöth, *J. Organomet. Chem.* **2002**, *643–644*, 189–193.

[55] I. Krummenacher, C. C. Cummins, *Polyhedron* **2012**, *32*, 10–13.

[56] F. F. Puschmann, D. Stein, D. Heift, C. Hendriksen, Z. A. Gal, H. F. Grützmacher, H. Grützmacher, *Angew. Chem. Int. Ed.* **2011**, *50*, 8420–8423.

[57] D. Heift, Z. Benko, H. Grützmacher, *Dalton Trans.* **2014**, *43*, 831–840.

[58] A. R. Jupp, J. M. Goicoechea, *Angew. Chem. Int. Ed.* **2013**, *52*, 10064–10067.

[59] J. M. Goicoechea, H. Grützmacher, *Angew. Chem. Int. Ed.* **2018**, *57*, 16968–16994.

[60] L. Weber, *Eur. J. Inorg. Chem.* **2018**, *2018*, 2175–2227.

[61] L. N. Grant, D. J. Mindiola, *Chem. Eur. J.* **2019**, *25*, 16171–16178.

[62] B. Cordero, V. Gómez, A. E. Platero-Prats, M. Revés, J. Echeverría, E. Cremades, F. Barragán, S. Alvarez, *J. Chem. Soc. Dalt. Trans.* **2008**, 2832–2838.

[63] S. Alidori, D. Heift, G. Santiso-Quinones, Z. Benkå, H. Grützmacher, M. Caporali, L. Gonsalvi, A. Rossin, M. Peruzzini, *Chem. Eur. J.* **2012**, *18*, 14805–14811.

[64] C. Camp, N. Settineri, J. Lefèvre, A. R. Jupp, J. M. Goicoechea, L. Maron, J. Arnold, *Chem. Sci.* **2015**, *6*, 6379–6384.

[65] L. N. Grant, J. Krzystek, B. Pinter, J. Telser, H. Grützmacher, D. J. Mindiola, *Chem.*

Commun. **2019**, *55*, 5966–5969.

[66] L. N. Grant, B. Pinter, B. C. Manor, R. Suter, H. Grützmacher, D. J. Mindiola, *Chem. Eur. J.* **2017**, *23*, 6272–6276.

[67] L. N. Grant, B. Pinter, B. C. Manor, H. Grützmacher, D. J. Mindiola, *Angew. Chem. Int. Ed.* **2018**, *57*, 1049–1052.

[68] L. Liu, D. A. Ruiz, F. Dahcheh, G. Bertrand, R. Suter, A. M. Tondreau, H. Grützmacher, *Chem. Sci.* **2016**, *7*, 2335–2341.

[69] O. Mundt, G. Becker, W. Uhl, W. Massa, M. Birkhahn, *ZAAC - J. Inorg. Gen. Chem.* **1986**, *540*, 319–335.

[70] M. T. Nguyen, A. F. Hegarty, M. A. McGinn, P. Ruelle, *J. Chem. Soc. Perkin Trans. 2* **1985**, 1991–1997.

[71] A. Hinz, R. Labbow, C. Rennick, A. Schulz, J. M. Goicoechea, *Angew. Chem. Int. Ed.* **2017**, *56*, 3911–3915.

[72] A. R. Jupp, J. M. Goicoechea, *J. Am. Chem. Soc.* **2013**, *135*, 19131–19134.

[73] A. R. Jupp, G. Trott, É. Payen De La Garanderie, J. D. G. Holl, D. Carmichael, J. M. Goicoechea, *Chem. Eur. J.* **2015**, *21*, 8015–8018.

[74] E. N. Faria, A. R. Jupp, J. M. Goicoechea, *Chem. Commun.* **2017**, *53*, 7092–7095.

[75] F. Wöhler, *Ann. Phys.* **1828**, *88*, 253–256.

[76] F. Wöhler, *Ann. Phys.* **1829**, *91*, 619–630.

[77] R. Suter, Y. Mei, M. Baker, Z. Benkő, Z. Li, H. Grützmacher, *Angew. Chem. Int. Ed.* **2017**, *56*, 1356–1360.

[78] A. M. Tondreau, Z. Benko, J. R. Harmer, H. Grützmacher, *Chem. Sci.* **2014**, *5*, 1545–1554.

[79] L. Liu, D. A. Ruiz, D. Munz, G. Bertrand, *Chem.* **2016**, *1*, 147–153.

[80] M. M. Hansmann, D. A. Ruiz, L. Liu, R. Jazzar, G. Bertrand, *Chem. Sci.* **2017**, *8*, 3720–3725.

[81] M. M. Hansmann, G. Bertrand, *J. Am. Chem. Soc.* **2016**, *138*, 15885–15888.

[82] M. M. Hansmann, R. Jazzar, G. Bertrand, *J. Am. Chem. Soc.* **2016**, *138*, 8356–8359.

[83] W. Gibbs, *Researches on the Ammonia-Cobalt Bases*, Smithsonian Institution, Washington D.C., **1856**.

[84] A. Werner, *Berichte der Dtsch. Chem. Gesellschaft* **1907**, *40*, 765–788.

[85] F. Basolo, G. S. Hammaker, *J. Am. Chem. Soc.* **1960**, *82*, 1001–1002.

[86] F. Basolo, G. S. Hammaker, *Inorg. Chem.* **1962**, *1*, 1–5.

[87] R. T. M. FRASER, *Linkage Isomerism*, **1967**.

[88] J. L. Burmeister, *Coord. Chem. Rev.* **1968**, *3*, 225–245.

[89] D. Heift, Z. Benko, H. Grützmacher, *Dalton Trans.* **2014**, *43*, 5920–5928.

[90] H. Wieland, *Berichte der Dtsch. Chem. Gesellschaft* **1909**, *42*, 4199–4206.

[91] G. A. Taylor, *J. Chem. Soc. Perkin Trans. 1* **1985**, 1181–1184.

[92] G. Trickes, H. Meier, *Angew. Chem. Int. Ed.* **1977**, *16*, 555–555.

[93] Z. Li, X. Chen, Z. Benkö, L. Liu, D. A. Ruiz, J. L. Peltier, G. Bertrand, C. Y. Su, H. Grützmacher, *Angew. Chem. Int. Ed.* **2016**, *55*, 6018–6022.

[94] R. B. King, *Inorg. Chem.* **1967**, *6*, 25–29.

[95] Z. Li, J. E. Borger, F. Müller, J. R. Harmer, C. Y. Su, H. Grützmacher, *Angew. Chem. Int. Ed.* **2019**, *58*, 11429–11433.

Chapter 2
Synthesis of a Phosphaethynolatoborane

2.1 Introduction and objectives

2.1.1 Coordination modes of the 2-phosphaethynolate anion

Owing to its resonance forms, the 2-phosphaethynolate anion is a bidentate ligand capable of coordinating to Lewis acids as a phosphaketenyl (PCO-κ-P) or a phosphaethynolato (PCO-κ-O) moiety. At the start of this project, the former coordination mode dominated the p- and d- block with numerous examples of structurally authenticated phosphaketenes reported in the literature.[1] The oxygen bound phosphaethynolato bonding mode is typically reserved for hard, charge-dense Lewis acids. The first reported example of a O-bound complex was published with Becker's original synthesis of the salt, in the form of $Li[OCP](DME)_2$ (Scheme 2.1; **A**). The poor stability of this species, and the fact that the reported synthesis could not be scaled up successfully, resulted in limited research on the anion for twenty years after it was first reported. The solid state structure of $Li[OCP](DME)_2$ reveals a O---Li tight ion pair (1.878(5) Å) with an interaction that is slightly shorter than the sum of the covalent radii for the constituent elements (Σr_{cov} O–Li = 1.94–1.96 Å).[2] This interaction decreases the stability of the anion through reduction of the ionic character, and in turn the coloumbic repulsion between the species which prevents them from reacting. Moreover, it increases the contribution from the phosphaethynolato resonance form, locating a greater degree of electron density on the C≡P π-manifold. As a result, this salt is prone to decomposition via oligermisation pathways. The heavier alkali metal salts A[PCO]L (A= Na, K; L= $(DME)_2$, 18-crown-6) display M---O interactions greater than the sum of their respective covalent radii (2.349(3) Å for $Na(DME)_2[PCO]$ (Σr_{cov} = 2.18 Å) and 2.901(2) Å for K(18-crown-6)[PCO] (Σr_{cov} = 2.59 Å)),[3,4] suggesting greater contribution from the phosphaketenyl resonance form. Furthermore, elongation of the C–P bond was noted (1.575(3) Å for $Na(DME)_2[PCO]$, 1.579(3) Å for K(18-crown-6)[PCO] vs. 1.555(3) Å for $Li(DME)_2[PCO]$), consistent with reduced C≡P multiple bond

character. As a result, both the sodium and potassium salts display remarkable stability and can be handled in air or water for short periods of time.

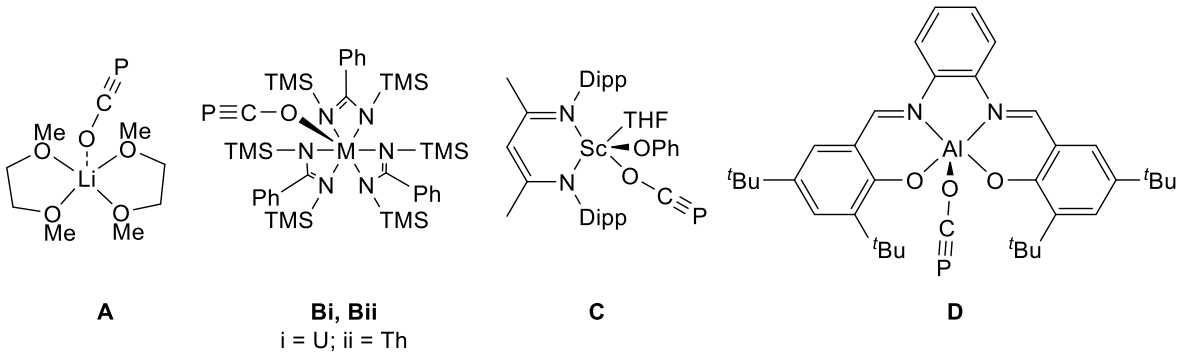

Figure 2.1. Selected phosphaethynolate species from the literature.

Westerhausen went on to synthesise a series of alkaline earth metal phosphaethynolate salts, which displayed similar stability issues as the lithium salt. From this series, they were able to structurally characterise the phosphaethynolato $Ca[OCP]_2(DME)_3$.[5] These investigations were furthered by Grützmacher and co-workers allowing for the isolation of the lighter, more ionic magnesium diphosphaethynolate complex $Mg[OCP]_2(THF)_4$.[6]

Oxygen binding can also be achieved by employing d-, and f-block metal centres that are highly ionic in character, first demonstrated in the coordination sphere of actinides by the $(amid)_3M(OCP)$ (M = U, Th; L = *N*,*N*′-bis-(trimethylsilyl)benzamidinate) complexes (Figure 2.1; **Bi** and **Bii**).[7] Reports on coordination with rare-earth metal complexes was expanded to include $[(^{Ad,Me}ArO)_3N]U(DME)(OCP)$, $[(DippForm)_2Ln(OCP)(thf)]$ (Ln = Y, Nd), [(DippForm)Sm(18-crown-6)(thf)][DippForm], in addition to the scandium complex $\{CH[N(Dipp)C(CH_3)]_2\}Sc(ODipp)(THF)(OCP)$ ($(^{Ad,Me}ArO)_3N^{3-}$ = trianion of tris(2-hydroxy-3-(1-adamantyl)-5-methylbenzyl)-amine; DippForm = *N*,*N*′-bis(2,6-diisopropylphenyl)-formamidinate)) (Figure 2.1; **C**).[8–10] In all of these ionic phosphaethynolate complexes the PCO^- moiety binds in a near-linear fashion, with M–O–C angles ranging from 170.9 (scandium) to 176.4° (thorium). The P–C bond is contracted

with concomitant C–O bond elongation when compared to reported phosphaketenes, consistent with greater C≡P triple bond character. This phenomenon was demonstrated in complex **Bii** through coordination to a nickel (0) centre through the C≡P π-manifold.

We chose to investigate the reactivity of the 2-phosphaethynolate anion with oxophilic main-group compounds, in an effort to promote coordination through the oxygen atom allowing for subsequent reductive deoxygenation and formation of a cyaphide ion (CP^-). Phosphaethynolato bonding between the 2-phosphaethynolate anion and p-block elements was first observed by the Grützmacher group with the addition of $Na[PCO](dioxane)_{2.1}$ to a THF solution of silyl trifluoromethanesulfonate (Scheme 2.1; **E**).[11] Calculations indicated the phosphaketene to be the more stable by 7.9 kcal/mol; the smallest energy difference of the group 14 compounds investigated. The authors were able to observe ^{31}P NMR resonances at –307.2 ppm, –371.3, and –368.4 ppm. The authors attribute two latter resonances as two isomers of the phosphaketenyl bonding mode, and the higher frequency resonance to the phosphaethynolate. The phosphaethynolate in this case being the kinetic product which rearranged upon warming to give exclusively the thermodynamic P-bound product. The products evaded isolation due to rapid, uncontrolled oligermerisation, however this report marked the first spectroscopic observation of a phosphaethynolato species.

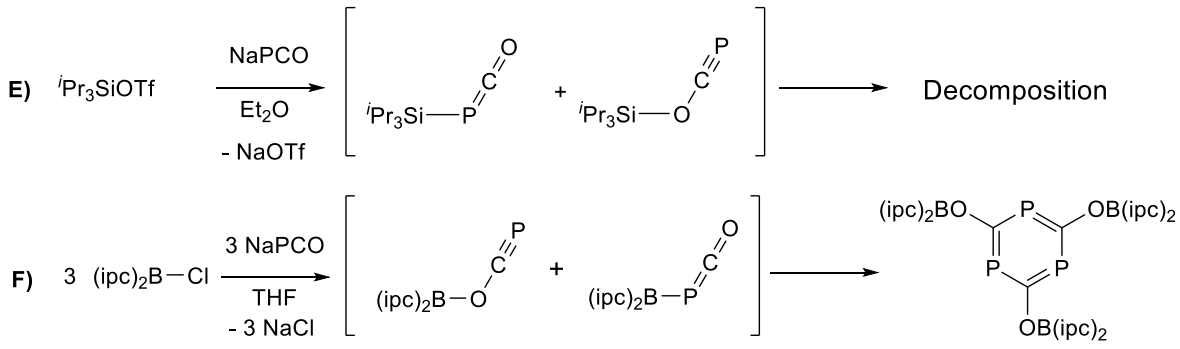

Scheme 2.1. Previous examples of spectroscopically detected phosphaethynolate species. ipc = (–)-B-chlorodiisopinocampheylborane.

The second report was published just after the start of this project. In it, (–)-B-chlorodiisopinocampheylborane was reacted with an equimolar amount of Na[PCO](dioxane)$_x$ resulting in formation of a triphosphabenzene species with the borane bound to the oxygen centre, implying the presence of a transient phosphaethynolate species (Scheme 2.1; **F**). At low temperature the authors were able to observe species consistent with both phosphaketene and phosphaethynolate bonding modes in the ^{31}P NMR spectrum. Interestingly, DFT investigations revealed the phosphaethynolate to be the more stable isomer by 5.9 kcal/mol when compared to the phosphaketenyl coordination mode, which to our knowledge is the only reported p-block system where this is the case.

It is worth noting that after our initial report on the phosphaethynolatoborane there has been one further example of a main-group system exhibiting this bonding mode in the form of a salen-supported aluminium complex (Figure 2.1; **D**).[12] Subsequent reactivity of this species is analogous to that of NaPCO, likely due to the high coordinative stabilisation and steric protection provided by the salen scaffold.

2.1.2 Chapter Outline

This chapter will detail our synthesis of a phosphaethynolatoborane, the first example of an isolable, covalently bound phosphaethynolate compound. We will explore how the reaction conditions affect the outcome of this reaction allowing for the synthesis of novel heterocycles. Using calculations, we will contrast the electronic structure of this species to more traditional phosphaalkynes with the aim of outlining possible reactivity trends.

2.2 A stable phosphaethynolatoborane ([B]OCP)

2.2.1 Synthesis of the phosphaethynolatoborane, [B]OCP

Our investigation focused on Yamashita's bromoborane, [B]Br ([B] = *N,N'*-bis(2,6-diisopropylphenyl)-2,3-dihydro-1H-1,3,2-diazaboryl), which upon heating with a slight excess of Na[PCO](dioxane)$_x$ in non-coordinating solvent for extended periods showed partial conversion to the desired phosphaethynolatoborane, [B]OCP (Scheme 2.2; **1**), as indicated by the presence of a singlet resonance in the $^{31}P\{^{1}H\}$ NMR spectrum at –285.9 ppm.

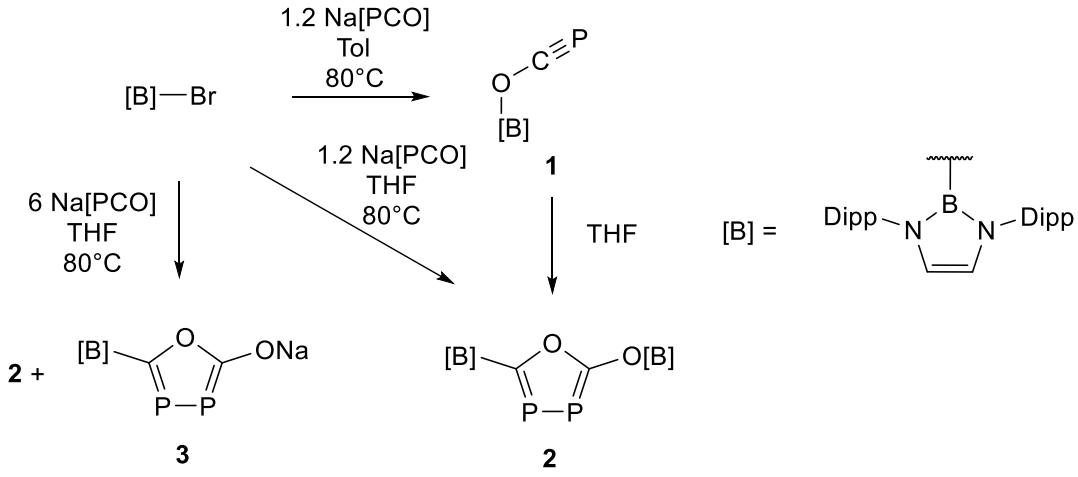

Scheme 2.2: Synthesis of [B]OCP and related heterocycles.

The reaction is solvent dependent, in the presence of a polar Lewis basic solvent, e.g. THF, **1** readily dimerises to quantitatively yield *cyclo*-$P_2\{C[B]\}O\{CO[B]\}$, **2**. Lewis bases able to induce this dimerization were expanded to include ether, pyridine, phosphines, and N-heterocyclic carbenes, with the rate of formation of the dimer approximately related to the donor capability of the base employed. This dimerization also proved to be a key challenge in our efforts to optimise reaction conditions.

Dioxane is present in the Na[PCO] salt as a solvate, and given its Lewis basic properties, induces dimerization when in too high a concentration. However, at

concentrations below 0.5 equivalents the salt becomes entirely insoluble in toluene and no reaction occurs. A number of attempts were made at bypassing this issue, such as using dioxane-free Na[PCO] followed by subsequent addition of substoichiometric amounts of dioxane to the reaction mixture, utilising phase transfer reagents, changing the solvate, and increasing the polarity of the solvent. However, none proved successful. Through trial and error, it was found that dioxane content of 0.5 to 1.2 equivalents proved ideal to yield **1** as the major product, with occasional trace formation of **2**. Due to the relative insolubility of the salt in non-polar solvents, the reaction proceeds *via* a somewhat heterogeneous pathway, as such the morphology of the Na[PCO] salt employed plays an important role in the conversion. Typically, the Na[PCO] salt is sonicated until it appears as a suspension, no longer settling at the bottom of the vessel even after several hours.

When the reaction was carried out in THF with an excess of Na[PCO] (6 equivalents), a second cyclisation product could be observed in the reaction mixture and was identified as *cyclo*-Na[P_2{C[B]}O{CO}], **3**. We propose that both **2** and **3** are formed from a Lewis base induced 1,2-boryl migration from the oxygen to the carbon centre, followed by a [3+2] cyclisation with **1** or Na[PCO], respectively.

The reaction to yield **1** was optimised for each batch of Na[PCO] used, utilising the diagnostic boryl backbone ^{1}H NMR shift to ensure complete consumption of [B]Br (typically 9–14 days at 80°C). Analytically pure, crystalline samples of **1** were obtained through cooling saturated hexane solutions to –30°C, with yields ranging from 40–70%.

2.2.2 Characterisation of [B]OCP

The ^{31}P{^{1}H} NMR spectrum of **1** in d_6-benzene contains a singlet resonance at –285.9 ppm, downfield-shifted relative to the free anion which typically appears between –368 and –397 ppm in polar solvents, and not at all in benzene (due to insolubility). The ^{11}B{^{1}H} NMR spectrum shows a broad resonance at 19.5 ppm, consistent with a three-

coordinate boron centre. The ^{1}H NMR spectrum is consistent with a single boryl moiety, with the diagnostic backbone proton resonance appearing at 5.88 ppm. The ^{31}P{^{1}H} NMR shift is not diagnostic of phosphaethynolato bonding, as reported phosphaketenes typically appear between –250 and –350 ppm. Interestingly, the ^{13}C NMR spectrum is diagnostic of this coordination mode. Phosphaketenes have been found to feature $^{1}J_{C–P}$ coupling of approximately 100 Hz, however in the case of **1** the carbon resonance corresponding to the phosphaethynolate carbon appears as a doublet at 140.15 ppm with a coupling constant of 17.6 Hz, almost an order of magnitude lower than similar linkage isomers. This observation is consistent with coupling constants reported in the aforementioned metal phosphaethynolates. While the origin of this phenomenon is not completely understood, it has been proposed that it is due to increased contribution from the phosphorus 3s orbital to the P–C bond in the phosphaketenyl bonding mode. The solid state IR spectrum of **1** exhibits a absorption band at 1648 cm^{-1} which can be assigned as the asymmetric P≡C–O stretch.

Compound **1** crystallises as yellow blocks in the triclinic space group *P*–1, and the asymmetric unit is shown in Figure 2.2. The hydrogen atoms were assigned idealised geometric coordinates after all other elements had been refined anisotropically.

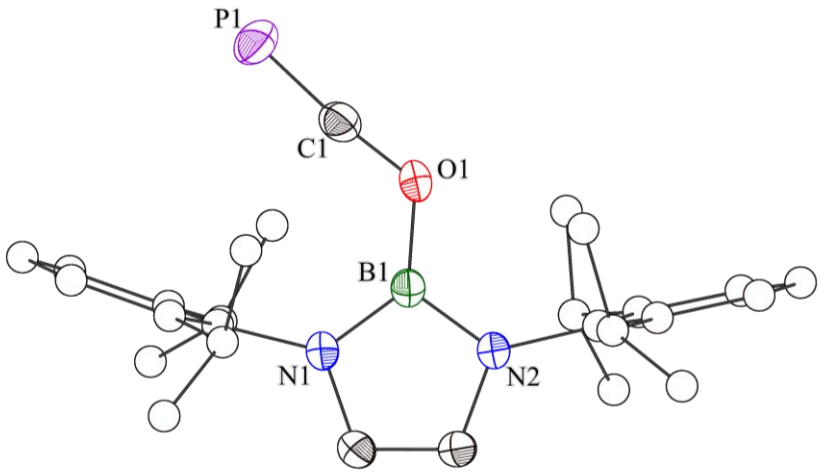

Figure 2.2. The solid state structure of [B]OCP, **1**. Anisotropic displacement ellipsoids are set at 50% probability. Hydrogen atoms omitted for clarity and Dipp carbon atoms shown as spheres of arbitrary radius.

The solid state structure of **1** reveals the phosphaethynolate moiety bound to the boron centre via the oxygen atom. The O1-C1-P1 bond angle remains almost linear (175.69(12)°). The C1–P1 bond length (1.545(2) Å) is shorter than that of the free PCO^- (1.579(3) Å) consistent with increased triple bond character. This bond contraction is accompanied by elongation of the C1–O1 bond (1.269(2) vs. 1.212(4) Å in the free anion). Perhaps the most important observation is the coplanarity between the phosphaethynolato moiety and the 1,3,2-diazaborole ring (deviation from planarity 0.0095 Å) indicative of p_π-delocalisation throughout the system. This is notable in the smaller than expected O1–B1 (1.425(2) Å) and O1–C1 bond lengths, both of which are shorter than the sum of the covalent radii for these elements (Σ_{cov} = 1.48 and 1.38 Å, respectively). We also suspect this delocalisation is responsible for the stability of this species, which is stable indefinitely in the solid state and can be heated to 120°C in toluene for weeks with no evidence for decomposition. Despite the presence of coplanarity in the solid state, the ^{1}H NMR spectrum indicates equivalence between the two protons on the boryl backbone, indicating rotation of the phosphaethynolato moiety is facile in the solution phase. Gas phase

calculations performed on the rotation of the N-B1-O1-C1 dihedral gave a barrier energy of 1.6 kcal/mol, consistent with the observation of rotation at room temperature.

Table 2.1: Selected bond lengths [Å] and angles [°] for **1**.

Bond length (Å)	
P1–C1	1.545(2)
C1–O1	1.269(2)
O1–B1	1.425(2)
B1–N1	1.415(2)
B1–N2	1.415(2)
Bond angle (˚)	
P1-C1-O1	175.69(12)
C1-O1-B1	126.16(11)
O1-B1-N1	129.64(12)
O1-B1-N2	123.27(12)
N1-B1-N2	107.09(11)

Gas phase calculations were performed on **1** using the functional PBE1PBE with the basis set 6-31G++(d,p) and revealed **1** to be the less stable than the phosphaketenyl isomer by 6.7 kcal/mol, calculated as:

$$\Delta E_{\text{linkage}} = E(\text{O-bound}) - E(\text{P-bound})$$

This value is comparable to that obtained for $^{i}Pr_3SiOCP$/ $^{i}Pr_3SiPCO$ (7.9 kcal/mol), for which both isomers are observed in solution.[11] We assume the lack of observation of the phosphaketenyl during the synthesis of **1** is due to the absence of a suitable isomerisation pathway. We were unable to compute a viable monomolecular isomerisation pathway, consistent with the lack of isomerisation even upon persistent heating. The HOMO of **1** is highly diffuse and shared across the entirety of the π-system, this delocalisation gives rise to the coplanarity between the OCP moiety and the boryl ring, observed both in the solid state and optimised gas phase structure. Furthermore, it is useful to note that the LUMO is

shared primarily between the phosphorus and carbon centre of the PCO, indicating potential electrophilic sites.

As the characterisation data for **1** show contraction of the C–P bond and increased triple bond character, it is useful to compare the frontier molecular orbitals of this species to the related phosphaalkynes. For the sake of simplicity, the frontier ortials of **1** are compared to those of the archetypal phosphaalkyne ^{t}BuCP. ^{t}BuCP and **1** show comparable LUMO energy (–0.64 and –0.28 eV, respectively), with the LUMO and the LUMO–1 located on C–P π* antibonding orbitals. One notable electronic difference between ^{t}BuCP and [B]OCP is the loss of degeneracy between the HOMO and HOMO–1, and LUMO and LUMO–1 induced by the reduction of symmetry from C_{3v} to C_s. This loss of symmetry results in the HOMO of **1** being higher in energy than that of ^{t}BuCP (–7.27 vs. –5.43 eV) implying this species will be a stronger nucleophile.

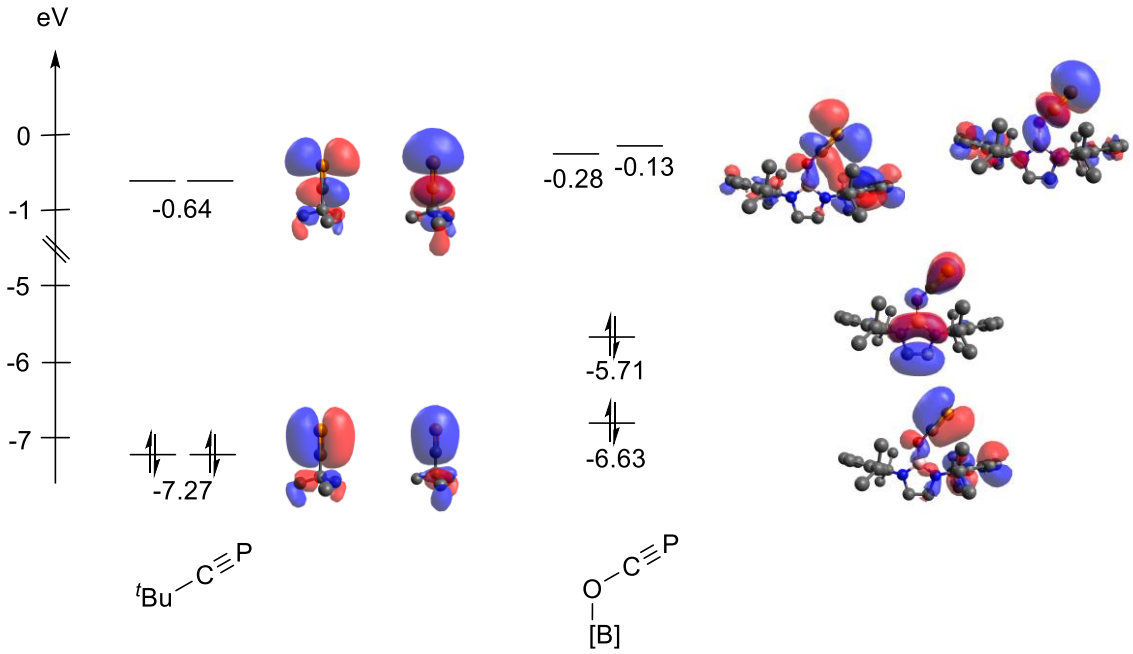

Scheme 2. 3: Frontier molecular orbital diagrams of ^{t}BuCP and [B]OCP from NBO analysis.

The difference in electronegativity between phosphorus and carbon results in a triple bond with partial positive charge at the phosphorus and partial negative charge at the

carbon, ie. $^{\delta-}C{\equiv}P^{\delta+}$. However, it is worth considering the influence of the carbon substituent on this dipole. Natural population analysis (NPA) was performed in order to gain insight into the polarity of the C≡P bond. In ^{t}BuCP the phosphaalkyne carbon has a calculated charge of –0.61 and the phosphorus has a charge of +0.57 (Δq_{NPA} = 1.18). In [B]OCP these are reduced to –0.13 and +0.26 (Δq_{NPA} = 0.39), respectively. A terminal alkyne, ^{t}BuCCH, has an overall difference in charge of 0.25, suggesting that the polarity of the C≡P bond in [B]OCP lies somewhere between that of ^{t}BuCP and ^{t}BuCCH.

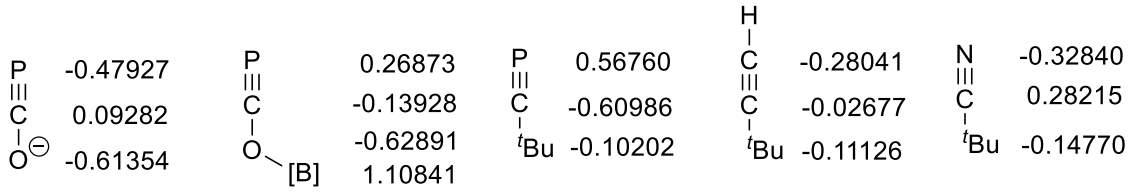

Figure 2.3: Natural population analysis charges (q) for [B]OCP, ^{t}BuCP and related species.

This reduced dipole can be illustrated using inductive and mesomeric effects. Substituting an electron-releasing (+*I*) ^{t}Bu group with an electron-withdrawing (–*I*) boryloxy group reverses the inductive effect at the phosphaalkyne carbon centre (Figure 2.4). These effects have the consequence of reducing the difference in electronegativity across the phosphaalkyne bond. The mesomeric effect can also explain the reduction of negative charge present at the phosphorus centre (Figure 2.4; +*M*). The boryloxy moiety in this case can act as a π-donator, influencing electron flow to induce a resonance form that places a negative charge at the phosphorus centre; a net reduction to the overall partial positive charge. This resonance form is analogous to the phosphaketenyl/phosphaethynolato resonance structures of PCO^{-}, however less electron density is available for redistribution.

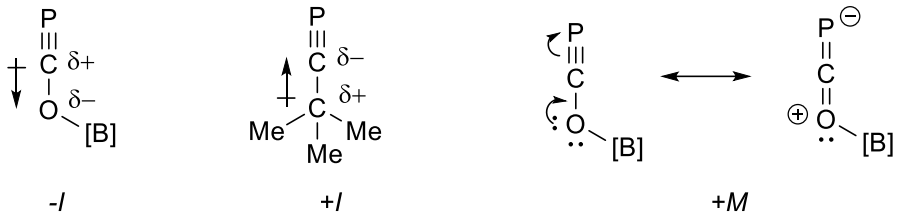

Figure 2. 4: Graphical illustration of the inductive effect (*-I* and *+I*) and mesomeric effect (*+M*) in phosphaalkynes

2.2.3 Characterisation of heterocycles 2 and 3

Compound **2** exhibits an AB spin system in the $^{31}P\{^{1}H\}$ NMR spectrum with doublet resonances at 223.3 and 38.3 ppm with a $^{1}J_{P-P}$ coupling constant of 386 Hz. The ^{1}H NMR spectrum is consistent with the presence of two distinct boryl moieties, with backbone ^{1}H resonances at 6.11 and 6.06 ppm. Whereas, the $^{11}B\{^{1}H\}$ NMR spectrum revealed a single broad resonance at 22.0 ppm, which is not unexpected for two similar three-coordinate boron environments.

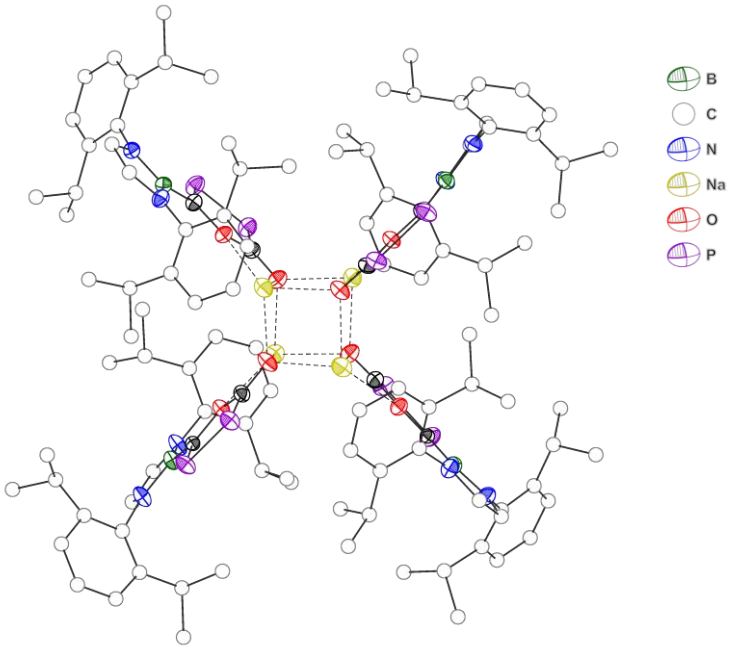

Figure 2.5: Solid state structure of tetrameric species **3**. Anisotropic displacement ellipsoids are set at 50% probability. Hydrogen atoms omitted for clarity and carbon atoms shown as spheres of arbitrary radius.

Crystals of **3** were grown from a layered toluene/hexane solution, in the triclinic spacegroup *P*–1. The solid-state structure revealed a tetramer, with four equivalents of the 1,3,4-oxadiphosphole bound through tight ion pairs to four sodium atoms in a cubane-like manner (Figure 2.5). Dissolution of the crystals results in the appearance of two AB systems in the $^{31}P\{^{1}H\}$ NMR, the major product has chemical shifts at 239.9 and –0.28 ppm with a coupling constant of 398 Hz. The minor product has a near identical coupling of 396 Hz, with doublets at 237.40 and –0.47 ppm. The two AB systems in the solution phase NMR can be tentatively assigned as the tetramer and the disassociated monomer in the solution phase. Further, the ^{1}H NMR spectrum shows broad peaks for the tetramer, consistent with slow tumbling on the NMR timescale, and sharper resonances for the monomer.

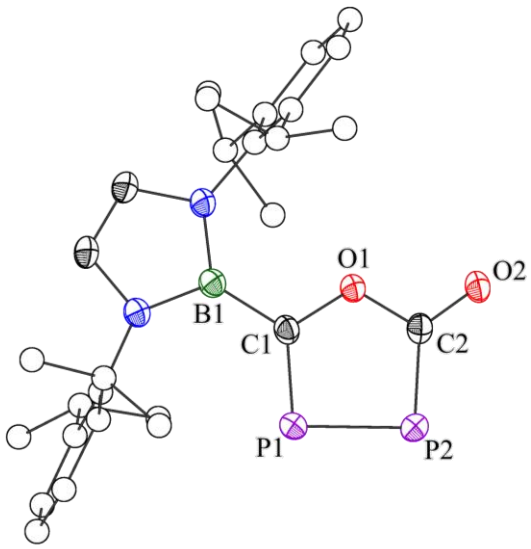

Figure 2.6. Solid state structure of a single anion of tetrameric species **3**. Anisotropic displacement ellipsoids are set at 50% probability. Hydrogen atoms omitted for clarity and Dipp carbon atoms shown as spheres of arbitrary radius.

Orange crystals of **2** were obtained by cooling a saturated solution of hexane to –30°C over several days, and crystallises in the monoclinic spacegroup $P2_1/c$ (Figure 2.7). The solid state structure revealed a five-membered 1,3,4-oxadiphosphole core. This motif contrasts with previously observed dimerisations for compounds of PCO^- and boranes,[13]

however a similar motif has been reported from the reaction of PCO^- with the electrophilic diazaphospholidine-4,5-dione, which afforded a *cyclo*-Na[P_2{C[NHP]}O{CO}] (NHP = diazaphospholidine-4,5-dione).[14]

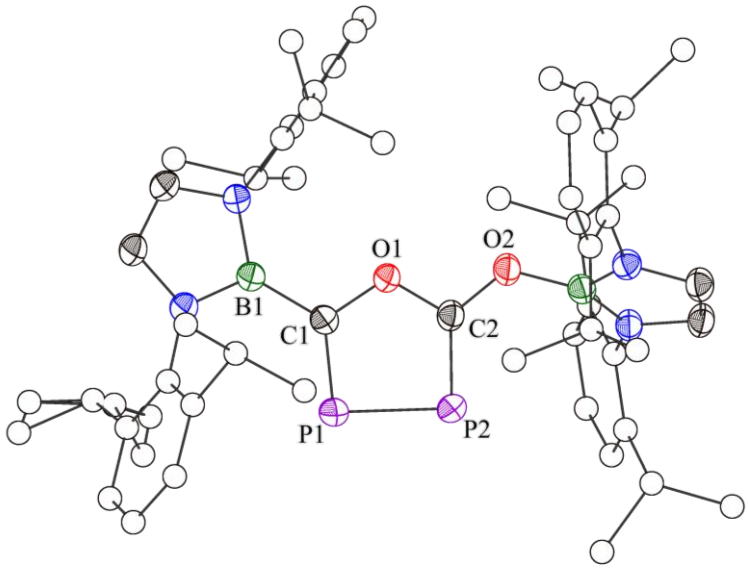

Figure 2. 7. Solid state structure of **2**. Anisotropic displacement ellipsoids are set at 50% probability. Hydrogen atoms omitted for clarity and Dipp carbon atoms shown as spheres of arbitrary radius.

Bond metrics for **2**, **3**, and the previously reported diazaphospholidine-4,5-dione *cyclo*-Na[P_2{C[NHP]}O{CO}] are given in Table 2.2. The five-membered heterocyclic core in all three compounds is comparable, with C1–P1 bonds in the range of 1.696-1.712 Å and P1–P2 bonds distances ranging from 2.096–2.141 Å. The P_2C_2O core of **2** is 6π electron system which exhibits aromaticity, NICS(0) and NICS(1) calculations performed on **2** gave values of –10.1 and –11.5 ppm, respectively.

Table 2.2: Select bond lengths for compound **2**, **3** and related literature compound.

Bond distance (Å)	**2**	**3**	*cyclo*-Na[P_2{C[NHP]}O{CO}]
P1–P2	2.141(1)	2.133(1)	2.096(3)
P1–C1	1.703(2)	1.712(2)	1.696(5)
C1–O1	1.374(2)	1.387(2)	1.231(7)
O1–C2	1.340(2)	1.381(2)	1.405(6)
C2–P2	1.721(2)	1.761(2)	1.795(6)

The formation of both **2** and **3** involve a 1,2-migration of the boryl moiety from the oxygen to the carbon centre followed by a cyclisation with a second equivalent of either **1** or PCO^-. The formation of **3** is perhaps better understood as PCO^- is known to be nucleophilic. We postulate that the nucleophilic phosphorus of PCO^- attacks the electrophilic phosphaethynolate phosphorus centre to induce boryl migration. This would then be followed by ring closure through an intramolecular attack of the oxygen on the electrophilic phosphaketenyl carbon centre (Scheme 2.4).

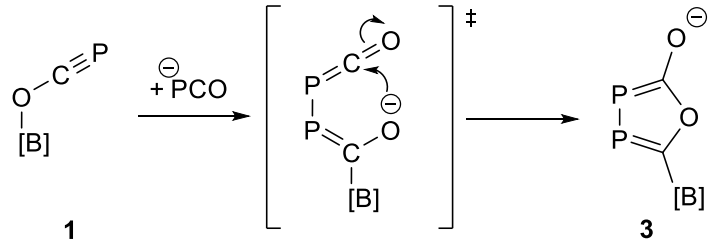

Scheme 2.4. Proposed mechanism for the transformation of **1** to **3**.

The mechanism for the formation of **2** is less well understood, seemingly two electrophilic phosphorus centres are bound in the final product. As discussed earlier, this transformation is highly solvent dependent. While the dimerization could be attributed to solvent polarity, it is noteworthy that no dimerization occurs in either difluorobenzene or dichloromethane. The role of the solvent in this dimerization is thought to be as a Lewis base catalyst and is consistent with the observation that addition of Lewis bases to

solutions of **1** also induces formation of **2**. We postulate that a Lewis basic solvent molecule induces the 1,2-boryl migration and facilitates a [3+2] cyclisation with a second equivalent of **1** (Scheme 2.5). Attempts to compute a viable mechanistic pathway for this mechanism were unsuccessful, primarily due to a large barrier of association of the Lewis base and **1**, and the possible concerted nature of both the boryl migration with base association, and the cyclisation accompanied with loss of the Lewis base.

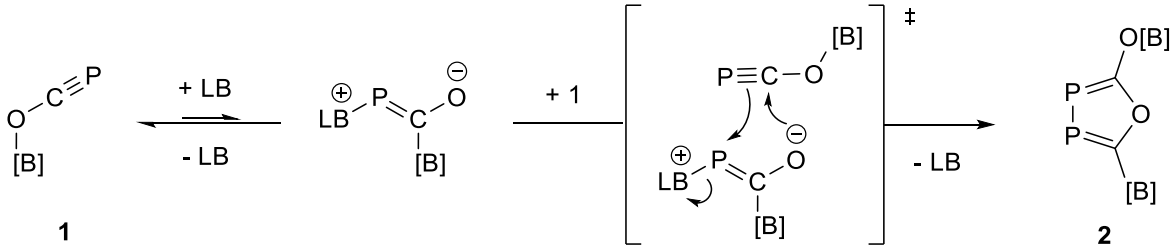

Scheme 2.5. Proposed mechanism for the transformation of **1** to **2**.

2.2.4 Further cyclisation chemistry

The ease with which **1** cyclises to **2** and **3** encouraged us to explore the viability of **1** as a synthon for novel heterocycle synthesis. Previous investigations into the reactivity of phosphaethynolate salts have found numerous cyclisation reactions, often involving an initial [2+2] cyclisation with heteroallenes. The first example of such a cyclisation was reported by Becker soon after the initial synthesis of the salt, who noted that the reaction of PCO^- with CS_2 generates PCS^- and SCO, through an unobserved cyclic four-membered intermediate.[15] Later, reports by the groups of Grützmacher and Goicoechea expanded the scope of heteroallene reactivity with [2+2] cyclisations with CO_2, ketenes, and carbodiimides to yield isolable four-membered heterocycles.[4,16] Stephan also reported [2+2] cyclisations upon addition of boranes, for which the composition of the heterocycle was dependent on the borane employed.[13] Many of the 5- and 6-membered heterocycles

generated from PCO^- and heteroallenes can be rationalised with an initial [2+2] cyclisation followed by either additional cyclisations and/or decarbonylation reactions.[1,17]

The cyclisation chemistry of the C≡P triple bond in phosphaalkynes has also been extensively investigated. Contrasting that of PCO^-, phosphaalkynes tend to undergo [2+1] cycloadditions with carbenes,[18] silylenes,[19] germylenes,[20] and phosphinidenes.[21] Additionally, [2+3] cycloadditions occur readily with compounds containing 1,3-dipoles, such as azides, giving access to heterophospholes.[22,23]

This section falls into two parts, initially we will discuss the chemistry that can be achieved from heterocycle **2**. Next, we attempt to expand the scope of heterocycles accessible from **1**.

2.2.5 Expanding the reactivity of 2

We sought to further develop the chemistry of heterocycle **2**. Due to the 6π aromatic nature of the ring, and the available lone pair at each phosphorus atom, we hypothesised that it may be possible to coordinate **2** to metal centres through displacement of weakly coordinating η^2 or η^6 ligands. However, **2** showed no reactivity towards M(mesitylene)CO_3 (M = W, Mo), $W(MeCN)_3(CO)_3$, $W(THF)CO_5$, or $(Me_2S)AuCl$.

Photolysis of solutions of **2** initially caused the solutions to turn bright green, and prolonged exposure gave dark red solutions. Removal of the solvent followed by recrystallization from a cooled, saturated hexane solution resulted in analytically pure crystals of 1*H*-diphosphirene *cyclo*-P{PO[B])(C[B]}, **5** in 39% yield.

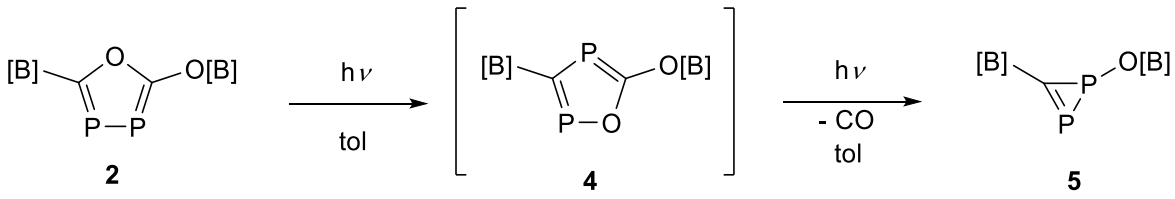

Scheme 2.6. Irradiation of **2** to yield **5**, via proposed intermediate **4**.

Following the reaction by ^{31}P NMR spectroscopy revealed the formation and consumption of an intermediate on route to **5**. The intermediate was partially characterised using multinuclear NMR spectroscopy. All attempts to isolate crystals suitable for single crystal X-ray diffraction were unsuccessful, likely due to **1** and **5** being present in the reaction mixture to varying degrees depending on the duration of the irradiation. However, from the data obtained we were able to assign the intermediate as *cyclo*-PO{CO[B]}P-{C[B]}, **4**.

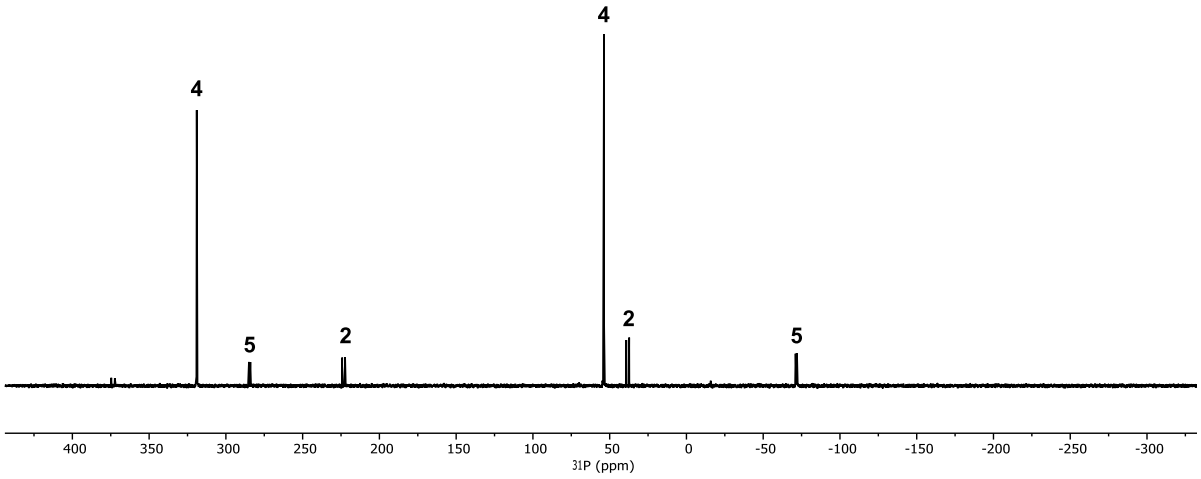

Figure 2.8. ^{31}P NMR spectrum in C_6D_6 showing products **2**, **4** and **5**.

The initial product of the irradiation, **4**, is formed from a rearrangement of the five membered core of **2**. Cooling a saturated solution of the reaction mixture yields green powders that contain small amounts of both **2** and **5**. Further purification results in diminishing yields and only slightly improved purity, likely due to the similar solubility of all three compounds. The $^{31}P\{^{1}H\}$ NMR spectrum displayed an AB spin system with resonances at 391.0 and 53.7 ppm with an unusually low $^{2}J_{P-P}$ coupling of 7 Hz. The core has previously been reported in the compound 3,5-dimesityl-1,2,4-oxadiphosphole, which shares the unusually small coupling constant in the ^{31}P NMR spectra, revealing a $^{2}J_{P-P}$ of

18 Hz.[24] The ^{1}H NMR spectrum is consistent with the presence of two distinct boryl moieties. The ^{13}C NMR spectrum has two resonances in the region of the heterocycle, one a doublet of doublets with coupling of 66 and 3 Hz, consistent with one and two bond carbon-phosphorus coupling, and a second resonance which is too broad to distinguish coupling, likely due to proximity to a quadrupolar ^{11}B{^{1}H} nucleus. A computational investigation into the possible isomers resulting from photolysis of **2** indicated **4** was in best agreement with the observed ^{31}P NMR shift (calc. 314 and 55 ppm).

Prolonged irradiation results in complete conversion to **5**, which can be isolated as analytically pure crystalline powders. The solution phase ^{31}P NMR spectrum is consistent with the presence of two inequivalent phosphorus environments with an AB spin system at 284.6 and –71.5 ppm ($^{1}J_{P–P}$ = 188 Hz). There are two previously reported examples of isolable 1*H*-diphosphirenes, which display different chemical shifts than those found in **5**.[25,26] *Cyclo*-P{PN(iPr)$_2$}{CN(iPr)-(SiMe$_3$)} reported by Niecke in 1989 displays an AB spin system at –14.9 and –118.7 ppm ($^{1}J_{P–P}$ = 104 Hz), and *cyclo*-P{PN(iPr)$_2$}{CN(iPr)$_2$} which displays resonances at –23.7 and –121.7 ppm ($^{1}J_{P–P}$ = 121 Hz). The large deviation in the shift of the σ^2-phosphorus atom is a consequence of the π-accepting ability of the boryl functionality, which contrasts the previously reported examples which both contain π-donating amide functionalities.

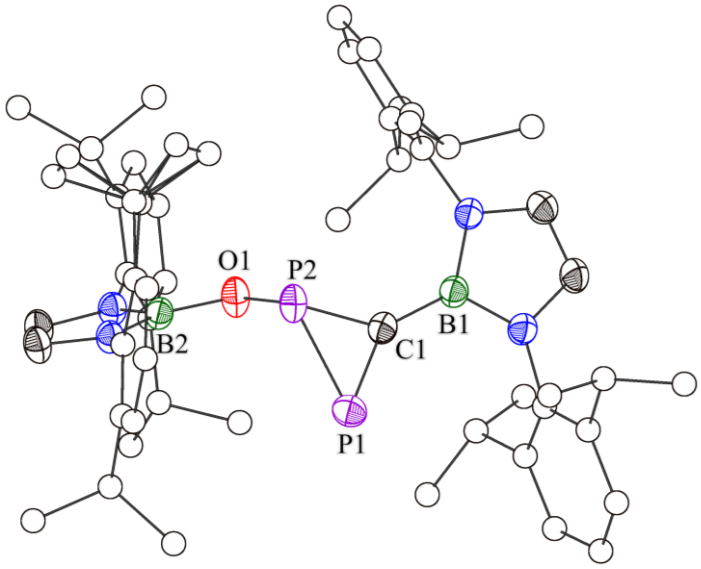

Figure 2.9: Molecular structure of **5** (major component of the positionally disordered molecule pictured). Anisotropic displacement ellipsoids are set at 50% probability. Hydrogen atoms omitted for clarity and Dipp carbon atoms shown as spheres of arbitrary radius.

The molecular structure of **5** reveals a triatomic core resulting from loss of carbon dioxide from the molecule and migration of the boryloxy moiety to a phosphorus centre. The structure is disordered about the diphosphirene ring, and only the major component will be discussed. The P–P bond length is consistent with that of a single bond (2.173(1) Å). The two P–C are significantly different, with interatomic distances of 1.802(2) and 1.670(2) Å, consistent with a single and double bond, respectively (Σ_{cov} = 1.86 (single) and 1.69 (double) Å).[2,27] The boryl moiety is coplanar to the three membered ring and the C–B bond is shorter than what would be expected of a single bond (1.534(3) Å vs. 1.550(2) Å in **2**). This bond contraction is consistent with π-delocalisation from the carbon to the boron atom. This observation corroborates both the broadening of the ^{13}C NMR resonance assigned to C1 and the unusually downfield shift of the σ^2-phosphorus. DFT investigations suggest that the rearrangement from **2** to **4** is thermodynamically downhill by 7.2 kcal/mol, and the decarbonylation step to yield **5** is an additional 14.3 kcal/mol downhill.

2.2.6 Attempts at click chemistry

Perhaps the most notable cyclisation reaction of the phosphaalkynes is their reaction with organic azides to yield triazaphospholes *via* [3+2] cyclisations (Scheme 2.7). Unlike organic click reactions involving alkynes, phosphaalkyne click chemistry proceeds without the need for increased temperatures or the presence of a catalyst.[28] The initial finding that **1** is able to undergo [3+2] cyclisations with itself to yield **2** was promising, and prompted us further investigate the cycloaddition chemistry of **1**.

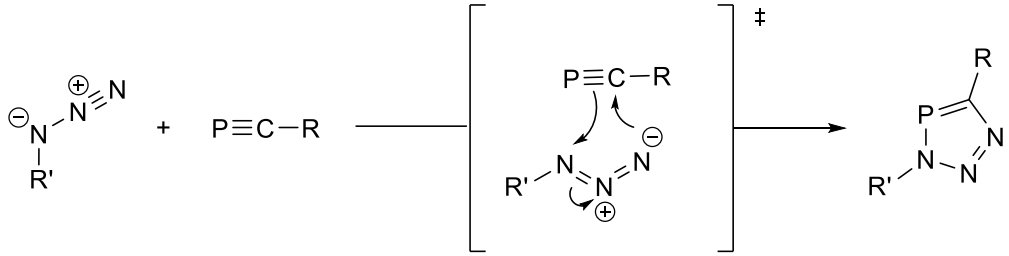

Scheme 2.7. The phosphaalkyne click reaction.

The selection of azide was limited by the solvent stability of **1**, as outlined in section 2.2.1., which prevented reactions from being conducted in coordinating solvent. Three azides were selected with varying electronic properties, the ionic sodium azide, trimethylsilyl azide, and benzyl azide.

Sodium azide showed no reactivity with **1** in toluene even at elevated temperatures. This is not surprising, as the solubility of the salt in non-coordinating salts is poor. Changing the solvent to THF yielded heterocycle **2** as the sole product. If instead trimethylsilyl azide was selected in toluene no reaction occurs. If instead THF is used the $^{31}P\{^{1}H\}$ NMR spectrum indicated the presence of multiple phosphorus-containing species, none of which are consistent with species **2**. The ^{1}H spectrum was consistent with a single boryl containing species. Crystallisation of the mixture allowed unambiguous assignment of the boryl species as boryl azide [B]N_3, which has previously been reported by the Braunschweig group.[29] While identification of the phosphorus species was not possible, it

is likely pseudohalide exchange occurs to yield trimethylsilyl phosphaethynolato compounds. Related species have been studied by the Grützmacher group and are known to readily oligermise.[11]

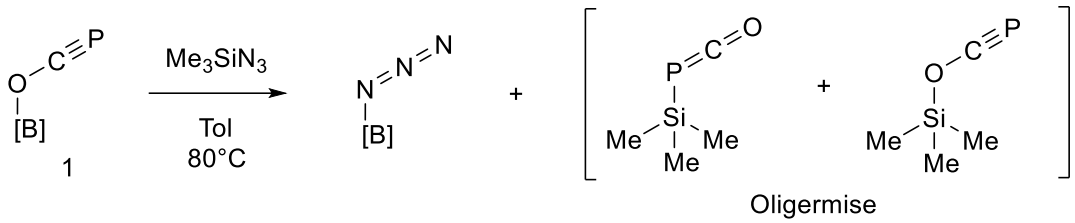

Scheme 2.8: Reactivity of **1** towards trimethylsilylazide.

Similar to the reactivity observed with trimethylsilyl azide, the reaction of benzyl azide and **1** in toluene at room temperature yields a mixture of products in the $^{31}P\{^{1}H\}$ NMR spectrum, while the ^{1}H NMR spectrum is indicative of a single boryl containing species. Unfortunately, it was not possible to separate the products. Although these reactions were not successful, it does contrast the reactivity of **1** with phosphaalkynes which typically undergo facile [3+2] cyclisations with azides. This difference could be attributed to the reduction in dipole across the C≡P bond, as discussed in section 2.2.2.

2.3 Conclusions

This chapter described the synthesis and characterisation of phosphaethynolatoborane ([B]OCP) **1** from the salt metathesis of $Na(PCO)(dioxane)_x$ and *N,N′*-bis(2,6-diisopropylphenyl)-2,3-dihydro-1H-1,3,2-diazaboryl. **1** represented the first isolable p-block oxygen bound 2-phosphaethynolate complex. A computational analysis of **1** found it to be less stable than its linkage isomer, [B]PCO, by 6.7 kcal/mol in the gas phase. Analysis of the frontier molecular orbitals indicated an increase in nucleophilicity with respect to the archetypal phosphaalkyne ^{t}BuCP, while natural populational analysis indicated a reduction in dipole across the C≡P bond.

Variation of the reaction conditions allowed for the synthesis and characterisation of heterocycles **2** and **3**. The chemistry of **2** was developed, finding that upon irradiation the five membered core rearranges to give a rare example of a 1,2,4-oxadiphosphole, **4**, in solution. Further irradiation induced decarbonylation to the 1*H*-diphosphirene, **5**.

The cycloaddition chemistry of **1** towards azides was also explored. Unlike traditional phosphaalkynes, no evidence of [3+2] cycloaddition was found . With trimethylsilyl azide a pseudohalide exchange occurs, resulting in a boryl azide and a mixture of phosphorus-containing species. The outcome of the reaction with benzylazide was inconclusive, however the NMR spectra obtained were not consistent with the expected triazophospholes. This reactivity deviates from that expected of phosphaalkynes, which typically undertake facile [3+2] additions with azides.

2.4 References

[1] J. M. Goicoechea, H. Grützmacher, *Angew. Chem. Int. Ed.* **2018**, *57*, 16968–16994.

[2] P. Pyykkö, M. Atsumi, *Chem. Eur. J.* **2009**, *15*, 12770–12779.

[3] F. F. Puschmann, D. Stein, D. Heift, C. Hendriksen, Z. A. Gal, H. F. Grützmacher, H. Grützmacher, *Angew. Chem. Int. Ed.* **2011**, *50*, 8420–8423.

[4] A. R. Jupp, J. M. Goicoechea, *Angew. Chem. Int. Ed.* **2013**, *52*, 10064–10067.

[5] M. Westerhausen, S. Schneiderbauer, H. Piotrowski, M. Suter, H. Nöth, *J. Organomet. Chem.* **2002**, *643–644*, 189–193.

[6] R. J. Gilliard, D. Heift, Z. Benko, J. M. Keiser, A. L. Rheingold, H. Grützmacher, J. D. Protasiewicz, *Dalton Trans.* **2018**, *47*, 666–669.

[7] C. Camp, N. Settineri, J. Lefèvre, A. R. Jupp, J. M. Goicoechea, L. Maron, J. Arnold, *Chem. Sci.* **2015**, *6*, 6379–6384.

[8] S. Bestgen, Q. Chen, N. H. Rees, J. M. Goicoechea, *Dalton Trans.* **2018**, *47*, 13016–13024.

[9] L. N. Grant, B. Pinter, B. C. Manor, H. Grützmacher, D. J. Mindiola, *Angew. Chem. Int. Ed.* **2018**, *57*, 1049–1052.

[10] C. J. Hoerger, F. W. Heinemann, E. Louyriac, L. Maron, H. Grützmacher, K. Meyer, *Organometallics* **2017**, *36*, 4351–4354.

[11] D. Heift, Z. Benko, H. Grützmacher, *Dalton Trans.* **2014**, *43*, 5920–5928.

[12] Y. Mei, J. E. Borger, D. J. Wu, H. Grützmacher, *Dalton Trans.* **2019**, *48*, 4370–4374.

[13] K. M. Szkop, A. R. Jupp, R. Suter, H. Grützmacher, D. W. Stephan, *Angew. Chem.*

Int. Ed. **2017**, *56*, 14174–14177.

[14] M. M. Hansmann, D. A. Ruiz, L. Liu, R. Jazzar, G. Bertrand, *Chem. Sci.* **2017**, *8*, 3720–3725.

[15] G. Becker, K. Hübler, *ZAAC - J. Inorg. Gen. Chem.* **1994**, *620*, 405–417.

[16] D. Heift, Z. Benko, H. Grützmacher, *Dalton Trans.* **2014**, *43*, 831–840.

[17] L. Weber, *Eur. J. Inorg. Chem.* **2018**, *2018*, 2175–2227.

[18] O. Wagner, M. Ehle, M. Regitz, *Angew. Chem. Int. Ed.* **1989**, *28*, 225–226.

[19] M. Regitz, *Chem. Rev.* **1990**, *90*, 191–213.

[20] A. H. Cowley, S. W. Hall, C. M. Nunn, J. M. Power, *J. Chem. Soc. Chem. Commun.* **1988**, 753–754.

[21] M. Regitz, U. Annen, E. P. O. Fuchs, *Phosphorus. Sulfur. Silicon Relat. Elem.* **1990**, *51*, 323.

[22] Y. Y. C. Yeung Lam Ko, R. Carrié, A. Muench, G. Becker, *J. Chem. Soc. Chem. Commun.* **1984**, 1634–1635.

[23] W. Rösch, M. Regitz, *Angew. Chem. Int. Ed.* **1984**, *23*, 900–901.

[24] A. Mack, U. Bergsträßer, G. J. Reiß, M. Regitz, *European J. Org. Chem.* **1999**, *1999*, 587–595.

[25] E. Niecke, R. Streubel, M. Nieger, D. Stalke, *Angew. Chem. Int. Ed.* **1989**, *28*, 1673–1674.

[26] D. Bourissou, Y. Canac, M. I. Collado, A. Baceiredo, G. Bertrand, *Chem. Commun.* **1997**, 2399.

[27] P. Pyykkö, M. Atsumi, *Chem. Eur. J.* **2009**, *15*, 186–197.

[28] L. Jin, D. R. Tolentino, M. Melaimi, G. Bertrand, *Sci. Adv.* **2015**, *1*, e1500304.

[29] H. Braunschweig, M. A. Celik, T. Dellermann, G. Frenking, K. Hammond, F. Hupp, H. Kelch, I. Krummenacher, F. Lindl, L. Mailänder, et al., *Chem. Eur. J.* **2017**, *23*, 8006–8013.

Chapter 3
Electrophilic reactivity of a phosphaethynolatoborane

3.1. Introduction and objectives

3.1.1. Phosphaalkynes as electrophiles

The chemistry of phosphaalkynes is dominated by reactivity studies into their nucleophilicity, which has been exploited to access organophosphorus species and a wealth of coordination complexes. Their utility as electrophiles, however, remains largely unexplored. The polarity of the carbon-pnictogen bond in phosphaalkynes is reversed relative to nitriles, indicating that nucleophilic reagents should display regioselectivity for the phosphorus centre. Cowley and co-workers demonstrated this inversion through addition of MeLi to Mes*CP (Mes*= 2,4,6-$^{t}Bu_3C_6H_2$), which resulted in methylation at the phosphorus centre and lithiation at the carbon atom.[1] Jones and co-workers later demonstrated similar reactivity could be observed using bulky Grignard reagents.[2] The limiting factor for these functionalisations is the requirement of steric bulk at either the phosphaalkyne substituent or the nucleophile to prevent further oligermisation, as a result further investigations into the scope of these transformations is limited.[3,4]

The reactivity of divalent tetrels towards phosphaalkynes has also been explored. Silylenes, germylenes, and stannylenes react with phosphaalkynes to generate three- or four-membered rings containing phosphaalkene structural elements.[5] Addition of cyclic carbenes leads to various heterocyclic products with the carbene generally associated at the carbon centre of the phosphaalkyne C≡P bond.[6] While this tends to run counter to the prediction of an electrophilic phosphorus centre, the lack of isolated intermediates on route to the cyclic products, in addition to the ambiphilic nature of divalent tetrels, makes drawing conclusions about the nature of the C≡P bond from these studies difficult.

As the 2-phosphaethynolate anion is itself a strong nucleophile its electrophilic behaviour has not yet been explored.

3.1.2. Objectives

The examples above demonstrate the electrophilicity of phosphaalkynes towards a limited number of nucleophiles. Our goal in these studies was to explore how [B]OCP, **1**, compares in reactivity to phosphaalkynes and to expand the range of chemical transformations possible utilising the C≡P multiple bond. This chapter will outline our findings on the addition of anionic nucleophiles to **1**, initially inspired by the work of Cowley, and later expanding this reactivity to enable synthesis of a new class of metallophosphaalkenes. The second half will explore the reactivity of **1** towards isocyanides, electron rich carbon monoxide analogues. Tertiary-butyl isocyanide (^{t}BuNC) was found to isomerise the phosphaethynolate to the more stable phosphaketenyl linkage isomer. The mechanism of isomerisation was investigated experimentally and computationally. Furthermore, we probed the reactivity of this species, including attempts at generating and detecting a triplet phosphinidene. Calculations on the mechanism of isomerisation were conducted in collaboration with Prof. John MCgrady and Mauricio Portiolli Franco. EPR and related calculations were performed in collaboration with Dr. William Myers.

3.2. Nucleophilic addition chemistry with Lithium Aryls and Na[Cp*Fe(CO)$_2$]

3.2.1. Synthesis of LiOC[B]P(Ar) complexes

The reaction of **1** with lithium aryls (aryl = Mes = 1,3,5-trimethylbenzene, Mes* = C_6H_3-2,6-Mes_2) in toluene/THF mixtures led to clean formation of compounds **6a** and **7**, respectively (Scheme 3.1), as evidenced by a single resonance in the $^{31}P\{^1H\}$ NMR spectra at δ = 107.1 and 162.3 ppm, respectively. A small amount of THF is required in the

reaction mixture to increase the solubility of the lithium aryls, without which no reaction occurs. **6a** exists as an adduct of THF in solution, and upon exposure to dynamic vacuum it can be desolvated to yield dimeric species **6b**, with a corresponding shift to higher frequency in the $^{31}P\{^{1}H\}$ NMR spectrum (136.7 ppm). Cooling a saturated hexane solution resulted in analytically pure, crystalline samples of phosphaalkene **6b**. **6b** can be cleaved into monomers through addition of stoichiometric amounts of 12-crown-4 to give compound **6c**, identified by a singlet resonance in the $^{31}P\{^{1}H\}$ NMR spectrum at 112.0 ppm.

The reaction shows tolerance for variation of the steric requirements of the aryl substituent. Increasing the bulk of the aryl from mesityl to Mes* produced analogous reactivity with the formation of compound **7**, revealing a singlet resonance by ^{31}P NMR spectroscopy at 112.0 ppm.

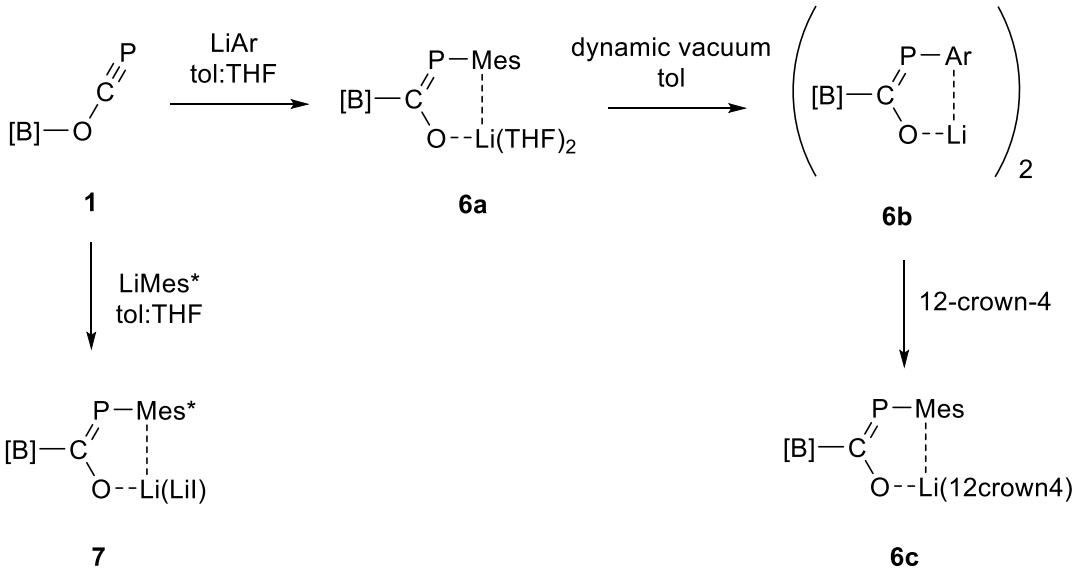

Scheme 3.1. Reactivity of **1** towards lithium aryls.

Both products arise from nucleophilic attack of the aryl anion at the phosphorus centre, accompanied by a 1,2-boryl migration from the oxygen to the carbon centre. Two resonance structures can be drawn for the central oxyphosphaalkene core, placing the

negative charge either on the oxygen to form an anionic phosphaalkene, or at the phosphorus atom to form an acyl phosphide (Scheme 3.2).

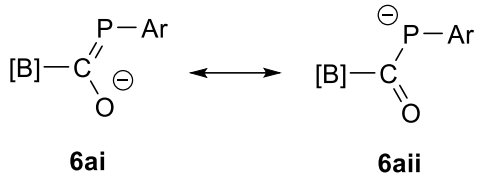

6ai **6aii**

Scheme 3. 2. Resonance forms of anion **6a**.

Crystals of **6a** grew as poor quality needles leading to unsatisfactory single crystal X-ray diffraction data. It was possible to obtain suitable crystals of both **6b** and **6c** from a cooled hexane solution. Crystals of **7** were obtained in a similar fashion, however the species co-crystallised with an equivalent of lithium iodide, likely an impurity carried forward from the synthesis of LiMes*. Attempts at separating the lithium salt were unsuccessful and further reactivity of this species was not explored, instead the subsequent reactivity focussed on **6**. A summary of the bond metrics for compounds **6** and **7** can be found in Table 3.1.

Table 3. 1. Summary of selected bond distance [Å] and angles [°] in compounds **6b**, **6c**, and **7**.

Bond distance (Å)	**6b**	**6c**	**7·LiI**
P1–C1	1.732(2)	1.740(2)	1.727(3)
C1–O1	1.318(3)	1.284(2)	1.330(3)
C1–B1	1.576(3)	1.586(3)	1.578(3)
O1–Li1	1.900(4)	1.850(4)	1.873(6)
Bond angle (˚)			
P1-C1-B1	114.06(14)	117.77(17)	116.89(18)
P1-C1-O1	128.92(16)	126.96(16)	125.75(18)
NMR (ppm)			
$^{31}P\{^{1}H\}$	136.7	162.3	112.0

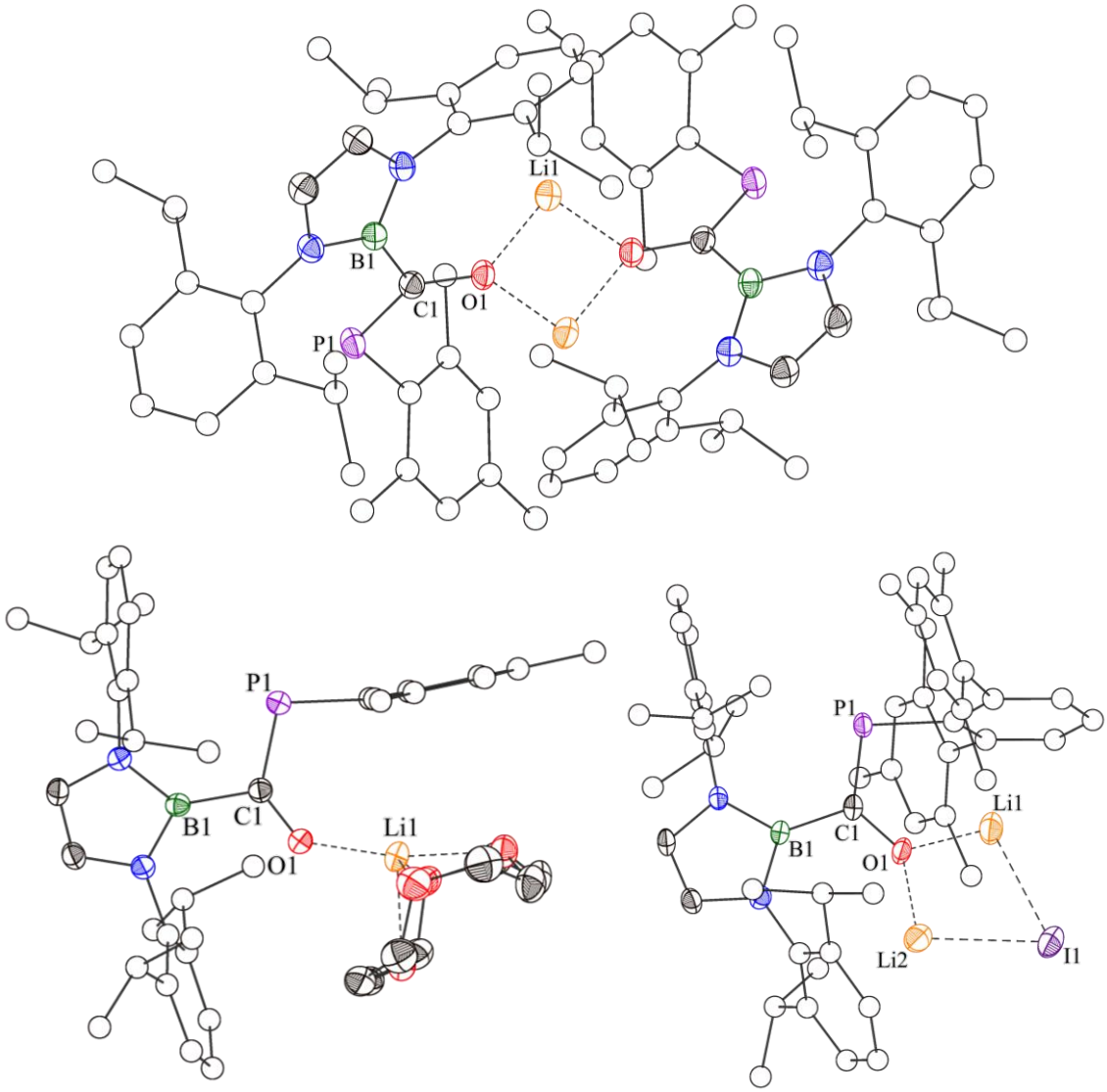

Figure 3.1. The solid state structures of **6b** (Top), **6c** (Left), **7** (Right). Anisotropic displacement ellipsoids are set at 50% probability. Hydrogen atoms omitted for clarity and aryl carbon atoms shown as spheres of arbitrary radius.

The core structure of the three structurally characterised phosphaalkenes are similar, with C–P bond lengths ranging from 1.727(3)–1.740(2) Å and C–O bonds ranging from 1.284(2)–1.330(3) Å. These distances are consistent with bond order between single and double bonds, with the sum of the covalent radii for C–P single and double bonds ranging from 1.86–1.69 and C–O between 1.38–1.24 Å.[7] This is consistent with the resonance structures outlined in Scheme 3.2 both contributing the electronic structure of these compounds. Increasing the steric requirement of the aryl substituent has little effect on the

core structure; **6b** and **6c** have comparable bond metrics to **7**. One of the more notable observations is that the addition of 12-crown-4 as a sequestering agent increases the double bond character of the C–O bond in **6** (1.318(3) in **6b** to 1.284(2) Å in **6c**).

The 1,3-aryl lithiation of **1** contrasts the previously reported reactivity of phosphaalkynes towards lithiated species which undergo 1,2-aryl lithiations. This transformation draws similarities to the dimerization observed in Chapter 2, in which a 1,2-boryl migration facilitates the transformation to the five-membered heterocycle **2**.

3.2.2. Further reactivity of compound 6a

Selective functionalisation of **6b** can be achieved through addition of hard or soft reagents. For example, addition of stoichiometric amounts of water to **6b** initially protonates the oxygen centre, affording [HOC[B]P(Mes)], **8a** (Scheme 3.3).

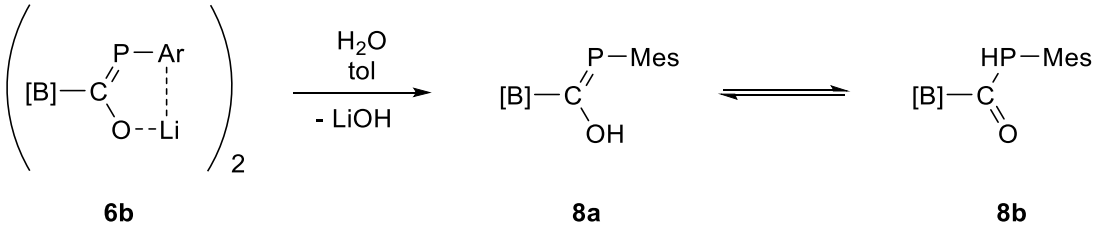

6b **8a** **8b**

Scheme 3.3. Reaction of **6b** with H_2O to yield **8**.

This species can be isolated as a pure compound if the work-up is completed within a few hours, however if left in solution an equilibrium is established between **8a** and its tautomeric acylphosphine [OC[B]P(Mes)H], **8b** (Figure 3.2). The rate of tautomerisation is dependent on the polarity of the solvent, in polar solvents such as pyridine the process is rapid and isolation of **8a** is not possible, while in non-polar toluene equilibrium is established at room temperature overnight. The isomers can be distinguished by their ^{31}P NMR resonances, with **8a** displaying a singlet resonance at 147.5 and **8b** at –29.0 ppm ($^1J_{P–H}$ = 240 Hz). These values are in good agreement with the gas phase DFT NMR

calculations for these species (141 and –17 ppm, respectively). DFT investigations predict the phosphine **8b** to be more thermodynamically stable than **8a** by only 0.7 kcal/mol, which falls within experimental error, suggesting that this transformation is energetically neutral. These calculations are consistent with the observation that, at equilibrium, equal amounts of each tautomer are present in solution.

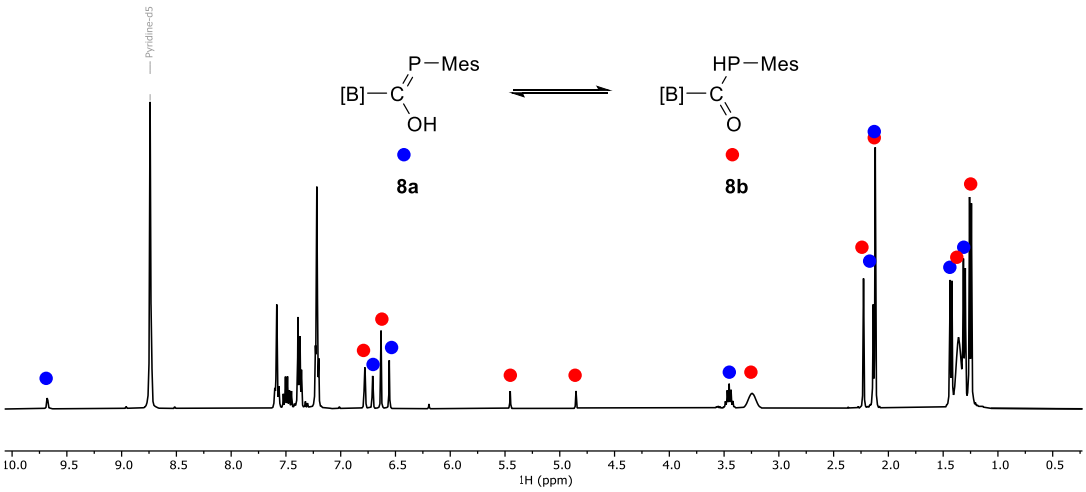

Figure 3.2. ^{1}H NMR (d_5-pyridine) spectrum of equilibrium between tautomers **8a** and **8b** with key regions assigned.

Compound **8a** arises from the phosphaalkene resonance structure (Scheme 3.2; **6ai**). Crystals of **8** were obtained by cooling a saturated hexane solution to –35°C. The solid state structure reveals a P1–C1 length with significant double bond character (1.699(2) Å) and a longer P1–C28 single bond (1.856 (2) Å), in addition to a short single C1–O1 bond (1.352(3) Å; the sum of the covalent radii for the constituent elements are 1.38 (single) and 1.24 (double) Å).[7] These bond lengths are consistent with protonation at the oxygen centre, corresponding to the kinetic product of this reaction, **8a**.

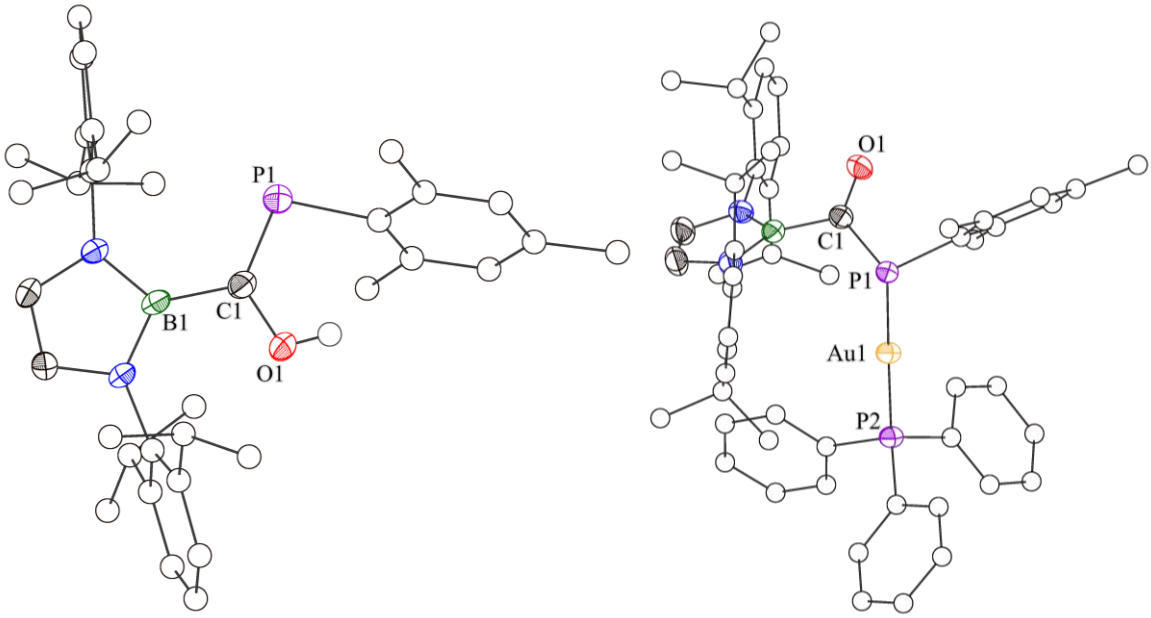

Figure 3.3. The solid state structure of **8a** (Left), **9** (Right). Anisotropic displacement ellipsoids are set at 50% probability. Hydrogen atoms omitted for clarity and non-core carbon atoms shown as spheres of arbitrary radius.

Examples of hydroxyl-phosphaalkenes are rare, a literature search found three examples of dialkyl-1-oylphosphines in reports from the group of Becker.[8] These species also exhibit keto-enol tautomerisation in solution (Scheme 3.4). Through variable temperature NMR the authors conclude the enol tautomer to be more stable by 1.0 kcal/mol in the case of R = *cyclo*-hexyl, comparable to the value calculated for our system (*cf.* 0.7 kcal/mol).

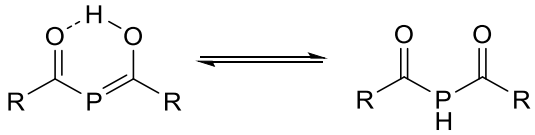

Scheme 3.4. Literature examples of hydroxylphosphaalkenes. R = Me, cyclo-hexyl, adamantyl

Softer electrophiles allow access to functionalisation at the phosphorus centre. This selectivity was demonstrated through the salt metathesis reaction between **6b** and (PPh_3)AuCl. Elimination of LiCl yields the stable gold complex [OC[B]P(Mes)Au(PPh_3)]

9 (Scheme 3.5). The $^{31}P\{^{1}H\}$ NMR spectrum features an AB spin system with doublet resonances at 50.3 and 44.0 ppm ($^{2}J_{P-P}$ = 145 Hz), while the ^{1}H NMR spectrum is consistent with a single boryl moiety.

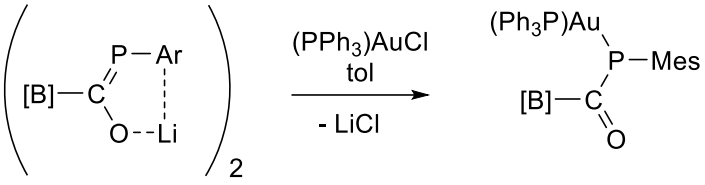

6b **9**

Scheme 3.5. The reaction of **6b** with chloro(triphenylphosphine)gold(I) to yield **9**.

Product **9** was crystallised by vapour diffusion of hexane into a toluene solution (Figure 3.3). The solid state structure reveals a linear gold atom (P–Au–P 175.86(3)°) with a slightly shorter bond to the triphenylphosphine substituent (Au1–P1 2.330(1), Au1–P2 2.307(1) Å). The two phosphorus carbon bonds in the acylphosphanido moiety are comparable in length (P1–C1 1.832(4), P1–C28 1.850(4) Å) with elongation of the P1–C1 in comparison to both the anionic precursor **6** and the hydroxyl-phosphaalkene **8**.

3.2.3. Synthesis of metallophosphaalkenes

The coordination chemistry of phosphaalkynes is dominated by the nucleophilicity of both the carbon-phosphorus π-bond and the lone pair at the phosphorus centre, allowing access to a wealth of coordination modes. To our knowledge, there have been no previous reports of metallo-organophosphorus complexes which exploit the relative positive dipole at the phosphorus centre. Encouraged by the aryl lithiation reactions described earlier, we set out to explore the reactivity of **1** towards the quintessential nucleophilic transition metal compound $Na[Cp^*Fe(CO)_2]$ (NaFp*, Cp* = pentamethylcyclopentadienyl).

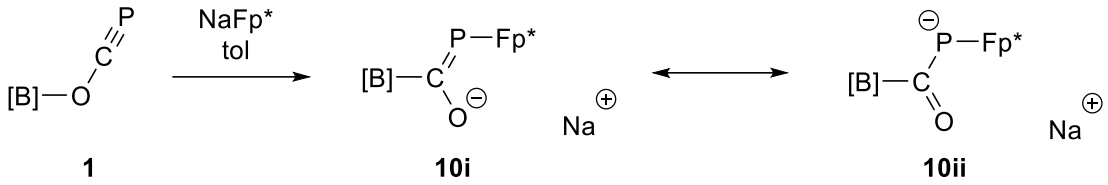

Scheme 3.6. Reaction of **1** with NaFp* to yield metallophosphaalkene **10**.

Addition of one equivalent of NaFp* to **1** affords the anionic metallopphosphaalkene {[B](NaO)C=PFp*}, **10** (Scheme 3.6). Upon addition of NaFp*, the solution immediately changed colour from yellow to red, accompanied by the appearance of a new singlet resonance in the $^{31}P\{^{1}H\}$ NMR spectrum at 188.6 ppm. The $^{13}C\{^{1}H\}$ NMR resonance corresponding to the central carbonyl carbon appears at 222.1 ppm, shifted to a higher frequency in comparison to the starting material, **1** (*cf.* 140.2 ppm).

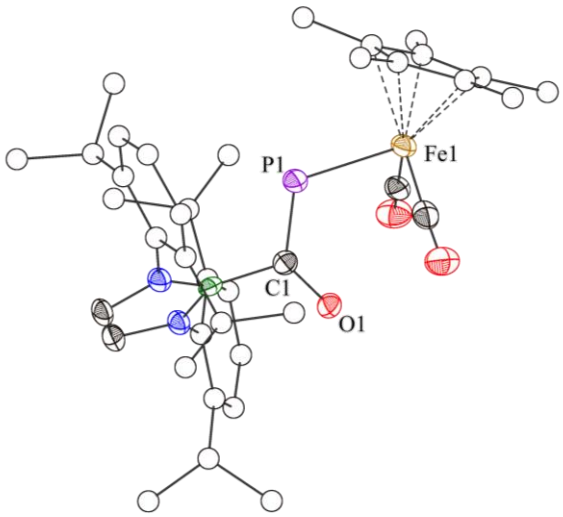

Figure 3.4. The solid state structure of anion **10**. Anisotropic displacement ellipsoids are set at 50% probability. Hydrogen atoms omitted for clarity and non-core carbon atoms shown as spheres of arbitrary radius.

Crystals of **10** suitable for X-ray diffraction studies were grown by slow evaporation of a toluene solution. The solid state structure reveals a tight ion pair featuring two distinct metallophosphaalkene moieties bridged by two sodium cations. For clarity the structural data for only one of the molecules will be discussed (Figure 3.4). The C=P bond in **10** is

significantly elongated (1.725(3) Å) relative to that of [B]OCP (1.545(2) Å). This distance falls between the values expected for a P–C single (1.86 Å) and double bond (1.69 Å). The sum of bond angles at the central carbon atom (359.8°) is consistent with a planar, formally sp^2 hybridised, carbon atom. As with the previously discussed lithium aryl product, **10** can be formally described as an anionic metallophosphaalkene with a formal negative charge on the oxygen atom (**10i**; Scheme 3.6.), or conversely as a phosphide bearing an acyl substituent (**10ii**). Again, further functionalisation can exploit either resonance structure dependent on the reagent employed, and in fact provides access to three phosphorus coordination modes, (σ^1-P)-, (σ^2-P)- and the serendipitous discovery of a cationic (σ^3-P)-Fp* complex.

Further functionalisation of metal complex **10** can be achieved by employing a salt metathesis strategy. Hard electrophiles, in this case chlorotrimethylsilane, functionalise the ligand at the oxygen centre yielding neutral metallophosphaalkene [B](Me$_3$SiO)C=PFp*), **11** (Scheme 3.7). The $^{31}P\{^1H\}$ NMR spectrum reveals a singlet resonance at 350.6 ppm, shifted to a higher frequency relative to **10** (*cf.* 188.6 ppm). A related species, ^{t}Bu(Me$_3$SiO)C=PFp*, exhibits a singlet resonance in its $^{31}P\{^1H\}$ NMR spectrum at 215.2 ppm.[9] The significant downfield shift observed for **11** can be attributed to the increased deshielding provided by the boryloxy functionality. Red crystals of **11** could be isolated in excellent yields (85%) from concentrated hexane solutions.

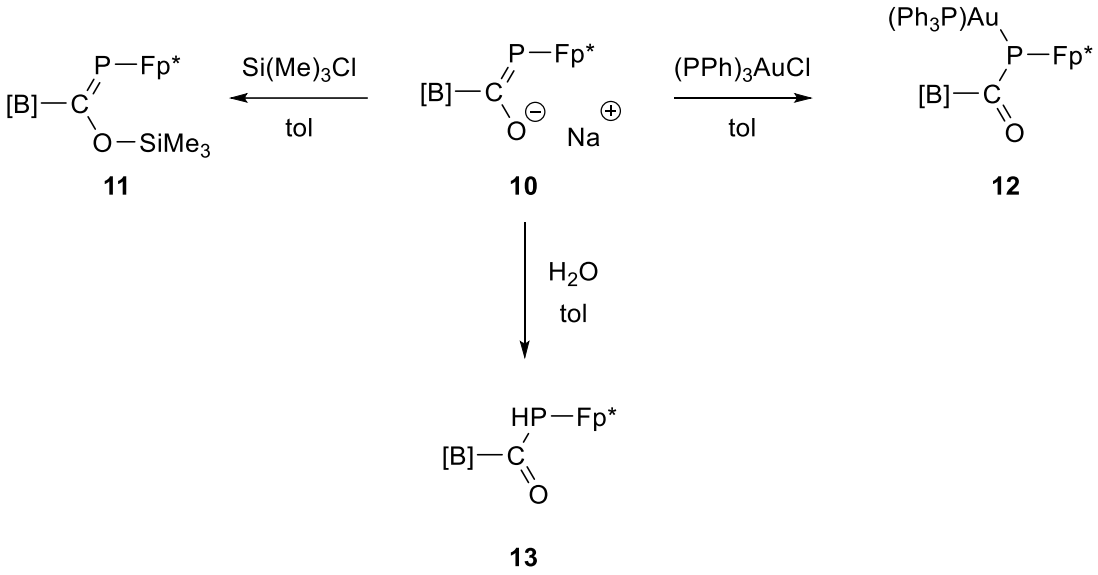

Scheme 3.7. Further reactivity of **10** with hard and soft electrophiles.

Structurally there is no significant change to the metallophosphalkene core of **10** upon silylation, with a modest contraction of the C–P bond in **11** (1.694(2); *cf.*1.725(3) Å in **10**), which is a result of increased localisation of electron density in the C–P π-bond. This contraction is accompanied by a shortening of the Fe–P bond on loss of any localised negative charge on the phosphorus atom (2.274(1); *cf.* 2.322(1) Å in **10**).

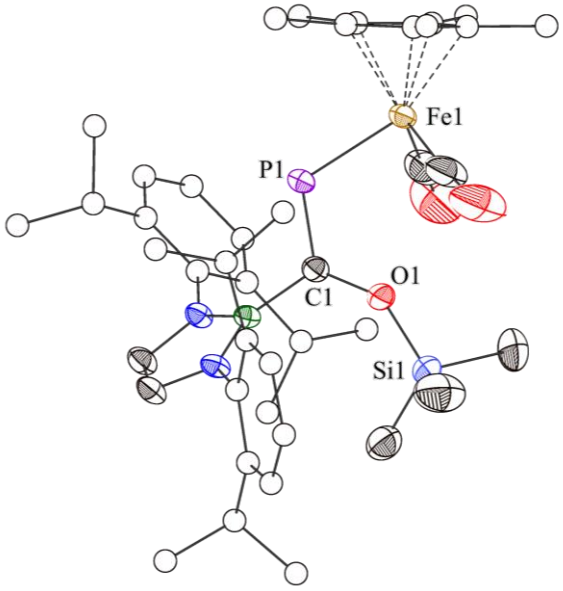

Figure 3.5. Molecular structure of **11.** Anisotropic displacement ellipsoids are set at 50% probability. Hydrogen atoms omitted for clarity and non-core carbon atoms shown as spheres of arbitrary radius.

If instead a soft electrophile is employed, such as triphenylphosphine gold chloride, functionalisation at the phosphorus can be achieved to yield heterobimetallic complex **12**. The $^{31}P\{^{1}H\}$ NMR spectrum exhibits two doublet resonances of equal intensity at 98.8 and 43.3 ppm ($^{2}J_{P-P}$ = 102.7 Hz), the former corresponds to the phosphide substituent, while the latter is due to the triphenylphosphine ligand. Crystallisation from a concentrated toluene solution afforded orange crystals of the linear gold(I) compound, **12**, in moderate yields (60%) (Figure 3.6).

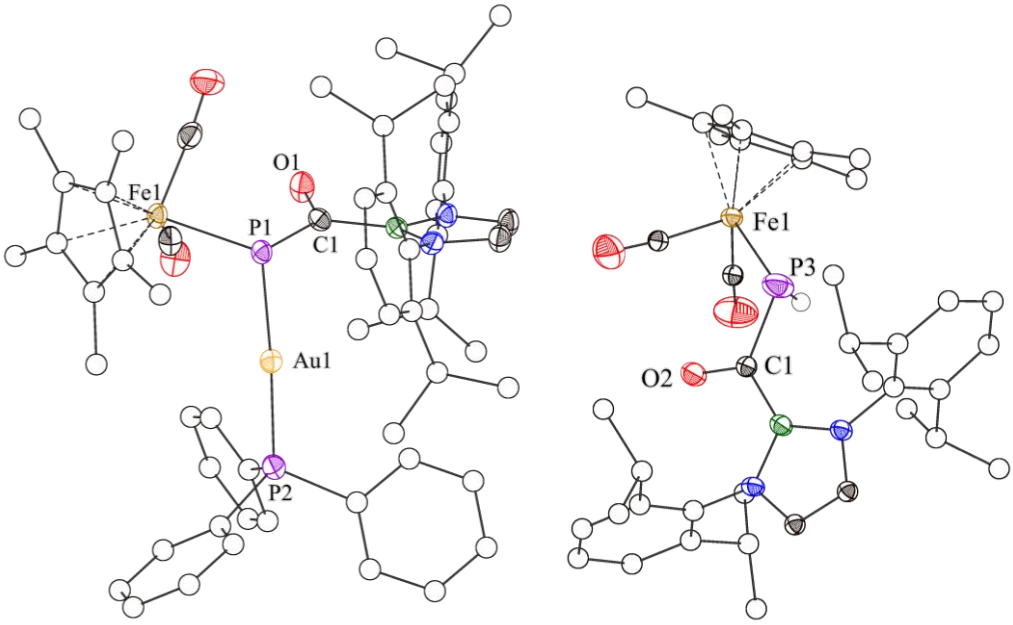

Figure 3.6. Molecular structures of **12** and **13**. Anisotropic displacement ellipsoids are set at 50% probability. Hydrogen atoms omitted for clarity and non-core carbon atoms shown as spheres of arbitrary radius.

The crystal structure of **12** confirms the presence of a linear gold(I) metal bonded to an anionic phosphido ligand and triphenylphosphine (P1–Au1–P2 175.51(4)°). There is significant lengthening of the C–P bond (1.846(4) Å; *cf.* 1.694(2) Å in **11**) in line with the value expected for a single bond. The gold–phosphorus bond distances are quite similar (Au1–P1 2.328(1) and Au1–P2 2.299(1) Å) with the bond to the triphenylphosphine substituent being somewhat shorter, presumably due to the presence of a stereochemically active lone-pair on the P{C(O)[B]}Fp*$^{-}$ substituent. Related gold(I) phosphane/phosphanido complexes, such as $(PPh_3)AuP(SnMe_3)_2$, have been found to exhibit comparable bond metrics with the bond to the phosphide functionality (2.320(1) Å) being slightly longer than that to the phosphine (2.293(1) Å).[10]

Interestingly, upon stoichiometric addition of water to **10** protonation occurs solely at the phosphorus centre to yield metallophosphide complex **13**. Contrasting the equilibrium between tautomers observed for species **8**, no such equilibrium is observed for this species.

The ^{31}P NMR spectrum displays a doublet resonance appearing at –8.98 ppm ($^{1}J_{P–H}$ = 198 Hz), collapsing to a singlet upon ^{1}H decoupling. Crystals can be obtained by cooling a hexane solution in moderate yields (43%). The solid state structure reveals a core phosphaalkene structure similar to that of **12** (Figure 3.6). The P1–C1 is elongated with respect to the starting material **10** (1.839(4) vs. 1.725(3) Å) and the C1–O1 bond contracted (1.242(5) vs. 1.315(3) Å), consistent with a formal single bond between the phosphorus and carbon and double bond between carbon and oxygen.

3.2.4. Attempts towards Fp*CP

In an effort to cleave the C1–O1 bond and generate a metal cyaphide complex (Fp*CP), we explored the further reactivity of **11**. Compound **11** bears some resemblance to the phosphaalkene precursors to phosphaalkynes, which thermally or catalytically release siloxane to yield phosphaalkynes (Scheme 3.8).[11] We sought to investigate if **11** thermally or catalytically release boranyloxysilane to yield Fp*CP.

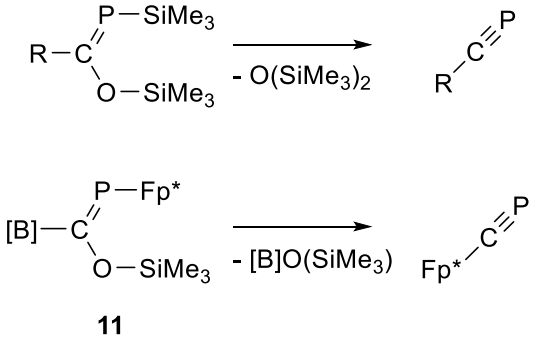

11

Scheme 3.8. Top: general procedure for phosphaalkyne synthesis. Bottom: Desired reactivity from compound **11**.

Thermal treatment of the metallophosphaalkene **11** showed no reactivity up to 120°C over several days. Addition of a catalytic amount of potassium *tert*-butoxide, a common catalyst for the conversion of phosphaalkenes to phosphaalkynes, showed small amounts of a new product formed which displayed a singlet resonance in the ^{31}P{^{1}H} NMR spectrum

at 178.3 ppm, however heating did not induce further conversion. When a stoichiometric amount of potassium *tert*-butoxide was employed quantitative formation of the new species could be observed by NMR spectroscopy, allowing for identification as potassium salt **14**. As this salt displays indistinguishable bond metrics to **10** it will not be discussed further.

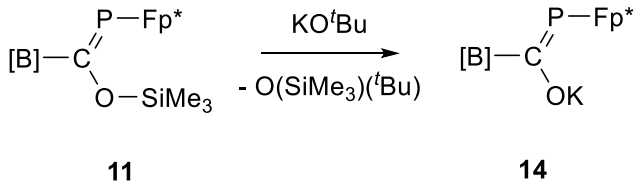

11 **14**

Scheme 3.9. Reactivity of **11** with potassium *tert*-butoxide to yield salt **14**.

An important feature of siloxane generation is the ability of the silicon centre to become hypervalent in the presence of KO^{t}Bu, allowing for the cleavage of the Si–E bond to form a stronger Si–O bond. The mechanism of this transformation has been investigated experimentally in a number of transformations, for example in C–H bond silylation catalysis, which highlights the importance of hypervalent five-coordinate intermediates.[12] Unfortunately, it seems [B] is less susceptible to this mechanism, perhaps due to the boron centre residing in a 6π aromatic ring, which reduces the Lewis acidity by occupying the typically vacant p-orbital. The steric protection provided by the Dipp groups may also prevent such reactivity.

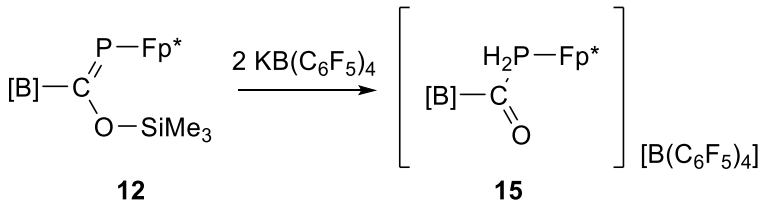

12 **15**

Scheme 3.10. Reactivity of **12** with potassium borate is yield **15**.

In a separate approach towards deoxygenation of Fp*CP, we hypothesised that an oxophilic Lewis acid may associate with the oxygen in **12** and facilitate bond cleavage.

Silylium cations ($[SiPh_3]^+$) were generated *in situ* through the reaction of chlorotriphenylsilane and potassium tetrakis(pentafluorophenyl)borate. In catalytic quantities, small amounts of a new product could be observed in the reaction mixture with a triplet ^{31}P resonance at –10.58 ppm ($^1J_{P–H}$ = 562.0 Hz), collapsing to a singlet upon ^1H decoupling. It was found that this product could be formed cleanly from the reaction of two equivalents of potassium tetrakis(pentafluorophenyl)borate and **11**, and was identified as a primary phosphine iron(II) complex {[B](O)C=P(H)$_2$Fp*}, **15**, in which the X-type (one electron donating) phosphaalkene ligand has undergone two protonations to yield an L-type (two electron donating) phosphine (Scheme 3.10). The source of the protons required for this formation remains unclear. However, during the reaction an oily substance is formed, we suspect polymerisation of the $SiMe_3$ cations generated by removal of the TMS group. Attempts were made to synthesise the triphenyl analogue of **12** in a similar fashion to deduce if the methyl groups were the source of these protons, however no reaction was observed, potentially due to the increased steric requirement of phenyl in comparison to methyl.

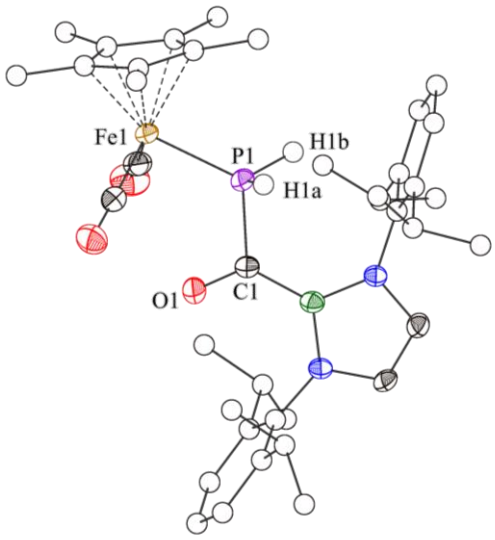

Figure 3.7. Molecular structure of **15.** Anisotropic displacement ellipsoids are set at 50% probability. Hydrogen atoms omitted for clarity and non-core carbon atoms shown as spheres of arbitrary radius.

Crystals suitable for X-ray diffraction studies of **15** can be obtained from concentrated toluene solutions in modest yields (38%). Once crystallised, the compound displayed diminished solubility in toluene, thus NMR characterisation was performed in THF. Compound **15** showed limited stability in THF and decomposed over the course of several hours, however a ^{31}P NMR resonance at –10.62 ppm (t, $^{1}J_{P–H}$= 352.0 Hz) could be identified, which further collapses to a singlet upon proton decoupling consistent with two proton substituents at the phosphorus centre. The ^{1}H and ^{19}F NMR are consistent with a single boryl and tris(pentafluorophenyl) environment, respectively.

The crystal structure reveals a Fe1–P1 bond length of 2.1709(10) Å, a significant contraction in comparison to **11** (2.2738(7) Å). The P1–C1 bond length is consistent with that of a single bond (1.915(4) Å), with concomitant contraction of the O1–C1 bond (1.217(5) Å). A summary of the bond parameters for the characterised metal complexes are summarised in Table 3.2.

Table 3. 2: Selected bond lengths [Å] and angles [°] for compounds **10**–**15**.

Bond distance (Å)	**10**	**11**	**12**	**13**	**15**
Fe1–P1	2.322(1)	2.2738(7)	2.3062(12)	2.2741(12)	2.1709(10)
P1–C1	1.725(3)	1.694(2)	1.846(4)	1.839(4)	1.915(4)
O1–C1	1.315(3)	1.381(3)	1.235(5)	1.242(5)	1.217(5)
C1–B1	1.578(4)	1.5568(3)	1.590(6)	1.593(6)	1.563(5)
Bond angle (˚)					
C1-P1-Fe1	111.03(9)	115.29(9)	107.89(14)	109.93(13)	116.57(12)

3.3. Neutral Nucleophiles: Isocyanides

The renaissance of phosphaethynolate chemistry brought on by the improved synthesis of PCO^- during 2012–2014 has led to a wealth of phosphaketenes, however there have only been three reports of p- and d-block phosphaethynolates. This limitation is somewhat expected, phosphaethynolates which display a particularly covalent E–O bond generate species with a localised C≡P π-bond, sacrificing a much stronger C=O double bond. For this reason, the ability to isolate a species such as **1** was quite surprising, especially after gas phase calculations revealed the phosphaketene to be more stable by 7.9 kcal/mol. As stated in Chapter 2, addition of most common Lewis bases to solutions of **1** results in dimerization into **2**. However, unexpected reactivity was observed with isocyanides (R–NC), electron rich carbon monoxide analogues. Isocyanides were found to induce isomerisation from the phosphaethynolate to the phosphaketene ([B]PCO) in catalytic loadings (in the case of ^{t}BuNC). While stoichiometric reactions with *tert*-butyl isocyanide (^{t}BuNC) and mesitylene isocyanide (MesNC) allowed for isolation of low valent phosphorus species from which a possible mechanism could be elucidated. We have also explored the reactivity of the generated phosphaketene [B]PCO, including an investigation into the photolytic decarbonylation. This section will initially focus on the stoichiometric reactions between **1** and isocyanides, and lead into the catalytic mechanism and subsequent phosphaketene chemistry.

3.3.1. Stoichiometric reactions

Addition of a stoichiometric amount of MesNC to **1** resulted in clean formation of a single product with a singlet resonance at –195.2 ppm in the $^{31}P\{^1H\}$ NMR spectrum after 24 hours, with no observation of any intermediates (Scheme 3.11).

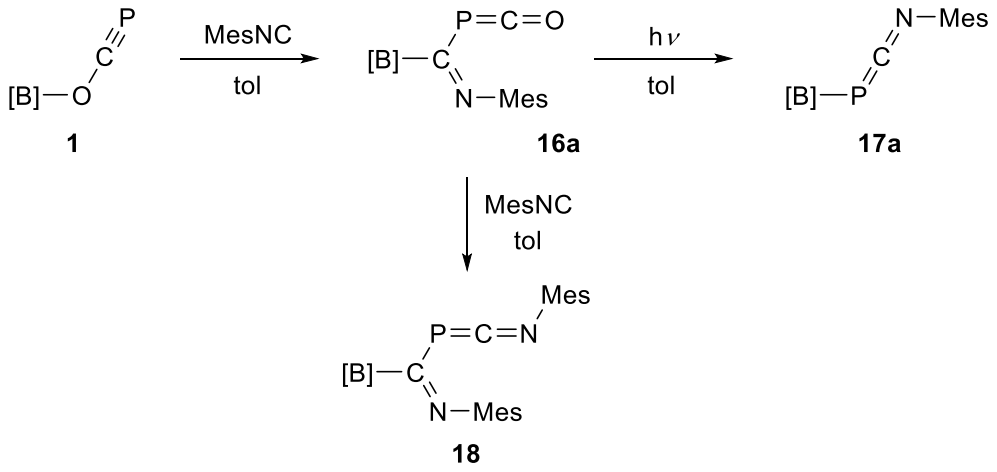

Scheme 3.11. Synthesis and further reactivity of phosphaketene **16a**.

Cooling the reaction mixture produced light orange crystals of **16a** in good yield (74%). The single crystal X-ray structure reveals the insertion of the isocyanide into the B–O bond of **1,** with concurrent isomerisation of the phosphaethynolate moiety from the phosphaethynolato to the phosphaketenyl bonding mode. The phosphaketene fragment is linear (P1-C1-O1 173.6(2)°) with a P–C distance of 1.670(2) Å and a C–O distance of 1.155(3) Å, these metrics are comparable to previously reported examples of phosphaketenes.

The outcome of this reaction implies that there is a nucleophilic attack of the isonitrile at the phosphorus centre of the OCP, in addition to a migration of the boryl group to the isocyanide carbon. The previous sections outlined similar boryl migrations induced by the attack of anionic nucleophiles at the phosphorus centre, however in this case isomerisation from the phosphaethynolate to the phosphaketene was induced.

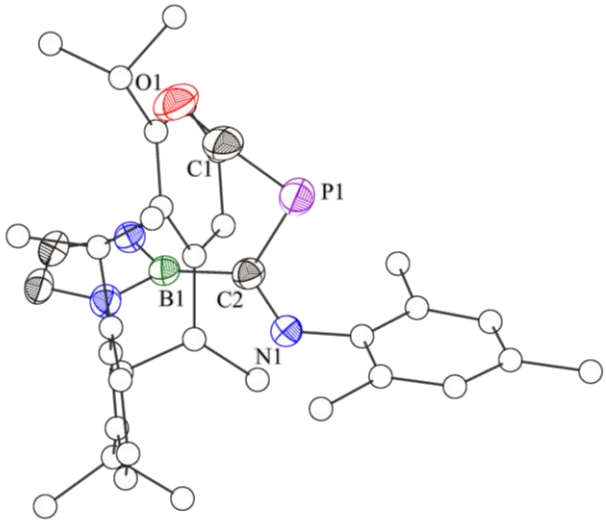

Figure 3.8. Molecular structure of **16a.** Anisotropic displacement ellipsoids are set at 50% probability. Hydrogen atoms omitted for clarity and non-core carbon atoms shown as spheres of arbitrary radius.

Compound **16a** can be decarbonylated either chemically or photolytically. The photolytic treatment of **16a** resulted in two products being observable in the $^{31}P\{^{1}H\}$ NMR spectrum, one at –262.6 ppm accompanied by an additional, unidentified product at 8.6 ppm. The former was identified through fractional crystallisation as the isocyanide-stabilised phosphinidene, **17a**, in which the boryl has migrated to the phosphorus centre with the loss of carbon monoxide (Scheme 3.11). Photolysis of phosphaketenes frequently induces decarbonylation to give heterocycles and diphosphenes, however to our knowledge base stabilised phosphinidenes have not been accessed *via* this method. A similar species can be synthesised using **1** and an excess of ^{t}BuNC without the need of photolysis. Three intermediates can be observed during this transformation, which will be discussed in detail later. The reaction reaches completion after 4 days, as indicated by a singlet resonance in the $^{31}P\{^{1}H\}$ NMR spectrum at –256.2 ppm (**17b**). The ^{1}H NMR displays resonances corresponding to the boryl backbone protons for **17a** and **17b** at 6.27 and 6.23 ppm, respectively, both with $^{4}J_{H-P} = 1.4$ Hz.

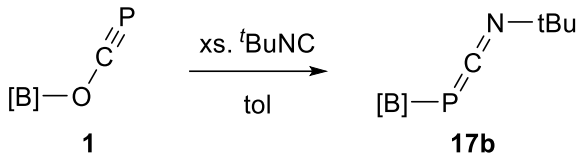

1 **17b**

Scheme 3.12. Synthesis of base stabilised phosphinidene **17b**.

17a and **17b** are structurally very similar, with a PCN core that is coplanar to the boryl ring (mean deviation from plane: 0.16 (**17a**) and 0.14 Å (**17b**)). The P–B and P–C bonds are 1.912(2)/1/916(3) and 1.674(2)/1.661(3) Å for **17a/b**. The former is in the range of a short single bond, the latter falls in the expected range of P=C double bond.

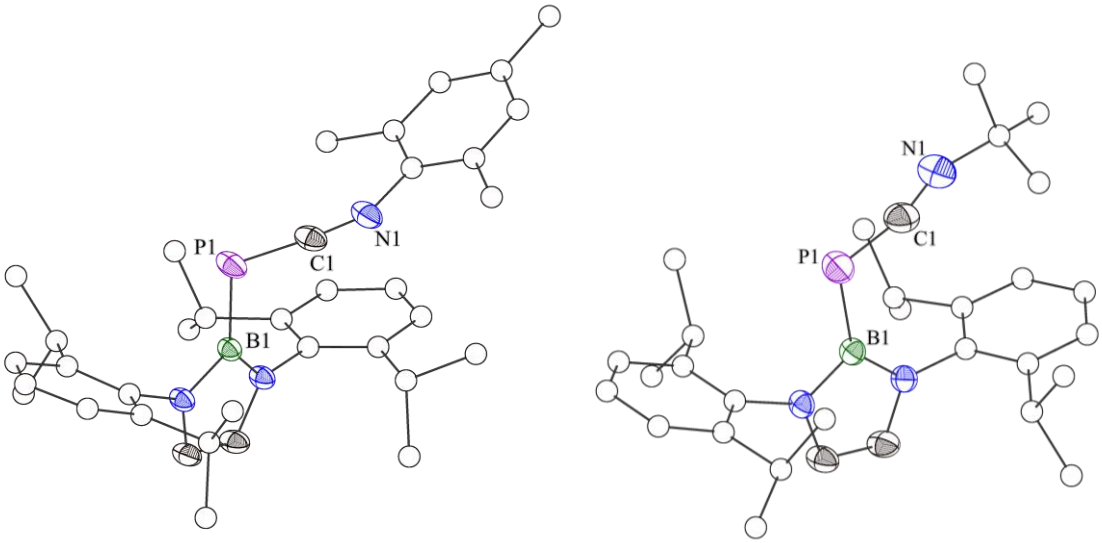

Figure 3.9. Molecular structure of **17a** and **17b.** Anisotropic displacement ellipsoids are set at 50% probability. Hydrogen atoms omitted for clarity and non-core carbon atoms shown as spheres of arbitrary radius.

Addition of a second equivalent of isocyanide to phosphaketene **16a** results in displacement of the carbon monoxide by MesNC, to yield base-stabilised phosphinidene **18**. The $^{31}P\{^{1}H\}$ NMR spectrum displays a singlet resonance at –136.1 ppm. Related chemodecarbonylation processes have been reported by the group of Bertrand, revealing that the phosphorus atom in phosphaketenes can act as a Lewis acid, allowing access to

ligand substitution reactions.[13] Crystals of **18** can be grown by cooling a saturated hexane solution in good yields (72 %).

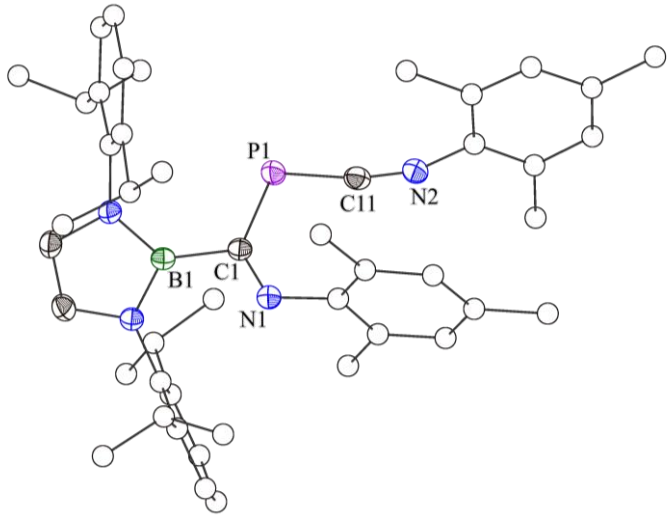

Figure 3.10. Molecular structure of **18.** Anisotropic displacement ellipsoids are set at 50% probability. Hydrogen atoms omitted for clarity and non-core carbon atoms shown as spheres of arbitrary radius.

Structurally **18** is related to **16a** and exhibits comparable bond metrics, with the exception of the B1-C2-P1-C1 dihedral angle which is inverted in **18** due to the increased steric requirement of the mesityl group (Figure 3.10). The C1–P1 bond is 1.841(2) Å, slightly shorter than that of **16a** (1.870(2) Å).

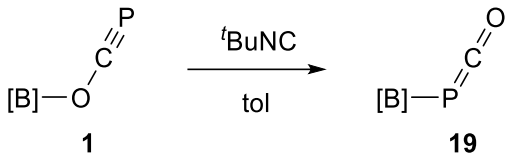

Scheme 3.13. Base induced isomerisation of phosphaethynolatoborane **1**.

The addition of a stoichiometric amount of ^{t}BuNC to **1** does not produce the ^{t}butyl analogue of **16**, but instead induces complete isomerisation to the linkage isomer of **1**, phosphaketene **19** (Scheme 3.13). This species displays a singlet resonance in the $^{31}P\{^{1}H\}$ NMR spectrum at –337.1 ppm, a significant upfield shift in comparison to the

phosphaethynolate (*cf.* –285.9 ppm). The phosphaketenyl carbon appears at 191.1 ppm (d, $^{1}J_{C–P}$ = 89.3 Hz) in the $^{13}C\{^{1}H\}$ NMR spectrum, the coupling constant being almost an order of magnitude higher than in that of the phosphaethynolate (*cf.* 140.2 ppm, d, $^{1}J_{C–P}$ = 17.6 Hz). This increase is due to a greater contribution from the phosphorus 3s orbital to the P–C bond in phosphaketenes in comparison to phosphaethynolates. The backbone protons display phosphorus coupling, appearing at 6.27 ppm ($^{4}J_{H–P}$ = 1.6 Hz), in the ^{1}H NMR spectrum. The product, [B]PCO **19**, could be crystallised by cooling a hexane solution in high yields (71%).

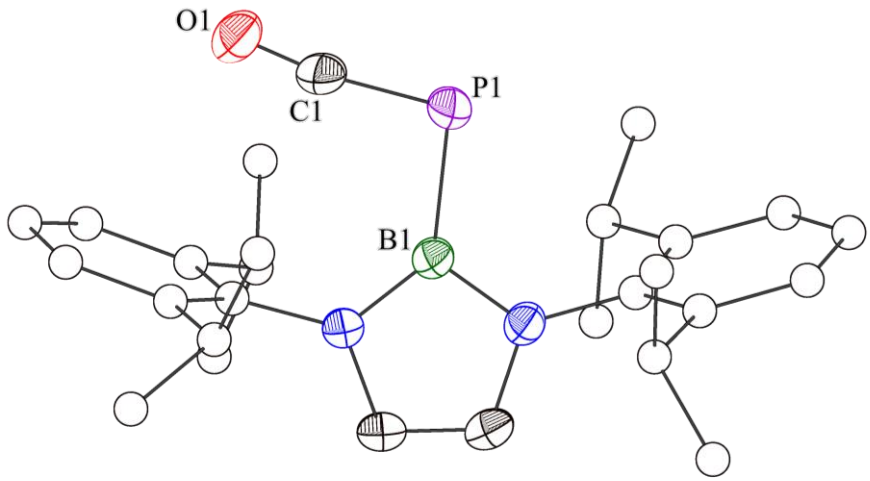

Figure 3.11. Molecular structure of **19.** Anisotropic displacement ellipsoids are set at 50% probability. Hydrogen atoms omitted for clarity and non-core carbon atoms shown as spheres of arbitrary radius.

The single crystal X-ray structure of **19** confirms the presence of a B–P bond with the phosphaketene moiety coplanar to the boryl ring (mean deviation from plane: 0.27 Å) (Figure 3.11). There is an elongation of the P–C bond in **19** relative to **1** (1.652(2) vs. 1.545(2) Å), and a concomitant shortening of the C–O bond (1.153(2) vs. 1.269(2) Å) consistent with an increased contribution from the phosphaketenyl resonance form placing formal double bonds between the three elements. At the time of writing, compounds **19** and

1 constitute the first structurally authenticated example of linkage isomers of the phosphaethynolate anion.

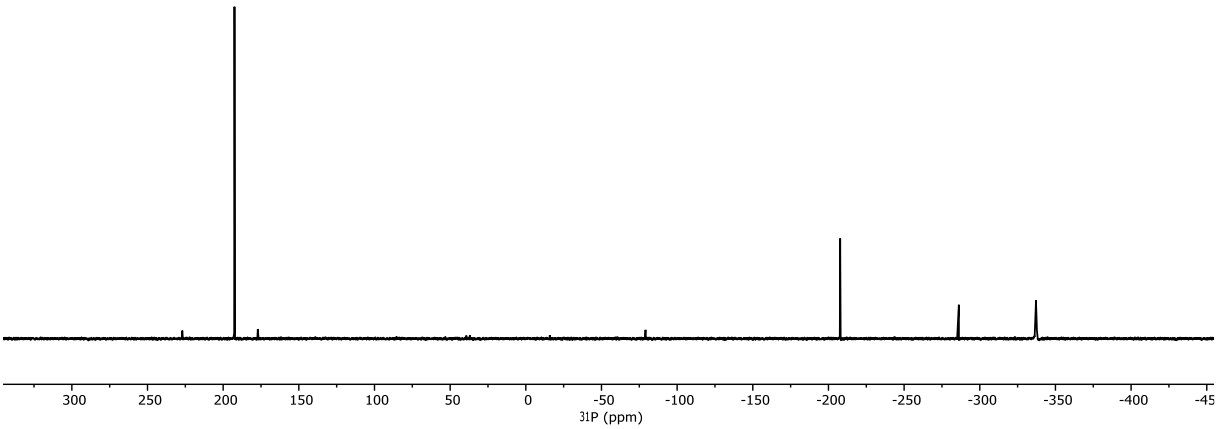

Figure 3.12. *In situ* $^{31}P\{^{1}H\}$ NMR spectrum (C_6D_6) of reaction mixture upon addition of ^{t}BuNC to **1**.

Monitoring this stoichiometric reaction by $^{31}P\{^{1}H\}$ NMR gives some insight into possible intermediates. Upon addition of ^{t}BuNC the solution turns bright purple and two main intermediates can be observed with singlet resonances at –207.8 ppm and 192.5 ppm (Figure 3.12). The former resonance can be attributed to **16b**, the ^{t}Butyl analogue of **16a** (*cf.* ^{31}P NMR δ = –195.2 ppm). The experimental ^{31}P NMR shift is in good agreement with the gas phase NMR calculation of –196 ppm. We were unable to find a satisfactory candidate for the resonance at 192.5 ppm, despite computing a range of possible intermediates. The bright purple colour encouraged us to monitor the reaction by UV/vis spectroscopy, allowing us to observe a species with an absorbance in the expected region for such a colour, around 560 nm (Figure 3.13). While this did allow us to conduct TDDFT calculations on proposed isomers, we were unable to find a species likely responsible for either this UV absorption or the $^{31}P\{^{1}H\}$ NMR shift. It is worth noting that the enolate-type species generated from the reaction of **1** with anionic nucleophiles, as outlined in Section 3.2, exhibit $^{31}P\{^{1}H\}$ NMR shifts similar to that observed for the intermediary species (for

example **10**, $^{31}P\{^{1}H\}$ NMR δ = 188.6 ppm); the analogous neutral species was considered, however the calculated ^{31}P NMR shift (–51 ppm) did not match that observed experimentally, nor did the calculated absorption spectra.

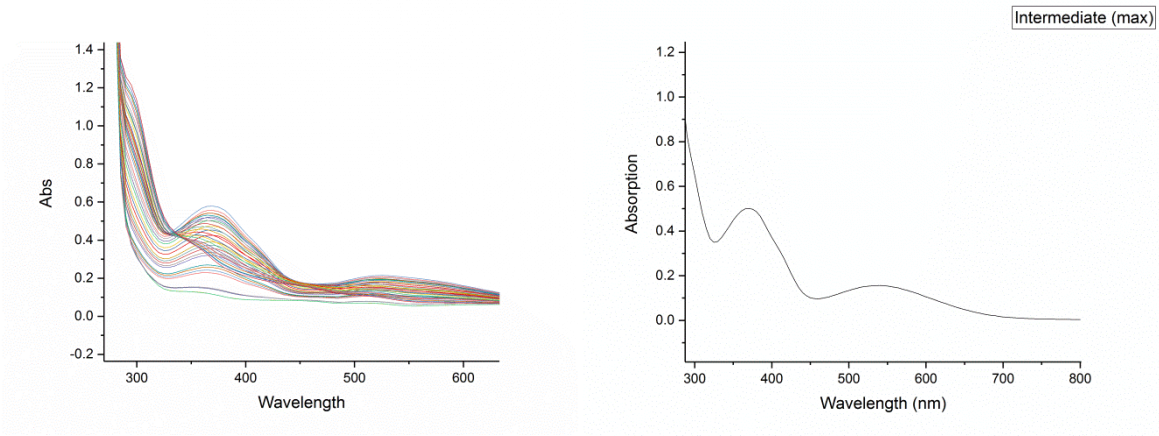

Figure 3.13. Left: Reaction monitoring using UV/vis absorption spectra. Right: Maximum intensity of intermediate with absorption around 550 nm.

3.3.2. Catalysis

The lack of integration of isocyanide into the final product prompted us to explore this process catalytically; with 10 mol% *tert*-butyl isocyanide loading the reaction (Scheme 3.13) went to completion within 24 hours. It is worth noting that catalytic amounts of mesityl isocyanide did not induce isomerisation, only small amounts of species **16** and starting material were observed in solution even after prolonged heating. Cyanide salts were also explored, however no reactivity was observed between either NaCN or $[Et_4N]CN$ and **1**.

3.3.3. DFT calculations

We turned to DFT investigation to map out key regions of the free-energy hypersurface. The calculations were performed by Professor John McGrady and Mauricio Portiolli Franco. Initially, optimisation of **1**, **16**, and **19** were performed using the M06-L functional. In all cases the structural parameters were found to be in good agreement with

the crystallographic data. **19** was found to be more stable than **1** by 10.0 kcal/mol, in agreement with previous calculations at the PBE1PBE level (6.5 kcal/mol, see Chapter 2), however of greater magnitude.

The isocyanide substituent was reduced to a model, HNC. The summary of the free-energy hypersurface between the transformations is shown in Figure 3.14. It was possible to locate a transition state that directly connects the two linkage isomers **1** and **19** (**TS1**, red line). The transition state displays an elongated B–O bond (1.84 Å), resulting in the phosphaethynolato carbon centre moving to within bonding distance of the boron (1.72 Å) to offset the loss of electron density caused by breaking the B–O bond.

In the transition structure, the B–O bond is substantially lengthened compared to **1** (1.84 Å vs. 1.41 Å) while the central carbon atom of the OCP unit approaches within bonding distance of the boron centre (1.72 Å vs. 2.40 Å in **1** and 2.70 Å in **5**) to offset the loss of electron density from the breaking B–O bond. The energy of this transition state lies 33.0 kcal/mol above **1**, consistent with the lack of isomerisation in solution even upon heating solutions for prolonged periods. The initial approach of HNC dictates the energy of the transition, a number of approaches were investigated with the lowest transition state connecting **1** and **16** having an energy of 19.1 kcal/mol (**TS2**, black line). ^{HNC}**16** can convert to **19** by a further transition (**TS3**), from which the HNC is extruded, which has a barrier of 12.9 kcal/mol, comparable in energy to **TS2**. Both **TS2** and **TS3** involve near-tetrahedral boron centres. Overall, it is possible to map out the conversion of **1** to **19** through the intermediate **16** by following the black path.

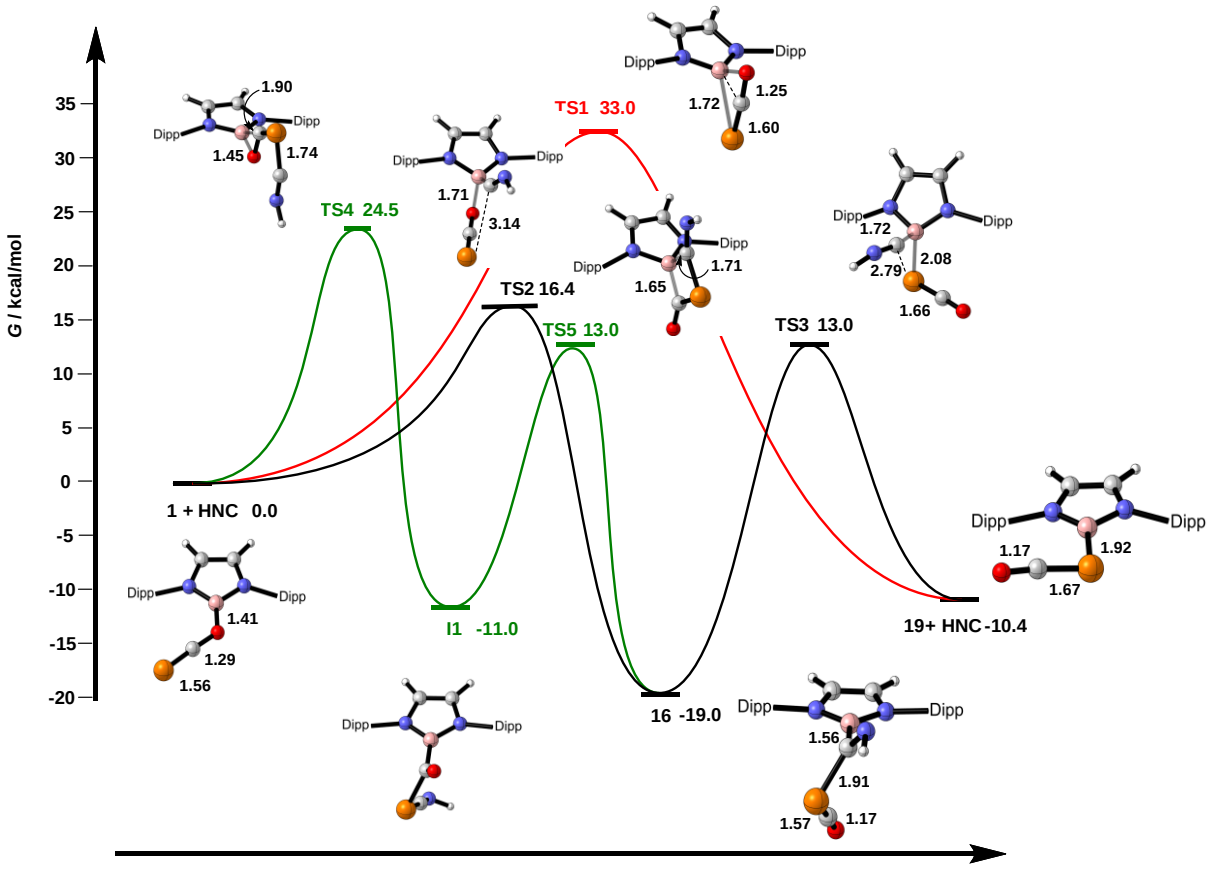

Figure 3.14. Free energy surface of key regions involved in conversion between linkage isomers **1** and **19**.

It can be seen from the model system that **19** is exergonic with respect to **16** (ΔG = 9.1 kcal/mol). This energy difference is sensitive the substituent on the base, by re-optimising the structures with either ^{t}Bu or Mes yields structures comparable to the model system, however the steric requirement destabilises **16** relative to **19** and **TS3**. With ^{t}BuNC, the overall transformation becomes slightly endergonic (+1.0 kcal/mol) and the barrier is reduced to 27.0 kcal/mol. The similarity in energy between ^{tBu}**16** and **19** + ^{t}BuNC results in sensitivity to concentration, with stoichiometric or lower loadings favouring **19**. If instead MesNC is used, the destabilising effect on ^{Mes}**16** is less severe and **19** remains 5.0 kcal/mol lower in energy, with an associated barrier of 34.9 kcal/mol for the transformation. These

energy profiles compliment the empirical data; the linkage isomer **19** is only accessible when employing ^{t}BuNC.

While the model isonitrile ligand is bound to the boron centre in both transition states (**TS2** and **TS3**) we have never located a stable minimum where it remains bound. The role of the isocyanide is to labilise the B–O bond by interaction with the boron centre only in the transition state. If we consider the outcome of the reaction with anionic nucleophiles, such as Fp^{*-} or Mes^{-}, which yield isolable enolates with the carbon centre of the phosphaethynolate moiety bound to the boron, we must also account for the size of the nucleophile and the role of the cation. We are not able to isolate or observe the analogous ketones upon addition of isonitriles as they would require a substantial separation of charge, provided in the former examples by the mobile cations. It is possible to compute a route to such a species (**I1**, green) by allowing HNC to approach the phosphorus centre of **1**. The transition state in this case (**TS4**) involves a four-coordinate boron bonding to both the carbon and oxygen of the phosphaethynolate, and has a barrier of 24.4 kcal/mol. This value is comparable to **TS2** and it is unclear as to why we do not observe this species spectroscopically, however it may be due to rapid conversion to its linkage isomer **16**, for which a transition state (**TS5**) could be computed, again involving a four-coordinate boron within a four-membered heterocycle, with an associated barrier of 23.9 kcal/mol.

The importance of the mobile cation in the transformation of **1** with NaFp* is further emphasized through reaction of **1** with the isoelectronic $[Co(Cp)(CO)_2]$, an example of a classic neutral nucleophilic metal complex. The term nucleophilic is used in this case due to its ability to perform formal oxidative addition reactions, without ligand dissociation, starting from an 18 valence electron configuration (for example with methyl iodide).[14] **1** shows no reactivity towards $[Co(Cp)(CO)_2]$ even at elevated temperatures, while reacts rapidly with NaFp* under ambient conditions. This is likely due to the cation stabilising

the negative charge, resulting in a lower barrier for conversion (Figure 3.14; **TS4**), in addition to stabilising the resultant enolate.

3.3.4. Further reactivity of [B]PCO

Next, we sought to explore the further reactivity of the phosphaketene **19**, the first isolable boron-substituted phosphaketene. In an attempt to isolate a terminal phosphinidene, [B]–P, **19** was photolyzed in a benzene solution. The $^{31}P\{^{1}H\}$ NMR spectrum of the reaction mixture reveals the formation of a single product with a singlet resonance at 596.2 ppm. The $^{11}B\{^{1}H\}$ and ^{1}H NMR spectra are consistent with a single boryl functionality. This data is consistent with the formation of diphosphene, [B]PP[B], **20**. Crystals suitable for X-ray diffraction studies were grown by cooling a saturated hexane solution in good yields (68%).

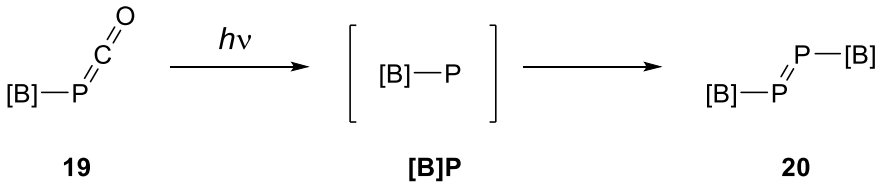

Scheme 3.14. Decarbonylation of **19** to **20** via intermediate phosphinidene.

The crystal structure reveals a diphosphene with a P–P distance of 2.027(1) Å, in line with the expected distance for a P–P double bond (2.04 Å). These metrics are indistinguishable from a closely related boryl-substituted diphosphene reported by Yamashita and coworkers.[15] The only difference between the two systems is saturation at the boryl backbone.

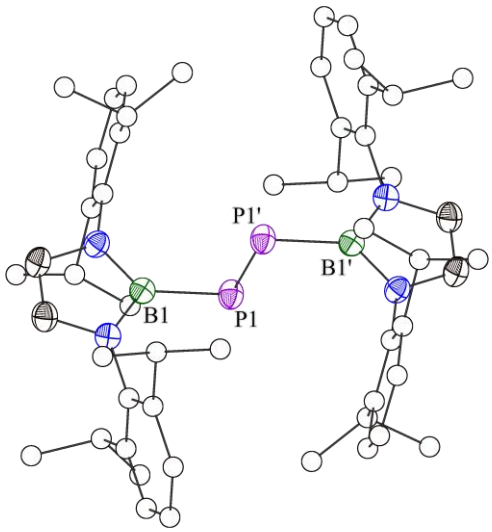

Figure 3.15. Molecular structure of **20.** Anisotropic displacement ellipsoids are set at 50% probability. Hydrogen atoms omitted for clarity and non-core carbon atoms shown as spheres of arbitrary radius.

The Bertrand group previously reported an example of a phosphaphosphinidene stabilised by significant steric bulk.[16] This species exists in the singlet state due to π-donation of the adjacent lone pair of the phosphorus into a vacant p-orbital of the phosphinidene (Figure 3.16). In the case of our expected phosphinidene, the boron does not have the requisite lone pair for donation and as such we would expect a transient triplet phosphinidene during the transformation of **19** to **20** with electrons occupying two orthogonal p-orbitals. Such species have been proposed as intermediates in a number of phosphaketene decarbonylation processes; however have never been observed spectroscopically.

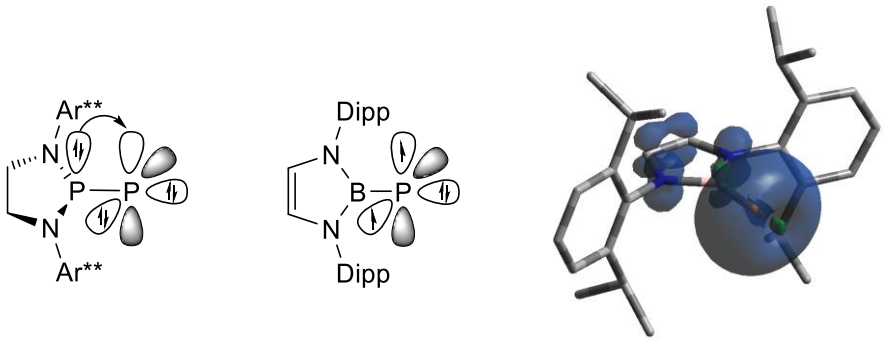

Figure 3.16. Left: Stabilising effect of Bertrand's singlet phosphinidene. Middle: Expected triplet state of **[B]P**. Right: Calculated spin-orbital density plot of **[B]P** (Mulliken spin densities: ρα−β(P) = 1.79 electrons, ρα−β(B) = –0.12 electrons).

We aimed to observe the triplet phosphinidene, **[B]P**, using EPR spectroscopy. Generation of **[B]P** from the photolysis of **19** resulted in the expected EPR signal at X-band (9.4 GHz) in the 1.15 to 1.25 Tesla field range characteristic of molecular oxygen, in fact during our early experiments we were also able to observe molecular oxygen leaking into the Young's tap EPR tube due to the vacuum generated at 5 K (Figure 3.17; b). Following this, we adjusted the reaction conditions, increasing the temperature to 30 K and flame sealing the EPR tube. Monitoring the photolysis using UV/vis spectroscopy at various time points identified an absorption in the spectra of **19** around 360 nm which was not present in **20**. As such, we used a 355 nm laser for the subsequent experiments, targeting only **19**. The calculated spin density plot of **[B]P** shows spin localisation over the p-orbitals of the phosphorus centre, the product of two orthogonal SOMOs (Figure 3.16).

As shown in Figure 3.17, the EPR signal obtained after experiment optimisation may be simulated with an axial zero-field splitting parameter, *D*, of 4 cm^{-1} and an orthorhombic parameter, *E*, of 3.7 × 10^{-3} cm^{-1} and hyperfine coupling of the electrons and ^{31}P nucleus, A(^{31}P)iso = 300 MHz. These values are in close agreement with a prior report of zero-field splitting parameters D = 4.116 cm^{-1}, E = 4 x 10^{-3} cm^{-1}, and hyperfine interactions

A_x,A_y(^{31}P) = 269, 356 MHz, respectively, for the related triplet mesitylphosphinidene reported by Akimov and co-workers.[17]

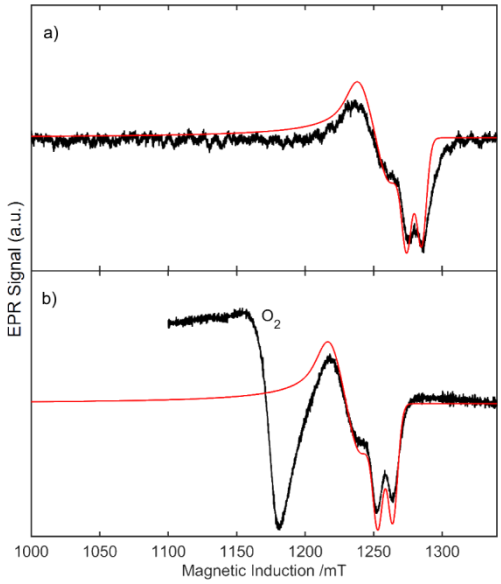

Figure 3.17. X-band EPR of **19** under two photolytic conditions with EPR simulations shown in red and the data is in black. In panel a., the temperature was 30 K with a flame-sealed sample and a pulsed LASER was used. In panel b., the temperature was 5 K with a J. Young sample tube and a xenon arc lamp was used.

The P–P bond of the diphosphene **20** could be cleaved by heating in the presence of N-heterocyclic carbene 1,3-diisopropyl-4,5-dimethyl-1H-imidazol-3-ium-2-ide (Scheme 3.15). Heating overnight reveals the presence of a new product in the ^{31}P{^{1}H} NMR spectrum with a singlet resonance at –196.7 ppm. This species was only stable for short periods, and upon isolation begins to convert to an unidentified product with a resonance at –245.0 ppm in the ^{31}P{^{1}H} NMR spectra. If the work up performed quickly it is possible to crystallise the product in reasonable yields (35%).

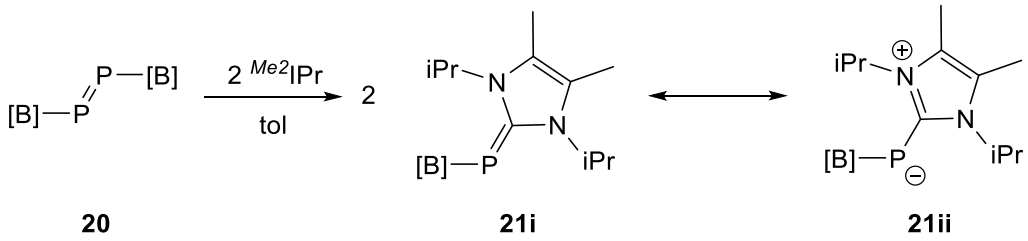

Scheme 3.15. Cleavage of a P=P double bond utilising an NHC.

Contrasting the related alkene analogues, relatively little is known about the cleavage of phosphorus double bonds. The first example of such a transformation was reported by Cowley and co-workers, who found facile cleavage of an aryl substituted diphosphene was possible upon oxidation with elemental sulphur.[18] The group of Stephan also reported Lewis acid bond cleavage through addition of gold chloride to vinyl-substituted diphosphenes which resulted in intramolecular C–P bond formation to yield heterocyclic species.[19] Matsuo and co-workers recently reported the first example of using a carbene to cleave a diphosphene bond into its constituent base stabilised phosphinidenes.[20]

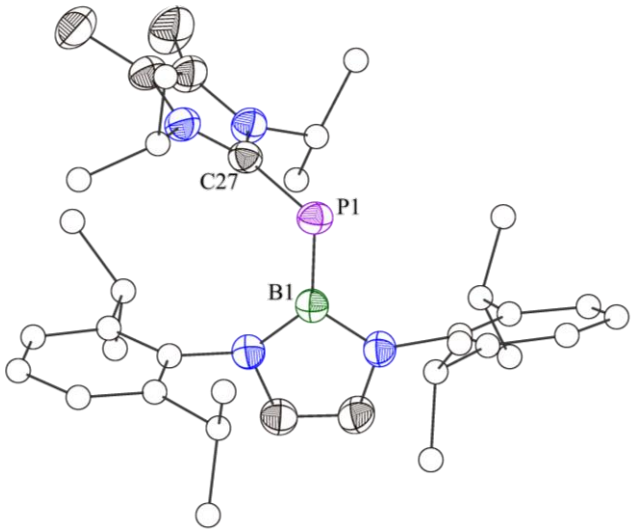

Figure 3.18. Molecular structure of **21.** Anisotropic displacement ellipsoids are set at 50% probability. Hydrogen atoms omitted for clarity and non-core carbon atoms shown as spheres of arbitrary radius.

The solid state structure reveals a P–C bond distance of 1.805(3) Å, lying between what is expected for a single (1.86 Å) and double (1.77 Å) bond (Figure 3.18). Similarly, the B–P distance is consistent with a shorter than usual single bond (1.892(3) Å), indicating some π-donation into the aromatic boryl ring. A resonance structure for the compound can be drawn in which a formal negative charge is placed on the phosphorus centre, with a single bond between the phosphorus and carbon. This rationalisation justifies both the intermediary P–C bond distance observed, as well as the upfield ^{31}P NMR shift (–196.72 ppm).

In an effort to chemically induce the decarbonylation of [B]PCO, in an analogous fashion to utilising ^{t}BuNC, NHC ^{Me2}IPr was added to a toluene solution of **19**. The ^{31}P{^{1}H} NMR spectrum of the reaction mixture reveals a single product AB spin system with resonances at 90.6 and – 22.5 ppm ($^{1}J_{P–P}$ = 191.0 Hz). The ^{1}H and ^{11}B{^{1}H} NMR spectra are consistent with the presence of two distinct boryl environments. Crystals suitable for X-ray diffraction studies were grown from a concentrated hexane solution.

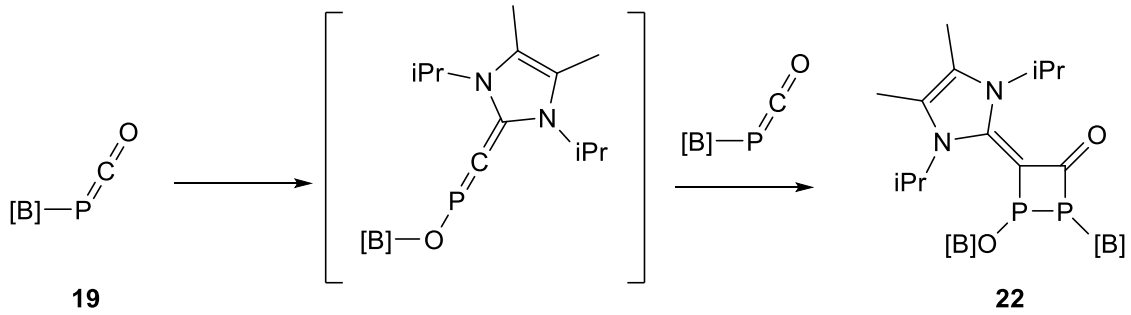

Scheme 3.16. Carbene induced cyclisation of phosphaketene **19** to yield **22**.

The solid state structure of **22** reveals a cyclic four membered core which can be rationalised as the [2+2] cycloaddition product of [B]OPC^{Me2}IPr and [B]PCO (Scheme 3.16). Such phosphorus containing fulminate analogues are not without precedent, related species have previously been reported from reactions of phosphaketenes, such as

Ph_3SiPCO, with NHCs.[21,22] These examples yield monomeric species due to increased steric bulk on the NHC nitrogen-substituents which prevents the additional cyclisation. The cyclic core of **22** is unusual, however is related to diphosphacyclobutenonyl ligand reported by Scheer and co-workers.[23]

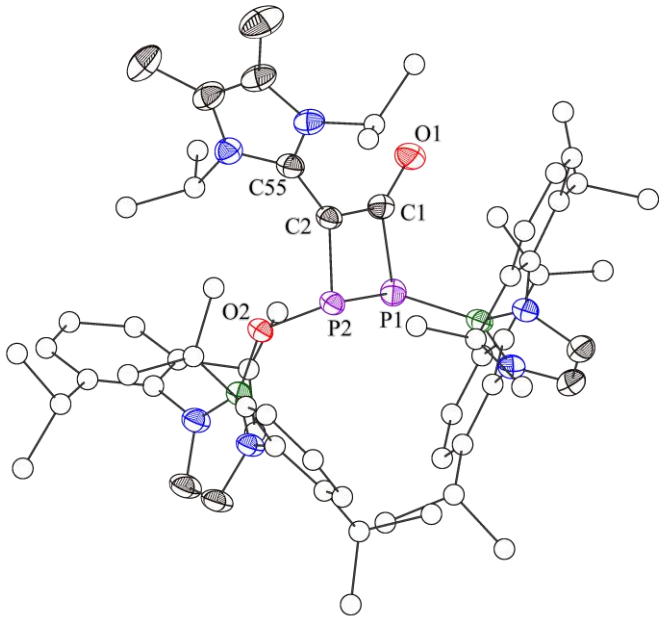

Figure 3.19. Molecular structure of **22.** Anisotropic displacement ellipsoids are set at 50% probability. Hydrogen atoms omitted for clarity and non-core carbon atoms shown as spheres of arbitrary radius.

3.4. Conclusion

We have described a novel route to phosphaalkenes and metallophosphaalkenes by exploiting the electrophilic character of a unique phosphaalkyne. In general, addition of anionic nucleophiles to **1** induces boryl migration from the oxygen to the carbon atom in [B]OCP. These species can be further functionalised to yield several phosphaalkenes, phosphines, and a number of metal complexes including (σ^1-P)-, (σ^2-P)- and (σ^3-P)-phosphorus based ligands, allowing for analysis of the different bonding modes. We have also shown that ^{t}BuNC can induce isomerization of the phosphaethynolatoborane to its

linkage isomer, [B]PCO. The isomerization mechanism was probed using stoichiometric reactions with MesNC and ^{t}BuNC, allowing for isolation of possible intermediates, in addition to DFT calculations. The [B]PCO can be chemically or photolytically decarbonylated yielding a base stabilised phosphinidene and diphosphene, respectively. The photolytic treatment was found to go via a transient triplet phosphinidene intermediate.

3.5. References

[1] A. M. Arif, A. R. Barron, A. H. Cowley, S. W. Hall, *J. Chem. Soc. Chem. Commun.* **1988**, 171–172.

[2] D. E. Hibbs, C. Jones, A. F. Richards, *J. Chem. Soc. - Dalt. Trans.* **1999**, *0*, 3531–3532.

[3] C. Jones, A. F. Richards, *J. Organomet. Chem.* **2002**, *645*, 256–261.

[4] S. Ito, H. Sugiyama, M. Yoshifuji, *Chem. Commun.* **2002**, *2*, 1744–1745.

[5] M. Regitz, *Chem. Rev.* **1990**, *90*, 191–213.

[6] L. Liu, J. Zhou, Y. Kim, L. L. Cao, D. W. Stephan, *Dalton Trans.* **2019**, *48*, 14242–14245.

[7] P. Pyykkö, M. Atsumi, *Chem. Eur. J.* **2009**, *15*, 12770–12779.

[8] G. Becker, M. Schmidt, W. Schwarz, M. Westerhausen, *ZAAC - J. Inorg. Gen. Chem.* **1992**, *608*, 33–42.

[9] D. Gudat, E. Niecke, A. M. Arif, A. H. Cowley, S. Quashie, *Organometallics* **1986**, *5*, 593–595.

[10] C. C. Cummins, C. Huang, T. J. Miller, M. W. Reintinger, J. M. Stauber, I. Tannou, D. Tofan, A. Toubaei, A. Velian, G. Wu, *Inorg. Chem.* **2014**, *53*, 3678–3687.

[11] J. F. Nixon, *Endeavour* **1991**, *15*, 49–57.

[12] W. B. Liu, D. P. Schuman, Y. F. Yang, A. A. Toutov, Y. Liang, H. F. T. Klare, N. Nesnas, M. Oestreich, D. G. Blackmond, S. C. Virgil, et al., *J. Am. Chem. Soc.* **2017**, *139*, 6867–6879.

[13] M. Joost, W. J. Transue, C. C. Cummins, *Chem. Commun.* **2017**, *53*, 10731–10733.

[14] A. J. Hart-Davis, W. A. G. Graham, *Inorg. Chem.* **1970**, *9*, 2658–2663.

[15] S. suke Asami, M. Okamoto, K. Suzuki, M. Yamashita, *Angew. Chem. Int. Ed.* **2016**, *55*, 12827–12831.

[16] L. Liu, D. A. Ruiz, D. Munz, G. Bertrand, *Chem.* **2016**, *1*, 147–153.

[17] A. V. Akimov, Y. S. Ganushevich, D. V. Korchagin, V. A. Miluykov, E. Y. Misochko, *Angew. Chem. Int. Ed.* **2017**, *56*, 7944–7947.

[18] A. H. Cowley, M. Pakulski, *Tetrahedron Lett.* **1984**, *25*, 2125–2126.

[19] L. L. Liu, L. L. Cao, J. Zhou, D. W. Stephan, *Angew. Chem. Int. Ed.* **2019**, *58*, 273–277.

[20] N. Hayakawa, K. Sadamori, S. Tsujimoto, M. Hatanaka, T. Wakabayashi, T. Matsuo, *Angew. Chem. Int. Ed.* **2017**, *56*, 5765–5769.

[21] Z. Li, X. Chen, Z. Benkö, L. Liu, D. A. Ruiz, J. L. Peltier, G. Bertrand, C. Y. Su, H. Grützmacher, *Angew. Chem. Int. Ed.* **2016**, *55*, 6018–6022.

[22] Z. Li, X. Chen, Y. Li, C. Y. Su, H. Grützmacher, *Chem. Commun.* **2016**, *52*, 11343–11346.

[23] M. Scheer, D. Himmel, B. P. Johnson, C. Kuntz, M. Schiffer, *Angew. Chem. Int. Ed.* **2007**, *46*, 3971–3975.

Chapter 4
Nucleophilic reactivity of a phosphaethynolatoborane

4.1 Introduction and objectives

4.1.1 Coordination chemistry of phosphaalkynes and phosphaethynolates

The reactivity of the C≡P triple bond in phosphaalkynes is more closely related to that of alkynes than to nitriles (R–C≡N). This is due to the reverse polarity of the carbon–pnictogen bond, i.e. $^{\delta-}C{\equiv}P^{\delta+}$ vs. $^{\delta+}C{\equiv}N^{\delta-}$.[1] The increased electron density at the carbon centre of phosphaalkynes has been investigated using electron density distribution maps and verified experimentally by reaction with electrophiles (H^+, NO_2^+ or $MeCO^+$), where attack at the carbon atom is observed, in contrast to nitriles where electrophilic attack occurs at the nitrogen atom.[2] This reverse dipole also has a profound effect on the coordination chemistry of phosphaalkynes where end-on coordination is disfavoured in lieu of η^2-type ligation though the π-manifold.[3] η^1-Coordination can be achieved by employing ligands that provide equatorial steric bulk and an axial binding pocket (Figure 4.1; **A**–**E**).[4–7] Examples of monomeric complexes in which phosphaalkynes bind in an η^1- or η^2-coordination mode are relatively rare due their propensity to oligomerize at metal centres. The first reported example of such reactivity was the head-to-head [2+2] cyclization of ^{t}BuCP in the coordination sphere of cobalt, rhodium and iridium to yield 1,2-diphosphacyclobutadienes (Figure 4.1; **F**).[8,9] Since then, numerous examples of metal-mediated oligomerization reactions of phosphaalkynes have been reported giving rise to dimers, trimers, tetramers and pentamers.[4,10,11]

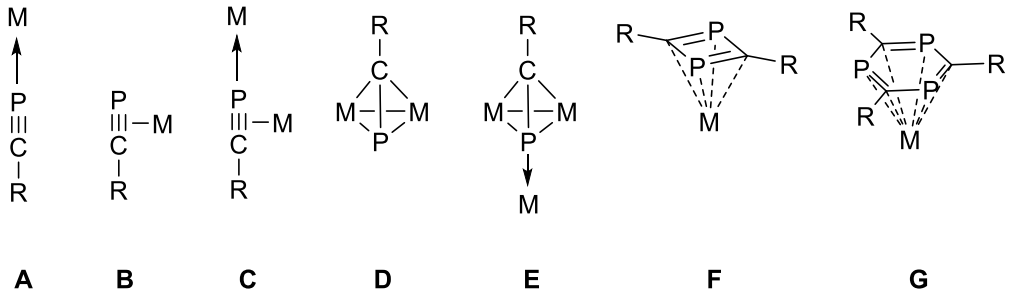

Figure 4.1. Common coordination modes of phosphaalkynes.

The coordination chemistry of phosphaethynolates, due to their paucity, has been less well developed. The only reported phosphaethynolate coordination complex is the heterobimetallic thorium complex (amid)$_3$Th(μ-η^1(O):η^2(C,P)-OCP)Ni(COD) (amid = *N*,*N*′-bis-(trimethylsilyl)benzamidinate, COD = cyclooctadiene) (Scheme 4.1).[12] In solution this compound was found to be in equilibrium with its constituent parts.

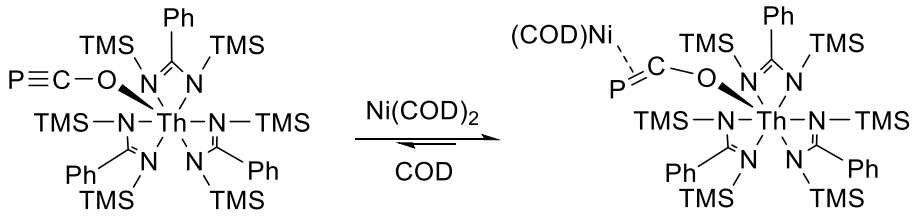

Scheme 4.1. Phosphaethynolate coordination complex (amid)$_3$Th(μ-η^1(O):η^2(C,P)-OCP)Ni(COD) (amid = *N*,*N*′-bis- (trimethylsilyl)benzamidinate, COD = cyclooctadiene).

4.1.2 Elementoboration Chemistry of Phosphaalkynes

Elementoboration, in which E–B (E = H, C) bonds are added across unsaturated C–E′ (E′ = C, N, O, etc.) bonds, has drawn widespread utility in organic synthesis since its initial development by H.C. Brown in the 1950s.[13] Typically these transformations rely on transition-metal catalysts, which have been developed to give stereo- and regio-chemical control over the products generated.[14] Catalyst-free elemento-boration reactions are less common however, and can be achieved by employing more reactive substrates. Wrackmeyer and co-workers developed a 1,1-carboboration reaction by allowing neutral alkenyl substituted acetylenes, i.e. trimethylstannylacetylene, to react with trialkylboranes. They

found that silyl, germyl, and plumbyl substituted acetylenes displayed increasing activity while moving down the group.[15] Metal-free alkynes can also undergo 1,1-carboborations with highly Lewis acidic boranes, in particular tris(pentafluorophenyl)borane (BCF) and related R–B(C_6F_5)$_2$ reagents.[16,17] The proposed mechanism involves an initial 1,2-carboboration across the unsaturated bond, followed by a 1,2-migration of the alkynyl substituent, resulting in the 1,1-carboboration product in the majority of cases. The migrating alkynyl group can include phosphorus, sulphur and boron containing substituents as well as terminal alkynes in which a hydrogen atom migrates.[18] It should be noted that alkyl and aryl substituted alkynes tend not to react with BCF at ambient temperature, however 1,1-carboboration can be achieved under forcing conditions. For example, 4-octyne reacts with BCF at 110°C to yield the *cis* and *trans* 1,1-carboborated products.[18]

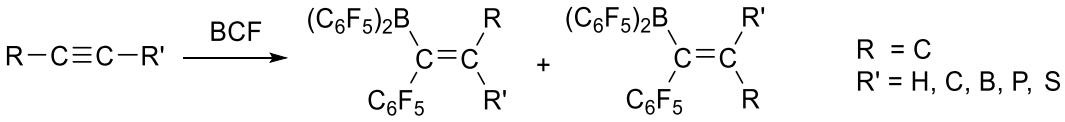

Scheme 4.2. General reactivity of alkynes with tris(pentafluorophenyl)borane.

Hydroboration is one of the most effective means of functionalizing carbon–carbon multiple bonds due to the development of palladium cross coupling reactions allowing for controlled functionalisation at boron substituted sites.[14] As such, it has garnered a considerable amount of interest in organic chemistry, resulting in significant development over the past decades. For simple substrates, the parent borane, BH_3, is a suitable reagent for such transformations. However, the poor regio- and diastereoselectivity of this compound has resulted in the development of more selective reagents, such as catecholborane (HBCat), 9-borabicyclo(3.3.1)nonane (9-BBN), 4,4,5,5-tetramethyl-1,3,2-dioxaborolane (HBPin), and bis(pentafluorophenyl)borane (Piers' borane).[19] As with carboboration, the more Lewis acidic the boron centre the greater the reactivity in hydroboration reactions. Typically, 1,2-hydroboration occurs across carbon–carbon multiple bonds, with regioselective control

attainable through tuning the steric and electronic properties of the alkynyl/alkenyl substituents (Scheme 4.3).

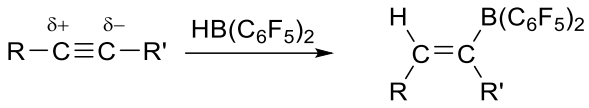

Scheme 4.3. General reactivity of alkynes towards Piers' borane. R = alkyl, aryl. R' = alkyl, aryl.

Despite its widespread development in organic chemistry, elementoboration in main-group inorganic chemistry is still in its infancy. The hydroboration of phosphaalkynes was first reported by Arbuzov and co-workers, who achieved the double hydroboration of ^{t}BuCP with HBCat yielding a gem-diboryl substituted primary phosphine (Scheme 4.4).[20] This work was expanded by the group of Stephan, who utilised Pier's borane to mono-hydroborate ^{t}BuCP and AdCP to their respective phosphaalkenylboranes.[21] Interestingly, the primary report gives the expected regiochemistry for addition across a polarised $^{\delta-}$C≡P$^{\delta+}$ bond, with protonation occurring at the more positive phosphorus centre. However, a latter report describes the synthesis of the inverse product, with protonation occurring at the carbon centre. The authors attribute this to the steric requirement of both reagents preventing addition of the bulky –B(C_6F_5)$_2$ group at the carbon centre.

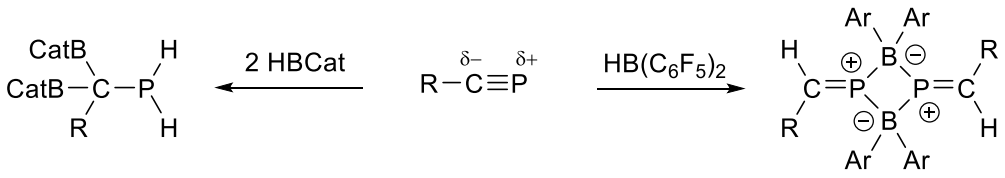

Scheme 4.4. Previously reported examples of hydroboration of phosphaalkynes. R = ^{t}Bu. Ar = C_6F_5.

To our knowledge only one example of the carboboration of phosphaalkynes has been reported. Martin and co-workers reported the insertion of AdCP into 9-phenyl-9-borafluorene resulting in a seven-membered 1,3-boraphosphaalkene (Scheme 4.5).[22]

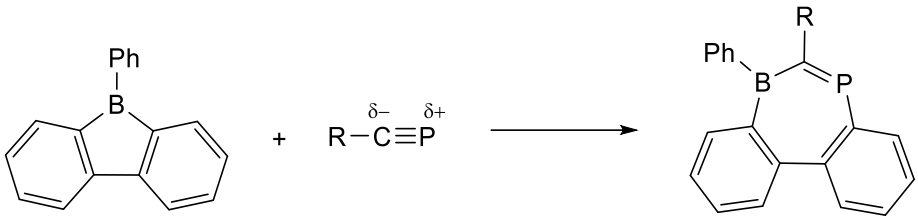

Scheme 4.5. Insertion of phosphaalkyne into 9-phenyl-9-borafluorene. R = adamantyl.

In Chapter 2 we outlined the increased energy of the HOMO of **1** with respect to ^{t}BuCP, which should allow access to nucleophilic reactivity hitherto inaccessible to phosphaalkynes. We also have an interest in exploring the elementoboration chemistry of **1** due to the inherent oxaphilicity of the boron reagents employed, potentially allowing access to O–C bond cleavage reactions.

4.1.3 Objectives

This chapter will explore the reactivity of phosphaethynolatoborane as a nucleophile. The first section will investigate the reductive dimerization of **1** in the coordination sphere of [Ni(COD)$_2$]. The chapter will then outline the synthesis of unusual tungsten carbonyl complexes which display solution phase isomerisation that was investigated using CPMAS and solution-phase NMR techniques.

The latter half of this chapter will focus on the behaviour of [B]OCP towards boranes, namely 9-BBN and tris(pentafluorophenyl)borane. Upon reaction with BCF varied reactivity towards [B]OCP and its linkage isomer [B]PCO was observed, with carboboration reactions allowing access to three constitutional isomers of the same compound.

4.2 Nickel coordination chemistry

4.2.1 Synthesis of a diphosphacyclobutadiene analogue

Preliminary investigations into the coordination chemistry of [B]OCP were performed. Upon reaction with $[Ni(COD)_2]$ (COD = cyclooctadiene) with **1**, the C≡P bond reacted with half an equivalent of the late transition metal complex to afford the dimerized η^4-1,3-diphosphacyclobutadiene complex $[([B]OCP)_2Ni(COD)]$ (Scheme 4.6). This dimerization is akin to the coordination chemistry of ^{t}BuCP, which has been reported to undergo such [2+2] cycloadditions at a range of metal centers (Co, Rh, Ir, Fe, Mo).[8,9] It is also possible to achieve a *bis*-diphosphacyclobutadiene nickel complex with ^{t}BuCP through *in situ* reduction of $Ni(acac)_2$ (acac = acetyl acetonate), which acts a nickel source.[23] The analogous reaction with the previously reported thorium phosphaethynolate and $[Ni(COD)_2]$ results in η^2-coordination through the C≡P π-manifold.[12]

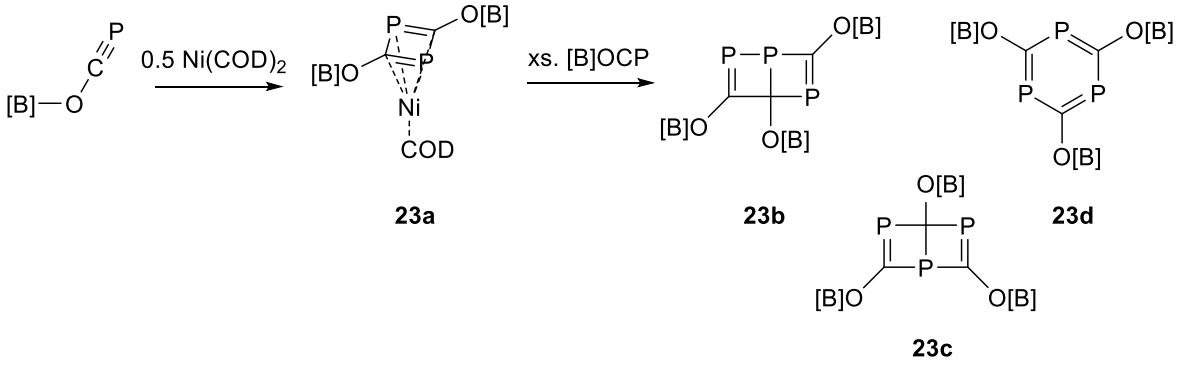

Scheme 4.6. Reductive coupling of **1** in the coordination sphere of nickel.

Single crystal X-ray diffraction analysis of **23a** reveals a slightly bent $[P(CO[B])]_2$ moiety (dihedral CPPC angle = 170.8(2)°). The C–P bond lengths are elongated with respect to the starting material, 1.803(2) and 1.814(2) Å (cf. 1.545(2) Å) due reduction of the bond order and donation of electron density from the Ni centre into a P–C π* antibonding orbital.

The Ni–C and Ni–P distances are 2.043(4) and 2.303(3) Å, respectively, comparable to those of the related [Ni((^{t}Bu)$_2$C$_2$P$_2$)$_2$] (average bond lengths 2.079 and 2.251 Å).

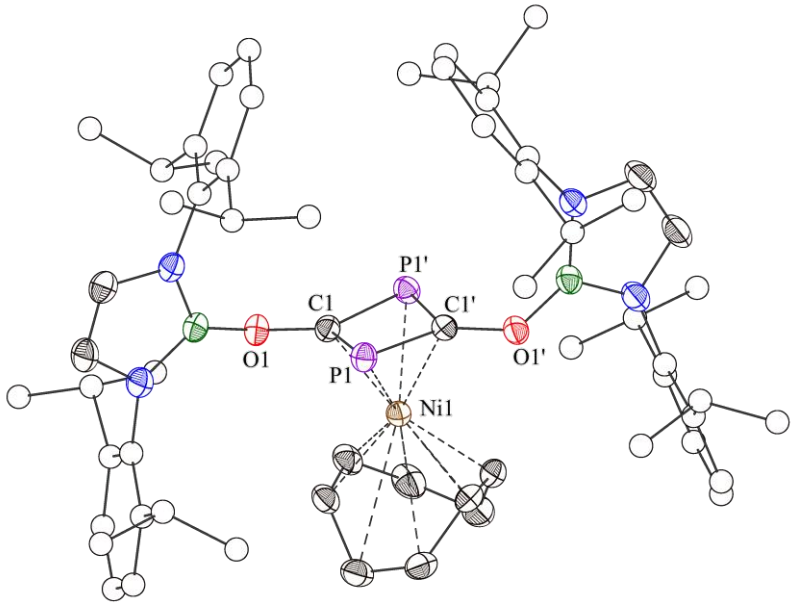

Figure 4.2. Solid state structure of **23a**. Anisotropic displacement ellipsoids are set at 50% probability. Hydrogen atoms omitted for clarity and Dipp carbon atoms shown as spheres of arbitrary radius.

Attempts were made to synthesise the sandwich complex, bis-(diphosphacyclobutadiene)nickel, by heating a solution of **23a** with an excess of **1**. After 12 hours of heating at 80 °C complete consumption of the starting material was observed. However, the products of this reaction evaded isolation. The ^{31}P{^{1}H} NMR spectra were characteristic of Dewar triphosphabenzenes **23a** and **23b**, and triphosphabenzene **23c**, with an ABX spin system corresponding to the asymmetrical **23c** with resonances at 294.6 (dd, $J_{P–P}$= 557, 49 Hz), 263.9 (dd, $J_{P–P}$ = 557, 32 Hz), and 218.3 ppm (dd, $J_{P–P}$ = 49, 32 Hz) and an AB spin system corresponding to the symmetrical **23b** at 277.5 (d, $^2J_{P–P}$ = 19 Hz), 137.6 ppm (t, $^2J_{P–P}$ = 19 Hz) (Scheme 4.6).

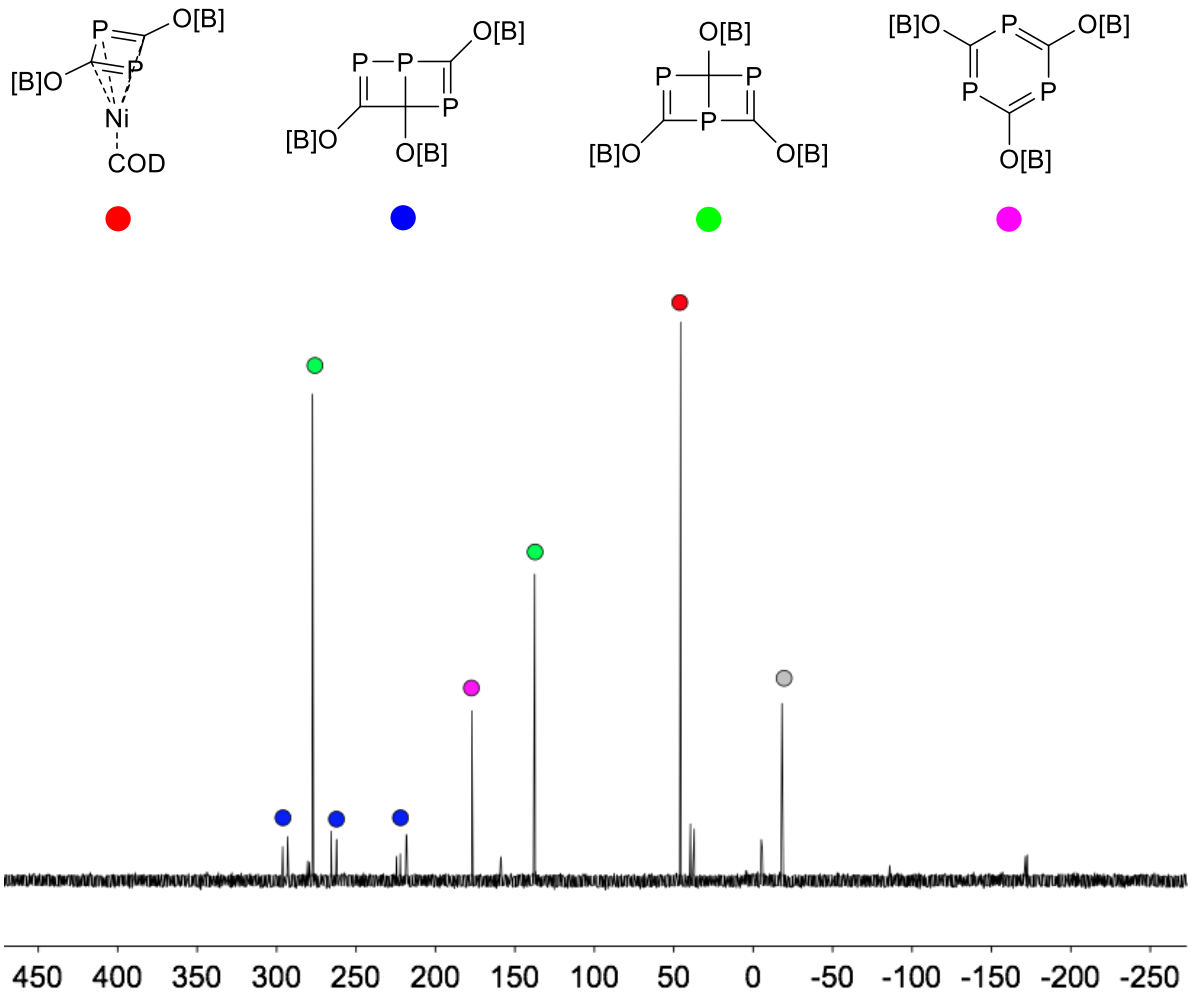

Figure 4.3. ^{31}P NMR spectrum (C_6D_6) of reaction mixture after heating **23a** with an excess of **1.**

The Grützmacher group have reported a catalytic, regioselective trimerization of triphenylphosphaalkyne to Dewar triphosphabenzenes using a Ni(0) complex.[24] The resulting Dewar triphosphabenzene has comparable shifts to those observed for **23c** with resonances in the ^{31}P{^{1}H} NMR spectrum at 346.4 (d, $^{2}J_{P-P}$ = 36 Hz), and 86.0 ppm (t, $^{2}J_{P-P}$ = 36 Hz). Thermal treatment of Dewar triphosphabenzenes results in rearrangement to triphosphabenzenes, reported by Binger and co-workers.[25] Therefore, we suspect that the resonance appearing at 177.1 ppm is the triphosphabenzene species **23d**. A comparable triphosphabenzene $[OB(ipc)_2]_3C_3P_3$ (ipc = (–)-B-chlorodiisopinocampheylborane) displays a singlet resonance at 182.7 ppm.[26]

4.3 Tris(phosphaalkyne)tungsten complexes

The reactivity of tungsten(0) reagents, such as $W(THF)(CO)_5$, towards phosphaalkynes has been extensively studied and the outcome of these reactions has been shown to be dependent on the steric bulk of the respective phosphaalkyne. Jones reported the first cyclodimerization of MeCP utilizing $W(THF)(CO)_5$, which resulted in a mixture of 1,2- and 1,3-diphosphacyclobutadiene complexes (**H** and **I**; Figure 4.4).[27] By contrast, analogous studies by Scheer showed that the stoichiometric reaction of ^{t}BuCP and $W(THF)(CO)_5$, yielded $[W(CO)_5\{\eta^4\text{-}(^t\text{BuCP})_2\}W(CO)_2\{\eta^2\text{-}(^t\text{BuCP})W(CO)_5\}]$ (**J**) as the sole product.[28] If instead MesCP is employed, a mixture of products is obtained, including the pentameric complex **K**.[29] Further increase of the steric bulk to Mes*CP prevents the reductive coupling to yield a spirocyclic complex with the phosphaalkynes bridging tungsten centers (**L**).[30]

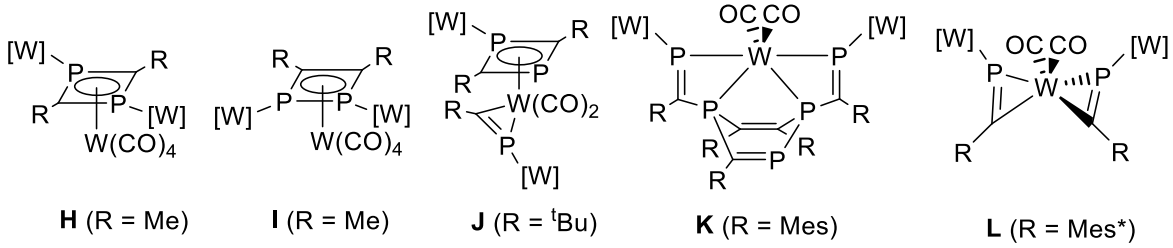

Figure 4.4. Previously reported tungsten phosphaalkyne complexes.

Due to the prevalence of tungsten phosphaalkyne complexes in the literature, we sought to explore the reactivity of [B]OCP towards tungsten carbonyl sources.

4.3.1 Tris(phosphaalkyne)tungsten complexes

4.3.1.1. Solution phase characterisation

Reaction of three equivalents of **1** with a tungsten(0) precursor (either $W(THF)(CO)_5$, $W(MeCN)_3(CO)_3$ or $W(\eta^6\text{-mesitylene})(CO)_3$) in difluorobenzene (DFB) leads to displacement of all but one of the ligands to afford $W(\eta^2\text{-PCO[B]})_3(CO)$ (**24**), which is present in solution as two isomers (**24a** and **24b**, Figure 4.7). The solution phase $^{31}P\{^1H\}$

NMR spectrum reveals three singlet resonances at 244.3, 244.2, and 109.6 ppm. The absence of coupling between the ^{31}P and ^{183}W nuclei is consistent with metal–ligand bonding occurring through the C≡P π-manifold. The ^{1}H NMR spectrum is consistent with the presence of three distinct boryl moieties (integrating in a 3:2:1 ratio). These data led us to hypothesize that two of the possible four isomers of **24** are present in solution (Figure 4.7). In one, all C≡P bonds are orientated in the same direction, with the three phosphorus atoms distal to the carbonyl (**24a**; ^{31}P{^{1}H} = 244.2 ppm). The second isomer consists of two ligands with phosphorus distal to the carbonyl (244.3 ppm) and one with phosphorus proximal to the carbonyl, the latter having a lower frequency ^{31}P{^{1}H} NMR resonance (109.6 ppm). These two resonances integrate in a 2:1 ratio. Both isomers are present in approximately equimolar amounts as determined by both ^{31}P and ^{1}H NMR spectroscopy.

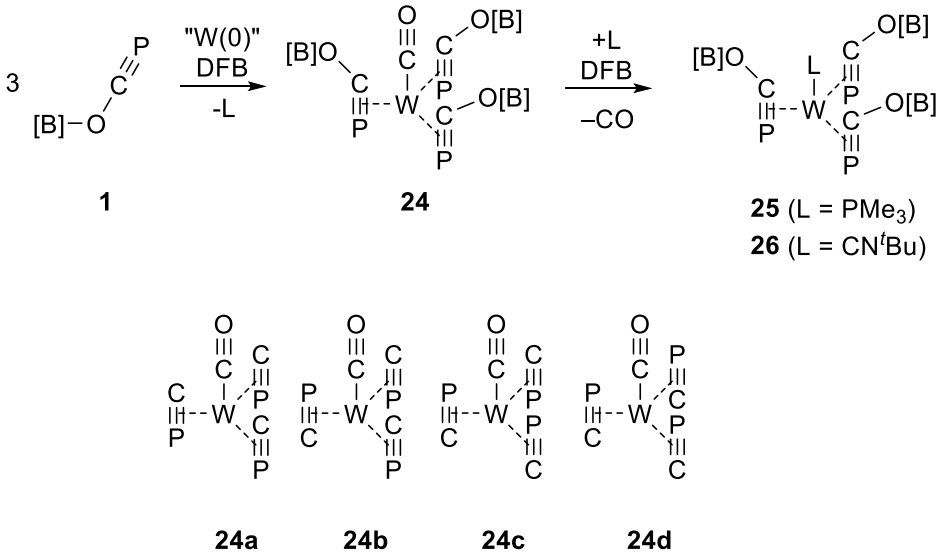

Scheme 4.7. Top: Synthesis of W(η^2-PCO[B])$_3$(CO) **24** (W(0) = (W(THF)(CO)$_5$, W(MeCN)$_3$(CO)$_3$ or W(η^6-mesitylene)(CO)$_3$) and ligand substitution reactions with PMe$_3$ and ^{t}BuNC. Bottom: The four possible isomers of **24** (boryloxy groups removed for clarity).

It is possible to displace the carbonyl ligand of **24** by addition of strong nucleophiles, such as trimethyl phosphine (**25**) and *tert*-butyl isocyanide (**26**). When trimethylphosphine (PMe$_3$, ca. 10 eq.) is added, the solution turns from dark red to light orange. The solution phase ^{31}P{^{1}H} NMR spectrum shows three singlets, at 264.8, 264.4 and 113.0 ppm,

corresponding to the C≡P phosphorus atoms, and two resonances with tungsten satellites at 7.11 ($^1J_{P–W}$ = 99 Hz) and 2.70 ($^1J_{P–W}$ = 80 Hz) ppm corresponding to the PMe_3 ligands. The ^1H NMR spectrum is consistent with the presence of three chemically distinct boryl groups and two PMe_3 environments at 0.97 (d, $^2J_{H–P}$ = 7 Hz) and 0.93 (d, $^2J_{H–P}$ = 13 Hz) ppm, further corroborating the presence of two isomers in solution (**25a** and **25b**), as was the case with solutions of **24**. The reaction mixture shows an isomer ratio of approximately 1:0.36; the more sterically demanding PMe_3 shifts the position of the equilibrium to favour the less sterically encumbered isomer **25a**. Mechanistic investigations conducted by Yeh and Chien on the conversion of $W(PhCCPh)_3(CO)$ to $W(PhCCPh)_3(PMe_3)$ concluded that the mechanism proceeds *via* displacement of one alkyne ligand by two equivalents of PMe_3 and were able to isolate metastable intermediate $W(PhC{\equiv}CPh)_2(CO)(PMe_3)_2$.[31] They propose this ligand displacement would be followed by decarbonylation and ligand exchange with the displaced alkyne to yield the final product. It should be noted that we were unable to observe any intermediates during our ligand displacement studies.

To better understand the relationship between the resonances observed in the NMR spectra of **24**, variable temperature ^1H and $^{31}P\{^1H\}$ NMR spectra were collected in d^8-toluene. In the $^{31}P\{^1H\}$ NMR spectra all three resonances show temperature dependence, moving downfield as the temperature increases. In contrast, the three ^1H NMR resonances corresponding to the boryl backbone protons shift upfield with increasing temperature. No significant interconversion between isomers was observed between –50°C and +50°C. Further increasing the temperature was not possible due to the thermal instability of the complex. The inability to observe coalescence in this system indicates that if an exchange mechanism exists, it is slow on the NMR timescale and variable temperature NMR is not suitable.

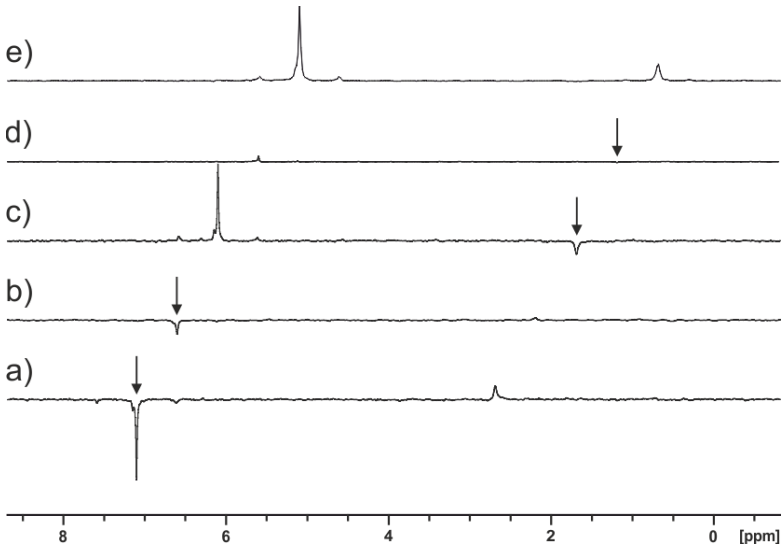

Figure 4.5. $^{31}P\{^{1}H\}$ selective inversion 1D-EXSY spectra of **25** highlighting the PMe_3 peaks of both isomers; a) major isomer peak inverted at mixing time 0s, b) major isomer peak inverted after 3s mixing time, c) minor isomer peak inverted at mixing time 0s, d) minor isomer peak inverted after 3s mixing time, e) $^{31}P\{^{1}H\}$ spectrum of same region (arrow indicates inverted peak).

However, in the case of **25**, where the CO ligand is replaced by PMe_3 (in order to provide an NMR handle with a reasonable relaxation time), it was possible to detect slow exchange between isomers **25a** and **25b** at room temperature using a ^{31}P 1D-EXSY experiment observing the PMe_3 resonances. In this experiment, the trimethylphosphine resonance in one of the two complexes is inverted and the relaxation process is monitored as a function of time as the inverted signal relaxes back to equilibrium. The intensity of the non-inverted signal is observed to reduce because of saturation transfer *via* chemical exchange, before relaxation returns both signals to equilibrium.

The rate at which spins relax is dependent on both the exchange rate and the relaxation time. This dependence is governed by the initial non-equilibrium state and if only one site is inverted the associated spins can relax both *via* their own spin relaxation mechanism and *via* exchange with the other site. Thus, upon selective inversion of one isomeric resonance, exchange to the second isomer results in inversion of the respective peak. Shown in figure 4.5, the initial inversion of the peak designated as the trimethylphosphine of **25a** (Figure 4.5; a) can be seen to affect the resonance associated with the trimethylphosphine of **25b** (Figure

4.5; b) after three seconds of mixing time. The analogous procedure can also be performed in reverse, where inverting the resonance of **25b** shows exchange with the major resonance of **25a** (Figure 4.5; c and d).

Density functional theory calculations were performed on all four isomers with reduced steric bulk at the substituents of the diazaboryl ring (diisopropylphenyl groups were replaced with methyl), except for **24a** which did not converge due to a low barrier of rotation around the boryl moieties, convergence was achieved for all the trimethylphosphine derivatives of **25**. The predicted ^{31}P NMR chemical shifts are in good agreement with the observed for the proposed isomers. The calculated free energy difference between the isomers is small 4.1 kcal/mol (Table 4.1). We propose the presence of only two isomers is due to the steric requirement of the boryloxy substituent rather than the relative thermodynamic stabilities of the isomers. The W–C bonds are notably shorter that the W–P bonds, causing the boryloxy groups to be canted inwards when the phosphorus is proximal to the carbonyl, allowing a maximum of one ligand to adopt this arrangement.

Table 4.1. Calculated energies of the model system. All geometry optimizations were computed using the functional PBE1PBE with 6-31G(d,p) basis sets except for W, where the pseudopotential ECP60MDF and the corresponding basis set ECP60MDF_VDZ (cc-pVDZ-PP VDZ-PP) were used. All values are given in kcal/mol. E represents the internal energy of the system and G represents the Gibbs energy.

	a	**b**	**c**	**d**
E R = CO	N.A.	0	–1.4	–4.0
G R = CO	N.A.	0	–2.1	–2.9
E (kcal/mol)	0	0.3	–0.6	–3.0
G (kcal/mol)	0	–0.2	–2.0	–4.0

4.3.1.2. Solid state characterisation

Purification of the crude reaction mixture of **24** proved troublesome, the dark red oil obtained upon removal of solvent was soluble in all common laboratory solvents and unstable on silica. Evaporation of a pentane solution of **24** in a narrow vial inside the glovebox yielded dark red crystals suitable for X-ray diffraction studies, and isolation of spectroscopically pure samples was possible by repeating this process multiple times, with removal of the crystals in between crystallisations.

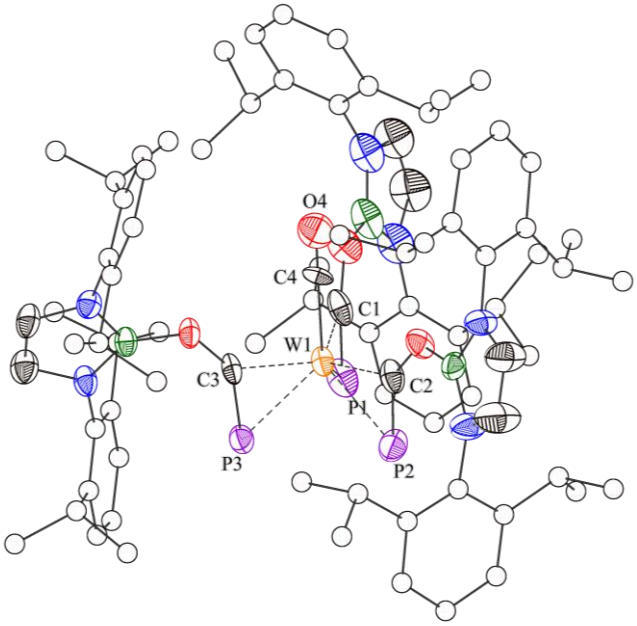

Figure 4.6. The solid state structure of **24a.** Anisotropic displacement ellipsoids are set at 50% probability. Hydrogen atoms omitted for clarity and Dipp carbon atoms shown as spheres of arbitrary radius.

Interestingly, single crystal X-ray analysis of the crystalline samples obtained from a solution of **2** reveals the presence of a single isomer, **24a**. The structure reveals a pseudo-tetrahedral tungsten monocarbonyl core surrounded by three η^2-[B]OCP molecules coordinated through the C≡P π-manifold (Figure 4.6). The structural parameters of all three ligands are equivalent within two standard deviations and will be discussed as average values. The C–P bonds are significantly elongated (1.672 Å) when compared to **1** (1.534 Å) and in line with the sum of the covalent radii for a double bond ($\sum_{cov}$ = 1.69 Å).[21] This elongation is consistent with a significant degree of σ-donation from the C≡P π-manifold to the tungsten centre and π-back-donation from the tungsten to the C≡P π* orbital. When comparing the C–P bond to known η^2-coordinated phosphaalkyne complexes, e.g. Ti(η^5-$C_5H_5)_2$\{η^2(2e)-P≡C^{t}Bu\}(PMe_3) and the related Ta(η^5-C_5Me_5)Cl_2\{η^2(4e)-P≡C^{t}Bu\}, the bond is longer than the former (1.636(2) Å) and indistinguishable from the latter (1.694(10) Å), indicating each ligand is donating, on average, more than two electrons to the tungsten centre.[32] The mean W–C bond length (2.066(8) Å) is similar to that of the related alkyne

complex W(η^2-PhC≡CPh)$_3$(PMe$_3$) (2.066(5) Å) and the W–P (2.433(2) Å) slightly longer than in [W(CO)$_2${(η^2-PCMes*)W(CO)$_5$}$_2$] (2.412(3) Å).[30,33]

The infrared (IR) spectrum of a crystalline sample of **24a** shows a sharp peak at 2064 cm^{-1}, consistent with the presence of a terminal carbonyl, and a broad band around 1600 cm^{-1} that can be assigned as the C≡P stretch, which is lower in frequency than that of the free ligand **1** (1649 cm^{-1}) and significantly broader. These absorptions further support the presence of a single isomer in the solid state.

When the crystals containing the single isomer are dissolved both isomers can be observed in solution by NMR spectroscopy in the same ratio as present in the reaction mixture, further supporting that a mechanism for ligand rotation is accessible and the two isomers are in equilibrium. The ^{31}P CPMAS confirms the existence of a single isomer in the solid state for both **24** and **25**; only 3 peaks of equal intensity are observed, relating to the three P≡C ligands with comparable shifts to isomer **a** in solution (Figure 4.7). No second set of peaks for a second isomer were observed.

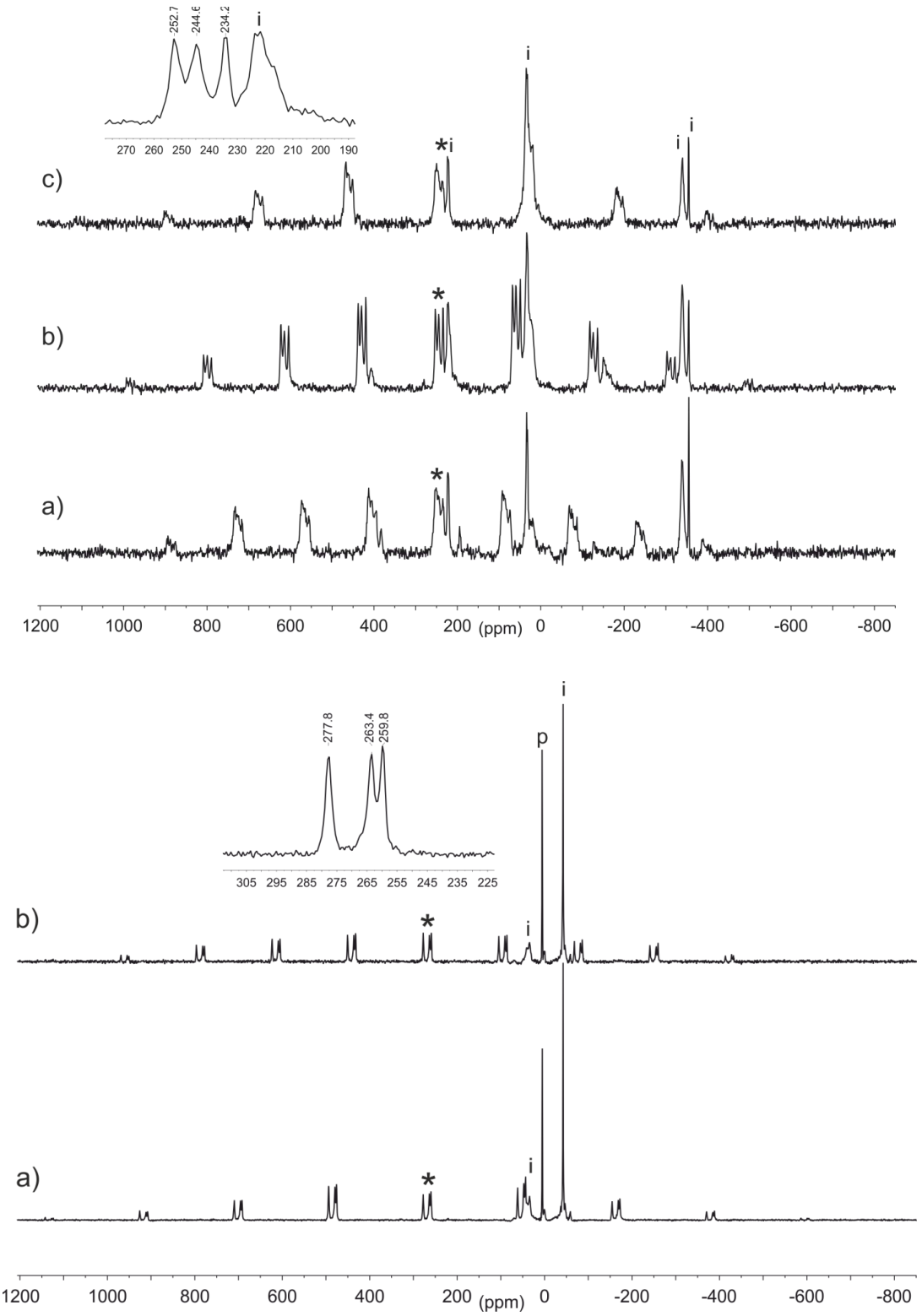

Figure 4.7. Top: $^{31}P\{^{1}H\}$ CPMAS spectra of **24a**; a) spinning speed 26 kHz, b) spinning speed 28 kHz, c) spinning speed 35 kHz, * indicates isotropic peak for P≡N resonances (see inset expansion) and i indicates impurity peaks. Bottom: $^{31}P\{^{1}H\}$ CPMAS spectra of **25a**; a) spinning speed 35 kHz, b) spinning speed 28 kHz, * indicates isotropic peak for P≡N resonances (see inset expansion), p indicates PMe_3 resonances, and i indicates impurity peaks.

The electronic structure of **2** is related to the landmark tris(alkyne) complexes $W(CO)(RC{\equiv}CR')_3$ (R/R′ = Ph/Ph, C_2H_5/C_2H_5, CH_3/Ph) first reported by Tate and Augl.[33,34] These complexes were of interest due to their unusual bonding situation. If one assumes that each alkyne ligand is able donate either two or four electrons, that gives the central metal an electron count of fourteen or twenty, respectively. An interpretation of the electronic structure of these compounds was put forward by King using group theoretical considerations which discussed the preference for $W(CO)(RC{\equiv}CR')_3$ geometry over $W(RC{\equiv}CR')_3$, which would satisfy the 18-electron rule if each alkyne donated four electrons.[35] In $W(CO)(RC{\equiv}CR')_3$ the six alkyne π orbitals form a basis for the irreducible representations $A_1 + A_2 + 2E$ ($3\pi_{\parallel} + 3\pi_{\perp}$). Symmetry-equivalent metal d-orbitals are available for the formation of three M–L σ interactions ($A_1 + E$), however only the E representation is suited for the formation of π interactions. There is no metal-based orbital of A_2 symmetry. Three alkynes substituents in C_{3v} symmetry can therefore donate a maximum of ten electrons, which when taken along with the six valence electrons of tungsten give rise to 16 valence electrons. The additional carbonyl ligand is thus needed to satisfy the eighteen electron rule. A similar treatment of $W(RC{\equiv}CR')_3$, with the same six alkyne π orbitals but this time with D_{3h} symmetry, results in the irreducible representation $A_1' + A_2' + E' + E''$ ($3\pi_{\parallel} + 3\pi_{\perp}$). As with the above case, the symmetry-equivalent metal d-orbitals are available for the formation of three M-L σ interactions ($A_1' + E' + E''$). There are no metal orbitals corresponding to the A_2' representation, while the (p_x, p_y) and ($d_{x^2-y^2}$, d_{xy}) sets of metal orbitals correspond to the E′ representation and are able to receive electron density through the π-bonds of a maximum of two ligands. Thus this conformation allows for a maximum of 10-electrons to be provided by the ligand, resulting in a 16-electron complex. Compound **24a** has the same C_{3v} symmetry as $W(CO)(RC{\equiv}CR')_3$ and the same bonding model can be applied, with two bidentate phosphaalkyne ligands donating 4-electrons and one donating 2-electrons. However, the core can be regarded as a superposition of the three possible

resonance forms, accounting for the equivalence between the three phosphaalkyne ligands observed in the solid state structure. Each ligand can be described as donating 3 1/3 electrons to the metal centre. Examples of η^2(2e)- and η^2(4e)-phosphaalkyne complexes have been reported in literature, however this compound is the first example of more than one η^2-ligand at a single metal site.

Crystals of the PMe_3 derivative, **25**, were obtained by allowing a pentane solution to evaporate in a narrow vial, forming red blocks on the walls of the vessel. The IR spectrum of **25** shows loss of the carbonyl stretch associated with **24**, and a broad band around 1600 cm^{-1} corresponding to the C≡P stretch. Analytically pure single crystals of **25** suitable for X-ray diffraction studies can be grown by slow evaporation of a pentane or hexane solution. The crystal structure reveals a single isomer, **25a** (Figure 4.8), and confirms the displacement of carbonyl by PMe_3. Structurally there is no change to the tungsten tris-phosphaalkyne core between complexes **24a** and **25a**.

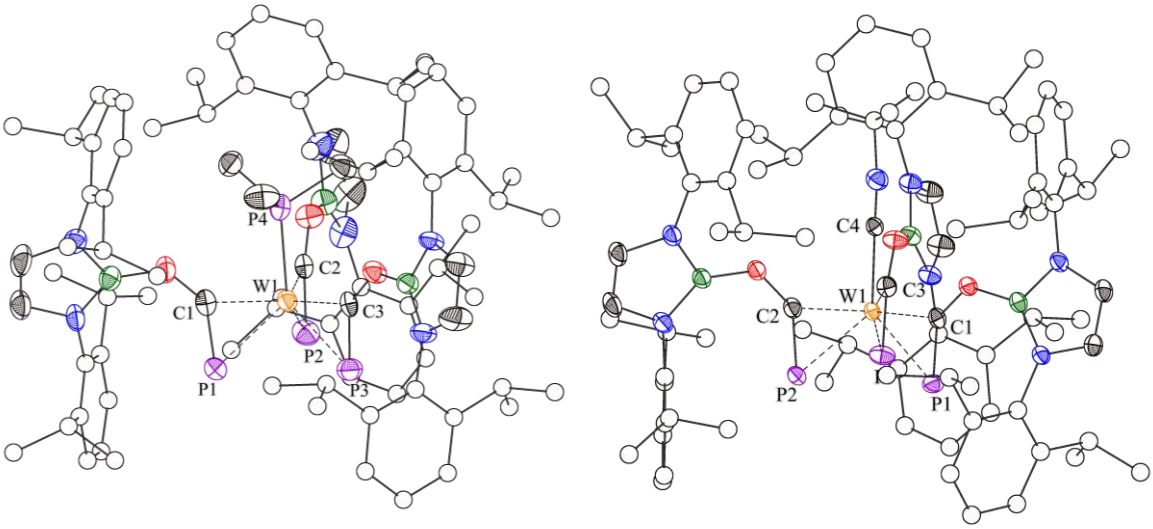

Figure 4.8. The solid state structure of **25** and **26.** Anisotropic displacement ellipsoids are set at 50% probability. Hydrogen atoms omitted for clarity and Dipp carbon atoms shown as spheres of arbitrary radius.

Similarly, reaction of **24** with an excess of *tert*-butyl isonitrile (^{t}BuNC) results in ligand substitution to yield **26**. The solution phase ^{31}P NMR spectrum indicates the presence of two isomers, **26a** and **26b** (ratio of 1:0.68), with singlet resonances at 256.0, 253.6 and 116.6 ppm, at a similar frequency to the phosphorus environments in **24** (*cf.* 264.8, 264.4 and 113.0 ppm). It is worth noting that increasing the steric requirement of the axial ligand results in a greater ratio of isomer **a**:**b** (where PMe_3 > ^{t}BuNC > CO). Slow evaporation of a pentane solution yielded large red crystals suitable for single crystal diffraction. The crystal structure revealed a single isomer, **26**, with two crystallographically unique molecules of present in the asymmetric unit, both of which exhibit comparable bond metrics to **24** and **25**.

The further reactivity of these compounds gave complicated results and typically resulted in mixtures of products. Thermal treatment of **24** gave compounds with varying numbers of carbonyl ligands, some of which could be identified by fractional crystallization however could not be rationally synthesized. Addition of decarbonylating agent trimethylamine N-oxide induces the desired effervescence; however ^{31}P NMR indicates a number of products are formed even at low temperatures. No further olimerisation-type reactions occurred when a further equivalent of **1** or ^{t}BuCP was added to solutions of **24**, **25** or **26**.

4.4 Elementoboration Chemistry

4.4.1 Hydroboration chemistry

Addition of 9-borabicyclo[3.3.1]nonane (9-BBN) to a benzene solution of **1** initially results in no reaction. Upon heating the solution to 60°C in benzene the appearance of a number of products was noted by ^{31}P{^{1}H} NMR spectroscopy. Complete consumption of the starting material is observed after 24 hours, resulting in a mixture of two major products. One consisting of an AB spin system with resonances at –112.3 and –213.5 ($^2J_{P–P}$ = 162.4

Hz), the second consisting of two broad resonances at –38.2 and –39.4 ppm. Fractional crystallisation of the reaction mixture allows for identification of latter product, **27**.

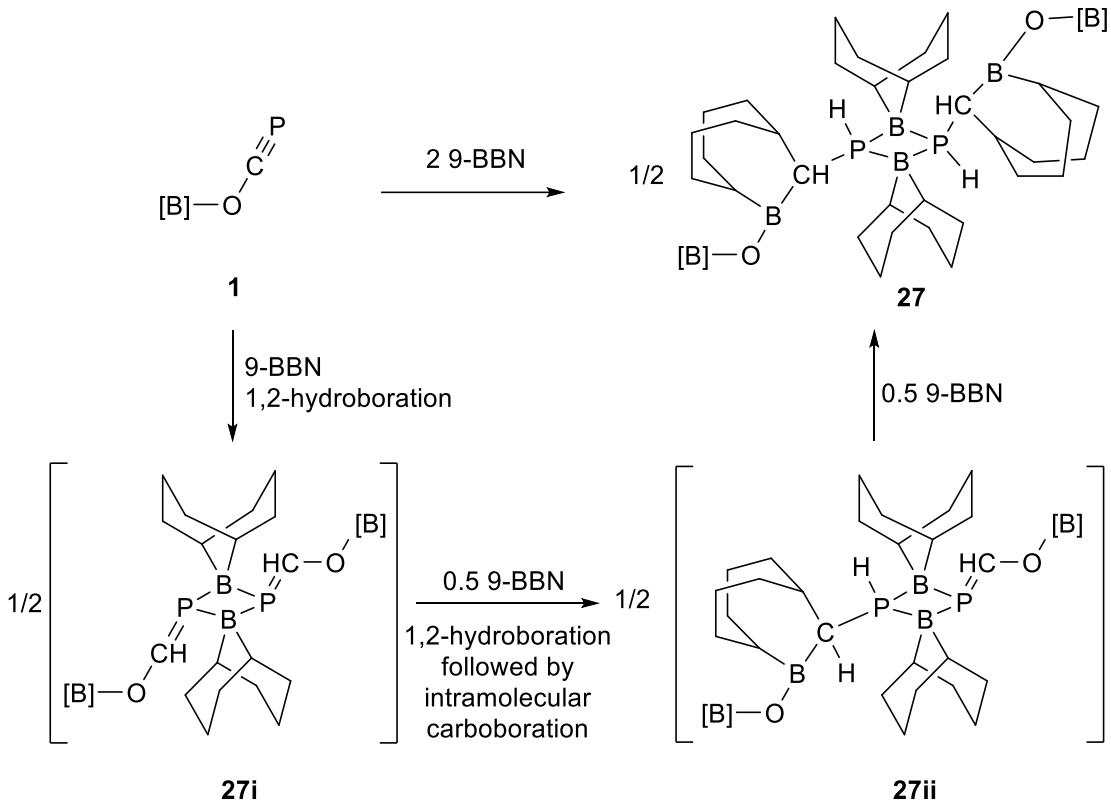

Scheme 4.8. Reactivity of **1** towards 9-BBN.

27 is a product of two equivalents of **1** reacting with four equivalents of 9-BBN. Dissolution of the crystals results in the two broad resonances previously mentioned, arising due to the *cis* and *trans* isomers being present in solution. There was also a significant amount of the AB product present in the crystals. After an initial 1,2-hydroboration reaction across the CP bond with formation of B–P and C–H bonds, a second, inverted, 1,2-hydroboration occurs across the same bond in addition to an intramolecular boron insertion into the C–O bond, leading to the formation of a O–B–C fragment.

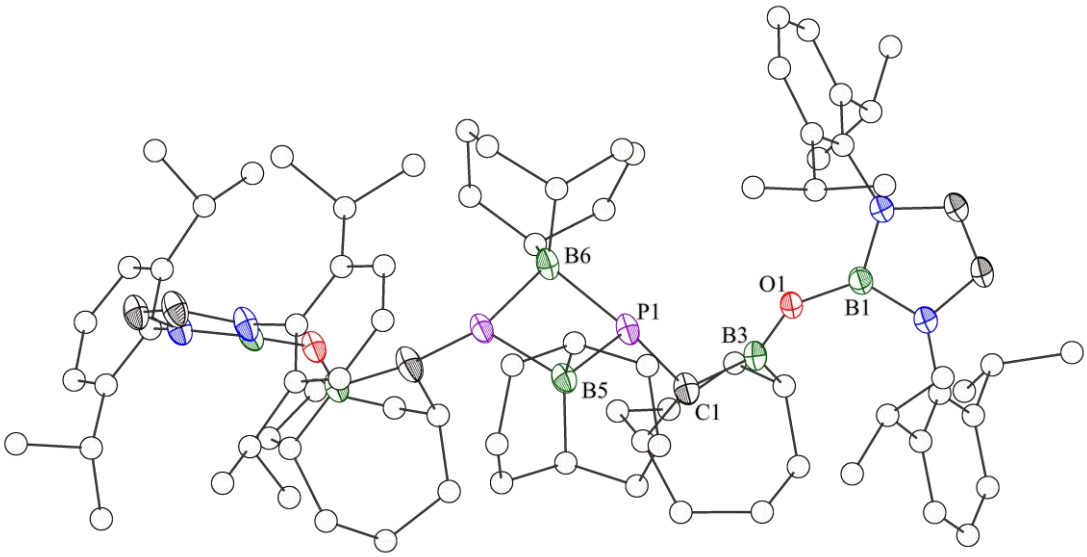

Figure 4.9. The solid state structure of **27.** Anisotropic displacement ellipsoids are set at 50% probability. Hydrogen atoms omitted for clarity and Dipp carbon atoms shown as spheres of arbitrary radius.

Periodic analysis of the reaction mixture gives some insight into the mechanism of formation. Initially, a set of broad singlet resonances at –116.1 and –117.0 ppm were present in the ^{31}P NMR spectrum. These resonances are consistent with a species displaying *cis-trans* isomerisation in solution, and we tentatively assign the signals as the singly hydroborated dimeric species (Scheme 4.8; **27i**). As with Stephan's report, we postulate that the steric requirements of the boryl fragment in 9-BBN leads to addition of the hydride at the less electrophilic carbon centre. The AB spin system with resonances -112.3 and –213.5 ppm displays higher order coupling in the ^{31}P proton coupled spectra, with the resonance at –213.5 becoming a triplet ($^{1}J_{P-H}$ = 164 Hz). The resonance at –112.3 ppm broadens out and coupling constants could not be resolved. Due to this we tentatively assign this resonances as the mono-carboborated species **27ii**. Upon proton coupling, the resonances corresponding to **27** overlap and become unresolvable.

The final product can be crystallised by cooling a concentrated hexane solution (Figure 4.9). The solid state structure reveals a dimeric species with a saturated C–P bond a central B_2P_2 ring. The solid state structure of **27** is dimeric; however for simplicity the bond metrics

of only one of the monomer fragments will be discussed. The P1–C1 bond is 1.871(2) Å, consistent with complete reduction of the C≡P triple bond to a single bond. The central four membered ring is slightly asymmetric, with P1–B5 and P1–B6 bond lengths of 2.016(2) and 2.041(2) Å, respectively. The insertion of B3 into the O1–C1 bond results in formation of an O1–B3 (1.365(2) Å) and C1–B3 bond (1.596(2) Å), both in good agreement with what would be expected of single bonds.[36]

4.4.2 Carboboration Chemistry

Addition of tris(pentafluorophenyl)borane (BCF) to a solution of [B]OCP results in an immediate colour change from yellow to dark red. The $^{31}P\{^{1}H\}$ and ^{1}H NMR spectra of the reaction mixture are consistent with the formation of a single product with a $^{31}P\{^{1}H\}$ NMR resonance at 174.0 ppm (**28**; Scheme 4.9). The ^{19}F spectrum is consistent with the presence of two pentafluorophenyl environments in a 2:1 ratio. Crystals can be obtained from a cooled hexane solution if the work up is performed quickly.

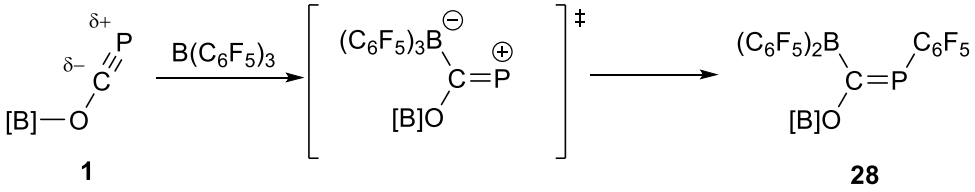

1 **28**

Scheme 4.9. Carboboration of **1** with BCF.

The solid state structure reveals that a *cis* 1,2-carboboration of the C≡P bond of [B]OCP has taken place with the formation of C–B and P–C bonds with a *cis*-arrangement of the C_6F_5 and $B(C_6F_5)_2$ groups (Figure 4.10). The C1–P1 bond distance (1.701(2) Å) is elongated with respect to the starting material consistent with the reduction of bond order from a triple to a double bond (double bond Σ_{cov} = 1.69 Å).[37] The C1–O1 bond distance of 1.356(2) Å is notably longer than that of the [B]OCP precursor (*cf.* 1.269(2) Å) due to diminishing π-conjugation throughout the phosphaethynolate moiety. This stereo- and regiochemical

outcome is inverse to that observed in Stephan's hydroboration of phosphaalkynes using Piers' borane, however is consistent with the expected stereo- and regiochemical outcome given the $^{\delta-}C{\equiv}P^{\delta+}$ dipole. This product is in keeping with a concerted interaction of the boron atom of BCF with the carbon of the phosphaalkyne and migration of the pentafluorophenyl to the phosphorus centre.

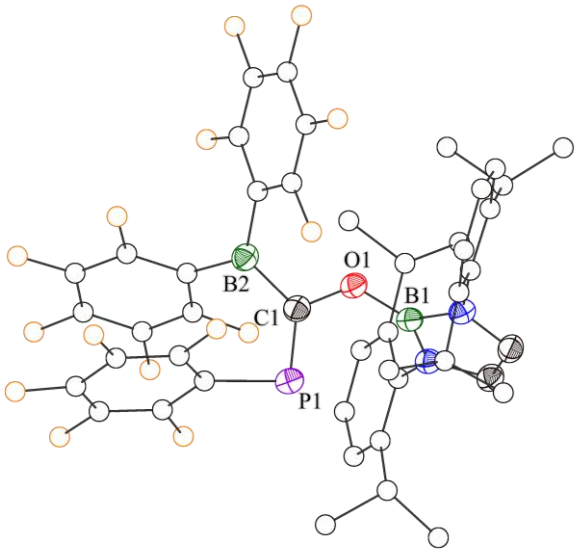

Figure 4.10. Molecular structure of **28**. Anisotropic displacement ellipsoids set at 50% probability. Hydrogen atoms have been omitted for clarity. Atoms of the Dipp and C_6F_5 moieties are pictured as spheres of arbitrary radius.

Interestingly, **28** undergoes a rearrangement in solution over the course of several hours to yield boryloxy(methylidene)phosphane, **29**. The ^{31}P NMR spectrum of **29** reveals a singlet at 409.1 ppm, shifted to significantly higher frequency relative to **28**. As with **28**, two distinct pentafluorophenyl environments are present in the ^{19}F NMR spectrum. Crystals of the product could be obtained by cooling a saturated hexane solution.

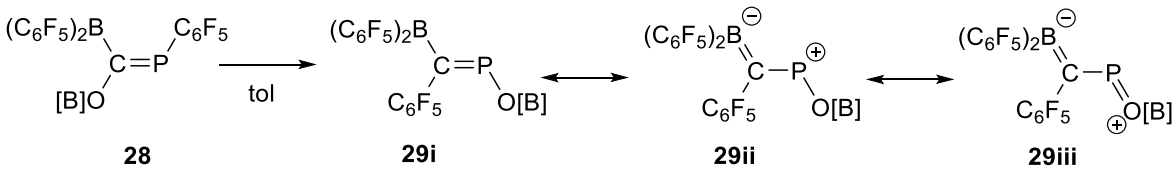

28 **29i** **29ii** **29iii**

Scheme 4.10. Rearrangement of **28** to **29**.

The solid-state structure of **29** (Figure 4.11) reveals a carbon phosphorus bond with significant double bond character (1.684(2) Å), in addition to short B1–O1 (1.339(2) Å), O1–P1 (1.593(2) Å) and C1–B2 (1.512(2) Å) which are all between what is expected for their respective single and double bonds (Σ_{cov} single/double bonds = 1.35/1.48, 1.59/1.74, 1.60/1.45 Å, respectively). The heteroatom chain O1-P1-C1-B2 is planar (mean deviation from plane = 0.0184 Å), which, when taken into consideration with the shorter than expected bond lengths, is consistent with delocalisation of electron density throughout the π-manifold. The boryl ring is out of plane with the heteroatom chain (deviation from planarity: 46.7°), a result of steric hinderence between the boryl Dipp groups and C_6F_5 substituents on the chain. This data, in combination with the unusually downfield $^{31}P\{^1H\}$ NMR signal, can be justified through resonance forms placing increased negative charge on the boron centre and a positive charge on the phosphorus (**29ii**; Scheme 4.10).

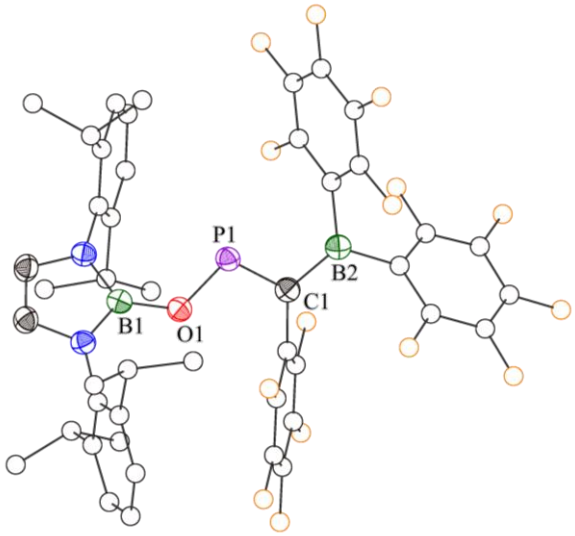

Figure 4.11. Molecular structure of **29**. Anisotropic displacement ellipsoids set at 50% probability. Hydrogen atoms have been omitted for clarity. Atoms of the Dipp and C_6F_5 moieties are pictured as spheres of arbitrary radius.

The final, 1,1-carboborated product of this reaction is analogous to the product of the reaction of BCF with alkynes. Despite the prevalence of alkyne carboborations with R-$B(C_6F_5)_2$ type species, very little has been done to probe the mechanism of such processes.

The better understood Wrackmeyer reaction proceeds by means of abstraction of a alkynyl to generate a transient zwitterionic heterocyclic intermediate, which in some cases have been structurally authenticated (M = Sn, Pb).[38,39] This zwitterionic intermediate then transfers the organyl substituent to the formerly alkenyl carbon centre to yield the final 1,1-carboborated product (Scheme 4.12). One consequence of this sequence is the stereoselectivity, in which the transferred organyl group is *trans* to the tetrel substituent. Carboborations with BCF do not display such stereoselectivity, typically giving rise to product mixtures containing both isomers. It can be assumed then to proceed via a different mechanism which has not been investigated in the literature. As phosphorus is often considered the 'carbon copy', in addition to providing a helpful NMR handle, we decided this system may provide insight into the mechanism of carboboration.

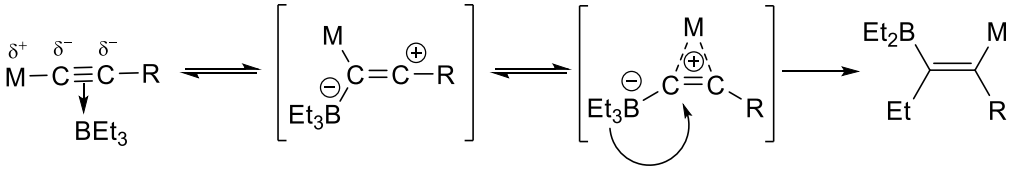

Scheme 4.11. The Wrackmeyer reaction mechanism: carboboration using activated alkynes. M = Si, Ge, Sn, Pb. R = alkyl

Kinetics experiments were performed using both the ^{1}H and ^{31}P nuclei. Upon heating a toluene solution of **28** to 50°C for 90 minutes complete consumption of the starting material is observed. Variation of the concentration of **28** did not yield any conclusive kinetic information, increasing the concentration did not result in a clear trend in rate of formation of the product. It was possible, however, to detect two intermediates by $^{31}P\{^{1}H\}$ NMR spectroscopy. A short-lived resonance appears at 196.5 ppm, which is possibly the *trans* isomer of **28**. Upon further heating, a second resonance appears at 17.2 ppm, with tdt coupling (J = 22 Hz, 16 Hz, 5 Hz) (Figure 4.12) which can be assigned as three, five, and four bond phosphorus–fluorine coupling.[40,41] While three bond coupling is frequently observed in $R_2P(C_6F_5)$ compounds, four and five bond coupling is much less common and it

is unclear why the five bond coupling is of a greater magnitude than the four bond. This resonance remains after all of the starting material is consumed, and may potentially be the product of a competitive pathway. Prolonged heating (6 hours) results in complete consumption of this intermediate and compound **29** is observed as the sole product. DFT calculations reveal **29** to be the thermodynamic product of the reaction, being 27.7 kcal/mol more stable than **28** in the gas phase.

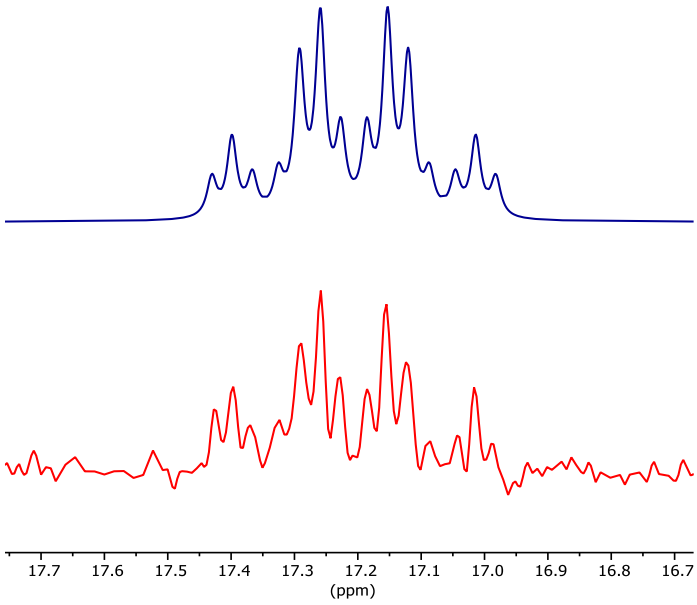

Figure 4.12. $^{31}P\{^{1}H\}$ NMR resonance of unknown intermediate (red trace) and the simulated spectrum (blue trace).

The rearrangement of **28** to **29** can be prevented through addition of the Lewis base trimethylphosphine to the reaction mixture (Scheme 4.12). The resulting compound displays an AB spin system in the $^{31}P\{^{1}H\}$ NMR spectrum with a doublet resonance at 145.4 ppm ($^{3}J_{P-P}$ = 14.7) and a broad resonance –10.7 ppm, the latter being broadened due to coupling to the quadrupolar boron nucleus. The $^{11}B\{^{1}H\}$ NMR in this case is quite diagnostic, revealing a broad resonance at 23.2 ppm corresponding to the three coordinate boryl boron, in addition to a sharper resonance at –13.0 ppm corresponding to the now four coordinate borane. Crystallisation of the species allows for its identification as the trimethylphosphine adduct of **28**, **30**.

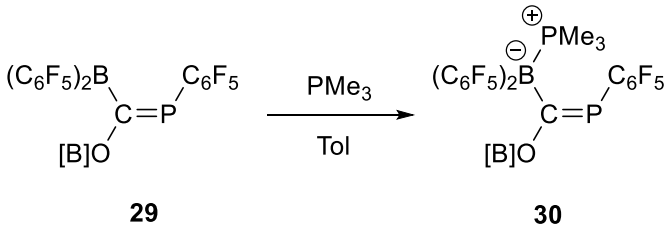

29 **30**

Scheme 4.12. Addition of trimethylphosphine to **29**.

The solid state structure reveals an elongation of the C1–B2 (1.638(2) Å) and C1–O1 (1.378(2) Å) bonds with respect to its base-free analogue (*cf.* 1.577(3) and 1.356(2) Å, respectively) with no significant change to the C1–P1 bond (Figure 4.15). These metrics are telling of a loss of conjugation through donation of the oxygen lone pair, and acceptance via the empty p-orbital of the borane, into the π-system, while electron density still remains localised on the C1–P1 π-orbital. The new P2–B2 bond distance (2.062(2) Å) is in line with that expected of a single bond (Σ_{cov} = 1.96 Å).[36] Compound **30** is thermally stable, with no change observed in the NMR spectra after heating at 80°C for 12 hours. This stability implies that the boron centre is integral to the rearrangement, either through its Lewis acidic nature or due to the conjugation of the final product providing a thermodynamic driving force for the rearrangement.

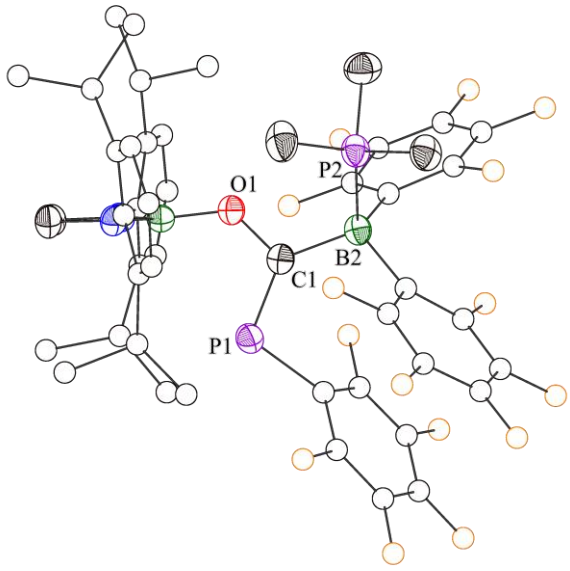

Figure 4.13. Molecular structure of **30**. Anisotropic displacement ellipsoids set at 50% probability. Hydrogen atoms have been omitted for clarity. Atoms of the Dipp and C_6F_5 moieties are pictured as spheres of arbitrary radius.

In contrast to the aforementioned reactions, if the linkage isomer of [B]OCP, [B]PCO (**19**), is treated with one equivalent of BCF a single product is formed with a singlet resonance in the $^{31}P\{^1H\}$ NMR spectrum at 142.2 ppm corresponding to 1,3-carboborated species **31** (Figure 4.13). The $^{11}B\{^1H\}$ NMR spectrum displays a single broad resonance for both three-coordinate boron centres, while the ^1H NMR spectrum is consistent with a single boryl moiety. Crystals were obtained from a cooled hexane solution.

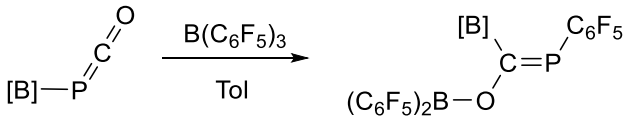

19 **31**

Scheme 4.13. The reaction of [B]PCO with BCF.

The solid state structure reveals a 1,3-carboboration product in which the boryl unit has migrated from the phosphorus to the carbon centre with formation of O–B and P–C bonds (Figure 4.16). The P1–C1 bond length is again consistent with significant π-character

(1.692(2) Å). Of note is the shorter than usual B2–O1 bond, which is closer to what is expected from a double bond (1.341(2) Å. Expected single/double bond: 1.48/1.35 Å).[36,37] This contraction is consistent with a contribution from the oxygen lone pair into the empty p-orbital of the boron centre.

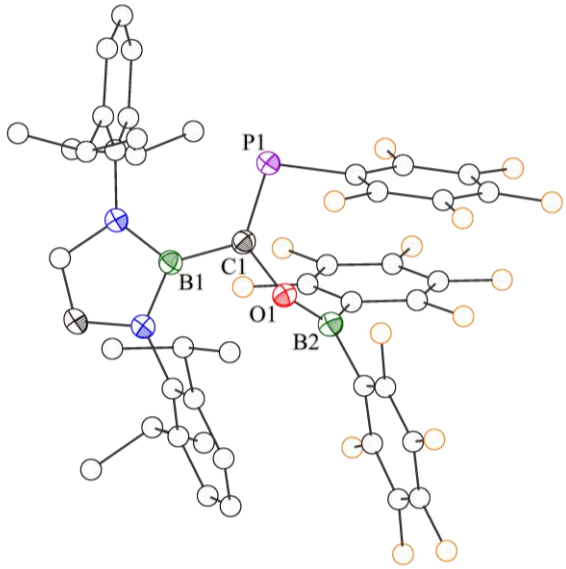

Figure 4.14. Molecular structure of **31**. Anisotropic displacement ellipsoids set at 50% probability. Hydrogen atoms have been omitted for clarity. Atoms of the Dipp and C_6F_5 moieties are pictured as spheres of arbitrary radius.

Similar boryl migrations have been observed for **1** as described in Chapters 2 and 3, however compound **32** is the first instance of such behaviour from the phosphaketene. It should also be noted that carboboration of phosphaketenes has not previously been reported. In a similar reaction, from the Bertrand group, addition of BCF to the more ionic (phospholidino)phosphaketene resulted in formation of a three membered heterocycle.[42] The carboboration of the isocyanates, the lighter analogues of phosphaketenes, has recently been explored by our group and were found to undergo an initial 1,2-carboboration across the C=O bond, followed by insertion of a second equivalent of isocyanate to yield six-membered heterocycles.[43]

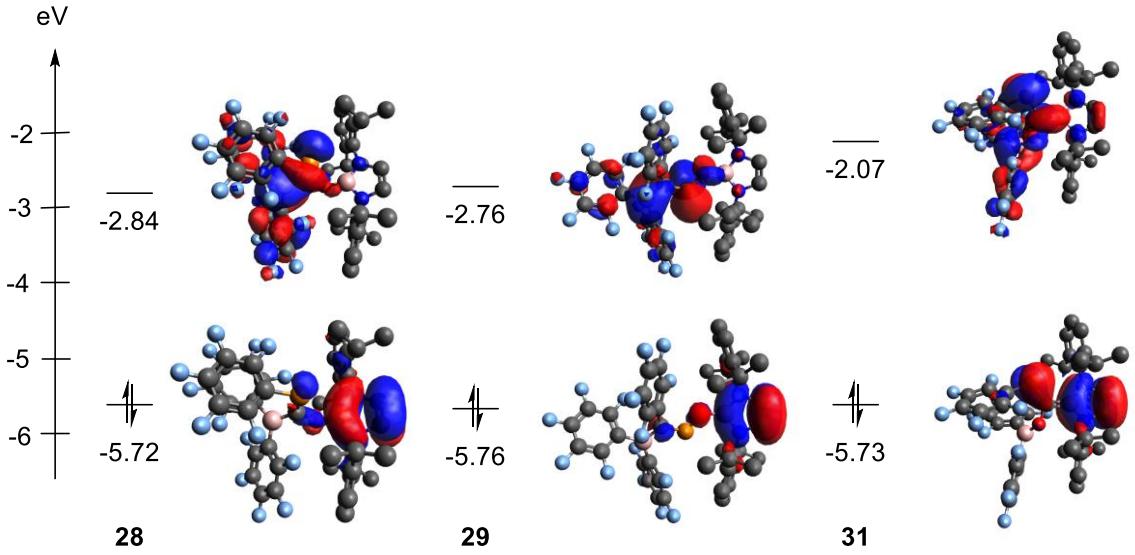

Figure 4.15. Frontier molecular orbital energies and visualisations of compounds **28**, **29**, and **30**. Values given in eV.

Compounds **28**, **29**, and **31** are constitutional isomers of a borylated phosphaalkene which display varying relative stability (ΔG = 0, –25.8, –13.6 kcal/mol, respectively). We aimed to investigate the relative reactivity of the series, however found that none of the three displayed reactivity towards small molecules (CO_2, CS_2, CO, H_2, N_2O). Addition of trimethylphosphine to any of the three resulted in NMR spectra consistent with association at the boron centre. Analysis of the frontier molecular orbitals revealed remarkably similar HOMO and LUMO energies. The HOMO of **28** and **29** is almost entirely located at the π-system of the boryl ring. The HOMO of **31** is also very similar; however there is some contribution from the C–P π-orbital. It is unsurprising then that the energies of these orbitals are comparable, at –5.72, –5.76, and –5.73 eV, respectively. The LUMOs are somewhat more varied, however are generally localised around the boron p-orbital and the C–P π*-antibonding orbital with energies of –2.84, –2.76, and –2.07 eV, respectively. Despite the substantial difference in relative energies across the series the energies of the frontier molecular orbitals are surprisingly similar, which results in consistent, if unremarkable, reactivity from these compounds.

4.5 Conclusions

This chapter described the ligand properties of phosphaethynolatoborane **1**. **1** dimerizes in the coordination sphere of nickel, analogous to reactivity previously reported with related phosphaalkynes. With tungsten carbonyl sources η^2-type coordination is achieved in a series of tungsten complexes displaying bonding previously only observed in the analogous alkyne species, with each η^2-bonded [B]OCP ligand donating an average of 3 1/3 electrons. The presence of different isomers in solution and the solid state was also explored.

We investigated the hydroboration chemistry of **1** towards 9-BBN which resulted in two consecutive hydroboration reactions occuring, with an inversion of the regioselectivity between consecutive hydroborations.

We have shown that tris(pentafluorophenyl)borane readily reacts with two isomers of a boryl-phosphaethynolate, [B]OCP and [B]PCO. In the case of **1** a concerted 1,2-carboboration reaction is observed initially, however the product ultimately rearranges to a more thermodynamically stable constitution isomer through a step-wise migratory process. By contrast the linkage isomer [B]PCO, a boryl-functionalized phosphaketene, undergoes a formal 1,3-carboboration in which O–B(C_6F_5)$_2$ and P–C_6F_5 bonds are formed accompanied by migration of the boryl functionality from phosphorus to carbon, the first time such a migration has been observed from the phosphaketenyl linkage isomer. The three resulting products from these reactions are all constitutional isomers of the same borylated phosphaalkenes, and allow for a mechanistic probing of the mechanism of carboboration.

4.6 References

[1] M. Y. Antipin, A. N. Chernega, K. A. Lysenko, Y. T. Struchkov, J. F. Nixon, *J. Chem. Soc. Chem. Commun.* **1995**, 505–506.

[2] P. M. Esteves, K. K. Laali, *Organometallics* **2004**, *23*, 3701–3713.

[3] J. C. T. R. James, P. B. Hitchcock, H. W. Kroto, J. F. Nixon, *J. Chem. Soc. Chem. Commun.* **1981**, 1141–1143.

[4] A. Chirila, R. Wolf, J. Chris Slootweg, K. Lammertsma, *Coord. Chem. Rev.* **2014**, *270–271*, 57–74.

[5] P. B. Hitchcock, M. J. Maah, J. F. Nixon, J. A. Zora, G. J. Leigh, M. A. Bakar, *Angew. Chem.* **1987**, *99*, 497–498.

[6] J. G. Cordaro, D. Stein, H. Rüegger, H. Grützmacher, *Angew. Chem. Int. Ed.* **2006**, *45*, 6159–6162.

[7] S. M. Mansell, M. Green, C. A. Russell, *Dalton Trans.* **2012**, *41*, 14360–14368.

[8] P. B. Hitchcock, M. J. Maah, J. F. Nixon, *J. Chem. Soc. Chem. Commun.* **1986**, 737–738.

[9] P. Binger, R. Milczarek, R. Mynott, M. Regitz, W. Rösch, *Angew. Chem.* **1986**, *98*, 645–646.

[10] J. F. Nixon, *Endeavour* **1991**, *15*, 49–57.

[11] M. Regitz, *Chem. Rev.* **1990**, *90*, 191–213.

[12] C. Camp, N. Settineri, J. Lefèvre, A. R. Jupp, J. M. Goicoechea, L. Maron, J. Arnold, *Chem. Sci.* **2015**, *6*, 6379–6384.

[13] H. C. Zweifel, B. George, *J. Am. Chem. Soc.* **1959**, *81*, 247.

[14] D. A. Evans, G. C. Fu, A. H. Hoveyda, *J. Am. Chem. Soc.* **1992**, *114*, 6671–6679.

[15] B. Wrackmeyer, *Coord. Chem. Rev.* **1995**, *145*, 125–156.

[16] D. J. Parks, W. E. Piers, *Organometallics* **1998**, *17*, 5492–5503.

[17] G. Kehr, G. Erker, *Chem. Commun.* **2012**, *48*, 1839–1850.

[18] G. Kehr, G. Erker, *Chem. Sci.* **2016**, *7*, 56–65.

[19] C. M. Crudden, D. Edwards, *European J. Org. Chem.* **2003**, *2003*, 4695–4712.

[20] A. S. Ionkin, S. N. Ignat'eva, B. A. Arbuzov, *Bull. Acad. Sci. USSR Div. Chem. Sci.* **1990**, *39*, 1315.

[21] L. E. Longobardi, T. C. Johnstone, R. L. Falconer, C. A. Russell, D. W. Stephan, *Chem. Eur. J.* **2016**, *22*, 12665–12669.

[22] S. Yruegas, J. H. Barnard, K. Al-Furaiji, J. L. Dutton, D. J. D. Wilson, C. D. Martin, *Organometallics* **2018**, *37*, 1515–1518.

[23] T. Wettling, G. Wolmershäuser, P. Binger, M. Regitz, *J. Chem. Soc. Chem. Commun.* **1990**, 1541–1543.

[24] M. Trincado, A. J. Rosenthal, M. Vogt, H. Grützmacher, *Eur. J. Inorg. Chem.* **2014**, *2014*, 1599–1604.

[25] P. Binger, J. Stannek, B. Gabor, R. Mynott, J. Bruckmann, C. Krüger, S. Leininger, *Angew. Chem. Int. Ed.* **1995**, *34*, 2227–2230.

[26] R. Suter, Y. Mei, M. Baker, Z. Benkő, Z. Li, H. Grützmacher, *Angew. Chem. Int. Ed.* **2017**, *56*, 1356–1360.

[27] C. Jones, C. Schulten, A. Stasch, *J. Chem. Soc. Dalt. Trans.* **2006**, 3733–3735.

[28] P. Kramkowski, M. Scheer, *Eur. J. Inorg. Chem.* **2000**, *2000*, 1869–1876.

[29] P. Kramkowski, M. Scheer, *Angew. Chem. Int. Ed.* **1999**, *38*, 3183–3186.

[30] P. Kramkowski, M. Scheer, G. Baum, *J. Organomet. Chem.* **1998**, *553*, 511–516.

[31] W. Y. Yeh, S. M. Chien, *J. Organomet. Chem.* **1997**, *548*, 191–194.

[32] A. D. Burrows, A. Dransfeld, M. Green, J. C. Jeffery, C. Jones, J. M. Lynam, M. T. Nguyen, *Angew. Chem. Int. Ed.* **2001**, *40*, 3221–3224.

[33] D. P. Tate, J. M. Augl, *A Novel Acetylenic Complex of Tungsten(0) Carbonyl*, American Chemical Society, **1963**.

[34] D. P. Tate, J. M. Augl, W. M. Ritchey, B. L. Ross, J. G. Grasselli, *J. Am. Chem. Soc.* **1964**, *86*, 3261–3265.

[35] R. B. King, *Inorg. Chem.* **1968**, *7*, 1044–1046.

[36] P. Pyykkö, M. Atsumi, *Chem. Eur. J.* **2009**, *15*, 186–197.

[37] P. Pyykkö, M. Atsumi, *Chem. Eur. J.* **2009**, *15*, 12770–12779.

[38] B. Wrackmeyer, S. Kundler, R. Boese, *Chem. Ber.* **1993**, *126*, 1361–1370.

[39] B. Wrackmeyer, K. Horchler, R. Boese, *Angew. Chem. Int. Ed.* **1989**, *28*, 1500–1502.

[40] A. Stute, G. Kehr, R. Fröhlich, G. Erker, *Chem. Commun.* **2011**, *47*, 4288–4290.

[41] Y. Ren, Y. Dienes, S. Hettel, M. Parvez, B. Hoge, T. Baumgartner, *Organometallics* **2009**, *28*, 734–740.

[42] M. M. Hansmann, D. A. Ruiz, L. Liu, R. Jazzar, G. Bertrand, *Chem. Sci.* **2017**, *8*, 3720–3725.

[43] M. Mehta, J. M. Goicoechea, *Chem. Commun.* **2019**, *55*, 6918–6921.

Chapter 5
Reduction and Deoxygenation chemistry of [B]OCP

5.1 Introduction and objectives

5.1.1 Cyaphide

Cyanide, C≡N⁻, is an ion of fundamental importance in both ionic salts and in the coordination sphere of metals. Its role in organic chemistry is equally important, allowing access to the linkage isomeric cyanides (R–CN) and isocyanides (R–NC). It is not surprising then that the heavier phosphorus analogue of cyanide, the cyaphide anion (C≡P⁻), in the form of salts and metal complexes, has been a much sought-after target for phosphorus and organophosphorus chemists. While salts of the ion have evaded isolation, several organo- and metallo-cyaphide species have been isolated by quite varied routes.

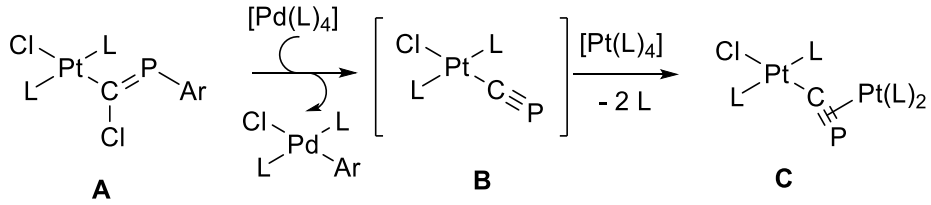

Scheme 5.1. Angelici's serendipitous platinum cyaphide complex. L = PEt_3.

The first spectroscopic evidence of a metal cyaphide complex was a result of the insertion of palladium into the C–Cl bond of **A** followed by transfer of the aryl substituent onto the palladium centre yielding platinum complex **B** (Scheme 5.1).[1] The cyaphide complex itself was too unstable to isolate, however a $^{31}P\{^{1}H\}$ NMR resonance at 68.0 ppm was observed with triplet splitting, assigned as coupling to two PEt_3 ligands ($^{3}J_{P–P}$ = 9.2 Hz). This resonance also exhibited satellites corresponding to ^{195}Pt coupling ($^{2}J_{Pt–P}$ = 303 Hz). While the authors were unable to isolate the terminal cyaphide complex **B**, addition of a second equivalent of the platinum complex $[Pt(PEt_3)_4]$ to the reaction mixture allowed for the isolation and characterisation of the trapped η^2-cyaphide complex **C**.

Following this report there have been two rational syntheses of cyaphide-containing compounds, both exploiting the oxophilicity of silicon to yield the desired $C{\equiv}P^-$ fragment. The first of these reports was from the groups of Lehmann and Willner, who achieved a Lewis-acid coordinated cyaphide through addition of $K[P(SiMe_3)_2]$ to the anionic complex $[(CF_3)_3B(COCl)][PPh_4]$ (Scheme 5.2; **D**), liberating KCl and siloxane to yield the anionic cyaphide adduct $[(CF_3)_3B(CP)][PPh_4]$ (Scheme 5.2; **E**).[2] The authors hoped that this strategy could be applied to a range of carbonyl complexes, however, there have been no further reports expanding on this methodology.

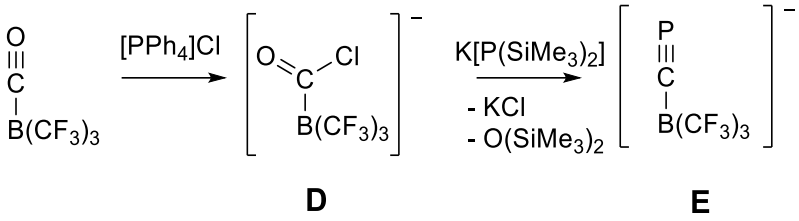

D **E**

Scheme 5.2. The first rational synthesis of a cyaphide adduct.

A different approach was adopted by Grützmacher and co-workers who found that by employing a ruthenium complex with equatorial steric bulk and an axial binding pocket they were able to achieve η^1-coordination of $(Ph)_3SiC{\equiv}P$, a strategy first reported by Nixon in 1987.[3] Subsequently the Si–C bond was cleaved through addition of nucleophilic sodium phenoxide, to yield the desired cyaphide complex and liberate $Ph–O–Si(Ph)_3$ (Scheme 5.3).[4] Further work has been conducted to expand the utility of these complexes by the group of Crossley, with a focus on increased conjugation between the cyaphide and the *trans* substituent.[5–7]

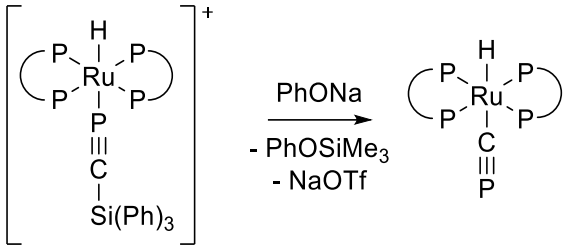

Scheme 5.3. Grützmacher's ruthenium cyaphide complex.

The 2-phosphaethynolate salt is, currently, the smallest stable molecule containing a C≡P triple bond, making it an attractive reagent for the synthesis of cyaphide-containing complexes. This potential reactivity of PCO^- was first demonstrated by the groups of Meyer and Grützmacher in the coordination sphere of uranium.[8] Addition of half an equivalent of Na[PCO] to [(($^{Ad,Me}ArO)_3N$)U(DME)] (($^{Ad,Me}ArO)_3N$ = the trianion of tris(2-hydroxy-3-(1-adamantyl)-5-methylbenzyl)-amine) followed by the addition of a sequestering agent 2.2.2-crypt (2.2.2-crypt = 4,7,13,16,21,24-hexaoxa-1,10- diazabicyclo[8.8.8]hexacosane) resulted in cleavage of the O–C bond, yielding the uranium(IV) cyaphide complex (Scheme 5.4.). The phosphaethynolate coordination complex is a proposed intermediate in this transformation, supported by a reaction between Na[PCO] and the analogous U(IV) chloride where the uranium phosphaethynolate complex was generated.[8]

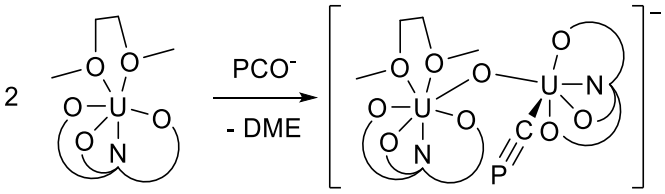

Scheme 5.4. Cleavage of the O–C bond in PCO^- by a uranium complex. O_3N^{3-} ligand = tris(2-hydroxy-3-(1-adamantyl)-5-methylbenzyl)-amine.

Mindiola and co-workers reported on the reduction of the scandium phosphaethynolate species (nacnac)Ti(OCP)(OAr) (nacnac = $[ArNC(CH_3)]_2CH$; Ar = 2,6-$^iPr_2C_6H_3$) using KC_8, which was found to produce the reductively coupled diisophosphaethynolate complex.[9] The ligand is formally the tetraanionic $[OCPPCO]^{4-}$.

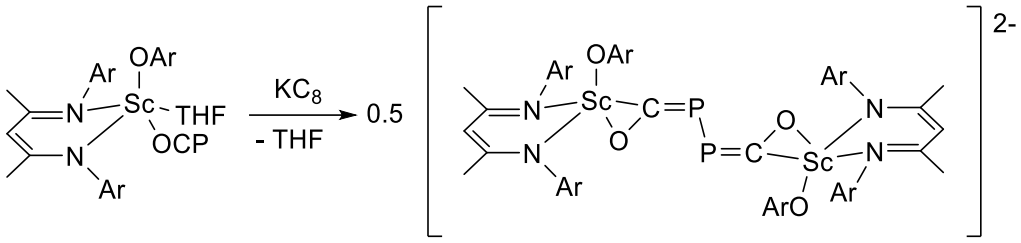

Scheme 5.5. The reduction of a scandium phosphaethynolate species to give a tetraanionic $[OCPPCO]^{4-}$ ligand.

5.1.2 Reduction chemistry of phosphaalkynes

The reduction chemistry of phosphaalkynes varies depending on the reducing agent used. Reaction of potassium or sodium metal with ^{t}BuCP results in formation of two products, the $(P_3C_2{}^{t}Bu_2)^-$ and $(P_2C_3{}^{t}Bu_3)^-$ anions shown in Scheme 5.6.[10] These cyclopentadienyl salt analogues have found use as ligands in a number of main-group complexes (Pb, Sr, Zn, Cd).

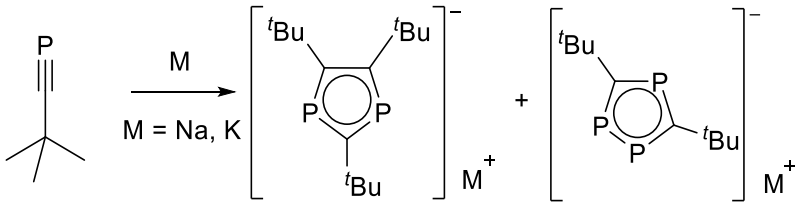

Scheme 5.6. Reduction of ^{t}BuCP with alkali metals.

Edelmann and co-workers described the unusual reductive dimerization of ^{t}BuCP by decamethylsamarocene $[Sm(Cp^*)_2(THF)_2]$, a lanthanide complex with a similar reduction potential to alkali metals. The product contains a dianionic 2,3-diphosphabutadiene unit linking two samarium centres, a result of reductive coupling of two phosphaalkynes.[11]

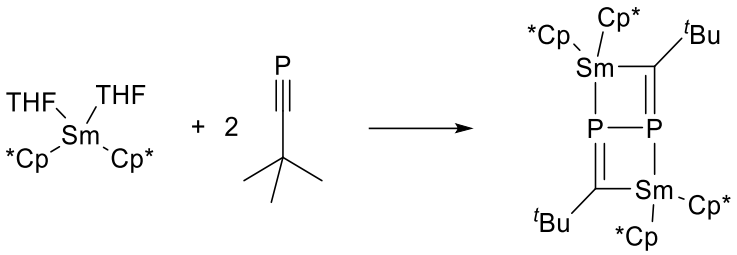

Scheme 5.7. Reductive coupling of phosphaalkynes with a samarium complex.

Binger, Regitz, and co-workers reported an unusual dimerization of ^{t}BuCP in the coordination sphere of zirconium through reduction of the Zr(II) precursor, $[Zr(Cp)_2Cl_2]$, over a magnesium amalgam (Scheme 5.8).[12,13] The reaction yields the zirconium complex $[Zr(Cp)_2(C_2P_2{}^{t}Bu_2)]$, in which the 1,3-diphosphabicyclo[l.l.0]butane ligand is bonded to the zirconium through two C–Zr σ-bonds. Calculations indicate that this diphosphabicyclo[l.l.0]butane arrangement of the $C_2P_2{}^{t}Bu_2$ fragment is thermodynamically more stable than the diphosphacyclobutadiene, and to date zirconium is the only transition metal known to display this bonding motif. The major advantage of this complex was the ease with which the $C_2P_2{}^{t}Bu_2$ moiety could be removed from the metal. For example, addition of PCl_3 to the complex resulted in the loss of the Zr(II) dichloride and formed a organophosphorus cage (Scheme 5.8). Alternatively, if two equivalents of I_2 are added the 1,2-diiodo-1,2-diphosphete is obtained.

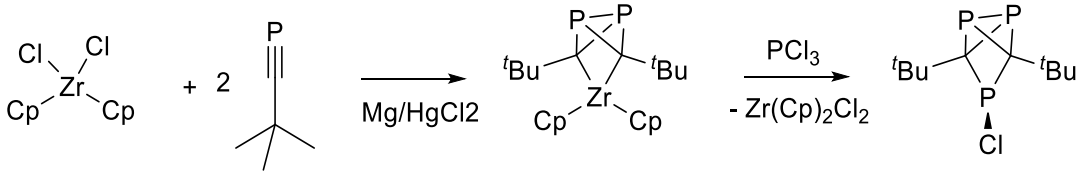

Scheme 5.8. Synthesis and reactivity of a $Cp_2Zr(C_2P_2{}^{t}Bu_2)$ complex.

A recent report from the Wolf group outlined a Ni(0) catalysed dimerization of phosphaalkynes to yield diphosphatetrahedranes $(RCP)_2$ (R = ^{t}Bu, Ad). The proposed mechanism for this transformation involves the diphosphacyclopentadienyl Ni(II) complex,

which was isolated and fully characterised, which rearranges to give the coordinated diphosphatetrahedrane which can subsequently be released from the metal.[14]

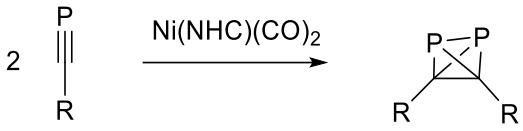

Scheme 5.9. Catalytic dimerization of phosphaalkynes to give diphosphatetrahedranes (NHC = 1,3-diisopropyl-4,5-dimethyl-1,3-dihydro-2λ^2-imidazole. R = ^{t}Bu, Ad).

5.1.3 Objectives

We hypothesized that through addition of a two-electron reductant to [B]OCP we could selectively cleave the O–C bond of the phosphaethynolato moiety, allowing access to the much desired cyaphide anion.

5.2 Alkali metals as reductants

The initial investigation into the reduction focussed on the alkali metals (Li, Na, and K). Typically, these reductions are carried out in a coordinating solvent such as ether or THF, however in the presence of basic solvents rapid formation of the respective 2-phosphaethynolate salt and dimeric species **2** was observed. Variation of the reaction conditions, such as decreasing the temperature, changed the ratio of the products formed, however no new products were observed. Dimerisation of **1** in the presence of THF typically requires several days at elevated temperatures to reach completion. Interestingly, the presence of alkali metal ions appears to catalyse this transformation, which goes to completion in less than an hour at –78 °C.

When toluene was employed as the solvent, the reaction between **1** and two equivalents of lithium showed no reaction even in the presence of sequestering agent 12-crown-4. Reduction of **1** with sodium metal required reduced temperatures to prevent formation of complex reaction mixtures. When the reaction was conducted at –78°C overnight three

products can be observed in the $^{31}P\{^{1}H\}$ NMR spectrum, the dimeric species **2**, a product with a singlet resonance at 120.4 ppm, and an AB spin system with resonances at 290.5 and 166.3 ppm (J_{P-P} = 39.7 Hz). It was possible to identify one of the products through fractional crystallisation from a hexane solution (Scheme 5.10; **32**).

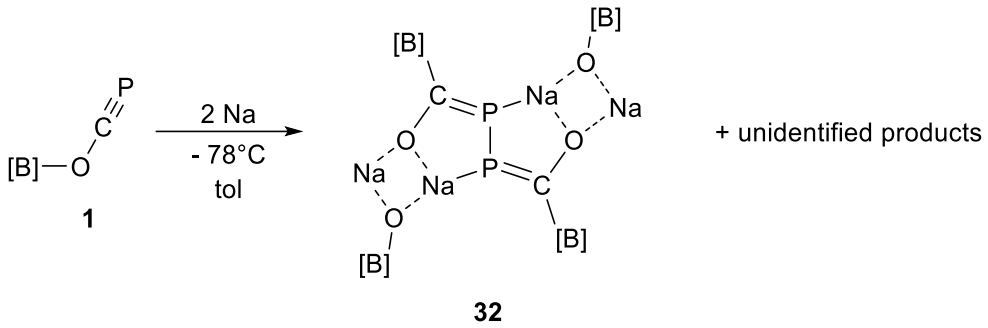

Scheme 5.10. Reduction of [B]OCP with sodium metal.

The solid-state structure of **32** reveals the reductive coupling of two units of [B]OCP, with formation of a P–P bond, accompanied by boryl migration from the oxygen to the carbon centre. This core is capped by two sodium cations in addition to two boryloxy anions with corresponding sodium cations, forming a ladder-like structure. The reductively coupled core of this species resembles Mindiola's titanium system, however with migration of the boryl moiety rather than η^2-coordination to the metal centre.[9]

Dissolving the crystals in deuterated benzene allowed for unambiguous assignment as the peak at 120.4 ppm in the $^{31}P\{^{1}H\}$ NMR spectrum. The ^{1}H NMR spectrum contained two peaks of equal intensity corresponding to the boryl fragments backbones at 6.33 and 5.98 ppm. The presence of two boryloxy anions in the product confirms that cleavage of the O–C bond is possible. However, the fate of two cleaved $C{\equiv}P^-$ fragments is unknown. It is probable they are related to the (as of yet) unidentified signals in AB spin system.

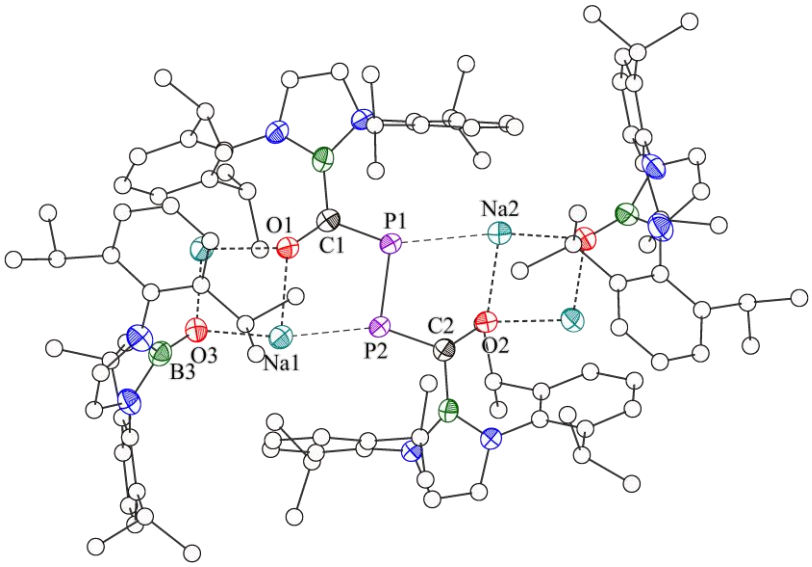

Figure 5.1. The solid-state structure of intermediate **32**. Anisotropic displacement ellipsoids are set at 50% probability. Hydrogen atoms omitted for clarity. Dipp and backbone carbon atoms shown as spheres of arbitrary radius.

If instead potassium is employed, in the presence of sequestering agent 18-crown-6, the ^{1}H NMR spectrum is consistent with the formation of a major boryl containing species while the ^{31}P{^{1}H} NMR spectrum displays two major products, an ABB spin system with resonances at 268.1 (d, $J_{P–P}$ = 44.8 Hz) and 254.6 (t, $J_{P–P}$ = 44.8 Hz), along with a singlet at 51.6 ppm. PCO^{-} could also be detected as a minor product.

Crystallisation of the reaction mixture allowed for identification of the major product in the ^{1}H NMR spectrum as [B]O[K(18-crown-6)]. A very similar compound has recently been utilised as a ligand by the Aldridge group.[15] Unfortunately, we were unable to crystallise either of the phosphorus-containing species from the reaction mixture.

These studies have demonstrated that while cleavage of the desired O–C bond is possible, selective, controlled reduction with alkali metals is poor.

5.3 [(^{Ar}Nacnac)Mg]$_2$

5.3.1 Reduction of [B]OCP, 1

Another family of reducing agents are Jones' magnesium(I) dimers in which the dimer acts as a two electron reductant.[16,17] This study employs the mesityl derivative, [(^{Ar}Nacnac)Mg]$_2$ (Ar = $C_6H_2Me_3$-2,4,6 (Mes)), [^{Mes}Mg]$_2$. Addition of one equivalent of [^{Mes}Mg]$_2$ to two equivalents of **1** results in only partial consumption of **1**. If instead a stoichiometric amount of dimer is added to **1** a complex reaction mixture can be observed by $^{31}P\{^1H\}$ NMR spectroscopy, by contrast the ^1H NMR spectra indicates a single major product in addition to a significant number of minor products (Scheme 5.11). Isolation of the major product observed in the ^1H NMR spectrum was possible by fractional crystallisation, allowing for identification of the magnesium stabilised boryloxy anion **33**.

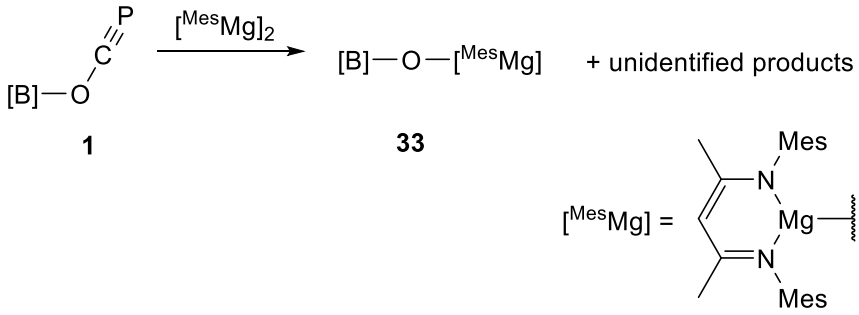

Scheme 5.11. Reduction of **1** with magnesium dimer to yield **33**.

Extraction of the reaction mixture with hexane, followed by cooling to –35°C results in pale yellow crystals suitable for X-ray diffraction analysis. The solid state structure reveals an O1–B1 bond distance of 1.326(2) Å, in line with what is typical of a double bond (Σ_{cov} = 1.35 Å).[18] The Mg1–O1 bond length is 1.803(1) Å, consistent with significant donation of electron density being donated from the oxygen lone pair into the π-system resulting in a double bond (Σ_{cov} = 1.89 Å). The B1-O1-Mg1 bond angle approaches linearity as noted by an angle of 174.6(1)° (Figure 5.2).

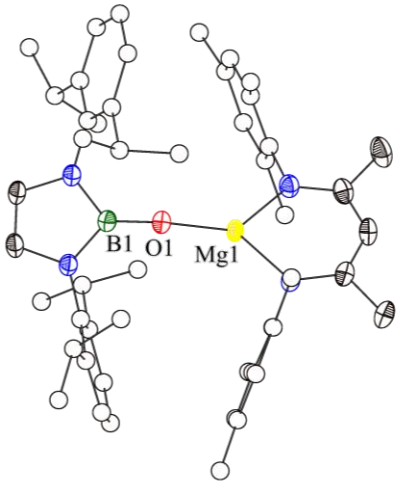

Figure 5.2. The solid state structure of **33**. Anisotropic displacement ellipsoids are set at 50% probability. Hydrogen atoms omitted for clarity. Dipp, Mes and ᵗButyl carbon atoms shown as spheres of arbitrary radius.

It was also possible to crystallise one of the phosphorus-containing species, however the crystals were very thin plates which diffracted poorly at high angle. This, in addition to a significant amount of positional disorder in the structure, results in poor data quality. It is possible, however, to deduce the presence of a $[C_2P_2]^{4-}$ fragment surrounded by five magnesium β-diketiminate complexes (Figure 5.3). There is also highly disordered region that may be cautiously described as a CP^- bridging between two magnesium centres. Despite multiple attempts at recollecting this structure, it was not possible to obtain data of an acceptable standard for the discussion of bond metrics.

The ^{1}H NMR spectrum of the crystals is consistent with presence of five magnesium ligands, however the $^{31}P\{^1H\}$ NMR spectra displays doublet resonances at 311.1 ppm ($^2J_{P-P}$ = 112.6 Hz) and 566.2 ppm ($^2J_{P-P}$ = 112.0 Hz), in addition to a broad singlet resonance appearing at 295.9 ppm.

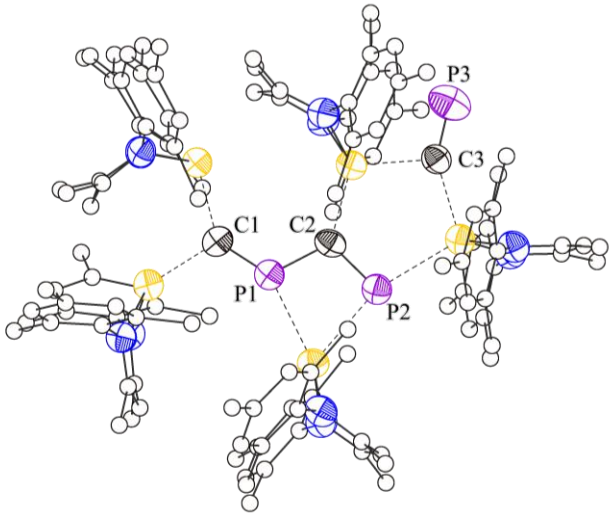

Figure 5.3. The solid state structure of **34**. Anisotropic displacement ellipsoids are set at 50% probability. Hydrogen atoms omitted for clarity. β-diketiminate carbon atoms shown as spheres of arbitrary radius.

34 is only present in the reaction mixture at around 16% of the total phosphorus-containing products, estimated using $^{31}P\{^{1}H\}$ NMR spectroscopy. Attempts to identify the any of the other phosphorus-containing species were unsuccessful. This study did indicate there is a possibility of cleaving the desired O–C bond. The selectivity of the initial step is very promising, with high yielding formation of **33**. The preliminary data for compound **34** suggests that generation of the target magnesium cyaphide, [Mg]CP, is possible. However, in this case it rapidly and uncontrollably reacts further, giving a mixture of phosphorus species, for example the oligomerised $[C_2P_2]^{4-}$ tetraanion.

5.3.2 Reactivity of magnesium(I) dimers with phosphaalkynes

We were unable to find any reports on the reactivity of phosphaalkynes towards Mg(I) dimers in the literature. In order to better understand the reactivity between the magnesium dimers and **1**, we began an investigation into the reduction of phosphaalkynes with $[^{Mes}Mg]_2$.

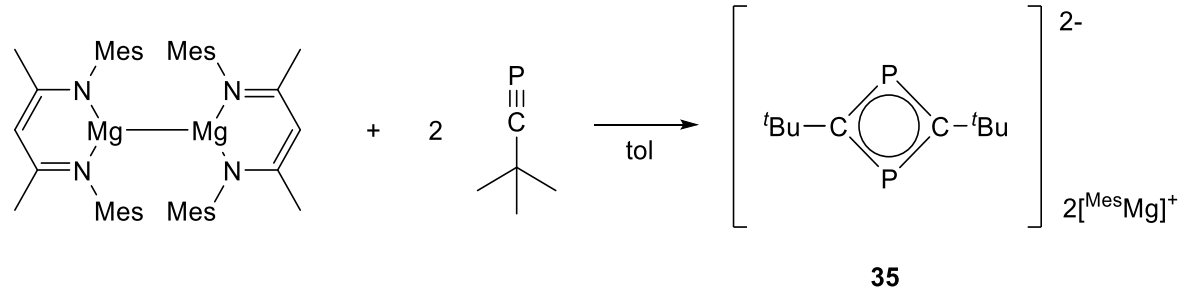

35

Scheme 5.12. The reactivity of ^{t}BuCP with $[^{Mes}Mg]_2$.

Addition of one equivalent of $[^{Mes}Mg]_2$ to one equivalent of ^{t}BuCP resulted in a complex reaction mixture. If instead half an equivalent of the dimer was employed, the reaction yielded a single product by $^{31}P\{^{1}H\}$ NMR spectroscopy after 24 hours with a singlet resonance at 202.3 ppm (Scheme 5.12). Crystals of this product were obtained by cooling a saturated toluene solution to –35°C overnight.

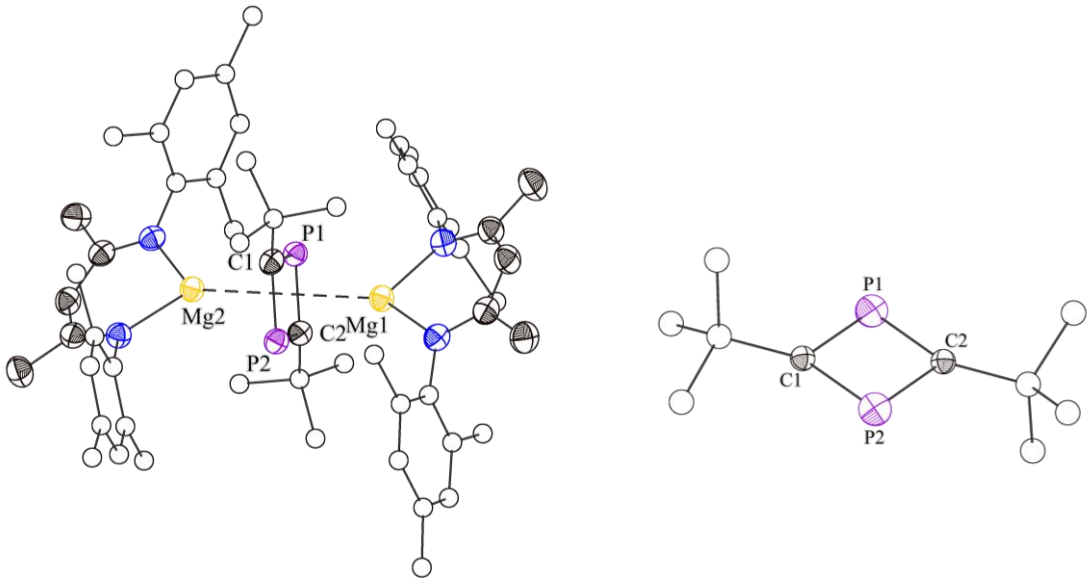

Figure 5.4. The solid-state structure of **35**. Anisotropic displacement ellipsoids are set at 50% probability. Hydrogen atoms omitted for clarity. Mes and ^{t}butyl carbon atoms shown as spheres of arbitrary radius. Right: The central $C_2P_2{}^{t}Bu_2$ core.

The solid-state structure revealed a 1,3-diphosphacyclobutadienediide, $[(^{t}Bu)_2C_2P_2]^{2-}$, the result of a reductive dimerization of two phosphaalkyne equivalents. The cyclic P–C bonds are identical within two standard deviations (Mean C–P distance = 1.820 Å) and are

in line with contracted single bonds (Σ_{cov} = 1.86 Å).[18] There is slight asymmetry between the four-membered ring and the two magnesium centres, both being closer to P1 than P2 (Mean Mg–P1 distance = 2.546 Å, Mg–P2 = 2.688 Å). This inequivalence is not present in the solution phase, the ^{13}C NMR spectrum displays a triplet resonance corresponding to the cyclic carbon centres ($^{1}J_{C-P}$ = 54 Hz). Notably the central four membered ring is not planar (deviation from plane = 0.00671 Å), which is unusual for what could be considered a 6π-aromatic system and contrasts with the planarity observed in the related transition metal complexes (discussed in Chapter 4) which all display planar C_2P_2 moieties. A closely related system has previously been reported by the group of Niecke.[19] Their synthetic route involves the reduction of 1,2-diphosphacyclobutane-2,4-diyl (Scheme 5.13). The P–aryl bonds are cleaved upon reduction with lithium or potassium resulting in the TMS derivative of the dianion. The solution phase NMR data for this compound is similar to **35**, with a ^{31}P NMR resonance appearing at 200.3 ppm. The reported solid-state data of the core C_2P_2 ring is indistinguishable within three standard deviations, with C–P bond lengths of 1.797(1) and 1.800(1) Å.

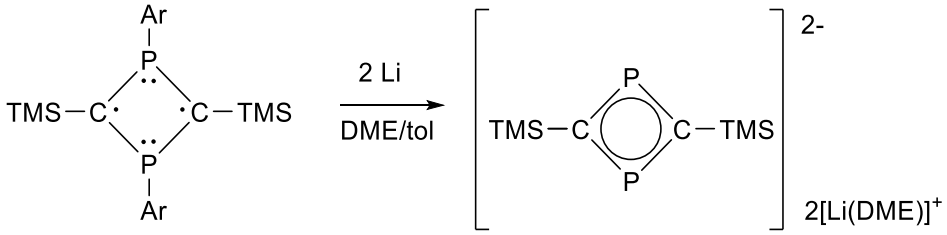

Scheme 5.13. Niecke's original synthesis of a 1,3-diphosphacycloburadiide.

Monitoring the reaction using ^{31}P{^{1}H} NMR spectroscopy revealed two intermediates during the transformation, a singlet resonance at 345.9 ppm and an AB spin system with doublet resonances at 382.4 and 287.1 ppm (J_{P-P} = 304 Hz) which converted to the dimeric product. During one of the NMR experiments, X-ray quality crystals formed at the top of the NMR tube, allowing for identification of the singlet species. The crystal structure contained

two crystallographically unique units of **36**, however for simplicity only one will be discussed.

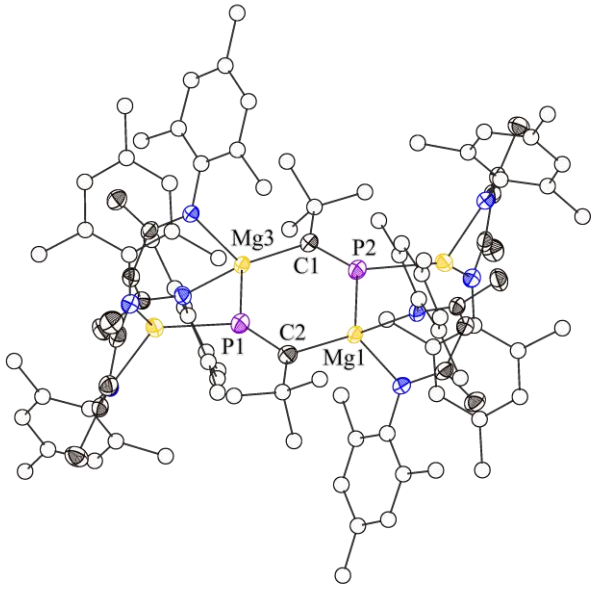

Figure 5.5. The solid-state structure of intermediate **36**. Anisotropic displacement ellipsoids are set at 50% probability. Hydrogen atoms omitted for clarity. Mes and ^{t}Butyl carbon atoms shown as spheres of arbitrary radius.

The solid-state structure reveals four magnesium centres and two equivalents of phosphaalkyne (Figure 5.5). The two phosphaalkynes and two of the magnesium centres form a six-membered heterocycle, while the additional two magnesium centres are coordinated to the phosphorus atoms. The C–P bonds are equivalent with an average bond length of 1.702 Å, consistent with reduction of multiple bond character to a single bond (Σ_{cov} = 1.69 Å).[18] The cyclic Mg–C bonds are slightly longer than the sum of the covalent radii for a single bond (mean bond length = 2.179 Å, Σ_{cov} = 2.14 Å), and the same is true for the P–Mg bonds (2.585 Å, Σ_{cov} = 2.50 Å). The exocyclic P–Mg bonds are slightly contracted with respect to the in-cycle bond (mean bond length = 2.525 Å).

One notable observation is the loss of planarity of the magnesium β-diketiminate ligand backbones, particularly those of the in-cycle magnesium complexes, which adopt a boat-like

conformation with long range interactions between the in-cycle β-diketiminate backbone carbons and the exocyclic magnesium cations (Mg–C = 2.504 Å). This bond length is consistent with a resonance form where there is increased negative charge on the backbone carbon, stabilised through interaction with the magnesium cations. Further structurally corroborated by pyramidalisation of the backbone carbon atoms and contraction of the ligand N–C bond length in the in-cycle magnesium complexes in comparison to the exocyclic complexes (average bond lengths 1.313 vs. 1.333 Å), consistent with a greater degree of electron density residing in the N–C π-bond in the in-cycle complexes.

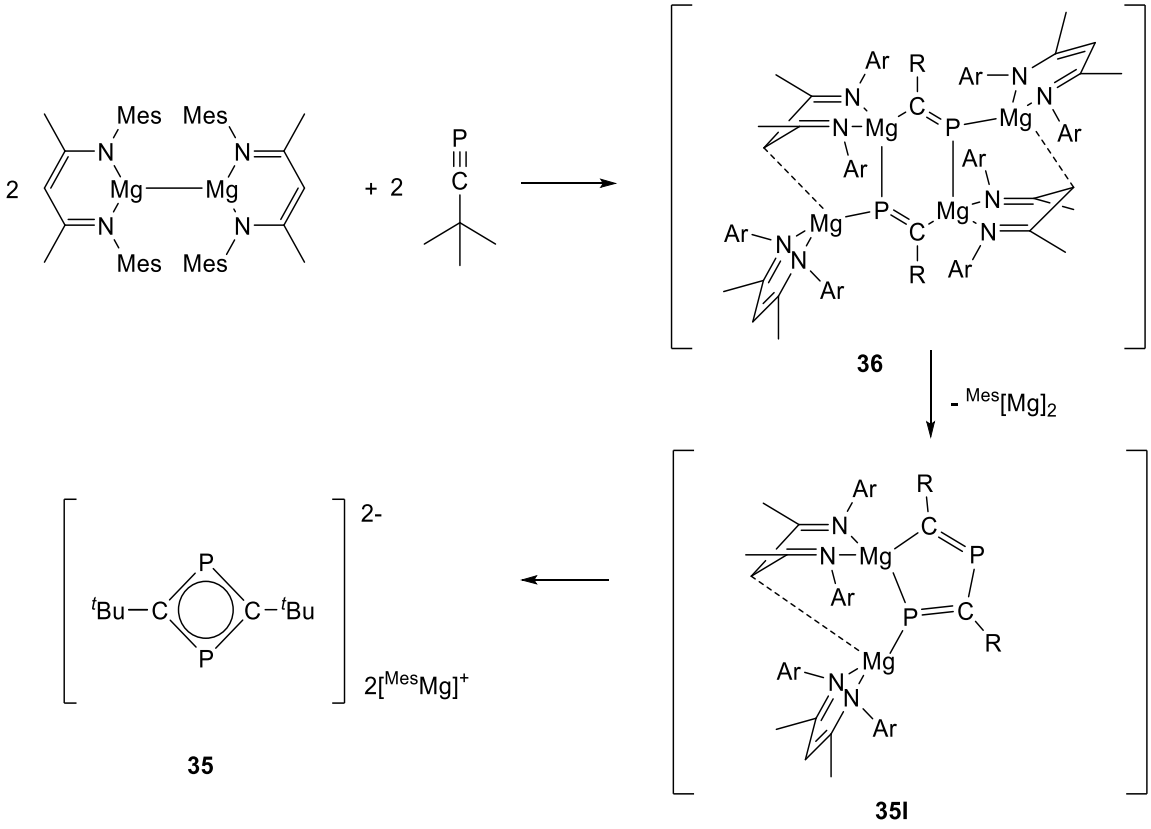

Scheme 5.14. Proposed mechanism for the formation of **35**. R = ^{t}Bu.

To our knowledge, this cooperative reactivity of magnesium β-diketiminate complexes has not been observed previously, and provides insight into the mechanism of these unusual reductants. Reversible redox behaviour has previously been observed during insertion reactions between magnesium dimers and 1,1-diphenylethylene.[20] We postulate that a

similar process is able to occur here, after 1,2-addition across the unsaturated C≡P bond, as is the case with the 1,1-diphenylethylene. This species then dimerises due to the presence of the lone pair at the phosphorus centre and a coordinatively unsaturated magnesium centre (Scheme 5.14). The dimer **36** undergoes further reactivity to the final product **35**, through release of two equivalents of the magnesium β-diketiminate. The complete consumption of phosphaalkyne implies the released magnesium species is able to undergo further reactions, likely in the form of the magnesium dimer, $[^{Mes}Mg]_2$ (Scheme 5.13), constituting a rare example of magnesium displaying redox behaviour more typical of transition metals.

During *in situ* reaction monitoring, an AB spin system could be observed, which was tentatively assigned to the 5-membered heterocycle **35I**, formed through the liberation of one magnesium(I) dimer from **36**. Similar η^3-coordinated phosphaalkyne dimers have been reported in the coordination sphere of rhodium(II) complexes.[21]

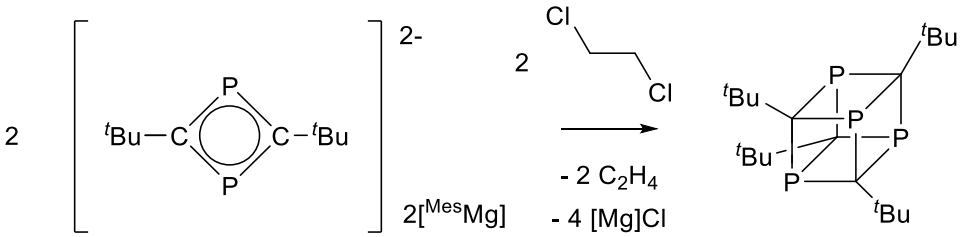

Scheme 5.15. Demetallation of **35** to yield a tetraphosphacubane.

As with the related zirconium complexes, demetallation of the C_2P_2 moiety is facile.[13] Addition of 1,2-dichloroethane to the reaction mixture results in liberation of [Mg]Cl and the tetraphosphacubane, identified by ^{31}P NMR spectroscopy (δ = 256.4 ppm), via a transient intermediary anti-aromatic diphosphacyclobutadiene (Scheme 5.15).[22,23] The instability of **33** in coordinating solvents negates its utility as a transfer agent for C_2P_2 ligands to other metals, and the prevalence of such complexes in literature would make such a reagent limited in scope.[24]

5.4 Deoxygenation chemistry

A recent report from the Grützmacher group showed addition of potassium bis(trimethylsilyl)amide (KHMDS) to a phosphanyl phosphaketene results in the deoxygenation to yield the respective phosphanyl cyanophosphide salts (Scheme 5.16).[25] This result encouraged us to investigate the chemistry of **1** towards KHMDS and its heavier phosphorus analogue, in an effort to probe the deoxygenation chemistry of the phosphaethynolate **1** relative to the reported phosphanyl phosphaketenes.

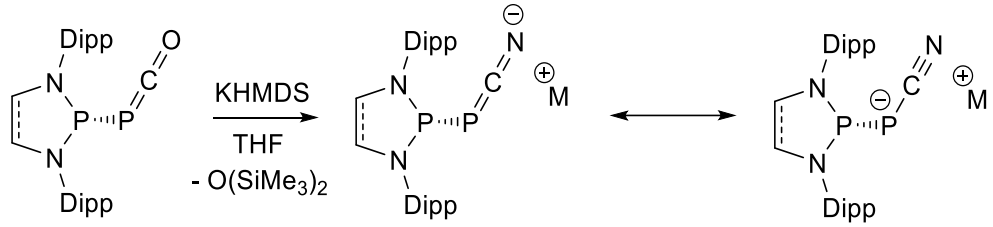

Scheme 5.16. The synthesis of phosphanyl cyanophosphide salts.

Addition of one equivalent of KHMDS to a THF solution of **1** results in quantitative formation of a single product in the NMR spectra with a ^{31}P NMR resonance at 156.7 ppm and a boryl backbone ^{1}H NMR resonance at 5.96 ppm (Scheme 5.17). While this species evaded crystallisation, the NMR data is consistent with attack of the $^{-}$N(SiMe$_3$)$_2$ at the phosphorus, initiating migration of the boryl moiety from the oxygen to the carbon to yield K[[B]C(O)PN(SiMe)$_2$], **37**. This reactivity is the same as what was observed with both lithium aryls and anionic metal complexes, outlined in Chapter 2. The ^{31}P{^{1}H} NMR shift is comparable to that of the LiMes* product, **7**, which displays a resonance at 162.3 ppm.

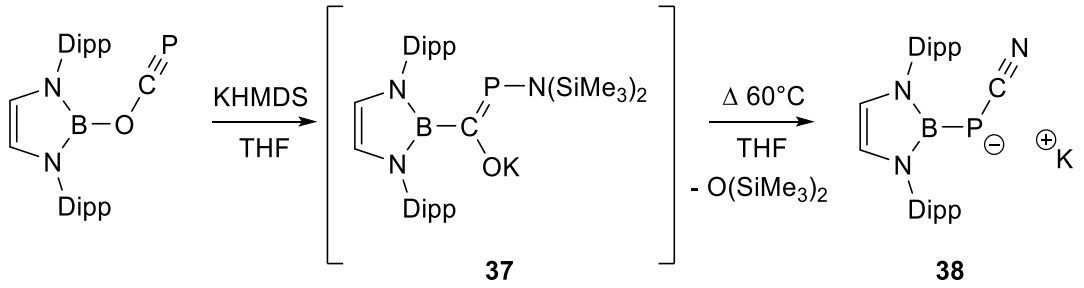

Scheme 5.17. Reaction of [B]OCP with KHMDS.

If a solution containing **37** is heated to 60°C for one hour, quantitative formation of a new product is observed by NMR spectroscopy. The new species displays a ^{1}H NMR resonance corresponding to a single boryl backbone at 6.10 ppm, and a singlet resonance in the ^{31}P NMR spectrum at –258.9 ppm. Crystals of this species can be obtained by cooling a saturated solution in hexane.

The solid-state structure reveals a cyanophosphide salt with a boryl bound to the phosphorus centre, [B]PCN^{-}. This product is related to that obtained in Grützmacher's report, however starting from the linkage isomeric phosphaethynolate rather than the phosphaketene.[26] The bond metrics for the PCN chain are indistinguishable from those of the previously reported phosphanyl cyanophosphide salts. The C–N bond in [B]PCN^{-} is 1.161(3) Å and the C–P is 1.757(2) Å, in comparison to reported averages of 1.75 and 1.16 Å, respectively.

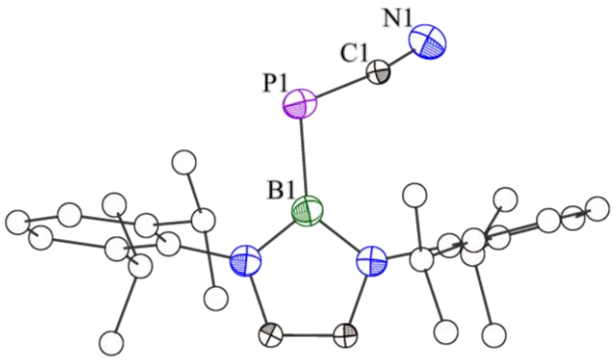

Figure 5.6. The solid-state structure of the anion **38**. Anisotropic displacement ellipsoids are set at 50% probability. Potassuim and hydrogen atoms omitted for clarity and Dipp carbon atoms shown as spheres of arbitrary radius.

We attempted to access carbodiimide analogues through salt metathesis, by substitution at the nitrogen centre using the bromoborane, [B]Br, or 2-bromosupermesitylene, Mes*Br. However, even after heating to 100 °C for prolonged periods no sign of reactivity could be observed in the NMR spectra. This lack of reactivity is consistent with the reported phosphanyl cyanophosphide salts, for which the HOMO lies predominantly on the phosphorus centre. Addition of electrophilic reagents to these species results in functionalisation at the phosphorus centre, with the exception of diazaborolidine $[(H_2C)_2(NAr)_2B]Br$ (Ar=2,6-diisopropylphenyl), which functionalises at the nitrogen due to the formation of an extended π-system.[25]

The mechanism of conversion is a step-wise migration of the boryl group, first migrating from the oxygen to the carbon centre, as observed with anionic nucleophiles (see Chapter 2), and then, upon heating, further migration to the phosphorus. Parallels can be drawn between this rearrangement and the isomerisation of [B]OCP to its linkage isomer, [B]PCO. However, the intermediate in this case is the 1,2-migrated anion stabilised through interaction with a mobile cation (analogous to I1 in Figure 3.14).

If an analogous procedure is carried out using the phosphorus analogue of KHMDS, bis(trimethylsilyl)phosphide, K[P(SiMe$_3$)$_2$], the initial product contains an AB spin system in the $^{31}P\{^1H\}$ NMR spectrum with resonances at 317.8 and –71.6 ppm ($^1J_{P–P}$ = 404 Hz). Consistent with previous observations, attempts to isolate this species were unsuccessful likely due to the increased solubility attributed to the trimethylsilyl functionalities. However, the $^{31}P\{^1H\}$ NMR resonance is consistent with the migratory species **39** (Scheme 5.18). We attempted to thermally treat this compound to induce migration of the boryl and generate a C≡P triple bond. However, no change to the NMR spectra of **39** was observed upon heating to 100°C overnight. A C≡P triple bond, being significantly weaker than the C≡N triple bond generated upon formation of **38**, may not provide an adequate thermodynamic driving force for this conversion.

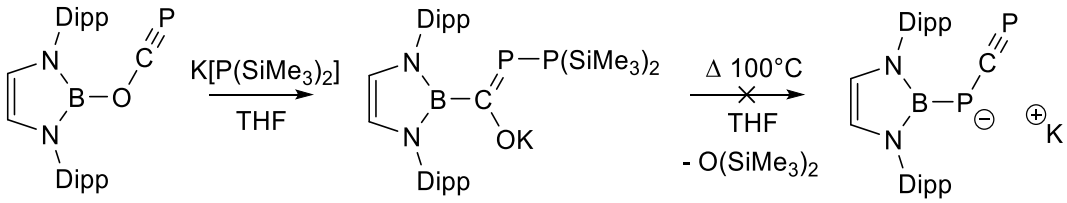

39

Scheme 5.18. Reactivity of [B]OCP with K[P(SiMe$_3$)$_2$].

5.5 Conclusions

This chapter discusses the reduction chemistry of [B]OCP. The selectivity upon reduction with alkali metals was poor, often yielding multiple products. In select cases, it was possible to isolate the boryloxy fragment, implying the possibility of generating the cyaphide ion. However, the phosphorus containing species that were isolated contained reductively coupled phosphorus centres, for example in the P–P bound complex **32**. Reduction with the magnesium(I) dimer [^{Mes}Mg]$_2$ resulted in similarly poor selectivity, however resulted in partial characterisation of a compound containing a $[C_2P_2]^{4–}$ tetraanionic

chain in addition to a CP^- fragment. Reduction of the archetypal phosphaalkyne ^{t}BuCP with $[^{Mes}Mg]_2$ results in a 1,3-diphosphacyclobutadiide **33**, allowing facile access to a species which was previously synthetically difficult and time consuming to access.

Finally, the deoxygenation chemistry of [B]OCP with $K[N(SiMe_3)_2]$ was explored, which was found to be similar to that reported for a series of phosphanyl phosphaketenes, resulting in formation of the cyanophosphidoborane salt $[B]PCN^-$, **38**. It was also possible to spectroscopically observe an intermediate, **37**, which displays comparable NMR data to the structurally characterised compound **7**. Interestingly, the reaction with $K[P(SiMe_3)_2]$ did not produce $[B]PCP^-$, indicating that siloxane formation alone is not an adequate driving force for this conversion.

5.6 References

[1] H. Jun, V. G. Young, R. J. Angelici, *J. Am. Chem. Soc.* **1992**, *114*, 10064–10065.

[2] M. Finze, E. Bernhardt, H. Willner, C. W. Lehmann, *Angew. Chem. Int. Ed.* **2004**, *43*, 4160–4163.

[3] P. B. Hitchcock, M. J. Maah, J. F. Nixon, J. A. Zora, G. J. Leigh, M. A. Bakar, *Angew. Chem.* **1987**, *99*, 497–498.

[4] J. G. Cordaro, D. Stein, H. Rüegger, H. Grützmacher, *Angew. Chem. Int. Ed.* **2006**, *45*, 6159–6162.

[5] S. K. Furfari, M. C. Leech, N. Trathen, M. C. Levis, I. R. Crossley, *Dalton Trans.* **2019**, *48*, 8131–8143.

[6] M. C. Levis, K. G. Pearce, I. R. Crossley, *Inorg. Chem.* **2019**, *58*, 14800–14807.

[7] M. C. Leech, I. R. Crossley, *Dalton Trans.* **2018**, *47*, 4428–4432.

[8] C. J. Hoerger, F. W. Heinemann, E. Louyriac, L. Maron, H. Grützmacher, K. Meyer,

Organometallics **2017**, *36*, 4351–4354.

[9] L. N. Grant, B. Pinter, B. C. Manor, H. Grützmacher, D. J. Mindiola, *Angew. Chem. Int. Ed.* **2018**, *57*, 1049–1052.

[10] N. Maigrot, L. Ricard, C. Charrier, F. Mathey, *Angew. Chem. Int. Ed.* **1990**, *29*, 534–535.

[11] A. Recknagel, D. Stalke, H. W. Roesky, F. T. Edelmann, *Angew. Chem. Int. Ed.* **1989**, *28*, 445–446.

[12] T. Wettling, R. Schneider, F. Zurmühlen, U. Bergsträsser, J. Hoffmann, G. Maas, M. Regitz, P. Binger, *Angew. Chem. Int. Ed.* **1991**, *30*, 207–210.

[13] P. Binger, B. Biedenbach, C. Krüger, M. Regitz, *Angew. Chem. Int. Ed.* **1987**, *26*, 764–765.

[14] G. Hierlmeier, P. Coburger, M. Bodensteiner, R. Wolf, *Angew. Chem. Int. Ed.* **2019**, *58*, 16918–16922.

[15] Y. K. Loh, L. Ying, M. Ángeles Fuentes, D. C. H. Do, S. Aldridge, *Angew. Chem. Int. Ed.* **2019**, *58*, 4847–4851.

[16] S. P. Green, C. Jones, A. Stasch, *Science.* **2007**, *318*, 1754–1757.

[17] C. Jones, *Nat. Rev. Chem.* **2017**, *1*, DOI 10.1038/s41570-017-0059.

[18] P. Pyykkö, M. Atsumi, *Chem. Eur. J.* **2009**, *15*, 12770–12779.

[19] M. Sebastian, M. Nieger, D. Szieberth, L. Nyulászi, E. Niecke, *Angew. Chem. Int. Ed.* **2004**, *43*, 637–641.

[20] A. J. Boutland, A. Carroll, C. Alvarez Lamsfus, A. Stasch, L. Maron, C. Jones, *J. Am. Chem. Soc.* **2017**, *139*, 18190–18193.

[21] P. Binger, B. Biedenbach, R. Mynott, C. Krüger, P. Betz, M. Regitz, *Angew. Chem.*

Int. Ed. **1988**, *27*, 1157–1158.

[22] P. Binger, J. Stannek, B. Gabor, R. Mynott, J. Bruckmann, C. Krüger, S. Leininger, *Angew. Chem. Int. Ed.* **1995**, *34*, 2227–2230.

[23] T. Wettling, J. Schneider, O. Wagner, C. G. Kreiter, M. Regitz, *Angew. Chem. Int. Ed.* **1989**, *28*, 1013–1014.

[24] A. Chirila, R. Wolf, J. Chris Slootweg, K. Lammertsma, *Coord. Chem. Rev.* **2014**, *270–271*, 57–74.

[25] Z. Li, J. E. Borger, F. Müller, J. R. Harmer, C. Y. Su, H. Grützmacher, *Angew. Chem. Int. Ed.* **2019**, *58*, 11429–11433.

[26] Z. Li, X. Chen, Z. Benkö, L. Liu, D. A. Ruiz, J. L. Peltier, G. Bertrand, C. Y. Su, H. Grützmacher, *Angew. Chem. Int. Ed.* **2016**, *55*, 6018–6022.

Chapter 6
Coordination chemistry of PCO^- and heavier group 13 elements

6.1 Introduction and objectives

6.1.1 Group 13 group 15 multiple bonds

Investigations into the chemistry of unsaturated group 13/15 bonded systems has been heavily focused on B–N bonds, which are isoelectronic to C–C bonds. Early research exploring the substitution of B–N groups into aromatic frameworks found that, despite retaining most of the structural properties of their carbon analogues, the photophysical and electrochemical properties of B–N substituted materials differ significantly.[1,2] For example, substituting the central C–C of pyrene with B–N bond results in a significant red-shift in the absorption and emission bands, and a reduction in quantum yield.[3]

Ammonia boranes, $R_2HN–BHR_2$ (R = H, aliphatic), which are isoelectronic to alkanes, display high gravimetric hydrogen storage capacity. Bearing both protic (NH) and hydridic (BH) hydrogen atoms, the proximity and inverse polarity of the two hydrogen sites allows for dihydrogen release under mild conditions.[4] While significant attention has been paid to developing catalysts for such dehydrogenation reaction, both for fuel cell applications and also for the controlled polymerisation of the generated B=N species to yield polyaminoboranes and polyborazylenes, regeneration of the amine boranes is still a key challenge in the field.[5,6]

While B–N systems have received significant interest over the past few decades, studies on heavier group 13/15 compounds featuring multiple bonds are much rarer. Examples of B–P and B–As multiple bonds, as well as group 13 metal imides have been reported.[7–10] However, of the heavier RM=ER’ species (M = Al, Ga, In, Tl; E = P, As, Sb, Bi) only three examples of gallaarsenes and a sole gallastibene have been reported.[11–13] These species, like their lighter congeners, contain hydridic and protic sites and have the potential to heterolytically split hydrogen, aided by the presence of a weak π–bond. Homolytic hydrogen

activation has previously been achieved employing main group compounds containing unsaturated homoleptic germanium and tin double bonds.[14,15]

The Schulz group recently reported a gallaarsene, a compound with a As=Ga double bond, from the reaction of Cp^*AsCl_2 ($Cp^* = C_5Me_5$) with two equivalents of Ga(nacnac) (nacnac = $HC[C(Me)N\text{-}(C_6H_3)\text{-}2,6\text{-}^iPr_2]_2$).[12,16] One equivalent of the gallium(I) species acts as a sacrificial reductant, to yield $Cl_2Ga(nacnac)$, and the authors were able to identify (η^1-Ga(nacnac)(μ-As_3)(η^2-Ga(nacnac)) and (nacnac)Ga=AsCp^* from the reaction mixture (Scheme 6.1.). The latter compound features a Ga=As double bond (average bond length 2.268 Å, Σ_{cov} = 2.31 Å).[17] The group optimised their synthesis to obtain related species containing Ga=As bonds from arsenic trihalides and three equivalents of Ga(nacnac).[13]

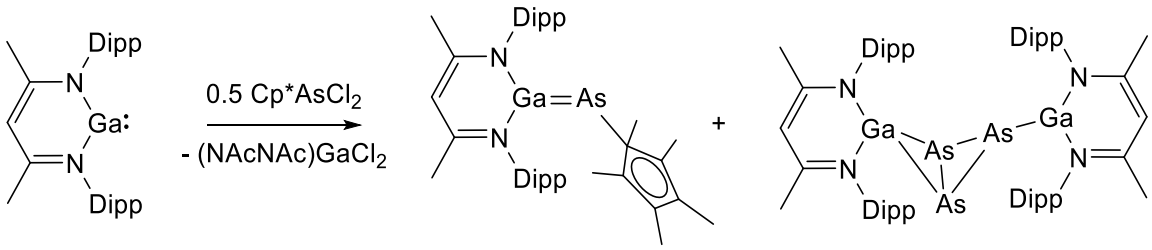

Scheme 6.1. Synthesis of a gallaarsene.

In a related synthesis, addition of two equivalents of Ga(nacnac) to one equivalent of Cp^*SbCl_2 results in a double oxidative addition reaction to afford the stilbene-bridged (nacnac)Ga(Cl)SbGa(Cl)(nacnac) (Scheme 6.2). This compound is subsequently reduced using KC_8 to afford (nacnac)Ga=SbGa(Cl)(nacnac).[11] The Ga–Sb distance is 2.469(2) Å, in line with a double bond (2.50 Å), and displays a Ga-Sb-Ga bond angle of 113.184(7)°.

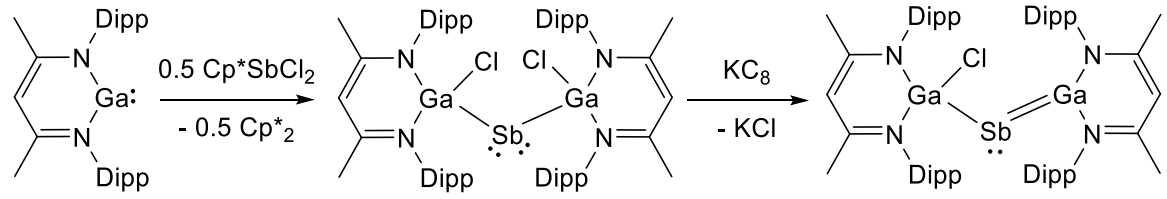

Scheme 6.2. Synthesis of a gallastibene.

While monomeric Ga=P bonds have yet to be structurally authenticated, they have been proposed as intermediates in other transformations. A study by the Grützmacher group investigated the reactivity between the 2-phosphaethynolate anion and a *bis*-amino functionalised gallium chloride, $(TMP)_2GaCl$ (TMP = 2,2,6,6,-tetramethylpiperidino).[18] The product of this reaction is a diphosphadigalletane, which forms a ladder like structure in the solid state. The authors propose that after generation of the phosphaketene, a 1,3-amino migration occurs to yield an acrylamide-type intermediate containing a Ga=P double bond, which dimerises to give the resultant diphosphadigalletane. The authors were not able to spectroscopically detect either of the proposed intermediates in this transformation.

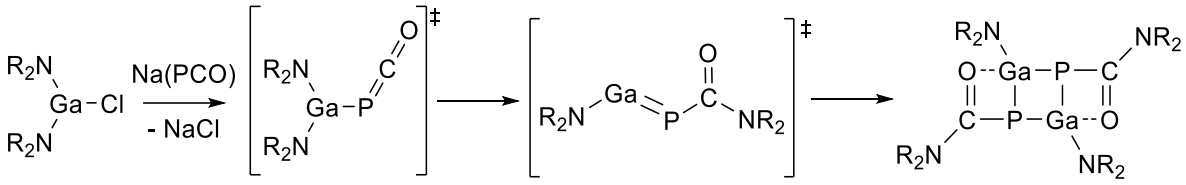

Scheme 6.3. Addition of Na(PCO) to a $(TMS)_2GaCl$ to yield a diphosphadigalletane.

6.1.2 Chapter outline

This chapter will explore the chemistry of the 2-phosphaethynolate towards gallium compounds. This chapter will describe the synthesis of gallium phosphaketenes. The reactivity of these species will be explored, with an emphasis on attempts to access Ga–P multiple bonds and their subsequent reactivity. Prior to beginning this work, there were no examples of gallium phosphaketenes reported in the literature. However, one example of a salen supported gallium phosphaketene has since been reported.[19] This compound reacts in an analogous fashion to alkali metal salts of PCO^- in examples of salt metathesis reactions and Diels Alder type cyclisations with tetrazine. We aim to expand on the known reactivity modes for such species.

6.2 Gallium phosphaketenes

6.2.1 Synthesis of gallium phospheketenes

Given the successful synthesis of compound **1**, we intended to keep the ligand backbone as close to the diimine used in **1** as possible. A literature search of monomeric aluminium and gallium halides bearing chelating diimine ligands yielded two prospective candidates (Figure 6.1) for both aluminium and gallium.[20,21] Attempts to repeat the synthesis of the aluminium halide complex was not successful, yielding mixtures of the desired product, a variety of what we assume to be ring closed and ring opened compounds, and an unknown number of radical species, some of which we were able to identify through fractional crystallisation.

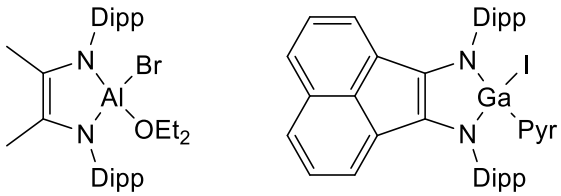

Figure 6.1. Examples of group-13 monohalides from the literature.

With limited success in synthesizing the aluminium precursor, we instead turned our attention to the Dipp-BIAN gallium iodide (Dipp-BIAN = 1,2-bis[(2,6-diisopropylphenyl)imino]acenaphthene) complex originally reported by Fedushkin and co-workers.[22,23] Modification of the literature procedure allowed a one-pot synthesis which produced good yields, bypassing a number of filtration and recrystallization steps, both of which can result in decomposition of this highly oxygen sensitive compound.

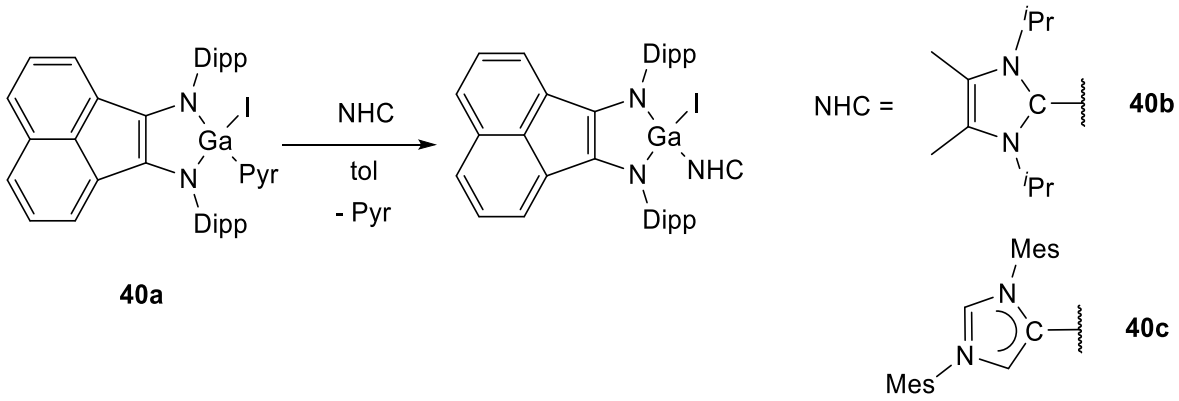

Scheme 6.4. Synthesis of gallium iodide precursors.

Ligand displacement reactions with N-heterocyclic carbenes (NHCs) allow for replacement of the pyridine; modifying the steric bulk around the gallium centre (Scheme 6.3). For example, addition of 1,3-diisopropyl-4,5-dimethyl-1,3-dihydro-2λ^2-imidazole (^{Me2}IPr) results in displacement of the pyridine ligand to give **40b**. The solid-state structure of this species displays increased pyramidalization with respect to the pseudotetrahedral pyridine derivative, a consequence of the steric hindrance between the diimine substituents and the isopropyl groups (Figure 6.2). Further increasing the steric requirement of the carbene by employing 1,3-dimesitylimidazol-2-ylidene,1,3-bis(2,4,6-trimethylphenyl)-imidazolium (IMes) forces abnormal coordination through the backbone of the NHC (**40c**; Figure 6.2). The solid-state structure in this case displays a lower degree of pyrimidalisation in comparison to the ^{Me2}IPr derivative due to one of the mesityl groups pointing away from the gallium centre.

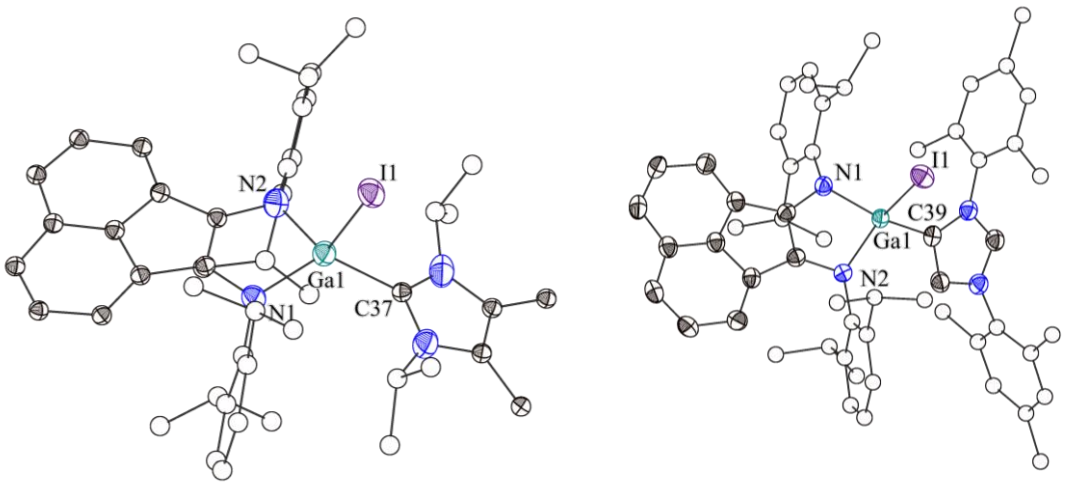

Figure 6.2. The solid state structure of **40b** and **40c**. Anisotropic displacement ellipsoids are set at 50% probability. Hydrogen atoms omitted for clarity. Dipp, Mes and ^{i}Pr carbon atoms shown as spheres of arbitrary radius.

Reaction of compounds **40a**–**c** with Na(PCO) in toluene results in the phosphorus-bound phosphaketenes **41a**–**c** as indicated by singlet resonances in the ^{31}P NMR spectra (δ = –394.6 (**41a**), –354.9 (**41b**), –374.2 ppm (**41c**)) and the characteristic phosphaketenyl carbon-phosphorus coupling in the ^{13}C NMR spectra (δ = 180.4 (d, $^{1}J_{P–C}$ = 101 Hz), 186.1 (d, $^{1}J_{P–C}$ = 86 Hz), 183.7 ppm (d, $^{1}J_{P–C}$ = 87 Hz) for **40a**–**c**, respectively). These values are comparable to the previously reported salen-supported gallium phosphaketene (*cf.* ^{31}P{^{1}H} NMR δ = –376.9 ppm, ^{13}C NMR δ = 182.5 ($^{1}J_{P–C}$ = 88 Hz)).[19]

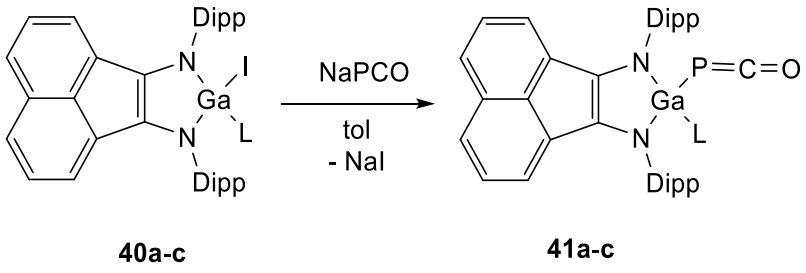

40a-c **41a-c**

Scheme 6.5. Synthesis of gallium phosphaketenes **39a**–**c**. L = Pyr (**41a**), ^{Me2}IPr (**41b**), IMes (**41c**)

The ^{1}H NMR spectra are consistent with an asymmetric tetrahedral geometry at the gallium centre, apparent from the presence of two isopropyl proton environments on the Dipp substituents. These species are all stable in solution for weeks, and stable in the solid

state for months. However, they are highly sensitive to oxygen and turn from blue/green to purple and then brown upon exposure to even trace amounts of oxygen.

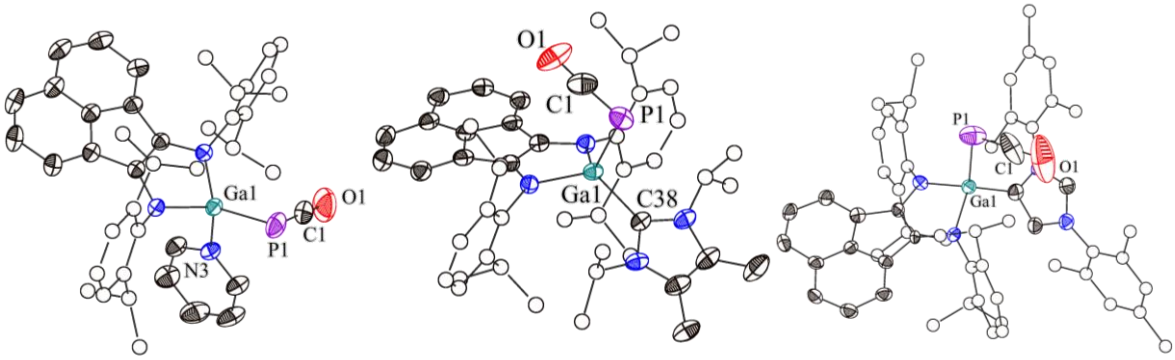

Figure 6.3. The solid state structure of **41a**–**c**. Anisotropic displacement ellipsoids are set at 50% probability. Hydrogen atoms omitted for clarity. Dipp, Mes and ^{i}Pr carbon atoms shown as spheres of arbitrary radius.

Crystals of **41a**–**c** were grown by cooling saturated toluene/ether solutions, and key bond lengths and angles can be found in Table 6.1. The bond angles about the phosphaketene are typical of compounds of this class, with approximately linear bond angle O1-C1-P1 (Mean value 177.3°) and Ga1-P1-C1 angles ranging from 85.6(1) to 91.0(5)°. Increasing the electron donating strength of the ligand (Pyr < ^{Me2}IPr < ^{ab}IMes) resulted in elongation of the C1-O1 bond with concurrent contraction of the C1−P1 bond, consistent with greater contribution from a resonance structure with increased C–P multiple-bond character, which correlates to the decreased coupling constant observed in the ^{13}C NMR spectrum.

Table 6. 1. Key bond parameters for gallium phosphaketenes **39a**–**c**.

Bond distance (Å)	**41a**	**41b**	**41c**
C1−P1	1.636(3)	1.598(9)	1.523(13)
O1−C1	1.166(3)	1.192(10)	1.230(13)
Ga1−P1	2.3270(5)	2.4303(17)	2.411(3)
Ga1−L	2.0559(14)	2.036(5)	1.978(7)
Bond angle (°)			
Ga1-P1-C1	85.6(1)	87.8(3)	91.0(5)
O1-C1-P1	177.3(2)	177.4(7)	177.2(11)
L-Ga1-P1	107.08(4)	98.79(17)	112.0(2)
^{13}C NMR P*C*O (ppm)	180.4	186.1	183.7
$^{1}J_{P-C}$ (Hz)	101	86	87
^{31}P NMR (ppm)	–394.6	–354.9	–374.2

6.2.2 Irradiation of phosphaketenes

In an effort to photolytically decarbonylate the phosphaketenes, which would allow access to terminal gallium–phosphinidenes, R_2Ga–P, toluene solutions of **41a**–**c** were irradiated using a medium pressure mercury-vapour lamp. This irradiation takes much longer than is typically required. A 100 mg/mL NMR sample requires 24 hours of irradiation time (6 hours a day for 4 days), a possible consequence of the photoabsorbing properties of the BIAN ligand.

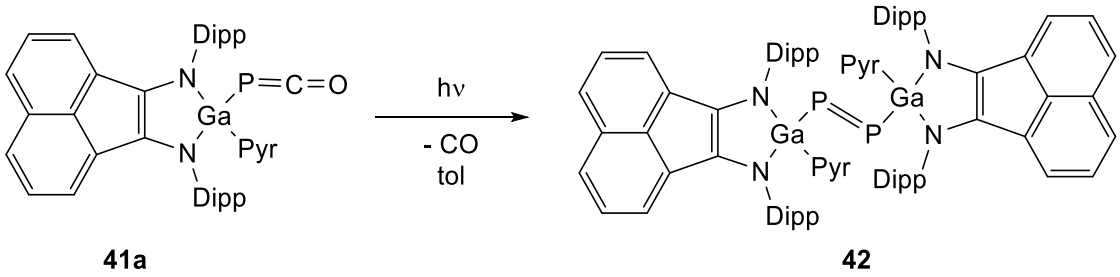

41a **42**

Scheme 6.6. Photolysis of **41a** to yield diphosphene **42**.

Over time, the NMR resonances corresponding to the phosphaketene diminish. In the case of **41a**, a broad resonance appears in the $^{31}P\{^{1}H\}$ NMR spectrum at 774.9 ppm. The ^{1}H resonances corresponding to **41a** are also consumed; however they are not replaced by a well-defined product, in effect going silent. The ^{31}P NMR resonance is shifted to a remarkably high frequency, the related boryl substituted diphosphene **20** displays the corresponding resonance at 596.2 ppm.

Crystallisation of the reaction mixture resulted in dark, heterochromic crystals. X-ray diffraction studies allowed for crystallographic identification of the diphosphene **42**, confirming the loss of carbon monoxide (Figure 6.4). The crystal structure contains an inversion centre at the P–P bond, resulting in symmetry between the two halves. The P–P bond is in the expected range of a double bond (2.037(1) Å) and the Ga–P distance is consistent with a single bond (2.340(1) Å). The Ga-P-P bond angle is 99.04(3)°, comparable to the boryl-substituted diphosphine, **20** (cf. 97.02(4)°, Chapter 3). The P_2 fragment and the BIAN backbone are almost coplanar (mean deviation from planarity: 0.1761 Å) indicating significant p_{π}–p^*_{π} donation from the phosphorus to the gallium atoms. The increased desheilding that results from this conjugation may be responsible for the high frequency $^{31}P\{^{1}H\}$ NMR resonance displayed by this compound.

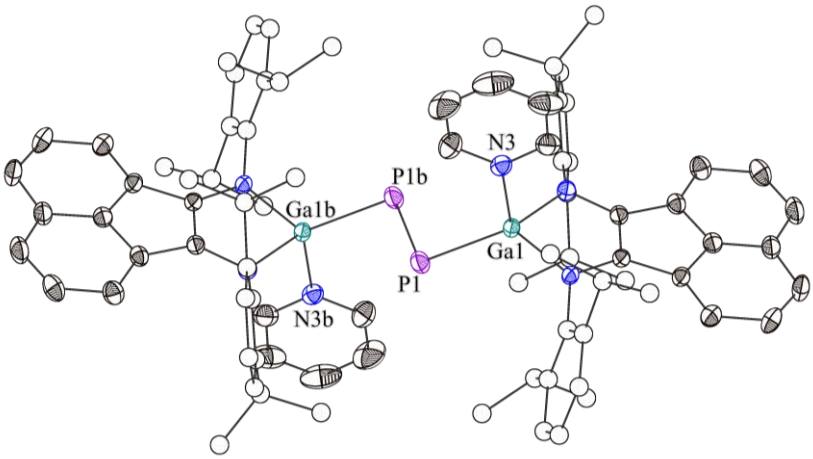

Figure 6.4. The solid state structure of **42**. Anisotropic displacement ellipsoids are set at 50% probability. Hydrogen atoms omitted for clarity. Dipp carbon atoms shown as spheres of arbitrary radius.

The NMR spectra of the dissolved crystals again displayed the broad resonance at 774.9 ppm in the $^{31}P\{^{1}H\}$ NMR spectrum, in addition to a silent ^{1}H NMR spectrum. Warming the sample to 40°C caused the ^{31}P NMR resonance to disappear, and cooling the solution did not cause it to return. EPR spectroscopy confirmed the presence of a radical species with comparable coupling to previously reported gallium Dipp-BIAN complexes.[22–25] By using EPR spectroscopy to monitor the irradiation of **41a** we were able to observe this species grow in intensity over time. Unfortunately, how this species is related to **42** remains unclear, as we were unable to further characterise it.

Irradiation of **41b** and **41c** resulted in no observable NMR resonances, including in the region corresponding to the diphosphene. The lack of observable diphosphene is likely a result of the increased steric requirement due to the carbene ligands, which prevents dimerisation. Reaction monitoring using EPR spectroscopy confirmed the presence of a radical species growing in over time in both cases. It should be noted that **41a–41c** all gave different signals, though **41b** and **41c** are visibly quite similar, implying the EPR signal is sensitive to substituents on the gallium centre (see appendix for details). Attempts to

crystallise these radical species frequently yielded yellow powders, likely to be the ligand, or bright green oils. We have so far been unable to obtain X-ray quality crystals.

6.2.3 Ligand substitution reactions

The substitution of the carbonyl ligand on phosphaketenes with stronger donors, yielding base-stabilised phosphinidenes, has previously been explored by the groups of Grützmacher and Bertrand utilising (phosphino)phosphaketenes, as outlined in Chapter 1.[26–28] Addition of trimethylphosphine to the phosphaketenes results in decarbonylation to yield the respective phosphine-stabilised phosphinidene. The base stabilised phosphinidenes can undergo subsequent ligand substitution reactions through addition of increasingly strong bases. It should be noted that phosphaketenes can also rearrange in the presence of carbenes due to the presence of an extended π–system; the rearrangement of **19** upon addition of ^{Me2}IPr in Chapter 3 is an example of such a case. In contrast to this, addition of carbenes to phosphine stabilised phosphinidenes results in ligand displacement reactions to yield carbene-stabilised phosphinidenes.

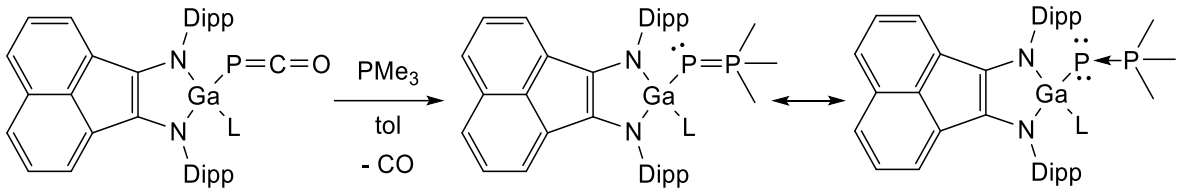

41a-b **43a-b**

Scheme 6.7. Carbonyl displacement using trimethylphosphine to give base stabilised phosphinidenes **43a**–**b**.

Inspired by this work, we sought to explore if similar ligand substitutions were accessible with the gallium phosphaketenes. Addition of the Lewis base trimethylphosphine to **39a** resulted in formation of a single product by ^{31}P NMR spectroscopy, with an AB spin system at 14.7 and –263.0 ppm (d, $^{1}J_{P–P}$ = 527 Hz), corresponding to the phosphine and phosphinidene resonances, respectively. Crystallisation from a cooled toluene solution

allowed for crystallographic characterisation of this compound as the expected base-stabilised phosphinidene, **43a**. Interestingly, the ^{1}H NMR spectrum is consistent with higher order symmetry than the solid state structure, indicative of fluxional behaviour which is rapid on the NMR timescale. We suspect pyridine dissociation makes the diisopropylphenyl groups equivalent. The sharpness of the peaks associated with pyridine would indicate this process is rapid on the NMR timescale. It could be assumed that the cause of this phenomenon is due to an increase in availability of the phosphinidene lone pair to donate into the gallium p–orbital, partially occupying the orbital and increasing the lability of the pyridine. This manifests in a longer than expected Ga1–N3(pyr) bond length of 2.115(2) Å, typically expected around 1.95 Å (*cf.* 2.056(2) Å for **41a**).[17,29] The increase in availability of the phosphinidene lone pair is a reflection of the reduced π–accepting ability of trimethylphosphine with respect to carbon monoxide, resulting in more donation to π–donation into the gallium p–orbital and a strong Ga1–P1 bond.

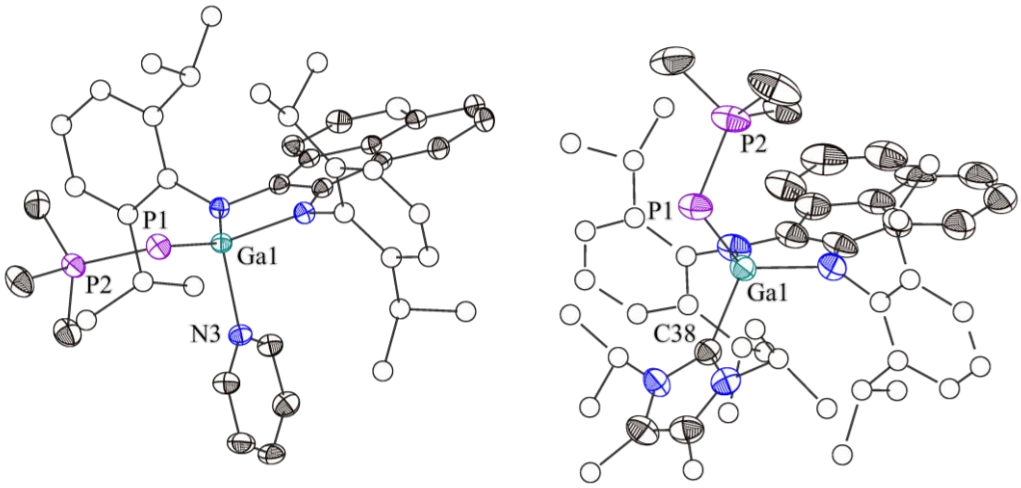

Figure 6.5. The solid state structure of **43a** and **43b**. Anisotropic displacement ellipsoids are set at 50% probability. Hydrogen atoms omitted for clarity. Dipp, Mes and ^{i}Pr carbon atoms shown as spheres of arbitrary radius.

The solid-state structure reveals a short P1–P2 bond (2.084(2) Å), in line with what is expected of a double bond (2.04 Å). This high bond order is also apparent from the large phosphorus–phosphorus coupling in the ^{31}P{^{1}H} NMR spectrum and can be rationalised

through dative bonding from the trimethylphosphine to the phosphinidene accompanied by back donation from the phosphinidene lone pair into the phosphine σ* orbital. The Ga1–P1 bond length is 2.265(1) Å, slightly shorter than a single bond (Σ_{cov} = 2.35 Å).

Addition of trimethylphosphine to **42b** results in no change to either the $^{31}P\{^{1}H\}$ or ^{1}H NMR spectra, consistent with both the increased steric protection given by the larger carbene ligand, in addition to the stronger P–C bond as noted in solid state structure of **41b** compared to **41a**. Irradiation of this reaction mixture results in a silent NMR spectrum. Crystals were obtained from a cooled toluene solution, allowing for identification of **43b** (Figure 6.5). This product confirms that irradiation is suitable for inducing decarbonylation in the NHC substuted phosphaketenes, however it is unclear why the NMR spectra of the solutions of the crystallised compounds are silent, however monitoring the irradiation using EPR spectroscopy allowed for observation of a radical species, as did dissolution of the crystals. The crystal structure contains three crystallographically unique molecules; consequently, all bond distances are discussed as mean values. Substituting the pyridine for a carbene results in a contraction of the P1–P2 bond (average length 2.008 Å) and concomitant elongation of the Ga1–P1 bond (2.318 Å). This is likely due to increased occupation of the gallium p–orbital in the case of the more strongly donating carbene preventing donation from the phosphinidene lone pair to gallium.

After the initial success with phosphines, we sought to expand this methodology to allow access to phosphorus–heteroatom multiple bonds. We hypothesized that addition of Power's gallium(I) carbenoid Ga(nacnac) to the phosphaketenes would result in decarbonylation. The resulting compound would display a gallium–phosphorus bond with significant double bond character due to donation of the phosphinidene lone pair into the vacant p–orbital of the gallium centre.

Addition of a stoichiometric amount of Ga(nacnac) to **41a** in toluene initially resulted in a mixture of two species in the $^{31}P\{^{1}H\}$ NMR spectrum, a singlet resonance at 157.3 ppm and a second singlet at –319.0 ppm.

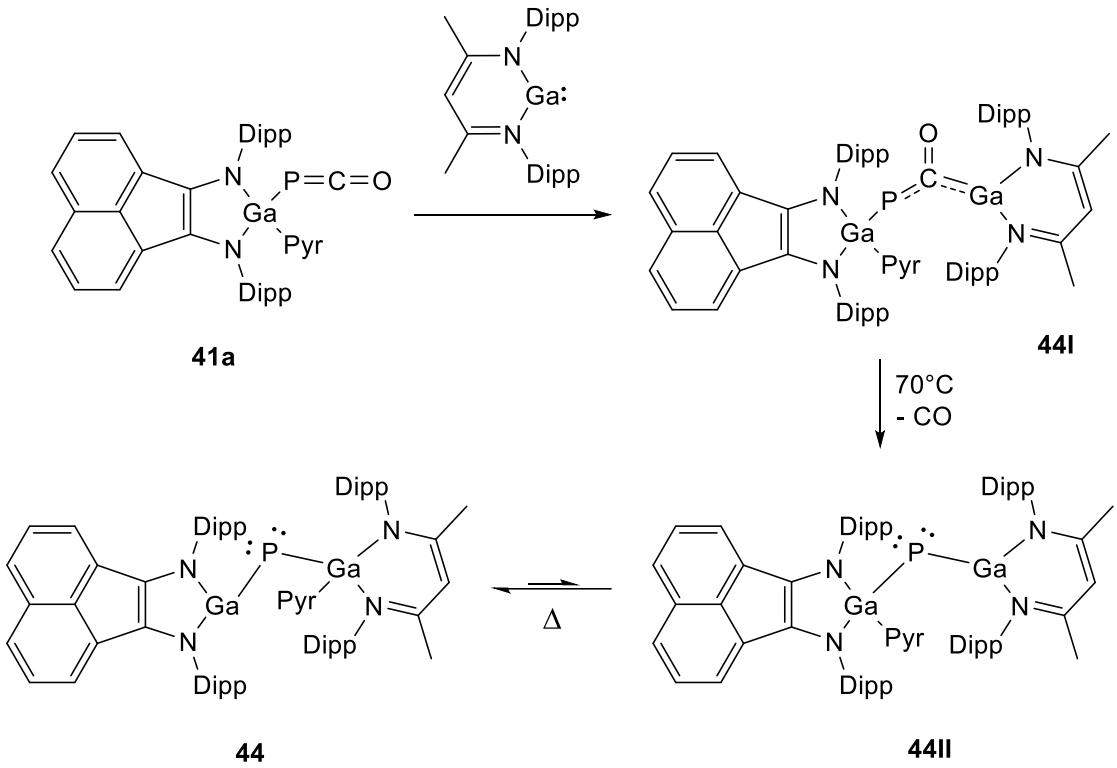

Scheme 6.8. Addition of gallium carbenoid to phosphaketene **41a** yielding gallaphosphene **44**.

The resonance at 157.3 ppm is tentatively assigned as the Ga(nacnac) adduct **44I**. A similar species obtained from the reaction of a saturated phosphanyl phosphaketene with IDipp has previously been structurally authenticated.[26] This imidazolium adduct displays a $^{31}P\{^{1}H\}$ NMR resonances at 142.5 and 129.8 ppm (d, $^{1}J_{P-P}$ = 325.1 Hz), the former of these resonances corresponding to the bridging phosphorus. It was not possible to isolate **42I** as it slowly converts to the species at –319.0 ppm. Heating the solution to 70°C expedites this process, which goes to completion in under 30 minutes. There is no change to the ^{31}P NMR spectrum upon proton coupling.

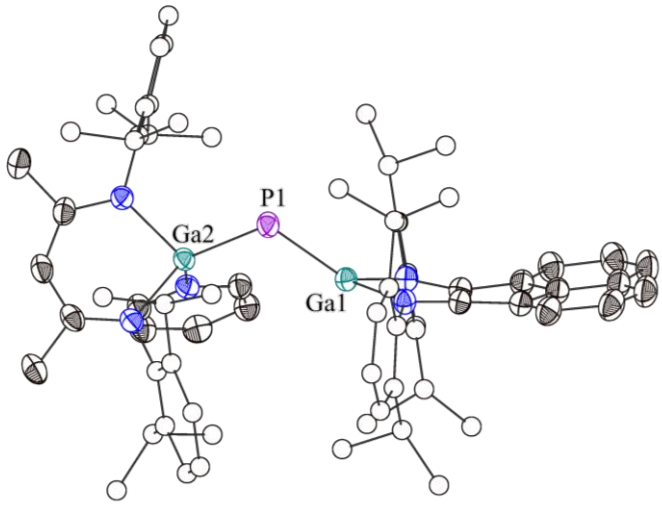

Figure 6.6. The solid state structure of **44**. Anisotropic displacement ellipsoids are set at 50% probability. Hydrogen atoms omitted for clarity. Dipp carbon atoms shown as spheres of arbitrary radius.

Crystals of **44** were obtained by allowing a refluxing saturated solution of toluene to cool slowly to room temperature. The solid-state structure reveals a bridging 2-coordinate phosphorus atom. The pyridine ligand has migrated to the less sterically congested Ga(nacnac) centre, and the Ga1–N3 bond length is longer than a typical single bond (2.071(2) Å, Σ_{cov} = 1.95 Å) suggesting back donation from the phosphorus lone pair into the gallium p-orbital. The Ga1–P1 and Ga2–P1 distances (2.215(1) and 2.207(1) Å, respectively) are consistent with double bonds (Σ_{cov} = 2.19 Å), and a search of structurally authenticated Ga–P bonds reveals them to be the shortest unsupported Ga–P bonds hitherto reported. However, Ga1-P1-Ga2 bond is significantly bent, 112.7(1)°, contrasting what would be expected of a phosphaallene-type species. Previously reported examples of bridging naked phosphorus atoms from the groups of Stephan and Cummins, in the complexes $(Cp_2Zr)_2(\mu–P)$ and $((Me_2N)_3Mo)(\mu–P)$, reveal linear bonding about the P centre.[30,31] In fact, the only example of a bent phosphorus bridge is between two tungsten centres with additional ancillary bridging ligands which may force this coordination mode.[32] The resulting W-P-W bond angle in this complex is much more acute (75.78(6)°) than that observed in **44**.

The Ga1-P1-Ga2 angle in **44** is perhaps due to the partial occupation of the β-diketiminate Ga p–orbital by the pyridine ligand, in addition to the two adjacent nitrogens. There is also poor π–overlap between the 3p and 4p orbitals, resulting in only partial multiple bond character in both Ga–P bonds. The bonding in this species can also be depicted using resonances shown in Figure 6.7. Compound **44** can be described as a zwitterion containing a monoanionic phosphorus with two lone pairs and a dative bond from the β-diketiminate Ga, which is formally cationic. The central resonance form is formally neutral, and involves donation of one of the lone pairs into the β-diketiminate Ga centre. Finally, moving the electron density to donate into the second Ga p–orbital results in a zwitterionic species with formal positive and negative charges on the two gallium centres. The contraction in Ga–P bond lengths supports significant contribution from the latter two resonance forms.

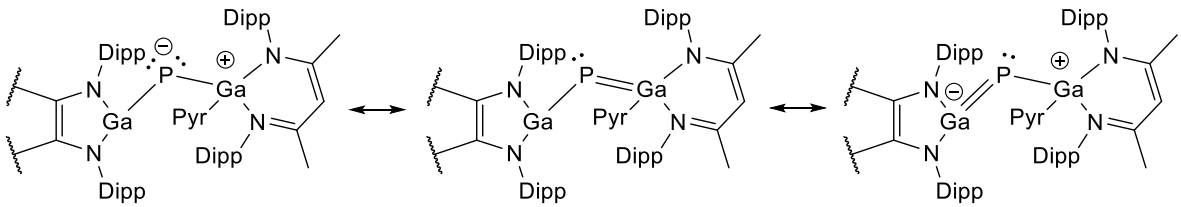

Figure 6.7. Resonance forms of **44**.

The $^{31}P\{^{1}H\}$ NMR spectrum of the dissolved crystals confirmed the identity of **44** as the species with a resonance at –319.0 ppm. The ^{1}H NMR spectrum is consistent with a symmetrical ligand environment for the Dipp-BIAN ligand, with a more complex set of resonances for the β-diketiminate ligand, which displays multiple broadened resonances for the Dipp and alkyl protons. The most notable observation is a significant broadening of the pyridine proton environments, likely due to a dissociative process taking place that is slow on the NMR timescale, similar to the dissociative process proposed for the phosphine stabilised-phosphinidene **43a**. When solutions of **44** are left for prolonged periods, a new species begins to appear with a ^{31}P resonance at –330.7 ppm, with a proton spectra consistent with the presence of both a Dipp-BIAN and β-diketiminate ligand environments. We

tentatively assign this as **44II**, in which the pyridine has migrated between gallium centres. The relative concentration of this species never increases above 10%, and upon refluxing temporarily disappears from the NMR spectra, indicating that it exists in equilibrium with **44**.

The analogous reaction between the more sterically demanding **41b** and the gallium carbenoid resulted in no reactivity, even upon prolonged heating.

6.3 Conclusions and ongoing work

This chapter has reported the synthesis of a series of gallium phosphaketenes obtainable in good yields through salt metathesis reactions. The photolytic decarbonylation of these compounds was explored, allowing access to the digallium diphosphene **42**. Chemical decarbonylation was also explored, addition of trimethylphosphine to phosphaketene **41a** allowed access to phosphine stabilised phosphinidene **43a**. This reactivity has previously been investigated for phosphanyl phospaketenes, however expansion of this ligand displacement strategy to include the gallium (I) β-diketiminate carbenoid, allowed access to **44**, which contains a Ga–P double with significant double bond character, the first of its kind.

This work is still ongoing; we are attempting to gain insight into the bonding situation of **44** through reactivity studies. Initially, we attempted to remove the pyridine ligand to obtain a phosphaallene analogue, $R_2Ga{=}P{=}GaR_2$, with each lone pair of the phosphorus able to donate into the vacant p-orbitals of the two gallium atoms. Addition of trispentafluorophenylborane (BCF) to the reaction mixture resulted in a sharpening of the pyridine peaks in the ^{1}H NMR spectra, in addition ^{11}B and ^{19}F NMR resonances consistent with formation of the pyridine-BCF adduct.[33] The ^{31}P NMR resonance corresponding to **44** rapidly broadens out, and after an hour both the ^{1}H and ^{31}P NMR spectra are silent (with the exception of the ^{1}H pyridine resonances). Further EPR studies are currently underway.

Attempts to crystallise this species have thus far been unsuccessful. Additionally, we are investigating the reactivity of **44** towards small molecules, namely H_2, CO_2, and NH_3, in the hopes of achieving bond activation reactions across the Ga–P bond.

6.4 References

[1] M. J. D. Bosdet, W. E. Piers, *Can. J. Chem.* **2009**, *87*, 8–29.

[2] P. G. Campbell, A. J. V. Marwitz, S. Y. Liu, *Angew. Chem. Int. Ed.* **2012**, *51*, 6074–6092.

[3] M. J. D. Bosdet, W. E. Piers, T. S. Sorensen, M. Parvez, *Angew. Chem. Int. Ed.* **2007**, *46*, 4940–4943.

[4] T. B. Richardson, S. De Gala, R. H. Crabtree, P. E. M. Siegbahn, *J. Am. Chem. Soc.* **1995**, *117*, 12875–12876.

[5] Z. Huang, T. Autrey, *Energy Environ. Sci.* **2012**, *5*, 9257–9268.

[6] P. G. Campbell, L. N. Zakharov, D. J. Grant, D. A. Dixon, S. Y. Liu, *J. Am. Chem. Soc.* **2010**, *132*, 3289–3291.

[7] A. Rosas-Sánchez, I. Alvarado-Beltran, A. Baceiredo, D. Hashizume, N. Saffon-Merceron, V. Branchadell, T. Kato, *Angew. Chem. Int. Ed.* **2017**, *56*, 4814–4818.

[8] E. Rivard, W. A. Merrill, J. C. Fettinger, P. P. Power, *Chem. Commun.* **2006**, 3800–3802.

[9] H. Zhu, J. Chai, V. Chandrasekhar, H. W. Roesky, J. Magull, D. Vidovic, H. G. Schmidt, M. Noltemeyer, P. P. Power, W. A. Merrill, *J. Am. Chem. Soc.* **2004**, *126*, 9472–9473.

[10] J. Li, X. Li, W. Huang, H. Hu, J. Zhang, C. Cui, *Chem. Eur. J.* **2012**, *18*, 15263–

15266.

[11] C. Ganesamoorthy, C. Helling, C. Wölper, W. Frank, E. Bill, G. E. Cutsail, S. Schulz, *Nat. Commun.* **2018**, *9*, 1–8.

[12] C. Helling, C. Wölper, S. Schulz, *J. Am. Chem. Soc.* **2018**, *140*, 5053–5056.

[13] J. Schoening, L. John, C. Wölper, S. Schulz, *Dalton Trans.* **2019**, *48*, 17729–17734.

[14] S. Wang, T. J. Sherbow, L. A. Berben, P. P. Power, *J. Am. Chem. Soc.* **2018**, *140*, 590–593.

[15] G. H. Spikes, J. C. Fettinger, P. P. Power, *J. Am. Chem. Soc.* **2005**, *127*, 12232–12233.

[16] N. J. Hardman, B. E. Eichler, P. P. Power, *Chem. Commun.* **2000**, 1991–1992.

[17] P. Pyykkö, M. Atsumi, *Chem. Eur. J.* **2009**, *15*, 12770–12779.

[18] J. E. Borger, G. Le Corre, Y. Mei, R. Suter, E. Schrader, H. Grützmacher, *Chem. Eur. J.* **2019**, *25*, 3957–3962.

[19] Y. Mei, J. E. Borger, D. J. Wu, H. Grützmacher, *Dalton Trans.* **2019**, *48*, 4370–4374.

[20] Y. Ju, Z. Yang, X. Ma, Y. Yang, H. W. Roesky, *Zeitschrift fur Anorg. und Allg. Chemie* **2015**, *641*, 521–524.

[21] H. Schumann, M. Hummert, A. N. Lukoyanov, I. L. Fedushkin, *Organometallics* **2005**, *24*, 3891–3896.

[22] I. L. Fedushkin, V. A. Dodonov, A. A. Skatova, V. G. Sokolov, A. V. Piskunov, G. K. Fukin, *Chem. Eur. J.* **2018**, *24*, 1877–1889.

[23] I. L. Fedushkin, A. A. Skatova, V. A. Dodonov, V. A. Chudakova, N. L. Bazyakina, A. V. Piskunov, S. V. Demeshko, G. K. Fukin, *Inorg. Chem.* **2014**, *53*, 5159–5170.

[24] I. L. Fedushkin, O. V. Kazarina, A. N. Lukoyanov, A. A. Skatova, N. L. Bazyakina, A. V. Cherkasov, E. Palamidis, *Organometallics* **2015**, *34*, 1498–1506.

[25] V. A. Dodonov, A. A. Skatova, A. V. Cherkasov, I. L. Fedushkin, *Russ. Chem. Bull.* **2016**, *65*, 1171–1177.

[26] Z. Li, X. Chen, Z. Benkö, L. Liu, D. A. Ruiz, J. L. Peltier, G. Bertrand, C. Y. Su, H. Grützmacher, *Angew. Chem. Int. Ed.* **2016**, *55*, 6018–6022.

[27] M. M. Hansmann, G. Bertrand, *J. Am. Chem. Soc.* **2016**, *138*, 15885–15888.

[28] M. M. Hansmann, R. Jazzar, G. Bertrand, *J. Am. Chem. Soc.* **2016**, *138*, 8356–8359.

[29] P. Pyykkö, M. Atsumi, *Chem. Eur. J.* **2009**, *15*, 186–197.

[30] M. C. Fermin, J. Ho, D. W. Stephan, *Organometallics* **1995**, *14*, 4247–4256.

[31] M. J. A. Johnson, P. Mae Lee, A. L. Odom, W. M. Davis, C. C. Cummins, *Angew. Chem. Int. Ed.* **1997**, *36*, 87–91.

[32] P. Kramkowski, M. Scheer, *Angew. Chem. Int. Ed.* **2000**, *39*, 928–931.

[33] F. Focante, I. Camurati, L. Resconi, S. Guidotti, T. Beringhelli, G. D'Alfonso, D. Donghi, D. Maggioni, P. Mercandelli, A. Sironi, *Inorg. Chem.* **2006**, *45*, 1683–1692.

Chapter 7
Conclusions and future work

7.1 Conclusions

This thesis has reported the synthesis of a phosphaethynolatoborane, [B]OCP OCP ([B] = *N,N′*-bis(2,6-diisopropylphenyl)-2,3-dihydro-1H-1,3,2-diazaboryl), *via* a salt metathesis reaction between Yamashita's bromoborane ([B]Br) and the 2-phosphaethynolate anion.[1] The synthesis was optimised to favour this product over associated heterocyclic compounds, which were also isolated and characterised.

The role of [B]OCP as an electrophile was explored. The reaction outcome is dependent on the nature of the nucleophile employed. With Lewis bases, such as phosphines or N-heterocyclic carbenes, a dimerization occurs, with concurrent migration of a boryl moiety from the oxygen to the carbon atom. With anionic nucleophiles, such as lithium aryls or NaFp*, it was possible to isolate monomeric species in which the nucleophile bonds with the phosphorus atom and the boron migrates from the oxygen to the carbon atom. The reactivity of [B]OCP towards isocyanides deviates from this trend and in the case of ^{t}BuNC, allowed access to the phosphaketenyl isomer, [B]PCO. The mechanism of this rearrangement was explored both computationally and experimentally. Calculations demonstrated that the isocyanide is able to interact with the boron p-orbital, labilising the B–O bond and allowing for isomerisation.

The ligand properties of [B]OCP were explored, allowing access to a diphosphacyclobutadiene nickel complex in addition to a series of trisphosphaalkyne tungsten carbonyl complexes. The tungsten complexes are reminiscent of the landmark organometallic trisalkyne complexes originally reported by Tate and Augl.[2] These complexes were of interest due to an unusual, symmetry enforced, electron configuration which they display in line with the phosphorus analogues reported herein.

Reactions with trispentafluorophenyl borane demonstrated an increase in nucleophilicity at [B]OCP in comparison to alkyl substituted phosphaalkynes such as ^{t}BuCP. This reaction, in addition to the reaction with the linkage isomeric [B]PCO, allowed access to three constitutional isomers of a carboborated phosphaalkyne.

The reductive cleavage of the O–C bond was also investigated. Attempts to reduce [B]OCP resulted in complex product mixtures. The most promising of these studies was the addition of $[^{Mes}Mg]_2$, which generated [B]O[Mg] as the major boryl-containing product as well as a magnesium species featuring CP^{-}. Unfortunately, thus far we have been unable to optimise the reaction conditions to favour any single phosphorus-containing product.

We have successfully synthesized a series of gallium 2-phosphaethynolate coordination compounds featuring Dipp-BIAN ligand scaffolds. As expected, moving down group 13 to the less charge-dense gallium resulted in the phosphaketenyl bonding mode. The ligand displacement chemistry of a series of gallium phosphaketenes was explored. Irradiation of these compounds resulted in persistent radical species, confirmed by EPR spectroscopy. In one case, fractional crystallisation allowed for identification of a diphosphene, consistent with decarbonylation. Remarkably, these species did not display well defined NMR resonances, the reasons for which are still under investigation. We went on to explore ligand substitution reactions at the phosphinidene, and adapted this methodology to allow access to a gallaphosphene, the first stable compound with a gallium–phosphorus double bond.

7.2 Future work

The preliminary results from the two electron reduction of [B]OCP showed some promise. The use of $[^{Mes}Mg]_2$ proved to be particularly encouraging, showing selectivity for the O–C bond. However, the resulting phosphorus containing compounds underwent further reactivity, often through uncontrolled oligermisation. Our studies on the reactivity of the

related phosphaalkyne, ^{t}BuCP, demonstrated that the magnesium centres are able to facilitate bond forming reactions through Lewis pair formation with the lone pair of the reduced phosphaalkene intermediates. This reactivity may explain why we are able to identify a complex containing a $[C_2P_2]^{4-}$ moiety (**34**).

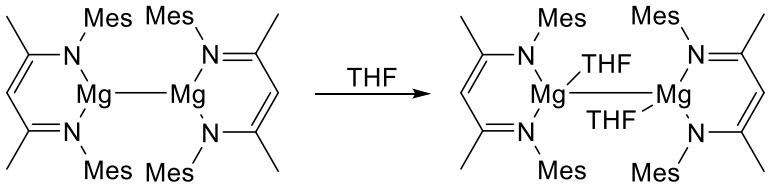

Scheme 7.1. Modification of $[^{Mes}Mg]_2$ with THF.

It is possible to further saturate the coordination sphere of $[^{Mes}Mg]_2$ through addition of THF, giving the isolable species $[^{Mes}Mg(THF)]_2$.[3] The coordinated THF displays fluxionality in solution, however may prevent oligermerisation of the CP^- salts generated by reducing the Lewis acidity of the magnesium centre.

Further characterisation of the gallium phosphaketenes decarbonylation compounds is required to elucidate why these species do not display well-defined NMR spectra. We also aim to expand on the ligand displacement chemistry at the phosphorus atom of phosphaketenes, a reaction first reported by the Bertrand group.[4] Through addition of carbenoids we hope to displace carbon monoxide to form a series compounds containing well defined P=E bonds (E = Al, Ga, In, Si, Ge). These compounds would constitute the first rational synthesis of such a series. Group 13 carbenoids are accessible supported by β-diketiminate ligands (Al, Ga, In),[5–7] while the group 14 carbenoids utilise a number of diimine ligands (Si, Ge, Sn).[8–10]

7.3 Publications

The work contained in this thesis can be found in the following publications:

1. D. W. N. Wilson, A. Hinz, J. M. Goicoechea, *Angew. Chem. Int. Ed.* **2018**, *57*, 2188–2193.
2. D. W. N. Wilson, J. M. Goicoechea, *Chem. Commun.* **2019**, *55*, 6842–6845.
3. D. W. N. Wilson, N. H. Rees, J. M. Goicoechea, *Organometallics* **2019**, *38*, 4601–4606.
4. D. W. N. Wilson, M. P. Franco, W. K. Myers, J. E. McGrady, J. M. Goicoechea, *Chem. Sci.* **2020**, *11*, 862–869.

A further publication is currently under review, and two manuscripts are in progress.

7.4 References

[1] Y. Segawa, M. Yamashita, K. Nozaki, *Science.* **2006**, *314*, 113–115.

[2] D. P. Tate, J. M. Augl, W. M. Ritchey, B. L. Ross, J. G. Grasselli, *J. Am. Chem. Soc.* **1964**, *86*, 3261–3265.

[3] S. J. Bonyhady, C. Jones, S. Nembenna, A. Stasch, A. J. Edwards, G. J. McIntyre, *Chem. Eur. J.* **2010**, *16*, 938–955.

[4] M. M. Hansmann, G. Bertrand, *J. Am. Chem. Soc.* **2016**, *138*, 15885–15888.

[5] C. Cui, H. W. Roesky, H. G. Schmidt, M. Noltemeyer, H. Hao, F. Cimpoesu, *Angew. Chem. Int. Ed.* **2000**, *39*, 4274–4276.

[6] N. J. Hardman, B. E. Eichler, P. P. Power, *Chem. Commun.* **2000**, 1991–1992.

[7] M. S. Hill, P. B. Hitchcock, *Chem. Commun.* **2004**, *10*, 1818–1819.

[8] P. Zark, A. Schäfer, A. Mitra, D. Haase, W. Saak, R. West, T. Müller, *J. Organomet. Chem.* **2010**, *695*, 398–408.

[9] S. M. Mansell, C. A. Russell, D. F. Wass, *Inorg. Chem.* **2008**, *47*, 11367–11375.

[10] T. Gans-Eichler, D. Gudat, K. Nättinen, M. Nieger, *Chem. Eur. J.* **2006**, *12*, 1162–1173.

Chapter 8
Experimental

8.1 General synthetic procedures

All reactions and product manipulations were carried out under an inert atmosphere of argon or dinitrogen using standard Schlenk or glovebox techniques (MBraun UNILab glovebox maintained at <0.1 ppm O_2 and <0.1 ppm H_2O) unless otherwise noted.

Tetrahydrofuran (THF; Fisher, HPLC grade), diethyl ether (Et_2O; Fisher, pesticide residue grade), and 1,4-dioxane (Alfa Aesar, 99+%, stab. 5-10 ppm BHT) were distilled from a sodium/benzophenone mixture. Pyridine (Alfa Aesar, 99+%) and 1,2-difluorobenzene (1,2-DFB; Fluorochem, 98%) were distilled from CaH_2. Hexane (Sigma Aldrich, HPLC grade), pentane (Sigma Aldrich, HPLC grade) and toluene (Sigma Aldrich, HPLC grade) were purified using an MBraun SPS-800 solvent system. d_8-THF (Eurisotop, >99.5%), d_5-pyridine (Eurisotop, >99.5%) were dried over CaH_2, vacuum distilled, and degassed before use. D_8-toluene (tol; Alfa Aesar, 99% (isotopic)) was dried over activated 3 Å molecular sieves and degassed before use. All dry solvents were stored under argon in gas-tight ampoules over 3 Å molecular sieves. Deionised water was obtained from a Millipore Milli-Q machine.

The suppliers and purification procedures for commercially available chemicals are detailed in Table 8.1.

Table 8.1: Supplier and purification procedures for commercially available chemicals.

Reagent	Supplier	Purity	Purification
Potassium	Strem	99.95%	Used as received
Phosphorus	Sigma Aldrich	99.99%	Dried under vacuum
Sodium	Acros Organics	99.8%, oiled sticks	Washed with hexane, dried under vacuum
18-crown-6	Alfa Aesar	99%	Dried under vacuum with heating
CO	CK Gas	Unspecified	Used as received

Naphthalene	Sigma Aldrich	99+%	Sublimed under vacuum
$[W(CO)_6]$	Strem	99%	Sublimed under vacuum
^{t}BuOH	Alfa Aesar	99%	Refluxed over Mg/I_2, distilled
KO^{t}Bu	Aldrich	≥98%	Used as received
Lithium	Strem	99.95%	Washed with hexane, dried under vacuum
NaN_3	Merck	≥99.5%	Used as recieved
Me_3SiN_3		95%	Used as received
12-crown-4	Sigma Aldrich	98%	Distilled and stored over 3 Å molecular sieves
$(PPh_3)AuCl$	Sigma Aldrich	≥99.5%	Used as received
Me_3SiCl	Sigma Aldrich	≥98%	Degassed prior to use
$K[B(C_6F_5)_4]$	Merck	Unspecified	Used as received
^{t}BuNC	Sigma Aldrich	98%	Used as received
9-BBN	Sigma Aldrich	0.4 M in hexanes	Used as received
$Ni(COD)_2$	Sigma Aldrich	Unspecified	Used as received
$W(CO)_3(MeCN)_3$	Sigma Aldrich	Unspecified	Used as received
KHMDS	Sigma Aldrich	95%	Used as received
PMe_3	Sigma Aldrich	1 M in toluene	Used as received

The following compounds were prepared according to literature procedures: $Na(dioxane)_{1.2}[PCO]$,[1] [B]Br,[2] LiMes and LiMes*,[3] NaFp*,[4] ^{Me2}IPr,[5] $B(C_6F_5)_3$,[6] $W(THF)(CO)_5$,[7], MesNC,[8] (^{Dipp}BIAN)Ga(I)(Pyr),[9] [(^{Mes}Nacnac)Mg]$_2$,[10] ^{t}BuCP,[11] $K[PSi(Me_3)_2]$,[12] [(^{Dipp}Nacnac)Ga].[13]

8.2 Syntheses of compounds

8.2.1 Chapter 2

8.2.1.1 Synthesis of [B]OCP (1)

To a solution of 2-bromo-1,3-bis(2,2-diisopropylphenyl)-1,3,2-diazaborole (500 mg, 1.07 mmol) in toluene (10 mL) [Na(dioxane)$_{1.7}$][PCO] (296 mg, 1.28 mmol, 1.2 eq.) was added The yellow suspension was heated to 70 °C for 10 days. The reaction mixture was allowed to cool to room temperature and all volatiles removed. The resulting orange solid was extracted with hexane (2 × 10 mL) and the combined extracts concentrated to approximately 3 mL. Storage of the solution at –30 °C overnight yielded yellow crystals. The solvent was decanted and the crystals dried under reduced pressure (202 mg, 42% crystalline yield). Crystals suitable for X-ray diffraction were obtained by slow evaporation of hexane. **CHN** Anal. Calcd. for $C_{27}H_{36}BN_2OP$ (446.36): C, 72.65%; H, 8.13%; N, 6.28%. Found: C, 72.11%; H, 8.25%; N, 6.12%. **^{1}H NMR** (500 MHz, C_6D_6): δ (ppm) 7.23 (t, $^{3}J_{H–H}$ = 8 Hz, 2H; *para*-Dipp*H*), 7.11 (d, $^{3}J_{H–H}$ = 8 Hz, 4H; *meta*-Dipp*H*), 5.88 (s, 2H; {(NC*H*)$_2$}), 3.19 (sept, $^{3}J_{H–H}$ = 7 Hz, 4H; {C*H*(CH$_3$)$_2$}), 1.33 (d, $^{3}J_{H–H}$ = 7 Hz, 12H; {CH(C*H*$_3$)$_2$}), 1.21 (d, $^{3}J_{H–H}$ = 7 Hz, 12H; {CH(C*H*$_3$)$_2$}). **^{13}C{^{1}H} NMR** (126 MHz, C_6D_6): δ (ppm) 140.2 (d, $^{1}J_{C–P}$ = 17.6 Hz, O*C*P) 146.6 (Dipp*C*), 140.5 (d, $^{1}J_{CP}$ = 17.6 Hz, O*C*P) 136.2 (Dipp*C*), 128.6 (Dipp*C*), 123.7 (Dipp*C*), 117.8 ({(N*C*H)$_2$}), 29.1 ({*C*H(CH$_3$)$_2$}), 24.3 ({CH(*C*H$_3$)$_2$}). **^{31}P{^{1}H} NMR** (162 MHz, C_6D_6): δ (ppm) –285.9 (s). **^{11}B{^{1}H} NMR** (128 MHz, C_6D_6): δ (ppm) 19.5 (s). **IR**: ν = 1649 cm^{-1} (vs, ν_{asym}, P≡C–O)

8.2.1.2 Synthesis of *cyclo*-P2{C[B]}O{CO[B]} (2)

To a solution of 2-bromo-1,3-bis(2,2-diisopropylphenyl)-1,3,2-diazaborole (500 mg, 1.07 mmol) in THF (5 mL) [Na(dioxane)$_{1.7}$][PCO] (296 mg, 1.28 mmol, 1.2 eq.) was added. The yellow suspension was heated to 100 °C for 5 days. The reaction mixture was allowed to

cool to room temperature and all volatiles were removed under reduced pressure. The resulting solid was extracted with hexane (2 × 10 mL) and the combined extracts concentrated to approximately 3 mL. After storing at –30 °C for several days a red, microcrystalline solid was obtained (240 mg, 50.3%). Crystals suitable for X-ray diffraction were obtained by slow evaporation and cooling of a saturated hexane solution.

CHN Anal. Calcd. for $C_{54}H_{72}B_2N_4O_2P_2$ (892.71): C, 72.65%; H, 8.13%; N, 6.28%. Found: C, 71.22%; H, 8.20%; N, 5.92%. **^{1}H NMR** (500 MHz, C_6D_6): δ (ppm) 7.26 – 7.01 (m, 12H; Dipp*H*), 6.11 (s, 2H; {(NC*H*)$_2$}), 6.06 (s, 2H; {(NC*H*)$_2$}), 3.21 (sept, $^3J_{H–H}$ = 7 Hz, 4H; {C*H*(CH$_3$)$_2$}), 3.08 (sept, $^3J_{H–H}$ = 7 Hz, 4H; {C*H*(CH$_3$)$_2$}), 1.20 – 1.09 (m, 12H; {CH(C*H*$_3$)$_2$}), 0.94 (d, $^3J_{H–H}$ = 7 Hz, 12H; {CH(C*H*$_3$)$_2$}). **^{13}C{^{1}H} NMR** (126 MHz, C_6D_6): δ (ppm) 202.9 (d, $^1J_{P–C}$ = 103 Hz; *C*(O)$_2$P), 187.9 (broad m; C(O)(B)P), 146.1 (Dipp*C*), 145.9 (Dipp*C*), 139.0 (Dipp*C*), 136.6 (Dipp*C*), 128.4 (Dipp*C*), 124.0 (Dipp*C*), 123.9 (Dipp*C*), 120.1 ({(N*C*H)$_2$}), 118.1 ({(N*C*H)$_2$}), 28.7 (*C*H(CH$_3$)$_2$), 25.4 (*C*H(CH$_3$)$_2$), 24.9 (CH(*C*H$_3$)$_2$), 24.5 (CH(*C*H$_3$)$_2$), 24.4 (CH(*C*H$_3$)$_2$), 23.6 (CH(*C*H$_3$)$_2$). **^{31}P{^{1}H} NMR** (162 MHz, C_6D_6): δ (ppm) 223.3 (d, $^1J_{P–P}$ = 386 Hz), 38.3 (d, $^1J_{P–P}$ = 386 Hz). **^{11}B{^{1}H} NMR** (128 MHz, C_6D_6): δ (ppm) 22.0 (s), –23.9 (s, br).

8.2.1.3 Synthesis of *cyclo*-P$_2${C}ONa{CO[B]} (3)

To a solution of 2-bromo-1,3-bis(2,2-diisopropylphenyl)-1,3,2-diazaborole (100 mg, 0.21 mmol) in THF (5 mL) [Na(dioxane)$_{1.7}$][PCO] (296 mg, 1.28 mmol, 6 eq.) was added. The yellow suspension was heated to 100 °C for 5 days. At which point, resonances corresponding to **2** and **3** were present. Washing with hexane resulted in extraction of **2**, and the white solid remaining could be recrystallized from toluene, revealing product **3** in low yields (10-15%). The NMR of the crystals revealed two products, assigned as the monomer (mon) and tetrameric (tet) forms of **3** in solution. No integrations are given due to broadening and overlap.

^{1}H NMR (500 MHz, C_6D_6): δ (ppm) 7.80–7.20 (br s, tet Ar*H*), 7.12 (t, J = 6.9 Hz, mon *para*-C*H*) 7.01 (d, *J* = 6.9 Hz, mon *meta*-C*H*), 6.33 (s, mon, {CH(CH_3)$_2$}), 6.03 (br s, tet {CH(CH_3)$_2$}), 5.51(br s, mon {C*H*(CH$_3$)$_2$}), 3.26 (br s, mon {C*H*(CH$_3$)$_2$}), 3.16 (sept, *J* = 7.0 Hz, 1H), 1.60 – 0.80 (br m, mon and tet (CH(*C*H$_3$)$_2$). **^{13}C{^{1}H} NMR** (126 MHz, C_6D_6): δ (ppm) 213.5 (d, $^{1}J_{C–P}$ = 98.1 Hz, (P)$_2$*C*O), 213.3 (d, $^{1}J_{C–P}$ = 98.1 Hz, (P)$_2$*C*B), 140.5 (s, ArC), 137.5 (s, ArC), 128.9 (s, ArC), 126.7 (s, ArC) 119.4 {(N*C*H)$_2$}), 28.8 (s, *C*H(CH$_3$)$_2$), 28.4 (s, *C*H(CH$_3$)$_2$), 21.1 (s, *C*H(CH$_3$)$_2$). **^{11}B{^{1}H} NMR** (128 MHz, C_6D_6): δ (ppm) 21.2 (br). **^{31}P{^{1}H} NMR** (162 MHz, C_6D_6): δ (ppm) 239.9 (d, $^{1}J_{P–P}$ = 398.1 Hz, tet), 236.8 (d, $^{1}J_{P–P}$ = 395.4 Hz, mon), -0.3 (d, $^{1}J_{P–P}$ = 398.1 Hz, tet), -0.5 (d, $^{1}J_{P–P}$ = 396.8, mon).

8.2.1.4 NMR data for cyclo-PO{CO[B]}P{C[B]} (4)

Irradiation of **2** for short periods of time in C_6D_6 led to the appearance of an AB spin system in the ^{31}P{^{1}H} NMR spectrum observed at 319.01 (d, $J_{P–P}$ = 7 Hz), 53.72 (d, $J_{P–P}$ = 7 Hz), alongside compounds **2** and **4**. Further irradiation led to complete conversion to **4**. Recrystallisation lead to cleaner product, however it was not possible to obtain a compositionally pure sample, or single crystals suitable for X-ray diffraction.

^{1}H NMR (500 MHz, C_6D_6): δ (ppm) 7.32 – 6.95 (m, Dipp*H*), 6.23 (s, 2H, {(NC*H*)$_2$}),), 5.95 (s, 2H, {(NC*H*)$_2$}),), 3.27 (sept, 2H, {C*H*(CH$_3$)$_2$}), 3.10 (sept, 2H, {C*H*(CH$_3$)$_2$}), 1.40 – 1.03 (m, {CH(CH_3)$_2$}). **^{13}C{^{1}H} NMR** (126 MHz, C_6D_6): δ (ppm) 201.5 (dd, $J_{P–P}$ = 66.2, 2.6 Hz (P)$_2$*C*O), 175.2 (m, br, (P)$_2$*C*B), 146.3 (s, Ar*C*), 146.2 (s, Ar*C*), 139.1 (s, Ar*C*), 137.1 (s, Ar*C*), 124.3 (s, Ar*C*H), 123.7 (s, Ar*C*H), 120.5 (s, {(N*C*H)$_2$}), 117.8 (s, {(N*C*H)$_2$}), 28.8 (s, *C*H(CH$_3$)$_2$), 23.9 (s, *C*H(CH$_3$)$_2$), 23.7 (s, *C*H(CH$_3$)$_2$). **^{31}P{^{1}H} NMR** (162 MHz, C_6D_6): δ (ppm) 318.9 (d, $J_{P–P}$ = 6.9 Hz), 53.7 (d, $J_{P–P}$ = 6.9 Hz). **^{11}B{^{1}H} NMR** (128 MHz, C_6D_6): δ (ppm) 22.3 (br).

8.2.1.5 Synthesis of cyclo-P{PO[B]){C[B]} (5)

A solution of **2** (100 mg, 0.11 mmol) was dissolved in benzene (0.5 mL) and irradiated continuously for 90 minutes. Volatiles were removed under reduced pressure and the resulting oily solid dissolved in pentane. Cooling the solution for a number of days resulted in red crystals suitable for single crystal X-ray diffraction (38 mg, 39%).

CHN Anal. Calcd. for $C_{53}H_{72}B_2N_4OP_2$ (864.70): C, 73.61%; H, 8.39%; N, 6.48%. Found: C, 72.77; H, 8.24%; N, 6.00%. **^{1}H NMR** (500 MHz, C_6D_6): δ (ppm) 7.22 (m, 6H; ArCH), 7.15–7.06 (m, 6H, 6H; ArCH), 6.22 (s, 2H; {(NC*H*)$_2$}), 5.84 (s, 2H; {(NC*H*)$_2$}), 3.35–3.21 (m, 2H; {C*H*(CH$_3$)$_2$}), 3.08 (m, 2H; {C*H*(CH$_3$)$_2$}), 2.97 (m, 4H; {C*H*(CH$_3$)$_2$}), 1.31–1.12 (m, 40H; {CH(C*H*$_3$)$_2$}), 1.04 (d, $^3J_{H–H}$ = 7 Hz, 6H; {CH(C*H*$_3$)$_2$}), 0.70 (d, $^3J_{H–H}$ = 7 Hz; 6H; {CH(C*H*$_3$)$_2$}). **^{13}C{^{1}H} NMR** (126 MHz, C_6D_6): δ (ppm) 147.2 (Ar*C*), 146.8 (Ar*C*), 146.7 (Ar*C*), 146.1 (Ar*C*), 145.7 (Ar*C*), 138.9 (Ar*C*), 138.6 (Ar*C*), 127.8 (Ar*C*H), 127.7 (Ar*C*H), 127.5 (Ar*C*H), 124.0 (Ar*C*H), 123.7 (Ar*C*H), 123.5 (Ar*C*H), 120.9 ({(N*C*H)$_2$}), 117.5 ({(N*C*H)$_2$}), 28.9 (Dipp*C*H), 28.8 (Dipp*C*H), 28.8 (Dipp*C*H), 28.8 (Dipp*C*H), 25.0 (Dipp*C*H$_3$), 25.0 (Dipp*C*H$_3$), 24.8 (Dipp*C*H$_3$), 24.6 (Dipp*C*H$_3$), 24.4 (Dipp*C*H$_3$), 24.3 (Dip*pC*H$_3$), 24.1 (Dipp*C*H$_3$), 23.9 (Dipp*C*H$_3$), 23.8 (Dipp*C*H$_3$), 23.7 (Dipp*C*H$_3$). **^{31}P{^{1}H} NMR** (162 MHz, C_6D_6): δ 284.7 (d, $^1J_{P–P}$ = 188 Hz), –71.5 (d, $^1J_{P–P}$ = 188 Hz). **^{11}B{^{1}H} NMR** (128 MHz, C_6D_6): δ (ppm) 19.7 (br).

8.2.2 Chapter 3

8.2.2.1 Synthesis of [LiOC[B]P(Mes)]$_2$ (6b)

1 (200 mg, 0.45 mmol) and mesityl lithium (56.5 mg, 0.45 mmol) were dissolved in benzene (2 mL). To this solution, a small amount of THF was added (approx. 0.2 mL) causing the suspended lithium mesitylide to dissolve and the colour change from yellow to orange. NMR spectroscopy indicated the presence of an intermediate (^{7}Li NMR: δ –0.91 (s), ^{31}P NMR: δ 107.13 (s)) which fully converted to the product after three lyophilisation cycles. The

resulting solid was dissolved in hexane and filtered. Concentration of the solution under reduced pressure followed by cooling to –30 °C yielded orange crystals suitable for X-ray diffraction (Yield: 131 mg, 52.8%). **CHN** Anal. Calcd. for $C_{76.5}H_{104.5}B_2Li_2N_4O_2P_2$: C, 75.96%; H, 8.71%; N, 4.63%. Found: C, 74.93%; H, 9.18%; N, 4.04%. **^{1}H NMR** (500 MHz, C_6D_6): δ 7.16 (m, 6H; Dipp*H*), 6.72 (s, 2H; Mes*H*), 6.09 (s, 2H; {(NC*H*)$_2$}), 3.35 (sept, $^3J_{H–H}$ = 6 Hz, 4H; {C*H*(CH$_3$)$_2$}), 2.24 (s, 6H; *ortho*-MesC*H*$_3$), 2.19 (s, 3H; *para*-MesC*H*$_3$), 1.39 (d, $^3J_{H–H}$ = 6 Hz, 12H; {CH(C*H*$_3$)$_2$}), 1.21 (d, $^3J_{H–H}$ = 6 Hz, 12H;{CH(C*H*$_3$)$_2$}). **^{13}C{^{1}H} NMR** (126 MHz, C_6D_6): δ (ppm) 212.9 (m, br, [B]*C*(PR)(OLi)) 145.5 (Ar*C*), 141.1 (d, $^2J_{P-P}$ = 5.6 Hz, Mes *ortho*-*C*), 140.4 (Ar*C*), 137.5 (d, $^1J_{C–P}$ = 55.5 Hz, Mes*C*), 135.8 (Ar*C*), 128.4 (Ar*C*), 123.2 (Ar*C*), 119.4 ((N*C*H)$_2$), 28.4 (Dipp*C*H(CH$_3$)$_2$), 25.3 (DippCH(*C*H$_3$)$_2$), 23.1 (Mes *ortho*-*C*H$_3$), 20.9 (Mes *para*-*C*H$_3$). **^{31}P{^{1}H} NMR** (162 MHz, C_6D_6): δ 136.7 (s). **^{11}B{^{1}H} NMR** (128 MHz, C_6D_6): δ 24.5 (s, br). **^{7}Li NMR** (156 MHz, C_6D_6): δ –3.2 (s).

8.2.2.2 Synthesis of [(12-crown-4)LiOC[B]P(Mes)] (6c)

To a solution of **6b** (78 mg, 0.13 mmol) in C_6D_6 was added 12-crown-4 (24 mg, 0.14 mmol). Volatiles were removed under reduced pressure and the off-white solid dissolved in hexane (1 mL). The solution was filtered and the solution concentrated to approximately 0.2 mL and cooled to –25 °C overnight to yield colourless crystals (82 mg, 80.4 %). **CHN** Anal. Calcd for $C_{44}H_{63}BLiN_2O_5P$ (748.68): C, 70.58%; H, 8.48%; N, 3.74%. Found: C, 68.67%; H, 7.98%; N, 2.98%. **^{1}H NMR** (500 MHz, C_6D_6): δ (ppm) 7.27–7.18 (m, 6H; Ar*CH*), 6.66 (s, 2H; Mes*CH*), 6.31 (s, 2H; {(NC*H*)$_2$}), 3.82 (sept, $^3J_{H–H}$ = 7 Hz, 4H; {C*H*(CH$_3$)$_2$}), 2.70 (broad s, 16H; 12-crown-4), 2.53 (s, 6H; Mes *ortho*-CH$_3$), 2.12 (s, 3H; Mes *para*-*CH$_3$*), 1.55 (d, $^3J_{H–H}$ = 7 Hz; 12H, {CH(C*H*$_3$)$_2$}), 1.38 (d, $^3J_{H–H}$ = 7 Hz, 12H; {CH(C*H*$_3$)$_2$}). **^{13}C{^{1}H} NMR** (126 MHz, C_6D_6): δ (ppm) 146.6 (Ar*C*), 142.7 (d, $^1J_{C–P}$ = 5.5 Hz, Mes*C*) 142.5 (Ar*C*), 133.1 (Ar*C*), 127.3 (Mes*C*H), 126.1 (Dipp*C*H), 123.0 (Dipp*C*H), 119.1 ((N*C*H)$_2$), 67.5 (12-crown-4 *C*H$_2$), 28.7 (Dipp*C*H), 25.4 (Dipp*C*H$_3$), 23.9 (Dipp*C*H$_3$), 23.3 (Mes*C*H$_3$), 21.0

(Mes*C*H_3). *Unable to find [B]*C*(PR)(OLi). **^{31}P{^{1}H} NMR** (162 MHz, C_6D_6): δ 112.0 (s). **^{11}B{^{1}H} NMR** (128 MHz, C_6D_6): δ 25.5 (s, broad). **^{7}Li NMR** (156 MHz, C_6D_6): δ –0.7 (s).

8.2.2.3 Synthesis of [LiOC[B]P(^{Mes}Terph)][LiBr] (7)

Compound **7** was synthesized using the same methodology **6b**. The lithium bromide was likely carried forward from the synthesis of Li^{Mes}Terph. An analytically pure sample of the compound could not be obtained due to small amounts of the LiBr free product can also be observed in the NMR. **^{1}H NMR** (500 MHz, C_6D_6): δ (ppm) 7.22 (t, 2H, 7.2 Hz, *para*-Ar*H*), 7.12 (d, 4H, $^{3}J_{H–H}$ = 7.7 Hz, *meta*-C*H*), 6.91 (s, 2H, Terph Ar*H*), 6.81 (s, 2H, TerphC*H*), 5.96 (s, 2H,{(NC*H*)$_2$})), 2.93 (sept, $^{3}J_{H–H}$ = 7 Hz, 4H; {C*H*(CH_3)$_2$}), 2.41 (s, 6H, TerphCH_3), 2.23 (s, 6H, TerphCH_3), 1.87 (s, 6H, TerphCH_3), 1.07 (d, $^{3}J_{H–H}$ =6.9, 12H), 1.02 (d, $^{3}J_{H–H}$ = 6.9, 12H). **^{31}P{^{1}H} NMR** (162 MHz, C_6D_6): δ (ppm) 162.7 (s). **^{11}B{^{1}H} NMR** (128 MHz, C_6D_6): δ 23.7 (s). **^{7}Li NMR** (156 MHz, C_6D_6): –1.8 (s).

8.2.2.4 Synthesis of [HOC[B]P(Mes)] (8a) and [OC[B]P(Mes)H] (8b)

Water (1.86 mg, 0.10 mmol) was added to a solution of **6b** (60 mg, 0.10 mmol) in C_6D_6 (0.5 mL). The colour changed from yellow to clear and a white precipitate formed. Volatiles were removed under reduced pressure and the resulting white solid was dissolved in hexane and filtered before being concentrated to approximately 0.2 mL. Cooling the solution for a number of days resulted in colourless blocks suitable for X-ray diffraction. (52 mg, 87.6%). **CHN** Anal. Calcd. for $C_{36}H_{47}BLiN_2OP$ (566.54): C, 76.32%; H, 8.54%; N, 4.94%. Found: C, 75.87%; H, 7.71%; N, 3.85%. **^{1}H NMR** (400 MHz, C_6D_6): δ (ppm) 7.26–7.04 (m, 3H, Dipp-C*H*), 6.52 (s, 2H, MesC*H*), 6.21 (s, 2H, {(NC*H*)$_2$}), 6.10 (s, 1H, OH), 3.33 (sept, $^{3}J_{H–H}$ = 7 Hz, 4H, {C*H*(CH_3)$_2$}), 2.08 (s, 6H, Mes *ortho*-CH_3), 1.97 (s, 3H, Mes *para*-CH_3), 1.39 (d, $^{3}J_{H–H}$ = 7 Hz, 12H, {CH(CH_3)$_2$}), 1.28 (d; $^{3}J_{H–H}$ = 7 Hz, 12H, {CH(CH_3)$_2$}). **^{13}C{^{1}H} NMR** (126 MHz, C_6D_6): δ (ppm) 198.5 (br, P*C*OH), 146.0 (Ar*C*), 142.6 (d, J_{PC} = 5.2 Hz, Ar*C*), 140.1 (Ar*C*), 138.9 (Ar*C*), 129.4 (Mes*C*H), 127.5 (Ar*C*H), 123.7 (Dipp*C*H), 120.4

({(NCH)$_2$}), 28.9 ({*C*H(CH$_3$)$_2$}), 25.1 ({CH(*C*H$_3$)$_2$}), 23.8 ({CH(*C*H$_3$)$_2$}, 22.2 (Mes *ortho*-*C*H$_3$), 22.1 (Mes *ortho*-*C*H$_3$), 21.0 (Mes *para*-*C*H$_3$). **^{31}P{^{1}H} NMR** (162 MHz, C$_6$D$_6$): δ (ppm) 147.5 (s). **^{11}B{^{1}H} NMR** (128 MHz, C$_6$D$_6$): δ (ppm) 23.83 (s).

Upon standing in solution for short periods a new resonance was observed in the ^{31}P NMR spectrum at –28.90 ppm (d, $^1J_{P–H}$ = 240 Hz) indicating an equilibrium between the phosphine and phosphaalkene, the corresponding coupling can also be observed for the phosphine proton in ^{1}H NMR spectrum. In benzene the equilibrium lies towards the phosphaalkene, whereas in pyridine the equilibrium moves towards the phosphine. Pure samples of the phosphine could not be obtained, however NMR assignment was possible from the equilibrium mixture. **^{1}H NMR** (500 MHz, [D$_5$]-pyridine): δ (ppm) 7.55–7.31 (m; Dipp C*H*), 6.78 (s, 2H; MesC*H*), 6.63 (s, 2H, {(NC*H*)$_2$}), 5.15 (d, $^1J_{H–P}$ = 240 Hz, 1H; P*H*), 3.23 (s, br; {C*H*(CH$_3$)$_2$}) 1.36 (s, br; 12H; {CH(C*H*$_3$)$_2$}), 1.25 (d, $^3J_{H–H}$ = 7 Hz, 12H, {CH(C*H*$_3$)$_2$}). **^{31}P{^{1}H} NMR** (162 MHz, [D$_5$]-pyridine): δ (ppm) –28.9 (d, $^1J_{H–P}$ = 240 Hz).

8.2.2.5 Synthesis of [OC[B]P(Mes)Au(PPh$_3$)] (9)

Compound **6b** (20 mg, 0.03 mmol) was dissolved in toluene (1 mL) and chloro(triphenylphosphine)gold(I) (17 mg, 0.03 mmol) was added. The solution was filtered, concentrated and cooled for a number of days to produce a yellow powder (18 mg, 58%).

A spectroscopically equivalent product can be synthesised through *in situ* generation of **6a**: **1** (100 mg, 0.22 mmol) was dissolved in benzene (2 mL) followed by the addition of mesityl lithium (27 mg, 0.21 mmol). THF was added dropwise until the suspension dissolved to give a bright orange solution. To this solution, chloro(triphenylphosphine)gold(I) (107 mg, 0.22 mmol) was added. The solution turned from orange to yellow and a white precipitate formed. Volatiles were removed under reduced pressure and the resulting pale yellow solid washed twice with hexane (2 mL), dissolved in toluene (1 mL) and filtered. The filtrate was cooled to –25 °C overnight to yield a pale yellow precipitate. Analytically pure samples could be obtained by vapour diffusion of hexane into a concentrated THF solution (110 mg, 49%).

Single crystals suitable for X-ray diffraction were grown from vapour diffusion of hexane into a toluene solution. **^{1}H NMR** (500 MHz, C_6D_6): δ (ppm) 7.43–7.20 (m, 12H; ArC*H*), 6.96 (m, 9H; ArC*H*), 6.82 (s, 2H; Mes ArC*H*), 6.28 (s, 2H, {(NC*H*)$_2$}), 3.52 (sept, $^{3}J_{H–H}$ = 7 Hz, 4H; {C*H*(CH$_3$)$_2$}), 2.63 (s, 6H; Mes *ortho*C*H*$_3$), 2.09 (s, 3H; Mes *para*C*H*$_3$), 1.32 (d, $^{3}J_{H–H}$ = 7 Hz, 12H; {CH(C*H*$_3$)$_2$}), 1.18 (d, $^{3}J_{H–H}$ = 7 Hz, 12H, {CH(C*H*$_3$)$_2$}). **^{13}C{^{1}H} NMR** (126 MHz, C_6D_6): δ (ppm) 146.3 (Ar*C*), 144.5 (d, $^{2}J_{C–P}$ = 10 Hz, Mes*C*), 139.9 (Ar*C*), 137.1 (Ar*C*), 134.6 (d, $^{2}J_{C–P}$ = 14 Hz; PPh$_3$), 133.4 (d, $^{1}J_{C–P}$ = 16.9 Hz; Mes*C*), 131.4 (Ar*C*H), 130.7 (d, $^{1}J_{C–P}$ = 49.0 Hz, PPh$_3$ *C*), 129.3 (d, $^{3}J_{C–P}$ = 10.9 Hz, P(Ph)$_3$ *C*H), 129.2 – 128.6 (m, P(Ph)$_3$ *C*H), 128.5 (Mes*C*H), 127.6 (Ar*C*H), 123.6 (Ar*C*H), 119.9 ({(N*C*H)$_2$}), 29.0 ({*C*H(CH$_3$)$_2$}), 26.1 ({CH(*C*H$_3$)$_2$}), 25.2 (d, $^{3}J_{C–P}$ = 12.3 Hz, Mes *ortho*C*H*$_3$), 24.1 ({CH(*C*H$_3$)$_2$}), 21.1 (Mes *para*C*H*$_3$). **^{31}P{^{1}H} NMR** (162 MHz, C_6D_6): δ (ppm) 50.3 (d, $^{2}J_{P–P}$ = 145.0 Hz; PC(O)[B]), 44.0 (d, $^{2}J_{P–P}$ = 144.6 Hz; PPh$_3$). **^{11}B{^{1}H} NMR** (128 MHz, C_6D_6): δ (ppm) 24.3 (s, br).

8.2.2.6 Synthesis of {[B](NaO)C=PFp*}$_2$ (10)

[B]OCP (150 mg, 0.34 mmol) was added to a suspension of NaFp* (92 mg, 0.34 mmol) in toluene (2 mL). The solution darkened from light to dark orange. The solution was filtered to remove any excess NaFp*, concentrated to approximately 50% of the original volume and cooled overnight to yield **10** as red crystals (195 mg, 80.6%) suitable for single crystal X-ray diffraction. **CHN** Anal. Calcd. for $C_{39}H_{51}BFeN_2NaO_3P$: C, 65.38%; H, 7.18%; N, 3.91%. Found: C, 66.25%; H, 7.63%; N, 4.17%. **^{1}H NMR** (500 MHz, C_6D_6): δ (ppm) 7.31 (br s, 6H; Ar*H*), 6.22 (s, 2H; (NC*H*)$_2$), 3.72 (br s, 2H; {C*H*(CH$_3$)$_2$}), 1.56 (br s, 26H; Cp* C*H*$_3$ and {CH(C*H*$_3$)$_2$}), 1.31 (d, $^{3}J_{H–H}$ = 7 Hz, 12H; {CH(C*H*$_3$)$_2$}). **^{13}C{^{1}H} NMR** (126 MHz, C_6D_6): δ (ppm) 222.1 (s, br; *C*P), 146.6 (*C*O), 140.8 (Ar*C*), 126.6 (Ar*C*), 123.3 (Ar*C*), 118.4 ((N*C*H)$_2$), 94.9 (Cp**C*), 28.2 (*C*H(CH$_3$)$_2$), 25.9 (Cp**C*H$_3$), 23.5 (*C*H(CH$_3$)$_2$), 9.3 (CH(*C*H$_3$)$_2$), 9.3 (CH(*C*H$_3$)$_2$). **^{11}B{^{1}H} NMR** (128 MHz, C_6D_6): δ (ppm) 25.5 (s). **^{31}P{^{1}H}**

NMR (162 MHz, C_6D_6): δ (ppm) 188.6 (s). **IR**: ν = 1899 cm^{-1} (ν_{asym}, C≡O), 1942 cm^{-1} 3 ν_{sym}, C≡O).

8.2.2.7 Synthesis of [B](Me$_3$SiO)C=PFp* (11)

To a solution of **10** (100 mg, 0.14 mmol) in toluene (2 mL) trimethylsilyl chloride (18.3 mg, 0.17 mmol; 1.2 equivalents) was added. A precipitate immediately formed and both the ^{1}H and ^{31}P NMR spectra revealed quantitative conversion to [B](Me$_3$SiO)C=PFp*. The solution was filtered and the solvent removed under reduced pressure, yielding an orange powder (91 mg, 85.0%). Recrystallisation from hexane yielded red crystals of [B](Me$_3$SiO)C=PFp* (**2**) suitable for X-ray diffraction. **CHN** Anal. Calcd. for $C_{42}H_{60}BFeN_2O_3PSi$: C, 65.80%; H, 7.89%; N, 3.65%. Found: C, 65.35%; H, 7.61%; N, 3.99%. **^{1}H NMR** (500 MHz, C_6D_6): δ(ppm) 7.27–7.20 (m, 6H; Ar*H*), 6.38 (s, 2H; (NC*H*)$_2$), 3.69 (sept, $^3J_{H–H}$ = 7 Hz, 4H; {C*H*(CH$_3$)$_2$}), 1.45 (d, $^3J_{H–H}$ = 7 Hz, 12H; {CH(C*H*$_3$)$_2$}), 1.40 (s, 15H; Cp* C*H*$_3$), 1.25 (d, $^3J_{H–H}$ = 7 Hz, 12H; {CH(C*H*$_3$)$_2$}), 0.15 (s, 9H; SiMe$_3$). **^{13}C{^{1}H} NMR** (126 MHz, C_6D_6): δ (ppm) 217.0 (s, br; *C*P), 145.9 (*C*O), 140.7 (Ar*C*), 127.0 (Ar*C*), 124.0 (Ar*C*), 120.1 ((N*C*H)$_2$), 95.9 (Cp**C*), 28.7 (*C*H(CH$_3$)$_2$), 26.4 (*C*H(CH$_3$)$_2$), 23.3 (Cp**C*H$_3$), 9.3 (CH(*C*H$_3$)$_2$), 1.2 (Si*C*H$_3$). **^{31}P{^{1}H} NMR** (162 MHz, C_6D_6): δ(ppm) 350.6 (s). **^{11}B{^{1}H} NMR** (128 MHz, C_6D_6): δ(ppm) 23.3 (s, br). **IR**: ν = 1947 cm^{-1} (ν_{asym}, C≡O), 1994 cm^{-1} (ν_{sym}, C≡O).

8.2.2.8 Synthesis of (PPh$_3$)AuP{C(O)[B]}Fp* (12)

To a solution of **10** (100 mg, 0.14 mmol) in toluene (2 mL) chloro(triphenylphosphene)gold(I) (69 mg, 0.14 mmol) was added. The suspension was sonicated for 30 minutes, after which the NMR spectra showed complete consumption of the starting material. The solution was filtered, and the solvent removed under reduced pressure. The resulting orange oil was washed with hexane and recrystallised from toluene yielding analytically pure orange crystals suitable for X-ray diffraction (87 mg, 60.1%). **CHN** Anal.

Calcd. for $C_{57}H_{66}AuBFeN_2O_3P_2$: C, 59.39%; H, 5.77%; N, 2.43%. Found: C, 58.91%, H5.34 %; N 2.40 %. **^{1}H NMR** (500 MHz, C_6D_6): δ(ppm) 7.65–7.56 (m, 5H; Ar*H*), 7.28–7.18 (m, 6H; Ar*H*), 7.11–6.99 (m, 11H; Ar*H*), 6.26 (s, 2H; {(NCH)$_2$}), 3.57 (sept, $^3J_{H–H}$ = 7, 4H; C*H*(CH$_3$)$_2$), 1.47 (s, 15H; Cp* CH$_3$), 1.39 (d, $^3J_{H–H}$ = 7, 12H, {CH(C*H*$_3$)$_2$}), 1.19 (d, $^3J_{H–H}$ = 7, 12H, CH(C*H*$_3$)$_2$). **^{13}C{^{1}H} NMR** (126 MHz, C_6D_6): δ(ppm) 218.9 (s, br; *C*P), 146.4 (*C*O), 140.7 (Ar*C*), 134.8 (Ar*C*), 134.7 (Ar*C*), 132.0 (Ar*C*), 131.6 (Ar*C*), 131.2 (Ar*C*), 131.2 (Ar*C*), 129.3 (Ar*C*), 129.2 (Ar*C*), 127.2 (Ar*C*), 123.4 (Ar*C*), 119.6 ((N*C*H)$_2$), 94.7 (Cp**C*), 29.0 (*C*H(CH$_3$)$_2$), 26.0 (*C*H(CH$_3$)$_2$), 24.3 (Cp**C*H$_3$), 9.7 (CH(*C*H$_3$)$_2$). **^{31}P{^{1}H} NMR** (162 MHz, C_6D_6): δ(ppm) 98.8 (d, $^2J_{P–P}$=102), 43.3 (d, $^2J_{P–P}$ =102). **^{11}B{^{1}H} NMR** (128 MHz, C_6D_6): δ(ppm) 21.8 (s). **IR**: ν = 1955 cm^{-1} (ν_{asym}, C≡O), 2003 cm^{-1} (ν_{sym}, C≡O).

8.2.2.9 13 Synthesis of HP{C(O)[B]}Fp*$^-$ (13)

To a solution of **10** (50 mg, 0.07 mmol) in toluene a small excess of water (2 μL, 0.15 mmol) was added. The reaction turned from bright red to light orange. The solvent was removed under reduced pressure and the resultant red oil taken up into hexane. Concentration, followed by cooling to –35 °C overnight resulted in pale yellow crystals of **13** (38 mg, 71%). **^{1}H NMR** (400 MHz, C_6D_6): δ (ppm) 7.33 – 7.18 (m, 6H, *meta*- and *para*-Ar*H*), 6.16 (s, 2H, {(NC*H*)$_2$}), 3.38 (sept, $^3J_{H–H}$ = 6.8 Hz, 5H, {C*H*(CH$_3$)$_2$}), 1.51 (d, $^3J_{H–H}$ = 6.8 Hz, 12H, {CH(C*H*$_3$)$_2$}), 1.30 (s, 15H, Cp*), 1.26 (d, $^3J_{H–H}$ = 6.8 Hz, 12H, {CH(C*H*$_3$)$_2$}),). **^{11}B{^{1}H} NMR** (128 MHz, C_6D_6): δ (ppm) 74.5. **^{31}P NMR** (162 MHz, C_6D_6): δ (ppm) –9.0 (d, $^1J_{P-H}$ = 199.0 Hz). **^{31}P{^{1}H}** NMR (162 MHz, C_6D_6): δ (ppm) -9.0 (s).

8.2.2.10 Synthesis of {[B](KO)C=PFp*}$_2$ (14)

KO^{t}Bu (6.7 mg, 0.06 mmol) was added to a toluene solution of **11** (50 mg, 0.06 mmol). A few drops of THF were added to aid solubility. The solution was filtered and concentrated. Crystals were obtained from a cooled toluene/hexane solution (21 mg, 41%). **^{31}P{^{1}H} NMR** (162 MHz, THF): δ (ppm) 178.3(s) ppm

8.2.2.11 Synthesis of [[B]OCPH$_2$Fp*][B(C$_6$F$_5$)$_4$] (15)

Potassium tetrakis(pentafluorophenyl)borate (150 mg, 0.21mmol) was added to a stirring solution of [B]O(SiMe$_3$)CPFp* (**11**) (80 mg, 0.10 mmol) and trimethylsilyl chloride (23 mg, 20mmol) in toluene (10 mL). Overnight the reaction mixture formed a thick oil, which was extracted with toluene (3 * 10 mL) and ether (2 * 5 mL) followed by filtration through celite. Concentration of the solution and cooling to –35 °C lead to the formation of red crystals of [[B]OCPH$_2$Fp*][B(C$_6$F$_5$)$_4$] (81 mg, 56.5%). Once formed, the crystals were no longer soluble in toluene, NMR characterisation was carried out in THF, however the stability of the compound was poor and it decomposed in solution over the course of a few minutes. **CHN** Anal. Calcd. for $C_{64}H_{56}B_2F_{19}Fe_1N_2O_3P_1$: C, 56.09%; H, 4.12%; N, 2.04%; Found: C, 54.19%; H, 4.14%; N, 2.12%. **^{1}H NMR** (400 MHz, THF–d_8): δ (ppm) 7.40 – 7.31 (m, 2H, Ar*H*), 7.27 (d, $^3J_{H–H}$ =7 Hz, 4H, Ar*H*), 6.64 (s, 2H, {(NC*H*)$_2$}), 4.17 (d, $^1J_{P–H}$= 349 Hz, 2H, R$_2$P*H*$_2$), 2.75 (hept, $^3J_{H–H}$= 7 Hz, 4H; {C*H*(CH$_3$)$_2$}), 1.18 (s, 15H; Cp*Methyl*H*), 1.15 – 1.02 (m, 24H; {CH(C*H*$_3$)$_2$}). **^{13}C{^{1}H} NMR** (126 MHz, THF): δ (ppm) 207.8 (d, $^1J_{C–P}$= 19 Hz; P*C*), 147.4 (BAr*C*), 145.5 (BAr*C*), 143.5 (Ar*C*), 137.3 (BAr*C*), 135.3 (BAr*C*), 133.4 (BAr*C*), 127.0 (Ar*C*), 126.2 (Ar*C*), 124.1 (Ar*C*), 123.4 ({(N*C*H)$_2$}), 122.2, 121.0, 102.5, 97.7 (Cp*), 27.9, 26.8, 6.5. **^{31}P{^{1}H} NMR** (162 MHz, THF–d_8): δ (ppm) –10.7. **^{31}P NMR** (202 MHz, THF–d_8): δ (ppm) –10.6 (t, $^1J_{P–H}$= 352.0 Hz). **^{11}B{^{1}H} NMR** (128 MHz, THF): δ (ppm) 18.6 (br, borane), –16.6 (sharp, borate). **^{19}F{^{1}H} NMR** (470 MHz, THF–d_8): δ (ppm) –130.7 (m), –164.9 (t, *J*=20 Hz), –168.4 (t, *J*=18 Hz).

8.2.2.12 Synthesis of [B]C(PCO)NMes (16a)

To a solution of [B]OCP (**1**) (100 mg, 22 mmol) in benzene (1 mL) was added 2,4,6-trimethylphenyl isocyanide (32 mg, 22 mmol). The solution immediately changed from pale yellow to orange. Removal of the solvent yielded an oily orange solid. Recrystallization from hexane yielded analytically pure orange crystals of [B]C(PCO)NMes (**2a**) (93 mg,

71.9% yield). **CHN** Anal. Calcd. for $C_{37}H_{47}BN_3OP$: C, 75.12%; H, 8.01%; N, 7.10%. Found: C, 74.96%; H, 8.14%; N, 7.00%. **^{1}H NMR** (400 MHz, C_6D_6): δ (ppm) 7.23 (dd, $^3J_{H–H}$ = 8.5 Hz, 6.8, 2H; *para*-Ar*H* Dipp), 7.14 (m, br, 4H; *meta*-Ar*H* Dipp), 6.57 (s, 2H; *meta*-Ar*H* Mes), 6.22 (s, 2H; {(NC*H*)$_2$}), 3.40 (sept, $^3J_{H–H}$ = 6.8 Hz, 4H; {C*H*(CH$_3$)$_2$}), 2.06 (s, 3H; *para*-C*H*$_3$ Mes), 1.53 (s, 6H; *ortho*-C*H*$_3$ Mes), 1.37 (d, $^3J_{H–H}$ = 6.9 Hz, 12H; {CH(C*H*$_3$)$_2$}), 1.21 (d, $^3J_{H–H}$ = 6.9 Hz, 12H; {CH(C*H*$_3$)$_2$}). **^{13}C{^{1}H} NMR** (126 MHz, C_6D_6): δ (ppm) 205.2 (d, $^1J_{C–P}$ = 117.2 Hz; P*C*O) , 154.2 (d, $^1J_{C–P}$ = 15.1 Hz; [B]*C*(NMes)(PCO)), 146.7 (Ar*C*), 138.4 (Ar*C*), 135.9 (Ar*C*), 129.1 (Ar*C*), 126.7 (Ar*C*), 123.7 (Ar*C*), 120.4 ({(N*C*H)$_2$}), 29.0 (methyl*C* Mes), 26.0 (methyl*C* Mes), 23.5 (methine*C* Dipp), 21.0 (methyl*C* Dipp), 17.1 (methyl*C* Dipp). **^{31}P{^{1}H} NMR** (162 MHz, C_6D_6): δ (ppm) –195.2 (s). **^{11}B{^{1}H} NMR** (128 MHz, C_6D_6): δ (ppm) 22.8 (s, br).

8.2.2.13 Irradiation of 16a to yield [B]PCNMes (17a) and an unidentified product

Irradiation of a solution of **16a** (50 mg) in toluene (1 mL) yields two products as determined by ^{1}H, ^{11}B and ^{31}P NMR spectroscopy, independent of the concentration and temperature at which irradiation is conducted. Attempts to separate these products were unsuccessful. Crystallisation from a concentrated hexane solution lead to the identification of a MesNC supported phosphinidene (**3a**), however it was not possible to identify the second product. Redissolving the crystals revealed a mixture of the two products observed during the reaction. A qualitative assignment of the observed peaks was still attempted.

^{1}H NMR (400 MHz, C_6D_6): A characteristic $^4J_{P–H}$ (1.4 Hz) coupling was observed at 6.27 ppm, consistent with the phosphaketene later characterised, likely belonging to the phosphinidene complex. The second product has a distinct boryl backbone resonance at 6.29 ppm, with no phosphorus coupling observed.

^{11}B{^{1}H} NMR (128 MHz, C_6D_6): Reveals two broad resonances at 28.2 and 23.4 ppm consistent with the presence of two boryl moieties.

$^{31}P\{^{1}H\}$ NMR (162 MHz, C_6D_6): The phosphinidene has a resonance at –262.6 ppm (s), in good agreement with the calculated structure. The unknown product is responsible for the phosphorus resonance at +8.6 ppm.

8.2.2.14 Synthesis of [B]C(PCNMes)NMes (18)

[B]C(PCNMes)NMes can be synthesised either from **16a** (i) or directly from [B]OCP (ii):

(i) **16a** (50 mg, 9 mmol) was dissolved in benzene (1 mL) and 2,4,6-trimethylphenyl isocyanide (15 mg, 10.8 mmol, 1.2 eq) was added. The reaction mixture was monitored by ^{31}P NMR spectroscopy and after 24 hours complete consumption of **16a** was observed. The solvent was removed and the oily orange solid recrystallized from hexane, yielding pale orange crystals of [B]C(PCNMes)NMes **16a** (42 mg, 73.5%).

(ii) [B]OCP (50 mg, 11 mmol) was dissolved in benzene (1 mL) and 2,4,6-trimethylphenyl isocyanide (35 mg, 24mmol, 2.2 eq) was added. The reaction was monitored by ^{31}P NMR spectroscopy and showed complete conversion after 24 hours. The solvent was removed and the oily orange solid recrystallized from hexane, yielding pale orange crystals of [B]C(PCNMes)NMes (**4a**) (46 mg, 60.0%). **CHN** Anal. Calcd. For $C_{46}H_{58}BN_4P$: C, 77.95%; H, 8.25%; N, 7.90%. Found: C, 77.56%; H, 8.34 %; N, 7.67%. **^{1}H NMR** (400 MHz, C_6D_6): δ (ppm) 7.25–7.12 (m, 2H; ArC*H* Dipp), 7.07–7.15 (m, 4H; ArC*H* Dipp), 6.32 (s, 2H; *meta*-Ar*H* Mes), 6.28 (s, 2H; *meta*-Ar*H* Mes), 6.21 (s, 2H; {(NC*H*)$_2$}), 3.49 (sept, $^{3}J_{H–H}$ = 6.9 Hz, 4H; {C*H*(CH$_3$)$_2$} Dipp), 1.78 (s with shoulder, 9H; *para*-C*H*$_3$ Mes and *ortho*-C*H*$_3$ Mes) 1.73 (s, 6H; *ortho*-C*H*$_3$ Mes), 1.48 (s, 3H, *para*-C*H*$_3$; Mes), 1.42 (d, $^{3}J_{H–H}$ = 6.9 Hz, 12H; {CH(C*H*$_3$)$_2$} Dipp), 1.22 (d, $^{3}J_{H–H}$ = 6.9 Hz, 12H; {CH(C*H*$_3$)$_2$} Dipp). **$^{13}C\{^{1}H\}$ NMR** (126 MHz, C_6D_6): δ (ppm) 165.3 (d, $^{1}J_{C–P}$ = 110.1 Hz; P*C*NMes) , 152.3 (d, $^{1}J_{C–P}$ = 11.3 Hz; [B]*C*(NR)(PCNMes)), 146.9 (Ar*C*), 139.5 (Ar*C*), 138.1 (Ar*C*), 135.0 (Ar*C*), 133.5 (Ar*C*), 128.8 (Ar*C*), 125.8 (Ar*C*), 123.6 (Ar*C*), 120.3 ({(N*C*H)$_2$}), 29.1 (methyl*C* Mes), 26.0 (methyl*C* Mes), 23.7 (methine*C* Dipp), 20.9 (methyl*C* Dipp), 20.4 (methyl*C* Dipp), 18.4

(methyl*C* Mes), 17.8 (methyl*C* Mes). **^{31}P{^{1}H} NMR** (162 MHz, C_6D_6): δ (ppm) –136.1 (s) (small amount of impurity observed at +152.90 ppm). **^{11}B{^{1}H} NMR** (128 MHz, C_6D_6): δ (ppm) 23.0 (s, br).

8.2.2.15 Synthesis of [B]PCN^{t}Bu (17b)

3b can by synthesised starting with [B]OCP (i) or [B]PCO (ii)**:**

(i) [B]OCP (30 mg, 6.7 mmol) was dissolved in benzene (1 mL) and ^{t}BuNC (25 mg, 30 mmol, 4.5 eq.) was added. After 2 hours complete conversion to **17b** was observed. The reaction was monitored for 2 days, after which *ca.* 95% of **4** had been consumed. The solvent and excess ^{t}BuNC was removed under vacuum and the orange oil recrystallized from hexane (1 mL concentrated to 0.3 mL) yielding orange crystals of **17b** (10 mg, 33%). The reduced yield is likely due to the high solubility of the species, as the only observed product of the reaction is **3b**. The NMR spectra of the crystalline material contained small amounts of impurities which were difficult to remove due to their solubility being similar to that of the desired product. Further recrystallizations gave diminishing improvements to purity and significantly lower yields.

(ii) [B]PCO (**5**) (50 mg, 11 mmol) was dissolved in benzene (1 mL) and ^{t}BuNC (23.5 mg, 28 mmol, 2.5 eq.) was added. The reaction was monitored for 4 days, by which time *ca.* 95% of the starting material had been consumed. Further stirring did not lead to substantial changes in the NMR spectrum. The solvent and excess ^{t}BuNC was removed under reduced pressure and the orange oil recrystallized from hexane (1 mL concentrated to 0.3 mL) yielding orange crystals (24 mg, 42 %). **CHN** Anal. Calcd. for $C_{31}H_{45}BN_3P$: C, 74.24 %; H, 9.04 %; N, 8.38 %. Found: C, 76.78 %, H, 9.84 %; N 6.25 %. Calcd. with 1 eq. of hexane as $C_{37}H_{59}BN_3P$: C, 75.62 %; H, 10.12 %; N, 7.15 %. **^{1}H NMR** (400 MHz, C_6D_6): δ (ppm) 7.24–7.09 (m, 6H; Ar*H*), 6.23 (d, $^{4}J_{P–H}$ =1.4 Hz, 2H; {(NC*H*)$_2$}), 3.39 (sept, $^{3}J_{H–H}$ =7.1 Hz, 4H; {C*H*(CH$_3$)$_2$}), 1.45 (d, $^{3}J_{H–H}$ = 6.9 Hz, 12H; {CH(C*H*$_3$)$_2$}), 1.31 (s, 11H; hexane), 1.23 (d,

$^{3}J_{H–H}$ = 6.9 Hz, 12H; {CH(CH_3)$_2$}), 0.91 (s, 5H, hexane), 0.70 (s, 9H; ^{t}Bu). **^{13}C{^{1}H} NMR** (126 MHz, C_6D_6): δ (ppm) 173.7 (d, $^{1}J_{C–P}$ = 70.4 Hz; isocyanide*C*), 147.0 (Ar*C*), 139.7 (Ar*C*), 124.0 (Ar*C*), 121.7 ({(N*C*H)$_2$}), 60.0 (d, $^{3}J_{C–P}$ = 5.3 Hz; N*C*(CH$_3$)$_3$), 38.8 (hexane), 31.9 (NC(*C*H$_3$)$_3$), 30.0 (methyl*C* Dipp), 29.0 (hexane), 25.1 (methyl*C* Dipp), 24.3 (methine*C* Dipp), 14.6 (hexane). **^{31}P{^{1}H} NMR** (162 MHz, C_6D_6): δ (ppm) –256.2 (s, br). **^{11}B{^{1}H} NMR** (128 MHz, C_6D_6): δ (ppm) 27.7 (s, br), impurity at 14.8 ppm.

8.2.2.16 Synthesis of [B]PCO (19)

[B]OCP (100 mg, 22 mmol) was dissolved in a benzene (1 mL) solution containing ^{t}BuNC (1.9 mg, 2 mmol, 10 mol%). The reaction was monitored by ^{31}P NMR spectroscopy, after 48 hours the starting material was completely consumed. The solvent and ^{t}BuNC were removed under vacuum, and the resulting oily solid recrystallized from hexane yielding [B]PCO (**19**) as a yellow powder (71 mg, 71%). Crystals suitable for X-ray diffraction were obtained from a cooled hexane solution. **CHN** Anal. Calcd. for $C_{27}H_{36}BN_2OP$: C, 72.65%; H, 8.13%; N, 6.28%. Found: C, 71.73%; H, 8.02 %; N, 6.66%. **^{1}H NMR** (400 MHz, C_6D_6): δ (ppm) 7.26–7.17 (dd, $^{3}J_{H–H}$ = 8.1, 6.9 Hz, 4H; *para*-Ar*H*), 7.14 (dd, $^{3}J_{H–H}$ = 7.2, 8.2 Hz, 2H; *ortho*-Ar*H*), 6.27 (d, $^{4}J_{H–P}$ = 1.6 Hz, 2H; {(NC*H*)$_2$}), 3.19 (sept, $^{3}J_{H–H}$ = 6.9 Hz, 4H; {C*H*(CH$_3$)$_2$}), 1.36 (d, $^{3}J_{H–H}$ = 6.9 Hz, 12H; {CH(CH_3)$_2$}), 1.19 (d, $^{3}J_{H–H}$ =6.9 Hz, 12H;{CH(CH_3)$_2$}). **^{13}C{^{1}H} NMR** (126 MHz, C_6D_6): δ (ppm) 191.1 (d, $^{1}J_{C–P}$ = 89.3 Hz; P*C*O), 146.6 (Ar*C*), 137.8 (Ar*C*), 128.7 (Ar*C*), 124.0, 121.9 ({(N*C*H)$_2$}), 28.8 (methyl*C* Dipp), 24.9 (methyl*C* Dipp), 23.9 (methine*C* Dipp). **^{31}P{^{1}H} NMR** (162 MHz, C_6D_6): δ (ppm) –337.1 (s, br). **^{11}B{^{1}H} NMR** (128 MHz, C_6D_6): δ (ppm) 25.6 (s, br).

8.2.2.17 Synthesis of [B]P=P[B] (20)

[B]PCO (**19**; 30 mg, 6.7 mmol) was dissolve in benzene (1 mL) and irradiated for 30 minutes, resulting in complete consumption of the starting material and formation a single product in the ^{31}P NMR spectrum at 596 ppm. The solvent was removed and the resulting orange solid

dissolved in hexane. Concentration of the solution and cooling to –35°C for a week resulted in orange crystals of **20** (19 mg, 67.6 %). **CHN** Anal. Calcd. for $C_{26}H_{36}BN_2P$: C, 74.64%; H, 8.67%; N, 6.70%. Found: C, 74.03%; H, 8.38%; N, 7.11%. **^{1}H NMR** (400 MHz, C_6D_6): δ (ppm) 7.23–7.16 (m, 4H; Ar*H*), 7.06–7.03 (m, 2H; Ar*H*), 6.26 (s, 2H; {(NC*H*)$_2$}), 3.14 (sept, $^3J_{H–H}$ = 7.1 Hz, 4H; {C*H*(CH$_3$)$_2$}), 1.17 (d, $^3J_{H–H}$ = 6.9 Hz, 12H; {CH(C*H*$_3$)$_2$}), 0.98 (d, $^3J_{H–H}$ = 6.9 Hz, 12H; {CH(C*H*$_3$)$_2$}). **^{13}C{^{1}H} NMR** (126 MHz, C_6D_6): δ (ppm) 146.2 (Ar*C*), 138.9 (Ar*C*), 123.5 (Ar*C*), 121.1 ({(N*C*H)$_2$}), 28.7 (methyl*C* Dipp), 25.4 (methyl*C* Dipp), 23.8 (methine*C* Dipp). **^{31}P{^{1}H} NMR** (162 MHz, C_6D_6): δ (ppm) 596.0 (s, br). **^{11}B{^{1}H} NMR** (128 MHz, C_6D_6): δ (ppm) 30.0 (s, br).

8.2.2.18 Synthesis of [B]P(*^{iPr}*NHC) (21)

Two equivalents of NHC 1,3-diisopropyl-4,5-dimethyl-1H-imidazol-3-ium-2-ide (20.6 mg, 11.5 mmol) were added to a solution containing [B]P=P[B] (50 mg, 5.7 mmol) in toluene. The solution was heated to 60 degrees for an hour, and the solvent immediately removed under reduced pressure. The resulting orange solid was extracted into hexane and concentrated to *ca.* 0.5 mL. Crystals were obtained from cooling the resultant solution to –35 °C overnight (25.7 mg, 35%). Upon isolation the compound slowly reacts to give an unknown species with a ^{31}P NMR resonance at –245.0 ppm. **^{1}H NMR** (400 MHz, C_6D_6): δ (ppm) 7.20 – 7.10 (m, 6H, *meta* and *para*-C*H*), 6.39 – 6.19 (m, 4H, {(NC*H*)$_2$}) and NHC {C*H*(CH$_3$)$_2$}, overlapping), 3.51 (sept, $^3J_{H–H}$ = 6.8, 4H, {C*H*(CH$_3$)$_2$}), 1.58 (s, 6H, NHC C*H*$_3$), 1.40 (d, $^3J_{H–H}$ = 7.0, 12H, {CH(C*H*$_3$)$_2$}), 1.33 – 1.14 (m, {CH(C*H*$_3$)$_2$}).), 0.95 (d, *J*=7.2, 12H, {CH(C*H*$_3$)$_2$}). **^{31}P{^{1}H} NMR** (162 MHz, C_6D_6): δ (ppm) –196.7 (s). **^{11}B{^{1}H} NMR** (128 MHz, C_6D_6): δ (ppm) 32.5 (s, br).

8.2.2.19 Synthesis of cyclo-[B]PP(O[B])C(*^{Me2}*IPr)C(O) (22)

Addition of one equivalent of 1,3-diisopropyl-4,5-dimethyl-1,3-dihydro-2λ^2-imidazole (19 mg, 11 mmol) to a toluene solution of [B]PCO (100 mg, 22 mmol) resulted in complete

consumption of the [B]PCO. The solvent was removed and product extracted with hexane and filtered to remove the excess carbene. Concentration of the hexane solution followed by cooling to –35 °C resulted in light orange crystals of **22** (57 mg, 47.9%). **CHN** Anal. Calcd. for $C_{65}H_{92}B_2N_6O_2P_2$: C, 72.76 %; H, 8.64 %; N, 7.83 %. Found: C, 73.86%; H, 8.89 %; N, 7.46 %. **^{1}H NMR** (500 MHz, C_6D_6): δ (ppm) 7.28–7.17 (m, 4H; Ar*H*), 7.12 (dd, *J* = 7.3, 1.7, 2H; Ar*H*), 7.09–7.02 (m, 6H; Ar*H*), 6.24 (d, $^4J_{H–P}$ = 1.1 Hz, 2H; {(NC*H*)$_2$}), 5.85 (s, 2H; {(NC*H*)$_2$}), 5.04 (s, very broad, 1H, NHC iPr), 3.86 (s, very broad, NHC iPr protons), 3.65 (sept, $^3J_{H–H}$ = 6.9 Hz, 2H, {C*H*(CH$_3$)$_2$}), 3.34 (sept, $^3J_{H–H}$ = 6.9 Hz, 2H; {C*H*(CH$_3$)$_2$}), 3.23 (d sept, *J* =13.8 Hz $^3J_{H–H}$ = 6.9 Hz, 4H; {C*H*(CH$_3$)$_2$}), 1.64 (s, 2H; hex), 1.52 (s, 4H; Ali*H*), 1.51 (s, 6H, NHC methyl*H*)), 1.33 (d, $^3J_{H–H}$ = 6.9 Hz, 10H, Dipp*H*), 1.29–1.21 (m, 29H; Dipp*H* and iPr *H*), 1.20 (d, $^3J_{H–H}$ = 6.9 Hz, 6H; Dipp*H)*, 1.01 (d, $^3J_{H–H}$ = 6.9, 6H; Dipp*H*), 0.91 (br, 16H, NHC Dipp*H*). **^{13}C{^{1}H} NMR** (126 MHz, C_6D_6): δ (ppm) 178.4 (dd, $^1J_{C–P}$ = 29.8 Hz, $^2J_{C–P}$ = 10.3 Hz, 1,2-diphosphetan-3-one carbon), 146.8 (Ar*C*), 146.2 (Ar*C*), 146.1 (Ar*C*), 145.7 (Ar*C*), 143.2 (t, $^2J_{C–P}$ = 11.2 Hz, carbene*C*), 139.8 (Ar*C*), 139.0 (Ar*C*), 126.7 (d, $^3J_{C–P}$ = 6.4 Hz; ({(N*C*H)$_2$}), 123.4 (NHC), 123.1 (NHC), 122.9 (NHC), 122.7 (NHC), 121.4 ({(N*C*H)$_2$}, 117.2 (NHC), 96.7 (dd, $^1J_{C–P}$ = 52.2 Hz, $^2J_{C–P}$ = 16.0 Hz, 1,2-diphosphetan-3-one carbon), 59.7 (NHC iPr), 38.2 (NHC iPr), 31.3 (hex), 29.9 (aliphatic C), 28.7 (aliphatic C), 28.2 (aliphatic C), 28.0 (aliphatic C), 25.8 (aliphatic C), 25.6 (aliphatic C), 25.0 (aliphatic C), 24.5 (aliphatic C), 24.4 (aliphatic C), 23.9 (aliphatic C), 23.7 (hex), 23.1 (aliphatic C), 14.0 (hex), 9.7 (aliphatic C). **^{31}P{^{1}H} NMR** (162 MHz, C_6D_6): δ (ppm) 90.6 (d, $^1J_{P–P}$ = 191.3 Hz), –22.5 (d, $^1J_{P–P}$ = 191.0 Hz). **^{11}B{^{1}H} NMR** (128 MHz, C_6D_6): δ (ppm) 26.5 (s, br), 19.2 (s, br).

8.2.3 Chapter 4

8.2.3.1 Synthesis of (COD)Ni[P(CO[B])]$_2$ (23)

Compound **1** (40 mg, 0.09 mmol) was added to a solution of bis(cyclooctadiene)nickel(0) (6 mg, 0.02 mmol) in C_6D_6 (0.5 mL). The solution was warmed to 50 °C, darkening in colour from yellow to orange. Volatiles were removed under reduced pressure and the resulting red solid dissolved in hexane. The solution was filtered and concentrated to approximately 0.2 mL. Cooling the solution to –25 °C for a number of days resulted in the formation of red blocks suitable for X-ray diffraction. (20 mg, 89%). **CHN** Anal. Calcd. for $C_{62}H_{84}B_2N_4NiO_2P_2$: C, 70.28%; H, 7.99%; N, 5.29%. Found: C, 70.33%; H, 7.81%; N, 4.84%. **^{1}H NMR** (500 MHz, C_6D_6): δ (ppm) 7.24 (t, $^3J_{H–H}$ = 8 Hz, 4H; ArC*H*), 7.12 (d, $^3J_{H–H}$ = 8 Hz, 8 H; ArC*H*), 5.88 (s, 4H; {(NC*H*)$_2$}), 3.46 (s, 4H; COD {C*H*R}$_2$), 3.13 (sept, $^3J_{H–H}$ = 7 Hz; 8H; {C*H*(CH$_3$)$_2$}), 2.55 (d, $^3J_{H–H}$ = 9 Hz, 2H; COD {C*H*$_2$R$_2$}), 2.02 (d, $^3J_{H–H}$ = 9 Hz, 4H; COD {C*H*$_2$R$_2$}), 1.36 (d, $^3J_{H–H}$ = 7 Hz, 24H; {CH(C*H*$_3$)$_2$}), 1.18 (d, $^3J_{H–H}$ = 7 Hz, 24H; {CH(C*H*$_3$)$_2$}). **^{13}C{^{1}H} NMR** (126 MHz, C_6D_6): δ (ppm) 146.3 (Dipp*C*), 137.6 (Dipp*C*), 127.7 (DippAr*C*H), 123.9 (DippAr*C*H), 117.8 ({(N*C*H)$_2$}), 92.1 (COD {*C*HR}$_2$), 31.2 (COD {*C*H$_2$R$_2$}), 28.8 (COD{*C*H$_2$R$_2$}), 25.4, 24.2. **^{31}P{^{1}H} NMR** (162 MHz, C_6D_6): δ (ppm) 45.7 (s). **^{11}B{^{1}H} NMR** (128 MHz, C_6D_6): δ (ppm) 19.6 (s, br).

8.2.3.2 Synthesis of [W([B]OCP)$_3$(CO)] (24)

Tris(acetonitrile)tricarbonyltungsten(0) (30 mg, 7.7 mmol) was suspended in difluorobenzene (DFB) (1 mL) and [B]OCP **1** (90 mg, 20 mmol, 2.6 eq.) was added. The reaction was vigorously stirred in a glove box overnight, the solution turning from pale yellow to dark red. The solution was filtered to remove excess tris(acetonitrile)tricarbonyltungsten(0) and the solvent removed under reduced pressure. The resulting red oil could be crystallised by evaporation of a concentrated hexane or pentane solution and collection of the crystals from the vessel wall. This process can be repeated

multiple times to yield bright red crystals of [W([B]OCP)$_3$(CO)] **2** (52 mg, 44.8 %). The reaction is quantitative by NMR spectroscopy; the relatively low yield is due to the difficulty crystallizing this species. Analysis was conducted on the isolated crystals, however further reactivity was primarily conducted on the filtrate of the reaction. Ratio of **24a** to **24b** is 1:1. **CHN** Anal. Calcd. for $C_{82}H_{108}B_3N_6O_4P_3W$: C, 63.50%; H, 7.02%; N, 5.42%. Found: C, 65.30%; H, 7.35%; N, 5.76%. **^{1}H NMR** (500 MHz, C_6D_6): δ (ppm) 7.19 (m, 10H, Ar*C*), 7.14 – 6.96 (m, 26H, Ar*C*), 5.98 (s, 2H, **24b**, {(NC*H*)$_2$}), 5.93 (s, 4H, **24b**, {(NC*H*)$_2$}), 5.93 (s, 6H, **24a**, {(NC*H*)$_2$}), 3.31 (sept, $^3J_{H–H}$ = 6.8 Hz, 4H, **24b** {C*H*(CH$_3$)$_2$} Dipp), 3.13 (Overlapping septets, 21H, **24a** and **24b** {C*H*(CH$_3$)$_2$} Dipp), 1.26 (d, $^3J_{H–H}$ = 6.9 Hz, 12H, **24b** {CH(C*H$_3$*)$_2$} Dipp), 1.23 (d, $^3J_{H–H}$ = 6.9 Hz, 12H, **24b** {CH(C*H$_3$*)$_2$} Dipp), 1.20 (d, $^3J_{H–H}$ = 6.9 Hz, 12H, **24a** {CH(C*H$_3$*)$_2$} Dipp), 1.17 (d, $^3J_{H–H}$ = 6.9 Hz, 36H, **24b** {CH(C*H$_3$*)$_2$} Dipp), 1.06 (d, $^3J_{H–H}$ = 6.9, 36H, **24a** {CH(C*H$_3$*)$_2$} Dipp), 1.03 (d, $^3J_{H–H}$ = 6.9 Hz, 12H, **24b** {CH(C*H$_3$*)$_2$} Dipp), 0.96 (d, $^3J_{H–H}$ = 6.9 Hz, 12H, **24b** {CH(C*H$_3$*)$_2$} Dipp). **^{13}C{^{1}H} NMR** (126 MHz, C_6D_6): δ (ppm) 146.2 (**24b** Ar*C*), 146.1 (**24a** Ar*C*), 146.0 (**24b** Ar*C*), 137.9 (**24a** Ar*C*), 137.7 (**24b** Ar*C*), 137.5 (**24b** Ar*C*), 123.3 (**24b** Ar*C*), 123.2 (**24a** Ar*C*), 117.7 (**24b** Ar*C*), 117.4 (**24b** {(N*C*H)$_2$}), 117.3 (**24a** {(N*C*H)$_2$}), 28.6 (**24b** {(N*C*H)$_2$}), 28.5 (methine*C*), 28.4 (methine*C*), 24.5 ({CH(*C*H$_3$)$_2$}), 24.3 ({CH(*C*H$_3$)$_2$}), 24.18 ({CH(*C*H$_3$)$_2$}), 24.0 ({CH(*C*H$_3$)$_2$}), 23.8 ({CH(*C*H$_3$)$_2$}), 23.7 ({CH(*C*H$_3$)$_2$}). **^{31}P{^{1}H} NMR** (162 MHz, C_6D_6): δ (ppm) 244.3 (s, **24b**), 244.2 (s, **24a**), 109.6 (s, **24b**). **^{11}B{^{1}H} NMR** (128 MHz, C_6D_6): δ (ppm) 21.3 (s). **IR** ν = 2064 cm^{-1} (ν_{asym}, C≡O), 1594 cm^{-1} (ν_{asym}, P≡C)

8.2.3.3 Synthesis of [W([B]OCP)$_3$(PMe$_3$)] (25)

To a solution of **24** (100 mg, 22 mmol) in DFB (1 mL) was added trimethylphosphine (20 mg, 263 mmol, 12 eq.). The solution was stirred for an hour; the solvent was removed under vacuum to yield a red oil. Extraction into hexane and crystallization as previously described for **24** yielded red crystals of **25** (53 mg, 51%). The ratio of isomers **25a** to **25b** in solution

was 1:0.36. **CHN**: Anal. Calc. for $C_{84}H_{117}B_3N_6O_3P_4W$: C, 63.09%; H, 7.38%; N, 5.26%. Found: C, 63.88%; H, 7.02%; N, 5.86%. **^{1}H NMR** (500 MHz, C_6D_6): δ (ppm) 7.35–7.17 (m, 9H, Ar*H*), 7.15 – 7.05 (m, 4H, Ar*H*), 6.14 (s, 0.75H, **25b** {(NC*H*)$_2$}), 6.09 (s, 1.5H, **25b** {(NC*H*)$_2$}), 6.07 (s, 6H, **25a** {(NC*H*)$_2$}), 3.58–3.42 (m, 2H, **25b** {C*H*(CH$_3$)$_2$} Dipp), 3.33 (m, 2H, **25b** {C*H*(CH$_3$)$_2$} Dipp), 3.25 (sept, $^3J_{H–H}$ = 6.8 Hz, 12H, **25a** {C*H*(CH$_3$)$_2$} Dipp), 3.15 (sept, $^3J_{H–H}$ = 6.8 Hz, 2H), 1.45–1.30 (m, 22H, **25b** {CH(C*H*$_3$)$_2$}), 1.29 (d, $^3J_{H–H}$ = 6.8 Hz, 36H, **25a** {CH(C*H*$_3$)$_2$}), 1.22 (m, 12H, **25b** {CH(C*H*$_3$)$_2$}), 1.14 (d, $^3J_{H–H}$ = 6.8 Hz, 36H, **25a** {CH(C*H*$_3$)$_2$}), 0.97 (d, $^2J_{H–P}$ = 6.9 Hz, 4H, **25b** PMe$_3$), 0.93 (d, $^2J_{H–P}$ = 12.8 Hz, 9H, **25a** PMe$_3$). **^{13}C{^{1}H} NMR** (126 MHz, C_6D_6): δ (ppm) 146.1 (s, **25b** Ar*C*), 146.1 (**25a** Ar*C*), 145.9 (**25b** Ar*C*), 138.8 (d, $^1J^{C–P}$ = 59.5 Hz, *C*P), 138.6 (**25a** Ar*C*), 138.2 (d, $^1J^{C–P}$ = 67.0 Hz, *C*P), 138.4 (**25b** Ar*C*), 138.1 (**25b** Ar*C*), 123.4 (**25b**, Ar*C*), 123.3 (**25b**, Ar*C*), 123.2 (**25a**, Ar*C*), 123.2 (**25b**, Ar*C*), 123.1 (**25b**, Ar*C*), 117.7 (**25a** {CH(*C*H$_3$)$_2$}), 117.6 (**25a** and **25b** {CH(*C*H$_3$)$_2$}), 28.5 (**25b** {*C*H(CH$_3$)$_2$}), 28.5 (**25a**{*C*H(CH$_3$)$_2$}), 28.4 (**25b** {CH(*C*H$_3$)$_2$}), 25.0 (**25b** {CH(*C*H$_3$)$_2$}), 24.9 (**25a** {CH(*C*H$_3$)$_2$}), 24.9 (**25b** {CH(*C*H$_3$)$_2$}), 24.6 (**25b** {CH(*C*H$_3$)$_2$}), 24.4 (**25b** {CH(*C*H$_3$)$_2$}), 24.1 (**25b** {CH(*C*H$_3$)$_2$}), 23.8 (**25b** {CH(*C*H$_3$)$_2$}), 23.8 (**25b** {CH(*C*H$_3$)$_2$}), 23.5 (**25a** {CH(*C*H$_3$)$_2$}), 23.2 (**25b** {CH(*C*H$_3$)$_2$}), 17.6 (d, $^1J_{C–P}$ = 68.9 Hz, **25a** PMe$_3$), 17.3 (d, $^1J_{C–P}$ = 28.8 Hz, **25b** PMe$_3$). **^{11}B{^{1}H} NMR** (128 MHz, C_6D_6): δ (ppm) 22.0 (s, br). **^{31}P{^{1}H} NMR** (162 MHz, C_6D_6): δ (ppm) 264.8 (**25a**), 264.4 (**25b**), 113.0 (**25b**), 30.74 (impurity), 7.1 (d, $^1J_{W–P}$ = 98.9 Hz, **25a**), 2.7 (d, $^1J_{W–P}$ = 79.4 Hz, **25b**). **IR** ν = 1594 cm^{-1} (ν_{asym}, C≡P).

8.2.3.4 Synthesis of [W([B]OCP)$_3$(^{t}BuNC)] (26)

To a solution of **24** (100 mg, 22 mmol) in difluorobenzene (1 mL) was added ^{t}BuNC (35 mg, 42 mmol, 2eq). The work up is analogous to compound **25**. (64 mg, 62%). Ratio of **26a** to **26b** in solution is approximately 1:1. **CHN** Anal. Calc. for $C_{86}H_{117}B_3N_7O_3P_3W$: C, 64.31%; H, 7.34%; N, 6.10%. Found: C, 64.12%; H, 7.52%; N, 6.15%. **^{1}H NMR** (500 MHz, C_6D_6):

δ (ppm) 7.26–7.11 (m, 8H, Ar*H*), 7.11–7.00 (m, 25H, Ar*H*), 6.04 (s, 1.9H, impurity), 5.99 (s, 1.8H, **26b** {(NC*H*)$_2$}), 5.95 (s, 3.4H, **26b** {(NC*H*)$_2$}), 5.93 (s, 6H, **26a** {(NC*H*)$_2$}), 3.55–3.39 (sept, $^3J_{H–H}$ = 6.8 Hz, 4H, **26b** {C*H*(CH$_3$)$_2$}), 3.21 (m, 12H, **26a** and **26b** {C*H*(CH$_3$)$_2$}), 3.11 (sept, $^3J_{H–H}$ = 6.8 Hz, 4H, **26b** {C*H*(CH$_3$)$_2$}), 2.99 (sept, $^3J_{H–H}$ = 6.9 Hz, 4H, {C*H*(CH$_3$)$_2$}), 1.64 (s, impurity), 1.42–0.78 (m, Dipp), 0.59 (s, 9H, ^{t}BuNC, **26b**), 0.30 (s, 8H, ^{t}BuNC, **26a**). **^{13}C{^{1}H} NMR** (126 MHz, C$_6$D$_6$): δ (ppm) 198.1 (s, **26a**, ^{t}BuN*C*), 194.5 (**26b**, ^{t}BuN*C*), 146.4 (**26a**, Ar*C*), 146.1 (**26b**, Ar*C*), 146.0 (**26b,** Ar*C*), 145.5 (**26b**, Ar*C*), 139.1 (**26a**, Ar*C*), 138.7 (**26b**, Ar*C*), 138.0 (**26b**, Ar*C*), 137.4 (d, $^1J_{C–P}$ = 13.7 Hz, *C*P), 136.2 (**26b**, Ar*C*), 123.6 (**26a**, Ar*C*), 123.5 (**26b**, Ar*C*), 123.3 (**26a**, Ar*C*), 123.2 (**26b**, Ar*C*), 123.2 (**26b**, Ar*C*), 120.5 (**26b**, Ar*C*), 117.7 (**26b**, {CH(*C*H$_3$)$_2$}), 117.5 (**26a**, {CH(*C*H$_3$)$_2$}), 117.4 (**26b**, {CH(*C*H$_3$)$_2$}), 57.0 (**26b**, ^{t}BuNC), 56.4 (**26b**, ^{t}BuNC), 31.6 (**26a**, {*C*H(CH$_3$)$_2$}), 29.8 (**26b**, {*C*H(CH$_3$)$_2$}), 28.5 (**26b**, {*C*H(CH$_3$)$_2$}), 28.4 (**26a**, {*C*H(CH$_3$)$_2$}), 24.7 (**26b,** {CH(*C*H$_3$)$_2$}), 24.5 (**26b,** {CH(*C*H$_3$)$_2$}), 24.4 (**26b,** {CH(*C*H$_3$)$_2$}), 24.4 (**26b,** {CH(*C*H$_3$)$_2$}), 24.3 (**26a,** {CH(*C*H$_3$)$_2$}), 24.2 (**26a,** {CH(*C*H$_3$)$_2$}), 23. 9 (**26b**, ^{t}BuNC), 23.7 (**26a**, ^{t}BuNC). **^{11}B{^{1}H} NMR** (128 MHz, C$_6$D$_6$): δ (ppm) 22.2, 14.9. **^{31}P{^{1}H} NMR** (162 MHz, C$_6$D$_6$): δ (ppm) 256.0 (s, **26b**), 253.6 (s, **26a**), 116.6 (s, **26b**), 28.0 (impurity). **IR** ν = 1594 cm^{-1} (ν_{asym}, C≡P)

8.2.3.5 Synthesis of {[B]OCHP(BBN)}$_2$ (27)

To a solution of **1** (30 mg, 6.6 mmol) in toluene 9-borabicyclo(3.3.1)nonane (16.4 mg, 13 mmol) was added. The solution was heated to 60 °C overnight before removal of the solvent under reduced pressure. The orange oil was taken up into hexane and concentrated. Storage at –35 °C overnight resulted in crystals of **27**. However, the NMR of these crystals was not spectroscopically pure, containing significant amounts of the proposed intermediate **27i**. **^{1}H NMR** (500 MHz, C$_6$D$_6$): δ (ppm) 7.30 – 7.08 (m, ArC*H*), 6.09 (s, {(NC*H*)$_2$} **27i**), 6.03 (s, {(NC*H*)$_2$}**27i**), 5.94 (s, {(NC*H*)$_2$}, **27**), 3.34 (m, {C*H*(CH$_3$)$_2$}), 2.2 – 0.6 (m, {CH(C*H*$_3$)$_2$}).

$^{31}P\{^{1}H\}$ NMR (162 MHz, C_6D_6): δ (ppm) –38.2 (s), –39.4 (s) (*cis* and *trans* isomers). **$^{11}B\{^{1}H\}$ NMR** (128 MHz, C_6D_6): δ (ppm) 29.3 (shoulder, BBN), 21.2 (br, [B]).

8.2.3.6 Synthesis of ([B]O){$(C_6F_5)_2$B}C=P(C_6F_5) (28)

Tris(pentaflourophenyl)borane (110 mg, 22 mmol) was added to a solution of [B]OCP (100 mg, 22 mmol) in toluene (3 mL). The solution immediately changed colour from pale yellow to red. Immediate removal of the solvent, followed by extraction in hexane (2 mL) and cooling to –35 °C overnight yielded red crystals of **1** suitable for single crystal X–ray diffraction. NMR studies of the crystals revealed a mixture of compounds **1** and **2**. Partial NMR data for **28** was obtained from the reaction mixture, with ~10% of [B]OCP present. Given the propensity for **28** to isomerize to **29** in solution, a compositionally pure sample of this compound could not be isolated. **^{1}H NMR** (400 MHz, C_6D_6): δ (ppm) 7.33–7.26 (m, 2H; *para*-Ar*H*), 7.15 (m, 4H; *meta*-Ar*H*), 6.17 (s, 2H; {(NC*H*)$_2$}), 3.33 (sept, $^{3}J_{H–H}$ = 6.5 Hz, 4H; {C*H*(CH_3)$_2$}), 1.27 (d, $^{3}J_{H–H}$ = 6.9 Hz, 12H; {CH(C*H*$_3$)$_2$}), 1.19 (d, $^{3}J_{H–H}$ =6.8 Hz, 12H;{CH(C*H*$_3$)$_2$}). **$^{31}P\{^{1}H\}$ NMR** (162 MHz, C_6D_6): δ (ppm) 174.0 (s). **$^{11}B\{^{1}H\}$ NMR** (128 MHz, C_6D_6): δ (ppm) 21.4 (s, br). **$^{19}F\{^{1}H\}$ NMR** (376 MHz, C_6D_6): δ (ppm) –125.8 (d, $^{3}J_{F–F}$ = 24.5 Hz, 2F, *ortho*-P(C_6F_5)), –126.2 (d, $^{3}J_{F–F}$ = 20.0 Hz, 4F, *ortho*-B(C_6F_5)$_2$), –144.4 (tt, $^{3}J_{F–F}$ = 20.7 Hz, $^{4}J_{F–F}$ = 5.8 Hz, 2F, *para*-B(C_6F_5)$_2$), –150.6 (t, $^{3}J_{F–F}$ = 20.5 Hz, 1F, *para*-P(C_6F_5)), –160.3 to –160.7 (m, 6F; *meta*-B(C_6F_5)$_2$ and *meta*-P(C_6F_5)).

8.2.3.7 Synthesis of [B]OP=C(C_6H_5){B(C_6F_5)$_2$} (29)

Tris(pentaflourophenyl)borane (110 mg, 22 mmol) was added to a solution of [B]OCP (100 mg, 22 mmol) in toluene (3 mL). The solution immediately changed colour from pale yellow to red. The solution was stirred for 24 hours at room temperature. The solvent was removed and the resulting red residue was extracted in hexane (5 mL) and filtered to afford an orange solution which was concentrated and cooled to –35 °C. After 7 days yellow crystals of **29** formed (148 mg, 70.5 % yield). Crystallization from toluene afforded a different solvate,

29·0.5tol. **CHN** Anal. Calcd. for $C_{45}H_{36}B_2F_{15}N_2OP$: C, 56.40%; H, 3.79%; N, 2.92%; **Found**: C, 56.32%; H, 3.84%; N, 3.16%. **^{1}H NMR** (400 MHz, C_6D_6): δ (ppm) 7.22 (t, $^3J_{H–H}$ = 7.7 Hz, 2H; *para*-Ar*H*), 7.00 (d, $^3J_{H–H}$ = 7.8 Hz, 4H; *meta*-Ar*H*), 5.83 (s, 2H; {(NC*H*)$_2$}), 2.93 (sept, $^3J_{H–H}$ = 6.9 Hz, 4H; {C*H*(CH$_3$)$_2$}), 1.07 (d, $^3J_{H–H}$ = 6.9 Hz, 4.4 Hz, 12H; {CH(C*H*$_3$)$_2$}), 1.05 (d, $^3J_{H–H}$ = 6.9 Hz, 4.4 Hz, 12H; {CH(C*H*$_3$)$_2$}). **^{31}P{^{1}H} NMR** (162 MHz, C_6D_6): δ (ppm) 401.9 (s). **^{13}C{^{1}H} NMR** (126 MHz, C_6D_6): δ (ppm) 155.7 (d, $^1J_{C–P}$ = 68.2 Hz; *C*P), 147.2 (C_6F_5), 145.9 (Ar*C*), 145.3 (C_6F_5), 142.5 (C_6F_5), 140.5 (C_6F_5), 138.2 (C_6F_5), 136.2 (C_6F_5), 135.4 (Ar*C*), 128.2 (Ar*C*), 123.5 (Ar*C*), 117.7 (C_6F_5), 117.1 ({(N*C*H)$_2$}), 111.9 (C_6F_5), 28.4 ({*C*H(CH$_3$)$_2$}), 23.9 ({CH(*C*H$_3$)$_2$}), 23.0 ({CH(*C*H$_3$)$_2$}). **^{11}B{^{1}H} NMR** (128 MHz, C_6D_6): δ (ppm) 21.1 (s, br). **^{19}F{^{1}H} NMR** (376 MHz, C_6D_6): δ (ppm) –129.7 (br s, 1F; *ortho*-P(C_6F_5)), –130.8 (br s, 1F; *ortho*-P(C_6F_5)), –138.5 (d, $^3J_{F–F}$ = 21.0 Hz, 4F; *ortho*-B(C_6F_5)$_2$), –146.8 (br s, 1F; *para*-P(C_6F_5)), –151.0 (br s), –155.5 (t, $^3J_{F–F}$ = 21.5 Hz, 2F; *para*-B(C_6F_5)$_2$), –159.4 to –162.6 (m, 6F; *meta*-B(C_6F_5)$_2$ and *meta*-(C_6F_5)).

8.2.3.8 Synthesis of ([B]O){(C_6F_5)$_2$B(PMe$_3$)}C=P(C_6F_5) (30)

Tris(pentaflourophenyl)borane (28 mg, 6 mmol) was added to a solution of [B]OCP (25 mg, 6 mmol) in toluene (1 mL). The solution immediately changed colour from pale yellow to red. Addition of trimethylphosphine (1 M in toluene, 0.1 mL, 10 mmol) resulted in the immediate colour change from red to pale yellow. Excess trimethylphosphine and toluene were removed under reduced pressure and the resulting pale yellow powder extracted into hexane. The eluent was filtered and cooled to –35 °C overnight to yield pale yellow crystals of **30** (29 mg, 54.7%). **CHN** Anal. Calcd. for $C_{48}H_{45}B_2F_{15}N_2OP_2$: C, 55.73%; H, 4.38%; N, 2.71%. Found: C, 56.53%; H, 4.73%; N, 2.71%. **^{1}H NMR** (400 MHz, C_6D_6): δ (ppm) 7.37–7.28 (m, 2H; *para*-Ar*H*), 7.18 (s, 4H; *meta*-Ar*H*), 6.11 (s, 2H; {(NC*H*)$_2$}), 3.49 (sept, $^3J_{H–H}$ = 6.4 Hz, 4H; {C*H*(CH$_3$)$_2$}), 1.25 (d, $^3J_{H–H}$ = 6.8 Hz, 12H; {CH(C*H*$_3$)$_2$}), 1.19 (d, $^3J_{H–H}$ = 6.8 Hz, 12H; {CH(C*H*$_3$)$_2$}), 0.41 (d, $^2J_{P–H}$ =11.2 Hz, 9H; PMe$_3$). **^{13}C{^{1}H} NMR** (126 MHz,

C_6D_6): δ (ppm) 149.5 (s, C_6F_5), 147.6 (C_6F_5), 146.6 (Ar*C*), 144.7 (C_6F_5), 141.2 (C_6F_5), 139.2 (C_6F_5), 138.4 (Ar*C*), 136.3 (C_6F_5), 124.2 (Ar*C*), 119.7 ({(N*C*H)$_2$}), 28.9 ({*C*H(CH$_3$)$_2$}), 26.4 ({CH(*C*H$_3$)$_2$}), 23.2 ({CH(*C*H$_3$)$_2$}), 11.0 (d, $^1J_{C-P}$ = 38.2 Hz, P(*C*H$_3$)$_3$). *B*C*(OR)P and *ipso* ArC not found. **^{31}P{^{1}H} NMR** (162 MHz, C_6D_6): δ (ppm) 145.4 (d, $^3J_{P-P}$ = 14.7 Hz; *P*=C), –10.7 (s, br, PMe_3). **^{11}B{^{1}H} NMR** (128 MHz, C_6D_6): δ (ppm) 23.2 (br s), –13.0 (s, {(PMe_3)B(C_6F_5)$_2$}). **^{19}F{^{1}H} NMR** (376 MHz, C_6D_6): δ (ppm) –152.6 (t, $^3J_{F-F}$ = 20.7 Hz; *ortho*-(C_6F_5)), –156.0 (t, $^3J_{F-F}$ = 20.2 Hz, *para*-(C_6F_5)), –161.6 (br s; *meta*-(C_6F_5)). Note: Integrations omitted due to significant broadening in the spectra.

8.2.3.9 Synthesis of (C$_6$F$_5$)P=C[B]{OB(C$_6$F$_5$)$_2$} (31)

Tris(pentaflourophenyl)borane (110 mg, 22 mmol) was added to a solution of [B]PCO (100 mg, 22 mmol) in toluene (3 mL). The solution darkened in colour. Removal of the solvent under a dynamic vacuum yielded a yellow powder. The solid was dissolved in hexane (5 mL), filtered and concentrated. Cooling the orange solution to –35 °C for 5 days resulted in yellow crystals of **4** (142 mg, 67.6 % yield). **CHN** Anal. Calcd. for $C_{45}H_{36}B_2F_{15}N_2OP$: C, 56.40%; H, 3.79%; N, 2.92%; Found: C, 57.06%; H, 3.71%; N, 3.80%. **^{1}H NMR** (500 MHz, C_6D_6): δ (ppm) 6.99–6.79 (m, 6H; Ar*H*), 6.19 (s, 2H; {(NC*H*)$_2$}), 3.20 (sept, $^3J_{H-H}$ = 6.6 Hz, 4H; {C*H*(CH$_3$)$_2$}), 1.33 (d, $^3J_{H-H}$ = 6.8 Hz, 12H; {CH(C*H*$_3$)$_2$}), 1.12 (d, $^3J_{H-H}$ = 6.8 Hz, 12H; {CH(C*H*$_3$)$_2$}). **^{13}C{^{1}H} NMR** (126 MHz, C_6D_6): δ (ppm) 202.3 (d, poorly resolved, $^1J_{C-P}$ = 76 Hz, [B]*C*), 148.9 (*C*$_6$F$_5$), 147.0 (*C*$_6$F$_5$), 146.3 (*C*$_6$F$_5$), 145.4 (Ar*C*), 144.4 (*C*$_6$F$_5$), 143.0(*C*$_6$F$_5$), 142.5 (*C*$_6$F$_5$), 140.9 (*C*$_6$F$_5$), 138.6 (Ar*C*), 138.3 (*C*$_6$F$_5$), 136.3 (*C*$_6$F$_5$), 123.6 (Ar*C*), 121.0 (Ar*C*), 109.2 (C_6F_5), 108.7 (C_6F_5), 107.5 (C_6F_5), 28.4 ({*C*H(CH$_3$)$_2$}), 25.8 ({CH(*C*H$_3$)$_2$}), 22.4 ({CH(*C*H$_3$)$_2$}). **^{31}P{^{1}H} NMR** (162 MHz, C_6D_6): δ (ppm) 142.2. **^{11}B{^{1}H} NMR** (128 MHz, C_6D_6): δ (ppm) 22.4 (br s). **^{19}F{^{1}H} NMR** (376 MHz, C_6D_6): δ (ppm) –128.5 (s, br weak), –147.2 (s, br), –151.1 (t, $^3J_{F-F}$ = 20.7 Hz), –160.8 (s, br), –161.2

(s, br). Note: Integrations and assignment omitted due to significant broadening in the spectra.

8.2.4 Chapter 5

8.2.4.1 Synthesis of 32

A solution of [B]OCP (35 mg, 7 mmol) was cooled to –78 °C. The solution was transferred by cannula into a pre-cooled schlenk containing a sodium mirror. The solution was stirred for an hour at –78 °C before being allowed to warm to room temperature overnight. The dark red solution was filtered and the volatiles removed under reduced pressure. The resultant red oil was extracted with hexane (2 mL) and filtered again, before being concentrated to *ca.* 0.5 mL and stored at –35°C. X-ray quality crystals grew over the course of a week. **^{1}H NMR** (400 MHz, C_6D_6): δ (ppm) 7.25 (m, 6H, Dipp Ar*H*), 7.09 – 6.85 (m, 6H, Dipp Ar*H*), 6.33 (s, 2H, {(NC*H*)$_2$}), 5.98 (s, 2H, {(NC*H*)$_2$}), 3.99 (sept, $^{3}J_{H–H}$ = 6.8 Hz, 4H, {C*H*(CH$_3$)$_2$}), 3.15 (sept, $^{3}J_{H–H}$ = 6.9 Hz, 4H, {C*H*(CH$_3$)$_2$}), 1.36 (d, $^{3}J_{H–H}$ = 6.8 Hz, 6H, {CH(C*H*$_3$)$_2$}), 1.29 (d, $^{3}J_{H–H}$ = 6.8 Hz, 6H, {CH(C*H*$_3$)$_2$}), 1.11 (d, $^{3}J_{H–H}$ = 7.0 Hz, 6H, {CH(C*H*$_3$)$_2$}), 1.01 (d, $^{3}J_{H–H}$ = 6.8 Hz, 6H, {CH(C*H*$_3$)$_2$}). **^{31}P{^{1}H} NMR** (162 MHz, C_6D_6): δ (ppm) 120.4 (s). **^{11}B{^{1}H} NMR** (128 MHz, C_6D_6): δ (ppm) 19.4 (s).

8.2.4.2 Synthesis of [^{Mes}Mg]O[B] (33) and [^{Mes}Mg]$_5$[C$_2$P$_2$][CP] (34)

An equimolar amount of [B]OCP in toluene was added to a suspension of [^{Mes}NacnacMg]$_2$ at –78.0 °C. The solution turned bright red and was allowed to warm slowly to room temperature. The volatiles were removed at reduced pressure and the resultant red oil extracted with hexane (3 mL). The filtrate was concentrated to *ca.* 0.5 mL and cooled at –35°C. Colourless crystals of **33** of X-ray quality had formed overnight. **^{1}H NMR** (500 MHz, C_6D_6): δ (ppm) 7.23 – 7.17 (m, 2H, Dipp *para*-Ar*H*), 7.10 (d, $^{3}J_{H–H}$ = 7.6 Hz, 4H, Dipp *meta*-Ar*H*), 6.67 (s, 4H, Mes Ar*H*), 5.92 (s, 2H, {(NC*H*)$_2$}), 4.73 (s, 1H, β-Diketiminate C*H*), 3.39

(sept, $^{3}J_{H–H}$ = 6.9, 4H, {C*H*(CH_3)$_2$}), 2.25 (s, 9H, β-Diketiminate C*H*$_3$), 1.79 (s, 12H, Mes C*H*$_3$), 1.38 (s, 6H, Mes C*H*$_3$), 1.22 (d, $^{3}J_{H–H}$ = 6.9 Hz, 12H, {CH(C*H*$_3$)$_2$}), 1.00 (d, $^{3}J_{H–H}$ = 6.9 Hz, 12H, {CH(C*H*$_3$)$_2$}). **^{13}C{^{1}H} NMR** (126 MHz, C_6D_6): δ (ppm) 170.2 (s, Ar*C*), 146.3 (s, Ar*C*), 143.5 (Ar*C*), 140.7 (Ar*C*), 133.11 (Ar*C*), 130.5 (Ar*C*), 129.6 (Ar*C*), 125.7 (Ar*C*), 122.8 ({(N*C*H)$_2$}), 115.0 (β-Diketiminate *C*H), 95.4 (β-Diketiminate *C*R$_2$), 28.1 (methyl*C* Mes), 23.6 (methyl*C* Mes), 23.6 (methine*C* Dipp), 22.7 (β-Diketiminate C*H*$_3$), 20.7 (methyl*C* Dipp), 17.7 (methyl*C* Dipp).

The remaining red oil was dissolved in toluene and concentrated to ca. 0.2 mL and placed in the freezer at –35°C. Colourless crystals of **34** formed over a few weeks. However, these thin places diffracted poorly at high angle, resulting in poor quality X-ray data. Recrystallization from toluene did not improve crystal quality. **^{1}H NMR** (400 MHz, C_6D_6): δ (ppm) 7.15 – 6.85 (m, 10H, Mes Ar*H*), 6.74 (s, 6H, Mes Ar*H*)), 6.58 (s, 4H, Mes Ar*H*), 5.17 (s, 1H, β-Diketiminate C*H*), 5.02 (s, 1H, β-Diketiminate C*H*), 4.80 (s, 1H, β-Diketiminate C*H*), 4.64 (s, 1H, β-Diketiminate C*H*), 3.95 (s, 1H, β-Diketiminate C*H*), 2.68 (s, 6H, s, β-Diketiminate C*H*$_3$), 2.47 (s, 6H, s, β-Diketiminate C*H*$_3$), 2.33 (S, 6H, s, β-Diketiminate C*H*$_3$), 2.24 (6H, s, β-Diketiminate C*H*$_3$), 2.11 (s, 6H, s, β-Diketiminate C*H*$_3$), 2.05 (s, 12H, Mes C*H*$_3$), 1.89 (s, 6H, s, β-Diketiminate C*H*$_3$), 1.82, 1.71 (s, 6H, s, β-Diketiminate C*H*$_3$). *It not possible to distinguish between 6H, s, β-Diketiminate back bone methyl groups and methyl groups on the mesityl ligand due to significant overlap. **^{31}P{^{1}H} NMR** (162 MHz, C_6D_6): δ (ppm) 566.2 (d, $^{2}J_{P–P}$ = 112.0 Hz), 311.1 (d, $^{2}J_{P–P}$ =112.0 Hz), 296.0.

8.2.4.3 Synthesis of [{(MesNacnac)Mg}2{cyclo-P$_2$C$_2$(^{t}Bu)$_2$}] (35)

A solution of tBuCP (21 mg, 0.210 mmol) in toluene (1 mL) was added to a suspension of [^{Mes}NacnacMg]$_2$ (70 mg, 0.102 mmol) in toluene (1 mL) at room temperature. The solution immediately darkens to red. The reaction mixture was stirred overnight, filtered and

concentrated to ~1 mL. Cooling the dark red solution to –35 °C overnight yielded pale orange crystals of **35** (48 mg, 53%). The compound was stable in the solid state over a period of weeks, however in solutions of toluene decomposes over days and in THF minutes. Elemental analysis calcd. for $C_{56}H_{76}Mg_2N_4P_2$: C, 73.44; H, 8.37; N, 6.12. Found: C, 72.91; H, 8.21; N, 6.02. **^{1}H NMR** (500 MHz, C_6D_6): δ (ppm) 6.85 (s, 8H, Ar*H*), 4.82 (s, 2H, NCC*H*), 2.26 (s, 12H, Mes *para*-CH_3), 2.25 (s, 24H, Mes *ortho*-CH_3), 1.57 (s, 12H, NCCH_3), 1.22 (s, 18H, *tBu*-CH_3). **^{13}C{^{1}H} NMR** (126 MHz, C_6D_6): δ (ppm) 168.8 (s, N*C*CH$_3$), 145.4 (Ar*C*), 138.1 (t, $^1J_{C\text{-}P}$ = 54.8 Hz, {C_2P_2}), 132.8 (Ar*C*), 132.0 (Ar*C*), 128.9 (Ar*C*), 94.6 (NC*C*H$_3$), 36.3 (*t*Bu*C*CH$_3$), 32.0 (*t*BuC*C*H$_3$), 23.8 (NC*C*H$_3$), 20.7 (Ar*C*H$_3$), 19.9 (Ar*C*H$_3$). **^{31}P{^{1}H} NMR** (162 MHz, C_6D6): δ (ppm) 202.3 (s).

In situ reaction monitoring indicates the presence of two intermediates by ^{31}P NMR spectroscopy, a singlet resonance at 345.9 ppm and an AB spin system with doublets at 382.4 and 287.1 ($J_{P–P}$ = 304 Hz) ppm. When the reaction is conducted at high concentrations colourless crystals form on the walls of the NMR tube. The crystal structure revealed one of the intermediates to be 8-membered heterocycle **36**.

8.2.4.4 Synthesis of [KOC[B]PN(SiMe$_3$)] (37)

Potassium bis(trimethylsilyl)amide (KHMDS) (10 mg, 0.05 mmol) was added to [B]OCP (23 mg, 0.05 mmol) in toluene (0.5 mL). The reaction was left overnight, by which time complete consumption of the starting material was observed by NMR spectroscopy. **^{1}H NMR** (400 MHz, C_6D_6): δ (ppm) 7.21 (m, 6H, Dipp Ar*H*), 6.10 (s, 2H, {(NC*H*)$_2$}), 3.42 (sept, $^3J_{H–H}$ = 6.6 Hz, 4H, {C*H*(CH$_3$)$_2$}), 1.36 (d, $^3J_{H–H}$ = 6.8 Hz, 12H, {CH(C*H*$_3$)$_2$}), 1.24 (d, $^3J_{H–H}$ = 6.8 Hz, 12H, {CH(C*H*$_3$)$_2$}), 0.14 (s, 18H, (Si(C*H*$_3$)$_3$)). **^{31}P{^{1}H} NMR** (162 MHz, C_6D_6): δ (ppm) 154.9 (s). **^{11}B{^{1}H} NMR** (128 MHz, C_6D_6): δ (ppm) 24.3 (s).

8.2.4.5 Synthesis of [K[B]PCN] (38)

Potassium bis(trimethylsilyl)amide (KHMDS) (10 mg, 0.05 mmol) was added to [B]OCP (23 mg, 0.05 mmol) in toluene (0.5 mL). The reaction was heated to 60°C for 2 hours, at which time complete consumption of **37** was observed by NMR spectroscopy. The solvent was removed under reduced pressure and the resultant orange solid taken up into hexane. The hexane was filtered and concentrated to *ca.* 0.5 mL. Crystals grew out of the hexane solution overnight (15 mg, 81.7%). **^{31}P{^{1}H} NMR** (162 MHz, C_6D_6): δ (ppm) –258.9 (s).

8.2.4.6 Synthesis of [KOC[B]PP(SiMe$_3$)] (39)

Potassium bis(trimethylsilyl)phosphide (11 mg, 0.05 mmol) was added to [B]OCP (23 mg, 0.05 mmol) in toluene (0.5 mL). The reaction was left overnight, by which time complete consumption of the starting material was observed by NMR spectroscopy. **^{31}P{^{1}H} NMR** (162 MHz, None): δ (ppm) 317.6 (d, $^{1}J_{P–P}$ = 405.5 Hz [KOC[B]*P*P(SiMe$_3$)]), –71.8 (d, $^{1}J_{P–P}$ = 404.3 Hz, [KOC[B]P*P*(SiMe$_3$)]).

8.2.5 Chapter 6

8.2.5.1 Synthesis of [Ga](I)L (40a–c)

The gallium iodides were made in one pot syntheses adapted from Fedshkin's original synthesis of **40a**.[9] Note: These compounds are extremely oxygen sensitive and require careful handling, in particular during filtration and crystallisation steps.

General procedure: Dipp-BIAN (0.5g, 1.0 mmol) was dissolved in toluene in an ampoule with an excess of gallium metal. The ampoule was sealed under vacuum, and heated to 130 °C overnight. The solution turns from orange to deep blue. The solution was cooled to room temperature and iodine (0.13 g, 0.5 mmol) was added with rapid stirring. The solution was stirred for two hours, turning brick red in colour. Volatiles were removed under reduced pressure, and the resulting red powder dissolved in pyridine (20 mL). Heating this suspension

to reflux causes the colour to turn bright blue. The remaining synthesis depends on the derivative (**a–c**):

40a: Volatiles were removed and the resulting blue powder crystallized by cooling a concentrated toluene solution (yields 40–65 %).

NMR characterisation can be found in the original publication.[9]

40b: Volatiles were removed and the blue powder redissolved in toluene, followed by the addition of 1,3-diisopropyl-4,5-dimethyl-1H-imidazol-3-ium-2-ide (^{iPr}NHC) (0.18 g, 1.0 mmol). The solution changed colour from blue to green. Concentration of the solution and cooling resulted in formation of analytically pure green powders of **40b** (typical yields 40–50%).

Alternatively route to **40b** from **40a**: To a solution of (dipp-Bian)GaI(pyr) (200 mg, 0.26 mmol) in toluene (10 mL) was added 1,3-diisopropyl-4,5-dimethylimidazole (46 mg, 0.26 mmol) and an immediate colour change from blue to green was observed. The reaction mixture was stirred overnight and the solvent removed. The green solid was extracted in toluene and filtered. The filtrate was concentrated and placed in the freezer to yield (dipp-Bian)GaI(NHC) as an emerald green crystalline powder (120 mg, 52.6 %). **CHN** Anal. Calcd. for $C_{47}H_{61}Ga_IN_4$: C, 64.25; H, 7.00; N, 6.38. Found: C, 65.21; H, 7.21; N, 6.49. **^{1}H NMR** (500 MHz, C_6D_6): δ (ppm) 7.36 (dd, $^3J_{H–H}$ = 7.6 Hz, 1.6, 2H, Ar*H*), 7.27 (t, $^3J_{H–H}$ = 7.6 Hz, 2H), 7.22 (dd, $^3J_{H–H}$ = 7.6 Hz, 1.6, 2H, Ar*H*), 7.14 – 7.10 (m, 2H, Ar*H*), 6.88 (dd, $^3J_{H–H}$ =8.2 Hz, 7.0, 2H, Ar*H*), 6.20 (d, $^3J_{H–H}$ =6.9 Hz, 2H, Ar*H*), 4.89 (sept, $^3J_{H–H}$ = 6.8 Hz, 2H, {C*H*$(CH_3)_2$}), 4.26 (sept, $^3J_{H–H}$ = 6.9 Hz, 2H, {C*H*$(CH_3)_2$}), 3.82 (sept, $^3J_{H–H}$ =6.9 Hz, 2H, {C*H*$(CH_3)_2$}), 1.55 (d, $^3J_{H–H}$ =6.9 Hz, 6H, {CH(C*H*$_3)_2$}), 1.42 (d, $^3J_{H–H}$ = 6.7 Hz, 6H, {CH(C*H*$_3)_2$}), 1.23 (s, 6H, NHC {CH(C*H*$_3)_2$}), 1.08 (dd, $^3J_{H–H}$ = 15.9 Hz, 6.9, 14H, {CH(C*H*$_3)_2$}), 0.92 (d, $^3J_{H–H}$ = 6.7 Hz, 12H, {CH(C*H*$_3)_2$}). **^{13}C{^{1}H} NMR** (126 MHz, C_6D_6): δ (ppm) 148.9 (s, Ar*C*), 148.2 (Ar*C*), 145.8 (Ar*C*), 136.2 (Ar*C*), 134.3 (Ar*C*), 127.5 (Ar*C*),

127.1 (Ar*C*), 125.8 (Ar*C*), 124.7 (Ar*C*), 124.3 (Ar*C*), 123.8 (Ar*C*), 118.5 (NHC N,N-*C*), 54.8 (NHC), 29.8 (DIPP methine*C*), 28.0 (DIPP methine*C*), 26.3 (DIPP methyl*C*), 26.0 (DIPP methyl*C*), 24.7 (DIPP methyl*C*), 24.1 (DIPP methyl*C*), 21.8 (NHC backbone methyl), 9.9 (NHC DIPP methyl*C*).

40c: Volatiles were removed and the blue powder dissolved in toluene, followed by the addition of IMes (0.30 g, 1.0 mmol) resulting in a colour change from blue to green. Concentration of the toluene solution and cooling resulted in precipitation of **40c** (typical yields ranging from 30–40%). **CHN** Anal. Calcd. for $C_{63}H_{76}Ga_IN_4$: C, 69.68; H, 7.05; N, 5.16. Found: C, 69.10; H, 6.61; N, 5.65. **^{1}H NMR** (500 MHz, C_6D_6): δ (ppm) 7.37 (d, $^3J_{H–H}$ = 9.3 Hz, 2H, Ar*H*), 7.27 (t, $^3J_{H–H}$ = 7.6 Hz, 2H, Ar*H*), 7.19 (d, $^3J_{H–H}$ = 9.5 Hz, 2H, Ar*H*), 7.02 (dd, $^3J_{H–H}$ = 14.3 Hz, 7.8 Hz, 5H), 6.93 (d, $^3J_{H–H}$ = 14.5, 2H, Ar*H*), 6.83 (t, $^3J_{H–H}$ = 7.6 Hz, 2H, $^3J_{H–H}$), 6.65 (d, $^3J_{H–H}$ = 17.4 Hz, 4H, Ar*H*), 6.44 (s, 2H), 6.28 (d, $^3J_{H–H}$ = 6.9 Hz, 2H), 6.24 (s, 1H, abnormal NHC C*H*), 4.64 (sept, $^3J_{H–H}$ = 6.8 Hz, 2H, {C*H*(CH_3)$_2$}), 3.96 (sept, $^3J_{H–H}$ = 6.8 Hz, 2H, {C*H*(CH_3)$_2$}), 2.14 – 2.09 (m, 9H, MesC*H*$_3$), 1.94 (s, 3H, MesC*H*$_3$), 1.76 (s, 6H, MesC*H*$_3$), 1.58 (s, 6H, MesC*H*$_3$), 1.54 (s, 6H, MesC*H*$_3$), 1.40 (d, $^3J_{H–H}$ = 6.7, 6H, {CH(C*H*$_3$)$_2$}), 1.34 (d, $^3J_{H–H}$ = 6.7, 6H, {CH(C*H*$_3$)$_2$}), 1.19 (d, $^3J_{H–H}$ = 6.7, 6H, {CH(C*H*$_3$)$_2$}), 1.13 (d, $^3J_{H–H}$ = 7.0, 6H, {CH(C*H*$_3$)$_2$}). **^{13}C{^{1}H} NMR** (126 MHz, C_6D_6): δ (ppm) 148.4 (s, Ar*C*), 146.7 (Ar*C*), 145.9 (Ar*C*), 140.4 (Ar*C*), 139.2 (Ar*C*), 137.7 (Ar*C*), 137.5 (Ar*C*), 137.4 (Ar*C*), 136.8 (Ar*C*), 135.4 (Ar*C*), 134.8 (Ar*C*), 133.5 (Ar*C*), 132.0 (Ar*C*), 130.6 (Ar*C*), 129.6 (Ar*C*), 129.4 (Ar*C*), 129.2 (Ar*C*), 129.0 (Ar*C*), 128.7 (Ar*C*), 126.8 (Ar*C*), 125.3 (Ar*C*), 124.4 (Ar*C*), 124.2 (Ar*C*), 123.2 (Ar*C*), 122.9 (Ar*C*), 120.3 (NHC *C*Ga), 117.43 (NHC backbone), 28.3 ({*C*H(CH_3)$_2$}), 28.0 (({*C*H(CH_3)$_2$})), 26.1 (C*H*$_3$), 25.2 (C*H*$_3$), 24.8 (C*H*$_3$), 21.1 (C*H*$_3$), 20.7 (C*H*$_3$), 20.7 (C*H*$_3$), 20.56 (C*H*$_3$), 17.8 (C*H*$_3$), 17.3 (C*H*$_3$), 16.7 (C*H*$_3$).

8.2.5.2 Synthesis of [Ga](Pyr)(PCO) (41a)

To a solution of (dpp-Bian)GaI(Pyr) (100 mg, 0.13 mmol) in toluene (2 mL) Na(dioxane)$_{0.6}$[PCO] (21 mg, 0.16 mmol) was added and the reaction mixture was stirred for 10 minutes. The solution was filtered and the solvent removed to yield (dpp-Bian)Ga(PCO)(Pyr) as a dark blue powder (81 mg, 88.7 %). Single crystals suitable for X-ray diffraction were grown by cooling a concentrated toluene solution to –35 °C. **CHN** Anal. Calcd. For $C_{42}H_{45}GaN_3OP$: C, 71.20; H, 6.40; N, 5.93. Found: C, 72.56; H, 6.43; N, 5.25. **^{1}H NMR** (500 MHz, C_6D_6): δ (ppm) 8.63 (d, $^3J_{H–H}$ = 5.0 Hz, 2H, pyr *ortho* C*H*), 7.29–7.31 (m, 4H, Ar*H*), 7.19–7.22 (m, 2H, Ar*H*), 7.09 (d, *J*=8.2 Hz, 2H, Ar*H*), 6.89 (dd, $^3J_{H–H}$ = 8.25, 6.94 Hz, 2H, Ar*H*), 6.68 (t, $^3J_{H–H}$ = 7.7 Hz, 1H, pyr *para* C*H*), 6.41 (d, $^3J_{H–H}$ = 6.8 Hz, 2H, Ar*H*), 6.27 (m, 2H, pyr *meta* C*H*), 3.96 (sept, $^3J_{H–H}$ = 6.7 Hz, 2H, {C*H*(CH$_3$)$_2$}), 3.29 (sept, $^3J_{H–H}$ = 6.8 Hz, 2H, {C*H*(CH$_3$)$_2$}), 1.54 (d, $^3J_{H–H}$ =6.9 Hz, 6H, {CH(C*H*$_3$)$_2$}), 1.25 (d, $^3J_{H–H}$ =6.9 Hz, 6H, {CH(C*H*$_3$)$_2$}), 1.15 (d, $^3J_{H–H}$ = 6.8 Hz, 6H, {CH(C*H*$_3$)$_2$}), 0.42 (d, $^3J_{H–H}$ = 6.8 Hz, 6H, {CH(C*H*$_3$)$_2$}). **^{13}C{^{1}H} NMR** (126 MHz, C_6D_6): δ (ppm) 180.8 (d, $^1J_{C–P}$ = 101.0 Hz, P*C*O), 148.3 (s, Ar*C*), 147.5 (pyr*C*), 146.4 (Ar*C*), 143.4 (Ar*C*), 141.2 (pyr*C*), 135.9 (Ar*C*), 127.4 (Ar*C*), 126.2 (Ar*C*), 125.3 (pyr*C*), 124.9, 124.2 (Ar*C*), 123.0 (Ar*C*), 118.0 (Ar*C*), 28.8 ({*C*H(CH$_3$)$_2$}), 28.7 ({*C*H(CH$_3$)$_2$}), 25.8 (({CH(*C*H$_3$)$_2$})), 25.0 (({CH(*C*H$_3$)$_2$})), 24.3 (({CH(*C*H$_3$)$_2$})), 24.2 ({CH(*C*H$_3$)$_2$})). **^{31}P{^{1}H} NMR** (162 MHz, C_6D_6): δ (ppm) –394.6 (s).

8.2.5.3 Synthesis of [Ga]($^{i\mathrm{Pr}}$NHC)(PCO) (41b)

This complex can be synthesised from (dipp-Bian)GaI(NHC), however due to the sensitivity of these compounds, which undergo decomposition during recrystalisation even in schlenk tubes, the compound is synthesised directly from the ligand with minimal filtration and recrystallisation steps.

Dipp-Bian (500 mg, 1.0 mmol) was refluxed (110 °C) in an ampoule fitted with a J young tap over an excess of gallium metal (> 10 eq.) for 12 hours. The resulting dark blue solution

was filtered and iodine (130 mg, 1.0 mmol) was added. The solution was stirred for 6 hours, forming a brick red suspension, and the solvent removed. Pyridine (20 mL) was added and the reaction heated to reflux, at which point the solution turns from red to blue. The solvent was removed and the blue solid redissolved in toluene. 1,3-diisopropyl-4,5-dimethylimidazole (180 mg, 1.0 mmol) was added and the solution turned from blue to green. After 2 hours [Na(dioxane)$_{0.6}$(PCO)] (1.2 eq, 1.2 mmol) was added and the solution filtered to a second ampoule before being concentrated and stored at 5 °C overnight to yield (dipp-Bian)Ga(PCO)(NHC) as a green powder (280 mg, 35%). The solution was then concentrated and cooled to yield a crop of crystals. **CHN** Anal. Calcd. for $C_{48}H_{61}GaN_4OP$: C, 71.11; H, 7.58; N, 6.91. Found: C, 69.43; H, 7.90; N, 6.86. **^{1}H NMR** (400 MHz, C_6D_6): δ (ppm) 7.34 (dd, $^3J_{H–H}$ = 7.4, 1.8, 2H, Ar*H*), 7.30 – 7.19 (m, 6H, Ar*H*), 7.11 (s, 2H, Ar*H*), 6.91 – 6.82 (m, 2H, Ar*H*), 6.20 (d, $^3J_{H–H}$ = 6.9, 2H, Ar*H*), 4.67 – 4.55 (m, 2H, NHC{C*H*(CH$_3$)$_2$}), 4.34 (sept, $^3J_{H–H}$ = 6.7, 2H, {C*H*(CH$_3$)$_2$}), 3.88 (sept, $^3J_{H–H}$ = 7.0, 2H, {C*H*(CH$_3$)$_2$}), 1.53 (d, $^3J_{H–H}$ = 6.9, 6H, {CH(C*H*$_3$)$_2$}), 1.43 (d, $^3J_{H–H}$ = 6.7, 6H, {CH(C*H*$_3$)$_2$}), 1.28 (s, 6H, C*H*$_3$), 1.09 (dd, $^3J_{H–H}$ = 13.9, 6.9, 12H, {CH(C*H*$_3$)$_2$}), 0.93 (d, $^3J_{H–H}$ = 6.8, 12H, {CH(C*H*$_3$)$_2$}). **^{13}C{^{1}H} NMR** (126 MHz, C_6D_6): δ (ppm) 186.4 (d, $^1J_{C–P}$ = 85.4 Hz, P*C*O), 160.2 (s, Ar*C*), 147.77 (Ar*C*), 145.8 (Ar*C*), 136.1 (Ar*C*), 134.9 (Ar*C*), 134.5 (Ar*C*), 125.1 (Ar*C*), 124.4 (Ar*C*), 123.7 (Ar*C*), 123.6 (Ar*C*), 123.4 (Ar*C*), 118.0 (Ar*C*), 54.4 (NHC {*C*H(CH$_3$)$_2$}), 30.0 ({*C*H(CH$_3$)$_2$}), 29.0 ({*C*H(CH$_3$)$_2$}), 27.5 ({CH(*C*H$_3$)$_2$}), 25.6 ({CH(*C*H$_3$)$_2$}), 24.4 ({CH(*C*H$_3$)$_2$}), 23.3 ({CH(*C*H$_3$)$_2$}), 21.7 ({CH(*C*H$_3$)$_2$}), 9.6 (NHC *C*H$_3$). **^{31}P{^{1}H} NMR** (162 MHz, C$_6$D6): δ (ppm) –354.9 (s).

8.2.5.4 Synthesis of [Ga](IMes)(PCO) (41c)

Dipp-Bian (500 mg, 1.0 mmol) was refluxed (110 °C) in an ampoule fitted with a J-Young tap over an excess of gallium metal (> 10 eq.) for 12 hours. The resulting dark blue solution was filtered and iodine (130 mg, 1.0 mmol) was added. The solution was stirred for 6 hours,

forming a brick red suspension, and the solvent removed. Pyridine (20 mL) was added and the reaction heated to reflux, at which point the solution turns from red to blue. The solvent was removed and the blue solid dissolved in toluene. IMes (0.30 g, 1.0 mmol) was added and the solution turned from blue to green. After 2 hours [Na(dioxane)$_{0.6}$(PCO)] (1.2 eq, 1.2 mmol) was added and the solution filtered to a second ampoule before being concentrated and stored at –35°C overnight to yield (dipp-Bian)Ga(PCO)(IMes) as a green powder (410 mg, 40%). **CHN** Anal. Calcd. for $C_{64}H_{76}GaN_4OP$: C, 75.51; H, 7.53; N, 5.50. Found: C, 74.75; H, 7.61; N, 6.03. **^{1}H NMR** (400 MHz, C_6D_6): δ (ppm) 7.40 – 7.26 (m, 6H, Ar*H*), 7.15 – 6.98 (m, 8H, Ar*H*), 6.89 (t, $^3J_{H–H}$ = 7.5 Hz, 2H, Ar*H*), 6.59 (s, 2H, Ar*H*), 6.51 (s, 2H, Ar*H*), 6.29 (d, $^3J_{H–H}$ = 6.8 Hz, 2H, Ar*H*), 5.48 (s, 1H, IMes C*H*), 4.40 (sept, $^3J_{H–H}$ = 8.4 Hz, 7.5, 2H, {C*H*(CH_3)$_2$}), 3.98 – 3.87 (sept, $^3J_{H–H}$ = 8.4 Hz, 2H, {C*H*(CH_3)$_2$}), 2.11 (s, 3H, IMes C*H*$_3$), 2.05 (s, 3H, IMes C*H*$_3$), 1.99 (s, 3H, IMes C*H*$_3$), 1.67 (d, $^3J_{H–H}$ = 10.8 Hz, 12H, {C*H*(CH_3)$_2$}),), 1.49 (d, $^3J_{H–H}$ = 6.8 Hz, 6H, {C*H*(CH_3)$_2$}),), 1.31 (dd, $^3J_{H–H}$ = 16.3 Hz, 6.7, 12H, {C*H*(CH_3)$_2$}), 1.19 (d, $^3J_{H–H}$ = 7.0 Hz, 6H, {C*H*(CH_3)$_2$}),). **^{13}C{^{1}H} NMR** (126 MHz, C_6D_6): δ (ppm) 203.4 (s, NHC *C*), 183.7 ($^1J_{C–P}$ = 87.3 Hz, P*C*O), 148.4 (Ar*C*), 146.7 ($^2J_{C–P}$ = 24.3 Hz, NHC Ga*C*), 146.1 (Ar*C*), 140.5 (Ar*C*), 140.3 (Ar*C*), 138.0 (Ar*C*), 137.5 (Ar*C*), 137.1 (Ar*C*), 136.6 (Ar*C*), 135.5 (Ar*C*), 134.4 (Ar*C*), 133.6 (Ar*C*), 132.4 (Ar*C*), 130.7 (Ar*C*), 129.5 (Ar*C*), 129.2 (Ar*C*), 129.0 (Ar*C*), 128.2 (Ar*C*), 126.8 (Ar*C*), 125.3 (Ar*C*), 124.5 (Ar*C*), 124.3 (Ar*C*), 122.9 (Ar*C*), 122.7 (Ar*C*), 117.5 (Ar*C*), 29.7 ({CH(*C*H$_3$)$_2$}), 28.5 ({*C*H(CH_3)$_2$}), 28.3 ({*C*H(CH_3)$_2$}), 25.7 ({*C*H(CH_3)$_2$}), 25.6 (*C*H$_3$), 25.5 (*C*H$_3$), 25.3 (*C*H$_3$), 24.2 (*C*H$_3$), 21.6 (*C*H$_3$), 20.6 (*C*H$_3$), 20.5 (*C*H$_3$), 17.5 (*C*H$_3$), 17.1 (*C*H$_3$). **^{31}P{^{1}H} NMR** (162 MHz, C_6D6): δ (ppm) –374.2 (s).

8.2.5.5 Synthesis of [Ga]PP[Ga] (42)

A solution containing **41a** (100 mg, 0.13 mmol) in toluene (0.5 mL) was irradiated for 4 × 9 hours, resulting in significantly reduced intensity in both the ^{31}P and ^{1}H NMR. Crystallisation

of the solution by cooling allowed for crystallographic characterisation of diphosphene **42**. The crystals were dissolved, and ^{31}P NMR allowed for identification of a peak at 774.9 ppm, which immediately and irreversibly disappeared upon warming. **^{31}P NMR** (162 MHz, C_6D6): δ (ppm) 774.9 ppm

8.2.5.6 Synthesis of [Ga](Pyr)(PPMe$_3$) (43a)

To a solution of **41a** (100 mg, 0.13 mmol) in toluene (2 mL) an excess of trimethylphosphine (20 mg, 0.26 mmol) was added. The volatiles were removed under reduced pressure and the resulting blue solid was taken up into toluene, filtered and concentrated. Cooling the solution to –35°C for a week resulted in bright blue, heterochromic crystals of **42a** (71 mg, 66.7 %). **CHN** Anal. Calcd. for $C_{44}H_{55}GaN_3O_2P_2$ + toluene: C, 69.47; H, 7.20; N, 4.77; Found: C, 70.81; H, 7.93; N, 4.21. **^{1}H NMR** (500 MHz, C_6D_6): δ (ppm) 9.08 (d, $^3J_{H–H}$ = 5.5 Hz, 2H,*ortho*- Pyr*H*), 7.27 (s, 6H, ArC*H*), 7.08 (d, $^3J_{H–H}$ = 8.2 Hz, 2H, ArC*H*), 6.91 (t, $^3J_{H–H}$ = 7.6 Hz, 2H, ArC*H*), 6.84 (t, $^3J_{H–H}$ = 7.7 Hz, 1H, *para*-Pyr*H*), 6.45 (t, $^3J_{H–H}$ = 6.7 Hz, 2H, ArC*H*), 6.36 (d, $^3J_{H–H}$ = 6.9 Hz, 2H, PyrC*H*), 3.71 (sept, $^3J_{H–H}$ = 6.9 Hz, 4H, {C*H*(CH_3)$_2$}), 3.27 (q, $^3J_{H–H}$ = 6.9 Hz, 2H), 1.21 (t, $^3J_{H–H}$ = 6.3 Hz, 12H, {C*H*(CH_3)$_2$}), 0.79 (dd, $^3J_{H–H}$ = 12.1 Hz, 2.1, 12H, {C*H*(CH_3)$_2$}). **^{13}C{^{1}H} NMR** (126 MHz, C_6D_6): δ (ppm) 149.3 (s, Ar*C*), 147.5 (Ar*C*), 145.7 (Ar*C*), 139.3 (Ar*C*), 136.0 (Ar*C*), 135.2 (Ar*C*), 126.9 (Ar*C*), 125.0 (Ar*C*), 123.8 (Ar*C*), 123.5 (Ar*C*), 123.3 (Ar*C*), 117.4 (Ar*C*), 65.5 ({*C*H(CH_3)$_2$}), 27.9 ({CH(*C*H$_3$)$_2$}), 24.6 ({CH(*C*H$_3$)$_2$}), 22.8 (dd, $^1J_{P–C}$ = 43.8 Hz, $^2J_{P–C}$ = 7.9 Hz, P(*C*H$_3$)$_3$). **^{31}P{^{1}H} NMR** (202 MHz, C_6D_6): δ (ppm) 14.7 (d, $^1J_{P–P}$ =527.4 Hz, *P*Me$_3$), –263.0 (d, $^1J_{P–P}$ = 527.4 Hz, phosphinidene).

8.2.5.7 Synthesis of [Ga]P[GaL] (44)

Ga(L), L = HC[C(Me)N-(C_6H_3)-2,6-^{i}Pr$_2$]$_2$ (24 mg, 0.05 mmol) was added to a solution of **41a** (36.5 mg, 0.05 mmol) in toluene (0.5 mL). The solution was heated to 90°C and allowed to cool slowly. Upon cooling blue crystals began to precipitate. The reaction mixture was

left overnight. The solvent was decanted and placed in the freezer. After a few days a second crop of crystals formed (combined yield 35 mg, 60%). **^{1}H NMR** (500 MHz, C_6D_6): δ (ppm) 8.81 (br s, 2H, Pyr*H*), 7.36 (s, 6H, Ar*H*), 7.02 (t, $^{3}J_{H–H}$ = 7.2 Hz, 6H, Ar*H*), 6.88 – 6.82 (m, 4H, Ar*H*), 6.35 (s br, 2H, Pyr*H*), 6.23 (d, $^{3}J_{H–H}$ = 7.0 Hz, 2H, Ar*H*), 4.79 (s, 1H, {*H*C(C(NR)(CH_3))$_2$), 3.90 (sept, $^{3}J_{H–H}$ = 6.9 Hz, 4H, Bian {C*H*(CH_3)$_2$}), 3.61 – 3.06 (m, 4H, β-Diketiminate {C*H*(CH_3)$_2$}), 2.11 (s, 1H, impurity), 1.45 (s, 6H, {HC(C(NR)(C*H*$_3$))$_2$)}), 1.31 (m, 12H,{CH(C*H*$_3$)$_2$}), 1.19 (d, $^{3}J_{H–H}$ = 6.9 Hz, 12H, β-Diketiminate {CH(C*H*$_3$)$_2$}), 1.07 (d, $^{3}J_{H–H}$ = 6.9 Hz, 12H), 0.99 (m br, 12H, {CH(C*H*$_3$)$_2$}). **^{13}C{^{1}H} NMR** (126 MHz, C_6D_6): δ (ppm) 169.4 (Ar*C*), 160.2 (br, Pyr*C*), 158.8, 148.4 (br, Pyr*C*), 146.5 (Ar*C*), 145.4 (Ar*C*), 143.0 (br, Pyr*C*), 141.0 (Ar*C*), 139.9 (Ar*C*), 137.5 (Ar*C*), 135.5 (Ar*C*), 134.9 (Ar*C*), 133.7 (Ar*C*), 129.0 (Ar*C*), 128.2 (Ar*C*), 126.9 (Ar*C*), 125.3 (Ar*C*), 124.8 (Ar*C*), 123.7 (Ar*C*), 123.1 (Ar*C*), 123.0 (Ar*C*), 117.0 (({HC(*C*(NR)(CH_3))$_2$), 96.7 ({H*C*(C(NR)(CH_3))$_2$), 59.7 ({HC(C(NR)(*C*H$_3$))$_2$), 38.2 ({(*C*H(CH_3)$_2$}), 31.3 ({(*C*H(CH_3)$_2$}), 29.9 ({(*C*H(CH_3)$_2$}), 29.0 ({(*C*H(CH_3)$_2$}), 28.3 (CH_3), 24.9 (CH_3), 24.3 (CH_3), 24.2 (CH_3), 23.5 (CH_3), 23.3 (CH_3), 22.8 (CH_3), 22.5 (CH_3), 21.1 (CH_3). **^{31}P{^{1}H} NMR** (162 MHz, C_6D_6): δ (ppm) –319.0 (s). **^{31}P NMR** (162 MHz, C_6D_6): δ (ppm) –319.0 (s).

8.3 Characterisation techniques

8.3.1 Single crystal X-ray diffraction

Single-crystal X-ray diffraction data were collected using an Oxford Diffraction Supernova dual-source diffractometer equipped with a 135 mm Atlas CCD area detector. Crystals were selected under Paratone-N oil, mounted on micromount loops and quench-cooled using an Oxford Cryosystems open flow N_2 cooling device. Data were collected at 150 K using mirror monochromated Cu K_α radiation (λ = 1.5418 Å; Oxford Diffraction Supernova) and processed using the CrysAlisPro package, including unit cell parameter refinement and inter-frame scaling (which was carried out using SCALE3 ABSPACK within CrysAlisPro).[14] Equivalent reflections were merged and diffraction patterns processed with the CrysAlisPro suite. Structures were subsequently solved using direct methods and refined on F^2 using the SHELXL package.[15–17]

8.3.2 NMR spectroscopy

NMR spectra were acquired on a Bruker AVIII 500 MHz NMR spectrometer (^{1}H 500 MHz, ^{13}C 126 MHz) and Bruker AVIII 400 MHz NMR spectrometer (^{1}H 400 MHz, ^{31}P 162 MHz, ^{11}B 128 MHz, ^{19}F 470 MHz, ^{7}Li 156 MHz). ^{1}H and ^{13}C NMR spectra were referenced to the most downfield solvent resonance (^{1}H NMR C_6D_6: $\delta_{(ppm)}$ 7.16 ppm; ^{13}C NMR C_6D_6: δ (ppm) 188.06 ppm). ^{31}P, ^{19}F, ^{11}B, ^{7}Li spectra were externally referenced to an 85% solution of H_3PO_4 in H_2O, $CFCl_3$, $BF_3{\cdot}Et_2O$ in C_6D_6, and 1 M LiCl in D_2O, respectively. Full details of the 1D-EXSY and ^{31}P{^{1}H} CPMAS can be found in the relevant publication.[18]

8.3.3 Elemental analysis

Elemental analyses were carried out by Elemental Microanalyses Ltd. (Devon, U.K.). Samples (approx. 5 mg) were submitted in sealed Pyrex ampoules.

8.3.4 IR spectroscopy

IR data were recorded as solid samples in Nujol mulls. Samples were prepared inside an inert atmosphere glovebox and the samples placed in airtight holders prior to data collection. Spectra were recorded on a Thermo Scientific iS5 FT-IR spectrometer in absorbance mode.

8.3.5 Computational details

Calculations were performed by Daniel Wilson, Alexander Hinz, John McGrady, Mauricio Franco, and William Myers. All calculations were performed using Gaussian09[19] or Orca 3.0.3 software packages. Explicit computational details for published compounds can be found in the following references:

- **1, 2, 4, 5, 6b**[20]
- **16a–21**[21]
- **24–26**[22]

8.3.6 EPR spectroscopy

EPR spectroscopy was performed by William Myers. Measurements of continuous wave electron paramagnetic resonance (CW-EPR) were performed in the Centre for Advanced ESR (CAESR) in the Department of Chemistry in the University of Oxford. X-band CW-EPR was acquired on a Bruker BioSpin EleXSys I E680 spectrometer with an XPB bridge, 1.5 T electromagnet, a Bruker BioSpin ER4122-SHQE-W resonator coupled to an Oxford Instruments ESR900 cryostat, and subsequently, a Bruker BioSpin ER4118X-MD-5-W resonator in an Oxford Instruments CF935W cryostat, both controlled with an Oxford Instruments ITC-503S temperature controller. Liquid helium was used as a cryogen. Samples were held in a J. Young adapted 4 mm O.D. clear fused quartz tube in the ER4122 resonator and other samples were collapsed and cut via a hydrogen/oxygen torch by Jose Goicoechea for a flame seal under vacuum to rigorously avoid O2 ESI 42 inclusion in

measurements within the ER4118X resonator. Illumination of the sample was achieved in two ways: one with a Newport/Oriel 1000W Xenon Arc lamp with a 10 cm water filter and liquid light guide with no other filter, having a total illumination power of 700 mW/cm2 as determined by a model 3W Ophir LASER power meter sensor. Alternative measurements were performed using the 355 nm pump wavelength of an OpoTek Opolette HE355 20 Hz pulsed OPO LASER with 1.5 mJ pulse energy and pulse length of 9 ns. Photolytic EPR signals were stable below 40 K, but may be complex with concentration and sample dependent species. Full experimental details can be found in the referenced manuscript.[21]

8.4 References

[1] D. Heift, Z. Benko, H. Grützmacher, *Dalt. Trans.* **2014**, *43*, 831–840.

[2] D. Herrmannsdörfer, M. Kaaz, O. Puntigam, J. Bender, M. Nieger, D. Gudat, *Eur. J. Inorg. Chem.* **2015**, *2015*, 4819–4828.

[3] E. L. Bennett, E. J. Lawrence, R. J. Blagg, A. S. Mullen, F. MacMillan, A. W. Ehlers, D. J. Scott, J. S. Sapsford, A. E. Ashley, G. G. Wildgoose, et al., *Angew. Chemie* **2019**, *131*, ange.201900861.

[4] R. B. King, *Acc. Chem. Res.* **1970**, *3*, 417–427.

[5] A. Levens, M. Kowalczyk, D. W. Lupton, in *Encycl. Reagents Org. Synth.*, John Wiley & Sons, Ltd, **2014**, pp. 1–4.

[6] W. E. Piers, T. Chivers, *Chem. Soc. Rev.* **1997**, *26*, 345–354.

[7] A. E. Seitz, U. Vogel, M. Eberl, M. Eckhardt, G. Balázs, E. V. Peresypkina, M. Bodensteiner, M. Zabel, M. Scheer, *Chem. Eur. J.* **2017**, *23*, 10319–10327.

[8] K. Bardsley, M. Hagigeorgiou, I. Lengyel, V. Cesare, *Synth. Commun.* **2013**, *43*, 1727–1733.

[9] I. L. Fedushkin, A. A. Skatova, V. A. Dodonov, V. A. Chudakova, N. L. Bazyakina, A. V. Piskunov, S. V. Demeshko, G. K. Fukin, *Inorg. Chem.* **2014**, *53*, 5159–5170.

[10] S. J. Bonyhady, C. Jones, S. Nembenna, A. Stasch, A. J. Edwards, G. J. McIntyre, *Chem. Eur. J.* **2010**, *16*, 938–955.

[11] G. Becker, G. Gresser, W. Uhl, *Zeitschrift fur Naturforsch. - Sect. B J. Chem. Sci.* **1981**, *36*, 16–19.

[12] M. Finze, E. Bernhardt, H. Willner, C. W. Lehmann, *Angew. Chemie Int. Ed.* **2004**, *43*, 4160–4163.

[13] N. J. Hardman, B. E. Eichler, P. P. Power, *Chem. Commun.* **2000**, 1991–1992.

[14] *CrysAlisPro*, Agilent Technologies, Version 1.171.35.8.

[15] G. M. Sheldrick in SHELXL97, *Programs for Crystal Structure Analysis (Release 97-2)*, Institut für Anorganische Chemie der Universität, Tammanstrasse 4, D-3400 Göttingen, Germany, 1998;

[16] G. M. Sheldrick, *Acta Crystallogr. Sect. A Found. Crystallogr.* **2008**, *64*, 112–122.

[17] G. M. Sheldrick, *Acta Crystallogr. Sect. A* **1990**, *46*, 467–473.

[18] D. W. N. Wilson, N. H. Rees, J. M. Goicoechea, *Organometallics* **2019**, *38*, 4601–4606.

[19] M. J. Frisch, G. W. Trucks, H. B. Schlegel, G. E. Scuseria, M. A. Robb, J. R. Cheeseman, G. Scalmani, V. Barone, B. Mennucci, G. A. Petersson, et al., *Gaussian, Inc. Wallingford CT* **2010**.

[20] D. W. N. Wilson, A. Hinz, J. M. Goicoechea, *Angew. Chemie Int. Ed.* **2018**, *57*, 2188–2193.

[21] D. W. N. Wilson, M. P. Franco, W. K. Myers, J. E. McGrady, J. M. Goicoechea,

Chem. Sci. **2020**, *11*, 862–869.

[22] D. W. N. Wilson, J. M. Goicoechea, *Chem. Commun.* **2019**, *55*, 6842–6845.

Appendix

EPR spectra for gallium phosphaketenes

Monitoring of irradiation of compound **41a:**

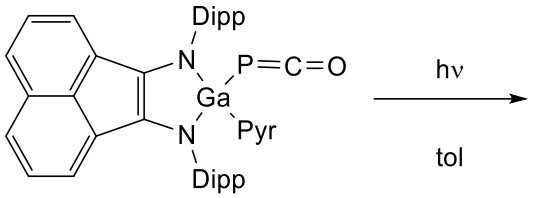

41a

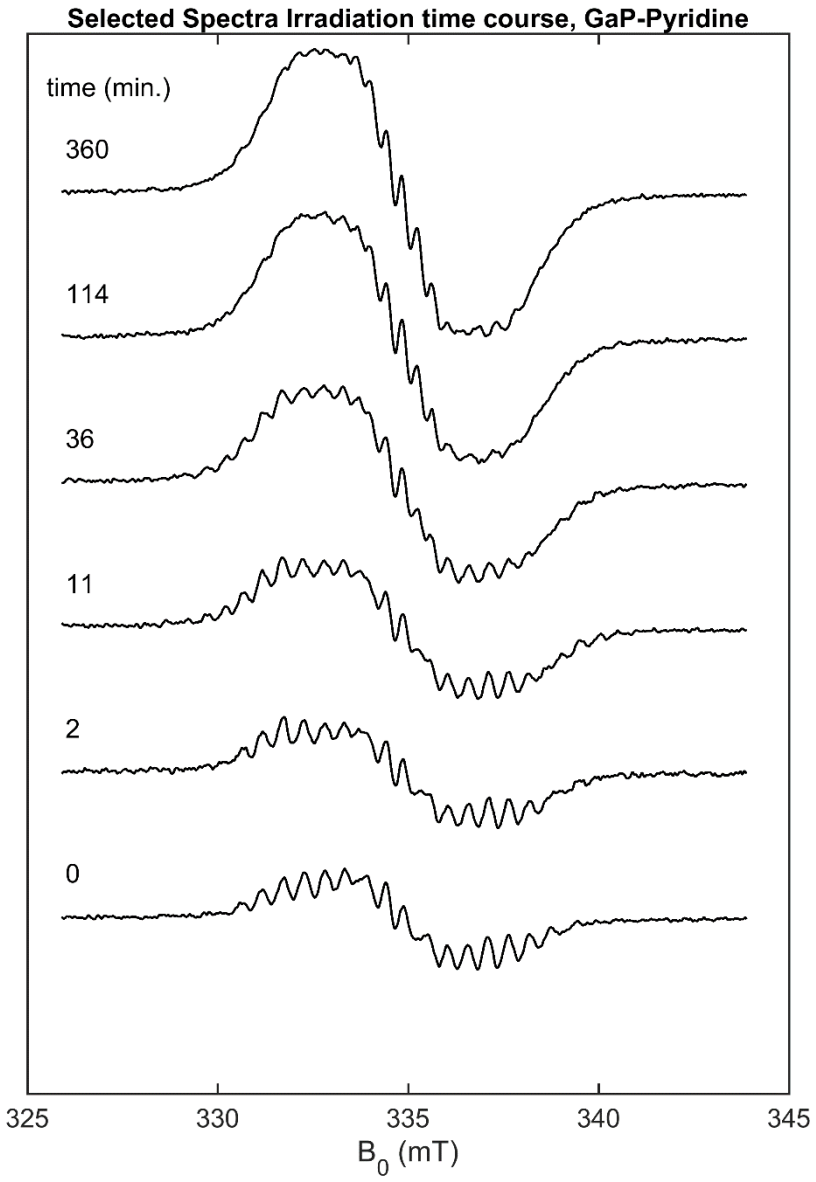

Figure A.1. EPR monitoring experiment of irradiation of a toluene solution of **41a**.

Irradiation of compound **41b** and **41c**

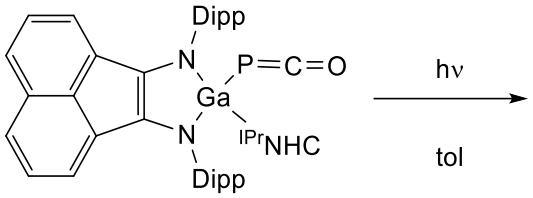

41b

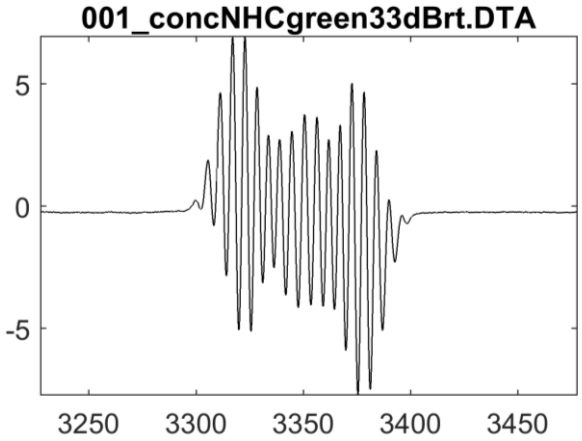

Figure A.2. EPR spectrum of irradiated solution of **41b**.

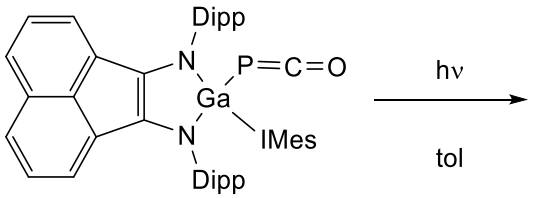

41c

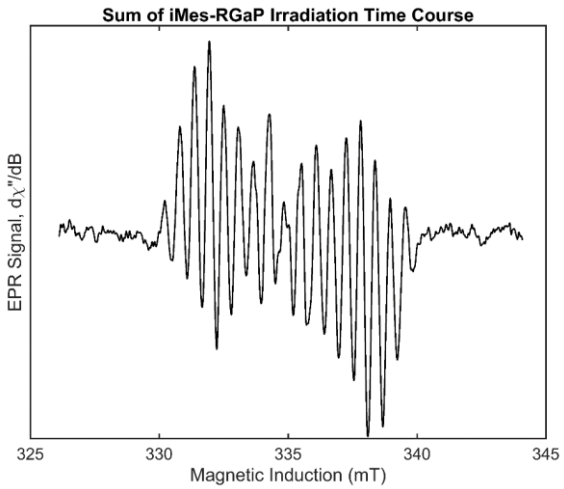

Figure A.3. EPR spectrum of irradiated solution of **41c**.

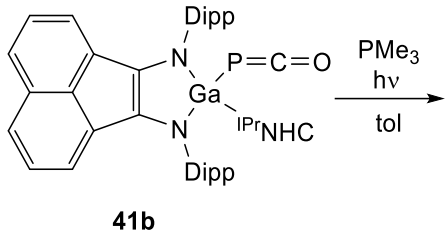

41b

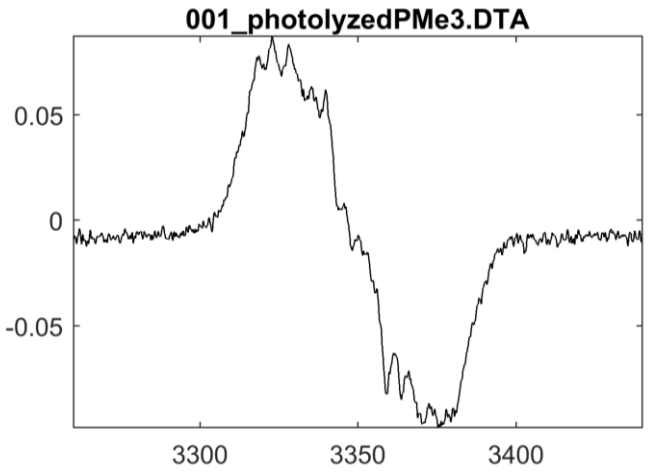

Figure A.4. EPR spectrum of photolysed solution of **41b** in the presence of trimethylphosphine.

Table A1. Selected X-ray data collection and refinement parameters for **1**, **2**, **4** and **5**.

	1	**2**	**3·2Et$_2$O**	**5**
Formula	$C_{27}H_{36}BN_2OP$	$C_{54}H_{72}B_2N_4O_2P_2$	$C_{121}H_{165}B_4N_8Na_4O_8P_8$	$C_{53}H_{72}B_2N_4OP_2$
CCDC	1589990	1589991		1589992
Fw [g mol^{-1}]	446.36	892.71	2242.56	864.70
Crystal system	triclinic	monoclinic	triclinic	monoclinic
Space group	*P*–1	$P2_1/c$	*P*–1	$P2_1/c$
a (Å)	9.5870(3)	10.5807(3)	16.9969(4)	10.7432(2)
b (Å)	10.6112(3)	13.7619(3)	18.8083(4)	13.3610(3)
c (Å)	13.1731(5)	36.2504(8)	21.5555(5)	35.7621(6)
α (°)	91.140(3)	90	108.067(2)	90
β (°)	98.412(3)	91.285(2)	102.546(2)	91.401(2)
γ (°)	93.989(2)	90	90.3910(18)	90
V (Å^3)	1321.85(8)	5277.1(2)	6374.3(3)	5131.75(17)
Z	2	4	2	4
Radiation, λ (Å)	Cu Kα, 1.54178	Cu Kα, 1.54184	Cu Kα, 1.54184	Cu Kα, 1.54184
Temp (K)	150(2)	150(2)	150(2)	150(2)
ρ_{calc} (g cm^{-3})	1.121	1.124	1.168	1.119
μ (mm^{-1})	1.063	1.065	1.587	1.064
Reflections collected	26544	31182	76220	31627
Independent reflections	5502	10945	26397	10645
Parameters	305	623	1571	618
R(int)	0.0268	0.0372	0.0568	0.0401
R1/wR2,[a] I ≥ 2σI (%)	4.32/11.59	4.61/11.01	5.03/12.45	4.83/12.06
R1/wR2,[a] all data (%)	4.93/12.22	6.22/12.16	6.67/14.06	7.04/13.40
GOF	1.055	1.017	1.037	1.031

[a] $R1 = [\Sigma||F_o| - |F_c||]/\Sigma|F_o|$; $wR2 = \{[\Sigma w[(F_o)^2 - (F_c)^2]^2]/[\Sigma w(F_o^2)^2\}^{1/2}$; $w = [\sigma^2(F_o)^2 + (AP)^2 + BP]^{-1}$, where $P = [(F_o)^2 + 2(F_c)^2]/3$ and the A and B values are 0.0342 and 0.00 for **1**, 0.0499 and 1.72 for **2**, 0.0702 and 1.1218 for **3·2Et$_2$O,** and 0.0638 and 1.12 for **5**.

Table A2. Selected X-ray data collection and refinement parameters for

	6b·0.75hex	**6c**	**7·LiI**	**8a**
Formula	$C_{76.5}H_{104.5}B_2Li_2N_4O_2P_2$	$C_{44}H_{63}BLiN_2O_5P$	$C_{51}H_{61}BILi_2N_2OP$	$C_{36}H_{48}BN_2OP$
CCDC	1589994	1589996		1589995
Fw [g mol^{-1}]	1209.57	748.68	900.57	566.54
Crystal system	triclinic	monoclinic	triclinic	triclinic
Space group	*P*–1	$P2_1/c$	*P*–1	*P*–1
a (Å)	13.6980(3)	24.3631(3)	11.5791(5)	9.5108(5)
b (Å)	20.6908(4)	31.7795(5)	11.8222(5)	9.9537(6)
c (Å)	27.1654(4)	16.4858(2)	20.0745(6)	18.2627(14)
α (°)	88.409(2)	90	75.549(3)	86.080(5)
β (°)	85.316(2)	94.3840(10)	78.015(3)	88.486(5)
γ (°)	71.177(2)	90	65.508(4)	78.165(5)
V (Å^3)	7263.2(3)	12726.7(3)	2404.63(18)	1688.05(19)
Z	4	12	2	2
Radiation, λ (Å)	Cu Kα, 1.54184	Cu Kα, 1.54184	Cu Kα, 1.54184	Cu Kα, 1.54184
Temp (K)	150(2)	150(2)	150(2)	150(2)
ρ_{calc} (g cm^{-3})	1.106	1.172	1.244	1.115
μ (mm^{-1})	0.887	0.923	5.814	0.929
Reflections collected	82381	73657	24485	15967
Independent reflections	25619	26286	9924	6944
Parameters	1641	1516	546	410
R(int)	0.0656	0.0538	0.0347	0.0688
R1/wR2,[a] $I \geq 2\sigma I$ (%)	5.62/14.58	6.06/15.54	4.37/11.82	5.95/14.40
R1/wR2,[a] all data (%)	7.55/15.83	8.66/17.70	4.84/12.27	9.00/16.72
GOF	1.037	1.030	1.048	1.002

[a] $R1 = [\Sigma||F_o| - |F_c||]/\Sigma|F_o|$; $wR2 = \{[\Sigma w[(F_o)^2 - (F_c)^2]^2]/[\Sigma w(F_o^2)^2\}^{1/2}$; $w = [\sigma^2(F_o)^2 + (AP)^2 + BP]^{-1}$, where $P = [(F_o)^2 + 2(F_c)^2]/3$ and the A and B values are 0.0851 and 0.73 for **6b**·0.75hex, 0.0823 and 4.56 for **6c,** 0.0653 and 0 for **8a**.

Table A3. Selected X-ray data collection and refinement parameters for

	9	**10**	**11**	**12**
Formula	$C_{54}H_{62}AuBN_2OP_2$	$C_{87}H_{123}B_2Fe_2N_4Na_2O_6P_2$	$C_{43.5}H_{63.5}BFeN_2O_3PSi$	$C_{57}H_{66}AuBFeN_2O_3P_2$
CCDC	1589997			
Fw [g mol^{-1}]	1024.77	1562.13	788.18	1152.68
Crystal system	monoclinic	triclinic	triclinic	triclinic
Space group	$P2_1/c$	$P\bar{1}$	$P\bar{1}$	$P\bar{1}$
a (Å)	14.6901(2)	12.4481(4)	12.6726(7)	12.5793(6)
b (Å)	12.4824(2)	16.8150(7)	14.4208(6)	12.6322(5)
c (Å)	26.8253(6)	22.2412(11)	25.6379(10)	17.8449(6)
α (°)	90	96.817(4)	78.827(4)	86.392(3)
β (°)	94.3483(16)	94.522(3)	86.973(4)	73.088(4)
γ (°)	90	107.257(4)	78.977(4)	81.048(4)
V (Å^3)	4904.72(16)	4382.4(3)	4511.1(4)	2679.5(2)
Z	4	2	4	2
Radiation, λ (Å)	Mo Kα, 0.71073	Mo Kα, 0.71073	Cu Kα, 1.54184	Cu Kα, 1.54184
Temp (K)	150(2)	150(2)	150(2)	150(2)
ρ_{calc} (g cm^{-3})	1.388	1.184	1.161	1.429
μ (mm^{-1})	6.544	0.429	3.556	8.145
Reflections collected	29825	35282	39615	28840
Independent reflections	10137	15427	18631	11081
Parameters	603	975	963	617
R(int)	0.0441	0.0424	0.0476	0.0453
R1/wR2,[a] $I \geq 2\sigma I$ (%)	3.51/8.16	5.05/10.25	5.38/13.81	3.96/9.55
R1/wR2,[a] all data (%)	4.84/8.88	8.12/11.31	7.17/15.56	4.83/9.93
GOF	1.017	1.042	1.039	1.029

[a] $R1 = [\Sigma||F_o| - |F_c||]/\Sigma|F_o|$; $wR2 = \{[\Sigma w[(F_o)^2 - (F_c)^2]^2]/[\Sigma w(F_o^2)^2\}^{1/2}$; $w = [\sigma^2(F_o)^2 + (AP)^2 + BP]^{-1}$, where $P = [(F_o)^2 + 2(F_c)^2]/3$ where A and B values are 0.0415and 2.44 for **9**, 0.0412 and 0.36 for **10**, 0.0725 and 1.76 for **11**, 0.0493 and 4.07 for **12**.

Table A4. Selected X-ray data collection and refinement parameters for **13** to **17a**

	13	**15**	**16a**	**17a**
Formula	$C_{39}H_{52}BFeN_2O_3P$	$C_{63}H_{49}B_2F_{20}FeN_2O_3P$	$C_{37}H_{47}BN_3OP$	$C_{36}H_{47}BN_3P$
CCDC				
Fw [g mol^{-1}]	735.95	1370.48	591.55	563.54
Crystal system	triclinic	triclinic	monoclinic	monoclinic
Space group	*P*–1	*P*1	$P2_1/n$	$P2_1/c$
a (Å)	12.54447(18)	10.5676(5)	10.6925(3)	18.9679(3)
b (Å)	16.6280(4)	12.4371(6)	19.6374(5)	7.4054(1)
c (Å)	19.7273(4)	13.3169(6)	17.0321(5)	25.1568(3)
α (°)	90.2559(17)	82.765(4)	90	90
β (°)	90.1291(13)	71.221(4)	101.118(3)	107.290(1)
γ (°)	109.4886(16)	67.263(5)	90	90
V (Å^3)	3879.08(13)	1528.30(14)	3509.16(17)	3373.97(8)
Z	4	1	4	4
Radiation, λ (Å)	Cu Kα, 1.54184	Cu Kα, 1.54184	Cu Kα, 1.54184	Cu Kα, 1.54184
Temp (K)	150(2)	150(2)	150(2)	150(2)
ρ_{calc} (g cm^{-3})	1.26	1.489	1.120	1.109
μ (mm^{-1})	4.089	3.198	0.923	0.914
Reflections collected	62591	24174	80990	29145
Independent reflections	16116	11822	7355	7067
Parameters	881	850	399	381
R(int)	0.0369	0.0330	0.0675	0.0300
R1/wR2,[a] $I \geq 2\sigma I$ (%)	8.00/20.94	3.91/10.09	5.67/15.64	4.71/12.27
R1/wR2,[a] all data (%)	8.29/21.12	4.10/10.30	6.66/16.75	5.37/12.83
GOF	1.123	1.016	1.071	1.048

[a] $R1 = [\Sigma||F_o| - |F_c||]/\Sigma|F_o|$; $wR2 = \{[\Sigma w[(F_o)^2 - (F_c)^2]^2]/[\Sigma w(F_o^2)^2\}^{1/2}$; $w = [\sigma^2(F_o)^2 + (AP)^2 + BP]^{-1}$, where $P = [(F_o)^2 + 2(F_c)^2]/3$ where A and B values are 0.0707 and 14.7302 for **13**, 0.0546 and 0.6246 for **15**, 0.0826 and 1.6499 for **16a**, 0.0592 and 1.4943 for **17a**.

Table A5. Selected X-ray data collection and refinement parameters for

	17b	**18**	**19**	**20**
Formula	$C_{31}H_{45}BN_3P$	$C_{46}H_{58}BN_4P$	$C_{27}H_{36}BN_2OP$	$C_{52}H_{72}B_2N_4P_2$
CCDC				
Fw [g mol^{-1}]	501.48	708.74	446.36	836.69
Crystal system	monoclinic	triclinic	monoclinic	monoclinic
Space group	$P2_1/n$	$P\bar{1}$	$P2_1/n$	$P2_1/n$
a (Å)	17.2385(2)	10.6744(3)	9.3904(1)	13.0269(2)
b (Å)	10.9928(1)	13.4621(4)	14.2038(1)	14.1779(1)
c (Å)	33.0859(4)	14.8146(4)	20.3914(2)	14.8915(2)
α (°)	90	82.534(2)	90	90
β (°)	96.506(1)	88.654(2)	99.177(1)	112.746(1)
γ (°)	90	84.679(2)	90	90
V (Å^3)	6229.38(12)	2101.57(10)	2684.98(4)	2536.47(6)
Z	8	2	4	2
Radiation, λ (Å)	Cu Kα, 1.54184	Cu Kα, 1.54184	Cu Kα, 1.54184	Cu Kα, 1.54184
Temp (K)	150(2)	150(2)	150(2)	150(2)
ρ_{calc} (g cm^{-3})	1.069	1.120	1.104	1.096
μ (mm^{-1})	0.932	0.836	1.046	1.045
Reflections collected	25322	37991	20355	41427
Independent reflections	10979	8780	5608	5310
Parameters	671	483	327	279
R(int)	0.0229	0.0336	0.0212	0.0281
R1/wR2,[a] $I \geq 2\sigma I$ (%)	6.41/18.42	3.63/9.14	4.00/10.51	3.70/9.67
R1/wR2,[a] all data (%)	7.56/19.46	4.40/9.69	4.59/11.06	4.33/10.16
GOF	1.110	1.041	1.017	1.037

[a] $R1 = [\Sigma||F_o| - |F_c||]/\Sigma|F_o|$; $wR2 = \{[\Sigma w[(F_o)^2 - (F_c)^2]^2]/[\Sigma w(F_o^2)^2\}^{1/2}$; $w = [\sigma^2(F_o)^2 + (AP)^2 + BP]^{-1}$, where $P = [(F_o)^2 + 2(F_c)^2]/3$ and the A and B values are 0.0995 and 3.40 for **17b**, 0.0444 and 0.54 for for **18**, 0.0556 and 0.78 for **19**, 0.0460 and 0.87 for **20**.

Table A6. Selected X-ray data collection and refinement parameters for

	21	**22·1.5hex**	**23a**	**24**
Formula	$C_{37}H_{56}BN_4P$	$C_{74}H_{113}B_2N_6O_2P_2$	$C_{62}H_{84}B_2N_4NiO_2P_2$	$C_{82}H_{108}B_3N_6O_4P_3W$
CCDC			1589993	
Fw [g mol^{-1}]	598.63	1202.26	1059.60	1550.93
Crystal system	orthorhombic	triclinic	tetragonal	orthorhombic
Space group	$P2_12_12$	P–1	$P4_12_12$	$Pna2_1$
a (Å)	12.1633(2)	14.0563(4)	13.7177(2)	19.763(4)
b (Å)	13.4908(3)	14.7947(4)	13.7177(2)	16.566(3)
c (Å)	22.3860(5)	20.1864(5)	32.5141(8)	25.827(5)
α (°)	90	73.781(2)	90	90
β (°)	90	76.257(2)	90	90
γ (°)	90	67.558(2)	90	90
V (Å^3)	3673.38(13)	3684.82(18)	6118.4(2)	8456(3)
Z	4	2	4	4
Radiation, λ (Å)	Cu Kα, 1.54184	Cu Kα, 1.54184	Cu Kα, 1.54184	Cu Kα, 1.54184
Temp (K)	150(2)	150(2)	150(2)	150(2)
ρ_{calc} (g cm^{-3})	1.082	1.084	1.150	1.218
μ (mm^{-1})	0.869	0.880	1.277	3.442
Reflections collected	15359	59780	19118	214640
Independent reflections	7031	15378	6309	17615
Parameters	402	797	368	915
R(int)	0.0291	0.0366	0.0289	0.0440
R1/wR2,[a] $I \geq 2\sigma I$ (%)	2.05/10.65	5.23/13.99	2.76/6.86	5.76/15.25
R1/wR2,[a] all data (%)	4.78/11.31	6.40/15.08	3.03/7.08	5.97/15.55
GOF	1.036	1.043	1.055	1.046

[a] $R1 = [\Sigma||F_o| - |F_c||]/\Sigma|F_o|$; $wR2 = \{[\Sigma w[(F_o)^2 - (F_c)^2]^2]/[\Sigma w(F_o^2)^2\}^{1/2}$; $w = [\sigma^2(F_o)^2 + (AP)^2 + BP]^{-1}$, where $P = [(F_o)^2 + 2(F_c)^2]/3$ and the A and B values are 0.0756 and 1.7565 for **21**, 0.0756 and 1.76 for **22**·1.5hex, 0.0354 and 0.73 for **23a**, and 0.0931and 24.65 for **24**.

Table A7. Selected X-ray data collection and refinement parameters for

	25	**26**	**27**	**28**
Formula	$C_{84}H_{117}B_3N_6O_3P_4W$	$C_{89}H_{124}B_3N_7O_3P_3W$	$C_{86}H_{132}B_6N_4O_2P_2$	$C_{45}H_{36}B_2F_{15}N_2OP$
CCDC				
Fw [g mol^{-1}]	1598.99	1649.13	1380.75	958.35
Crystal system	orthorhombic	triclinic	monoclinic	monoclinic
Space group	*Pna*2$_1$	*P*–1	*P*2$_1$/*n*	*P*2$_1$/*n*
a (Å)	20.0708(1)	14.7117(1)	19.4274(2)	11.1556(2)
b (Å)	16.5566(1)	22.5626(2)	11.7836(2)	34.4444(4)
c (Å)	26.1693(2)	28.9916(3)	36.2597(3)	11.3887(1)
α (°)	90	70.417(1)	90	90
β (°)	90	82.498(1)	91.0320(10)	91.954(1)
γ (°)	90	87.337(1)	90	90
V (Å^3)	8696.17(10)	8989.02(15)	8299.39(18)	4373.54(10)
Z	4	4	4	4
Radiation, λ (Å)	Cu Kα, 1.54184	Cu Kα, 1.54184	Cu Kα, 1.54184	Cu Kα, 1.54184
Temp (K)	150(2)	150(2)	150(2)	150(2)
ρ_{calc} (g cm^{-3})	1.221	1.219	1.105	1.455
μ (mm^{-1})	3.520	3.260	0.825	1.477
Reflections collected	92841	250052	48052	36336
Independent reflections	14752	37334	12163	9069
Parameters	938	1909	925	603
R(int)	0.0456	0.0426	0.0486	0.0374
R1/wR2,[a] I ≥ 2σI (%)	5.38/13.96	2.80/6.81	5.23/12.09	4.69/12.03
R1/wR2,[a] all data (%)	6.03/14.76	3.23/7.11	7.74/13.77	5.89/12.88
GOF	1.032	1.033	1.024	1.044

[a] $R1 = [\Sigma||F_o| - |F_c||]/\Sigma|F_o|$; $wR2 = \{[\Sigma w[(F_o)^2 - (F_c)^2]^2]/[\Sigma w(F_o^2)^2\}^{1/2}$; $w = [\sigma^2(F_o)^2 + (AP)^2 + BP]^{-1}$, where $P = [(F_o)^2 + 2(F_c)^2]/3$ and the A and B values are 0.0903 and 22.05 for **25**, 0.0326 and 8.97 for **26**, 0.0530 and 2.6520 for **27**, and 0.0616 and 1.73 for **28**.

Table A8. Selected X-ray data collection and refinement parameters for

	29	**30**	**31**	**32·1.33benz**
Formula	$C_{45}H_{36}B_2F_{15}N_2OP$	$C_{48}H_{45}B_2F_{15}N_2OP_2$	$C_{45}H_{36}B_2F_{15}N_2OP$	$C_{114}H_{146}Mg_4N_8P_2$
CCDC				
Fw [g mol^{-1}]	958.35	1034.42	958.35	1787.56
Crystal system	triclinic	triclinic	triclinic	triclinic
Space group	*P*–1	*P*–1	*P*–1	*P*–1
a (Å)	11.2406(2)	10.0611(3)	13.6128(4)	14.0074(3)
b (Å)	12.8123(4)	12.6527(4)	17.7940(4)	14.3950(4)
c (Å)	16.0763(3)	19.1586(9)	19.2912(5)	40.3577(4)
α (°)	95.774(2)	81.253(3)	104.027(2)	81.701(2)
β (°)	95.372(2)	75.996(4)	102.959(2)	85.6580(10)
γ (°)	105.189(2)	88.193(3)	90.090(2)	81.280(2)
V (Å^3)	2205.63(9)	2338.85(16)	4410.3(2)	7947.2(3)
Z	2	2	4	3
Radiation, λ (Å)	Cu Kα, 1.54184	Cu Kα, 1.54184	Cu Kα, 1.54184	Cu Kα, 1.54184
Temp (K)	150(2)	150(2)	150(2)	150(2)
ρ_{calc} (g cm^{-3})	1.443	1.469	1.443	1.121
μ (mm^{-1})	1.465	1.737	1.465	0.979
Reflections collected	27341	28673	49435	79170
Independent reflections	9098	9686	18221	27976
Parameters	603	642	1205	1731
R(int)	0.0237	0.0308	0.0206	0.0369
R1/wR2,[a] $I \geq 2\sigma I$ (%)	3.97/9.95	4.24/10.99	3.62/9.56	8.52/23.80
R1/wR2,[a] all data (%)	4.87/10.53	5.24/12.02	4.06/9.98	9.91/25.04
GOF	1.029	1.023	1.016	1.016

[a] $R1 = [\Sigma||F_o| - |F_c||]/\Sigma|F_o|$; $wR2 = \{[\Sigma w[(F_o)^2 - (F_c)^2]^2]/[\Sigma w(F_o^2)^2\}^{1/2}$; $w = [\sigma^2(F_o)^2 + (AP)^2 + BP]^{-1}$, where $P = [(F_o)^2 + 2(F_c)^2]/3$ and the A and B values are 0.0455 and 0.99 for **29**, 0.0690 and 0.58 for **30**, 0.0523 and 1.30 for **31**, and 0 and 0.0807 for **32**.

Table A9. Selected X-ray data collection and refinement parameters for

	33·0.5hex	**34**	**35**	**36**
Formula	$C_{52}H_{72}BMgN_4O$	$C_{118}H_{145}Mg_5N_{10}P_3$	$C_{56}H_{76}N_4Mg_2P_2$	$C_{114}H_{146}Mg_4N_8P_2$
CCDC				
Fw [g mol^{-1}]	804.25	1917.89	915.76	1787.56
Crystal system	triclinic	monoclinic	monoclinic	triclinic
Space group	*P*–1	$P2_1/n$	$P2_1/n$	*P*–1
a (Å)	12.7324(4)	14.2205(11)	14.9746(3)	14.0074(3)
b (Å)	13.9468(5)	18.800(2)	17.9972(3)	14.3950(4)
c (Å)	15.1879(4)	47.113(5)	19.8583(3)	40.3577(4)
α (°)	69.599(3)	90	90	81.701(2)
β (°)	77.946(3)	91.323(9)	92.360(2)	85.6580(10)
γ (°)	77.883(3)	90	90	81.280(2)
V (Å^3)	2444.29(15)	12592(2)	5347.29(16)	7947.2(3)
Z	2	4	4	3
Radiation, λ (Å)	Cu Kα, 1.54184	Cu Kα, 1.54184	Cu Kα, 1.54184	Cu Kα, 1.54184
Temp (K)	150(2)	150(2)	150(2)	150(2)
ρ_{calc} (g cm^{-3})	1.093	1.012	1.138	1.121
μ (mm^{-1})	0.603	1.02	1.253	0.979
Reflections collected	24784	125325	42898	79170
Independent reflections	10088	22172	11068	27976
Parameters	558	1279	598	1731
R(int)	0.0203	0.2856	0.0378	0.0369
R1/wR2,[a] I ≥ 2σI (%)	4.24/11.34	11.15/29.59	4.25/10.98	8.52/23.80
R1/wR2,[a] all data (%)	4.82/11.90	19.09/36.77	6.16/12.15	9.91/25.04
GOF	1.093	0.873	1.022	1.016

[a] $R1 = [\Sigma||F_o| - |F_c||]/\Sigma|F_o|$; $wR2 = \{[\Sigma w[(F_o)^2 - (F_c)^2]^2]/[\Sigma w(F_o^2)^2\}^{1/2}$; $w = [\sigma^2(F_o)^2 + (AP)^2 + BP]^{-1}$, where $P = [(F_o)^2 + 2(F_c)^2]/3$ where A and B are 0.0601 and 0.5283 for **33·0.5hex**, 0.2000 and 0 for **34**, 0.0695 and 0.7173 for **35**, and 0.1410 and 15.7790 for **36**.

Table A10. Selected X-ray data collection and refinement parameters for

	38	**40b·tol**	**40c·2tol**	**41a·tol**
Formula	$C_{30}H_{43}BKN_3P$	$C_{49.33}H_{59.67}GaIN_4$	$C_{71}H_{80}GaIN_4$	$C_{49}H_{53}GaN_3OP$
CCDC				
Fw [g mol^{-1}]	526.55	905.29	1186.01	800.63
Crystal system	triclinic	trigonal	orthorhombic	monoclinic
Space group	*P*–1	*R*3*c*	$P2_12_12_1$	$P2_1/n$
a (Å)	16.4541(5)	30.5012(5)	13.65400(10)	12.4092(2)
b (Å)	17.6172(6)	30.5012(5)	18.29020(10)	19.3221(3)
c (Å)	19.7041(6)	25.1712(7)	24.71570(10)	17.8085(3)
α (°)	63.866(3)	90	90	90
β (°)	65.771(3)	90	90	90.204(2)
γ (°)	79.970(3)	120	90	90
V (Å^3)	4676.0(3)	20280.0(9)	6172.36(6)	4269.95(12)
Z	6	18	4	4
Radiation, λ (Å)	Cu Kα, 1.54184	Cu Kα, 1.54184	Cu Kα, 1.54184	Cu Kα, 1.54184
Temp (K)	150(2)	150(2)	150(2)	150(2)
ρ_{calc} (g cm^{-3})	1.122	1.334	1.276	1.245
μ (mm^{-1})	2.126	6.484	4.861	1.53
Reflections collected	54188	43818	76989	47742
Independent reflections	19300	9219	12864	8915
Parameters	980	509	710	505
R(int)	0.0413	0.0571	0.0392	0.0259
R1/wR2,[a] I ≥ 2σI (%)	5.17/13,27	3.28/7.52	2.59/6.62	3.32/9.26
R1/wR2,[a] all data (%)	6.96/14.81	3.97/8.16	2.79/6.83	3.62/9.52
GOF	1.026	1.035	1.082	1.234

[a] $R1 = [\Sigma||F_o| - |F_c||]/\Sigma|F_o|$; $wR2 = \{[\Sigma w[(F_o)^2 - (F_c)^2]^2]/[\Sigma w(F_o^2)^2\}^{1/2}$; $w = [\sigma^2(F_o)^2 + (AP)^2 + BP]^{-1}$, where $P = [(F_o)^2 + 2(F_c)^2]/3$ where A and B are 0.0765 and 1.3879 for **38**, 0.0352 and 24.0515 for **40b·tol**, 0.0413 and 0.9451 for **40c·2tol**, and 0.0466 and 0.9783 for **41a·tol**.

Table A11. Selected X-ray data collection and refinement parameters for **41b**, **41c**, **42**, and **43a**

	41b·0.5tol	**41c·tol**	**42·Et$_2$O**	**43a**
Formula	$C_{51.5}H_{64}GaN_4OP$	$C_{72}H_{80}GaN_4OP$	$C_{90}H_{110}Ga_2N_6O_2P_2$	$C_{44}H_{54}GaN_3P_2$
CCDC				
Fw [g mol^{-1}]	855.75	1118.09	1509.21	756.56
Crystal system	orthorhombic	orthorhombic	Monoclinic	monoclinic
Space group	*Fdd*2	$P2_12_12_1$	$P2_1/c$	$P2_1/c$
a (Å)	39.4865(13)	13.6214(10)	12.2300(3)	9.35570(10)
b (Å)	36.1344(15)	18.3845(12)	22.2691(4)	19.1486(2)
c (Å)	12.8743(6)	24.7906(11)	15.9009(4)	22.4817(2)
α (°)	90	90	90	90
β (°)	90	90	111.732(3)	96.9660(10)
γ (°)	90	90	90	90
V (Å^3)	18369.3(13)	6208.1(7)	4022.83(18)	3997.83(7)
Z	16	4	2	4
Radiation, λ (Å)	Cu Kα, 1.54184	MoKα, 0.71073	MoKα, 0.71073	Cu Kα, 1.54184
Temp (K)	150(2)	150(2)	150(2)	150(2)
ρ_{calc} (g cm^{-3})	1.238	1.196	1.246	1.257
μ (mm^{-1})	1.458	0.515	0.761	1.947
Reflections collected	18275	25542	58229	47290
Independent reflections	8777	10916	11317	8269
Parameters	544	728	470	462
R(int)	0.0448	0.0727	0.0456	0.0397
R1/wR2,[a] $I \geq 2\sigma I$ (%)	4.91/12.08	6.51/11.17	4.13/8.73	3.26/7.92
R1/wR2,[a] all data (%)	6.71/13.94	11.13/12.79	6.76/9.90	4.30/8.28
GOF	1.013	1.009	1.026	1.081

[a] $R1 = [\Sigma||F_o| - |F_c||]/\Sigma|F_o|$; $wR2 = \{[\Sigma w[(F_o)^2 - (F_c)^2]^2]/[\Sigma w(F_o^2)^2\}^{1/2}$; $w = [\sigma^2(F_o)^2 + (AP)^2 + BP]^{-1}$, where $P = [(F_o)^2 + 2(F_c)^2]/3$ where A and B are 0.0730 and 11.2096 for **41b·0.5tol**, 0 and 0.0436 for **41c·tol**, 0.0348 and 3.3566 for **42·Et$_2$O**, and 0.0291 and 3.1474 for **43a**.

Table SA12. Selected X-ray data collection and refinement parameters for

	43b·0.66Et$_2$O	**44·tol**
Formula	$C_{52.67}H_{75.67}GaN_4O_{0.67}P_2$	$C_{84}H_{102}Ga_2N_5P$
CCDC		
Fw [g mol^{-1}]	907.16	1352.11
Crystal system	trigonal	orthorhombic
Space group	*P*–3	*Pbca*
a (Å)	46.3247(5)	27.3275(2)
b (Å)	46.3247(5)	17.6404(2)
c (Å)	12.9618(2)	31.0011(3)
α (°)	90	90
β (°)	90	90
γ (°)	120	90
V (Å^3)	24089.1(6)	14944.6(2)
Z	18	8
Radiation, λ (Å)	Cu Kα, 1.54184	Cu Kα, 1.54184
Temp (K)	150(2)	150(2)
ρ_{calc} (g cm^{-3})	1.126	1.202
μ (mm^{-1})	1.541	1.432
Reflections collected	264237	136257
Independent reflections	33572	15813
Parameters	1639	827
R(int)	0.0572	0.0656
R1/wR2,[a] I ≥ 2σI (%)	8.54/22.66	4.12/10.01
R1/wR2,[a] all data (%)	9.39/23.22	6.13/11.08
GOF	1.248	1.036

[a] $R1 = [\Sigma||F_o| - |F_c||]/\Sigma|F_o|$; $wR2 = \{[\Sigma w[(F_o)^2 - (F_c)^2]^2]/[\Sigma w(F_o^2)^2\}^{1/2}$; $w = [\sigma^2(F_o)^2 + (AP)^2 + BP]^{-1}$, where $P = [(F_o)^2 + 2(F_c)^2]/3$ where A and B are 0.0480 and 78.6176 for **43b·0.66Et$_2$O**, and 0.0484 and 11.7582 for **44·tol**.